Journal of the Anatomical Society of India

Print ISSN: 0003-2778

GENERAL INFORMATION

About the Journal

Journal of the Anatomical Society of India (ISSN: Print 0003-2778) is peer-reviewed journal. The journal is owned and run by Anatomical Society of India. The journal publishes research articles related to all aspects of Anatomy and allied medical/surgical sciences. Pre-Publication Peer Review and Post-Publication Peer Review Online Manuscript Submission System Selection of articles on the basis of MRS system Eminent academicians across the globe as the Editorial board members Electronic Table of Contents alerts Available in both online and print form. The journal is published quarterly in the months of January, April, July and October.

Scope of the Journal

The aim of the *Journal of the Anatomical Society of India* is to enhance and upgrade the research work in the field of anatomy and allied clinical subjects. It provides an integrative forum for anatomists across the globe to exchange their knowledge and views. It also helps to promote communication among fellow academicians and researchers worldwide. The Journal is devoted to publish recent original research work and recent advances in the field of Anatomical Sciences and allied clinical subjects. It provides an opportunity to academicians to disseminate their knowledge that is directly relevant to all domains of health sciences.

The Editorial Board comprises of academicians across the globe.

JASI is indexed in Scopus, available in Science Direct.

Abstracting and Indexing Information

The journal is registered with the following abstracting partners:

Baidu Scholar, CNKI (China National Knowledge Infrastructure), EBSCO Publishing's Electronic Databases, Ex Libris – Primo Central, Google Scholar, Hinari, Infotrieve, Netherlands ISSN center, ProQuest, TdNet, Wanfang Data

The journal is indexed with, or included in, the following:

SCOPUS, Science Citation Index Expanded, IndMed, MedInd, Scimago Journal Ranking, Emerging Sources Citation Index.

Impact Factor® as reported in the 2020 Journal Citation Reports® (Clarivate Analytics, 2021): 0.15

Information for Authors

Article processing and publication charges will be communicated by the editorial office. All manuscripts must be submitted online at https://review.jow.medknow.com/jasi.

Subscription Information

A subscription to JASI comprises 4 issues. Prices include postage. Annual Subscription Rate for non-members-		
Rates of Membership (with effect from 1.1.2019)		
	India	**International**
Ordinary membership	INR 1500	US $ 100
Couple membership	INR 2250	
Life membership	INR 8000	US $ 900
Subscription Rates (till 31st August)		
Individual	INR 6000	US $ 650
Library/Institutional Trade discount of 10% for agencies only	INR 12000	US $ 1000
Subscription Rates (after 31st August)		
Individual	INR 6500	US $ 700
Library/Institutional	INR 12500	US $ 1050
The Journal of Anatomical Society of India (ISSN: 0003-2778) is published quarterly **Subscriptions** are accepted on a prepaid basis only and are entered on a calendar year basis. Issues are sent by standard mail Priority rates are available upon request.		

Information to Members/Subscribers

All members and existing subscribers of the Anatomical Society of India are requested to send their membership/existing subscription fee for the current year to the Treasurer of the Society on the following address: Prof (Dr.) Punit Manik, Treasurer, ASI, Department of Anatomy, KGMU, Lucknow - 226003. Email: punitamanik@yahoo.co.in. All payments should be made through an account payee bank draft drawn in favor of the **Treasurer, Anatomical Society of India,** payable at **Lucknow** only, preferably for **Allahabad Bank, Medical College Branch, Lucknow.** Outstation cheques/drafts must include INR 70 extra as bank collection charges.

All complaints regarding non-receipt of journal issues should be addressed to the Editor-in-Chief, JASI at editorjasi@gmail.com. The new subscribers may, please contact wkhlrpmedknow_subscriptions@wolterskluwer.com.

Requests of any general information like travel concession forms, venue of next annual conference, etc. should be addressed to the General Secretary of the Anatomical Society of India.

For mode of payment and other details, please visit www.medknow.com/subscribe.asp

Claims for missing issues will be serviced at no charge if received within 60 days of the cover date for domestic subscribers, and 3 months for subscribers outside India. Duplicate copies cannot be sent to replace issues not delivered because of failure to notify publisher of change of address. The journal is published and distributed by Wolters Kluwer India Pvt. Ltd. Copies are sent to subscribers directly from the publisher's address. It is illegal to acquire copies from any other source. If a copy is received for personal use as a member of the association/ society, one cannot resale or give-away the copy for commercial or library use.

The copies of the journal to the subscribers are sent by ordinary post. The editorial board, association or publisher will not be responsible for non receipt of copies. If any subscriber wishes to receive the copies by registered post or courier, kindly contact the publisher's office. If a copy returns due to incomplete, incorrect or changed address of a subscriber on two consecutive occasions, the names of such subscribers will be deleted from the mailing list of the journal. Providing complete, correct and up-to-date address is the responsibility of the subscriber.

Nonmembers: Please send change of address information to subscriptions@medknow.com.

Advertising Policies

The journal accepts display and classified advertising. Frequency discounts and special positions are available. Inquiries about advertising should be sent to Wolters Kluwer India Pvt. Ltd, advertise@medknow. com.

The journal reserves the right to reject any advertisement considered unsuitable according to the set policies of the journal.

The appearance of advertising or product information in the various sections in the journal does not constitute an endorsement or approval by the journal and/or its publisher of the quality or value of the said product or of claims made for it by its manufacturer.

Addresses

Editorial Office

Dr. Vishram Singh, Editor-in-Chief, JASI
OC-5/103, 1st floor, Orange County Society,
Ahinsa Khand-I, Indirapuram, Ghaziabad,
Delhi, NCR- 201014.
Email: editorjasi@gmail.com

Published by

Wolters Kluwer India Pvt. Ltd
A-202, 2nd Floor, The Qube,
C.T.S. No.1498A/2 Village Marol, Andheri (East),
Mumbai - 400 059, India.
Phone: 91-22-66491818
Website: www.medknow.com

Printed at

Nikeda Art Printers Pvt. Ltd Bhandup (W) , Mumbai - 400078, India.

Journal of the Anatomical Society of India

Print ISSN: 0003-2778

EDITORIAL BOARD

Journal of the Anatomical Society of India

Print ISSN: 0003-2778

EXECUTIVE COMMITTEE

Journal of the Anatomical Society of India

Volume 71 | Issue 1 | January-March 2022

CONTENTS

Superspecializations in Anatomy: A Step Forward in Order to Improve Medical Education and Clinical Practice

The anatomy has been the cornerstone of medical education, since time immemorial.[1] For it lays the foundation of all medical curricula and provides the anatomical basis of clinical practice.[2]

Traditionally, anatomy is mainly taught to 1st-year medical students, although the knowledge attained is required by them throughout their clinical careers. Anatomical knowledge is vital for a clinician, helping them identify the embryological and anatomical basis of various diseases. It is also required for proper clinical examination, interpretation of signs and symptoms, and radiological images.[3] The curriculum is designed in such a way that even though it is taught, during the clinical posting of medical students but, the teacher here is the clinician and not an anatomist. This editorial talks about the need for specialized anatomists.

For the past 30 years or so, clinicians, particularly surgeons, have felt that there is a definite decline in knowledge of the anatomy of newly passed medical graduates. The students with decreasing knowledge of anatomy show their disability to apply knowledge in diagnosis and problem-solving.[3]

Although it is difficult to assess the reason objectively, the possible reasons could be (a) drastic reduction in allocated time for anatomy teaching, (b) poor teacher–student ratio,[4] (c) lack of proper cadaveric dissection, (d) use of new technologies in teaching, (e) too much research work by teachers without proper facilities and guidance,[5](f) nonexposure of teaching faculty to patients care, etc.

The proper knowledge of anatomy is the utmost for doctors in order to do the proper and safe clinical practice. The decline in knowledge of anatomy is hazardous not only to medical profession but also to society.

Recently, National Medical Commission (NMC) has been constituted in India by an act of parliament known as NMC Act, 2019, which came into force on September 25, 2020, by a gazette notification dated: September 24, 2020, with mission and vision to improve access to quality and affordable, medical education, and ensure availability of adequate and high-quality medical professional in all parts of country.[6]

The competencies provided by NMC are well thought and well planned to teach anatomy but difficult to implement properly, due to limited time allocation, late admission, decreased teacher–student ratio, and nonexposure of faculty to clinical procedures and practice.

As discussed earlier, the knowledge of anatomy is of paramount importance to successful medical practice. The inadequate anatomical knowledge of clinicians is hazardous for successful clinical practice.[7] Further, nowadays, there is a huge public and media pressure on clinicians to have proper knowledge of anatomy. This is because public interest and knowledge of anatomy has been increased in the recent past due to adequate public exposure through various educational programs run on YouTube and television talking about the structure and functions of the human body.

In one of the recent polls, it has been found that about 90% general public think that clinicians should have practical experience of real human anatomy. The inadequate anatomical knowledge for clinicians is hazardous for successful clinical practice.[7]

The discrepancy in public expectation and actual knowledge of the clinical anatomy of a clinician may lead to future legal claims. Therefore, it has been thought that the following reforms should be done by the competent authorities.

The anatomy should not only be taught to students during 1st year but also during their clinical years subject-wise by specialist anatomists in that field.

This is possible only if the anatomists are superspecialized in the area related to a particular clinical subject, namely anatomy in radiology, forensic medicine, general surgery, orthopedic surgery, pediatric surgery, ENT surgery, skull base surgery, cardiac surgery, reproductive biology, and so on.

Therefore, it is felt that the time has come when during postgraduation in anatomy, the topic of their thesis should be related to one of the specialties of clinical medicine. There must be a collaboration between the anatomy and the clinical departments. The thesis work should be done in collaboration of the faculty of that particular clinical specialty. After passing their postgraduation these, the concerned students should be awarded, their postgraduate degrees as under:

- MD Anatomy (Radiology and imaging)
- MD Anatomy (Forensic science)
- MD Anatomy (Reproductive biology)
- MD Anatomy (Orthopedic surgery)
- MD Anatomy (ENT surgery)
- MD Anatomy (Skull base surgery), and so on.

After getting MD degree in specialized anatomy, these anatomists can, provide clinical anatomy education to students during their clinical years with ease and efficiency. This will not only improve rather greatly enhance the

knowledge of the anatomy of clinicians to do the safe and efficient clinical practice.

Vishram Singh, Gaurav Singh[1]

Department of Anatomy, Kasturba Medical College, Mangalore, Manipal Academy of Higher Education, Manipal, Karnataka, India, [1]Clinical Editor, BMJ India, Delhi, India

Address for correspondence: *Prof. Vishram Singh, B5/3 Hahnemann Enclave Plot No. 40, Sector 6 Ph-2 Dwarka, New Delhi - 110 075, India.*
E-mail: drvishramsingh@gmail.com

References

1. Staden HV. The Art of Medicine in Early Alexandria. Cambridge, Mass USA: Cambridge University Press; 2004.
2. Standring S. Gray's Anatomy: The Anatomical Basis of Clinical Practice. 41st ed. Canada: Elsevier; 2016. [Last accessed on 2022 Feb 09].
3. Doomernik DE, van Goor H, Jan GM, Kooloos, Richard P, Brock T. Longitudinal retension of anatomical knowledge in second year medical students. Anat Sci Edu 2017;10:242-8.
4. Singh V, Sahai A. Implementation of competency based medical education in anatomy with poor teacher-student ratio: The utopia. J Anat Soc India 2020;69: 193-5.
5. Singh V, Reddy KC, Rashi S. Medical research and publication: Concerns and way forward. J Anat Soc India 2021;70:195-6.
6. Curricula of Postgraduate Medical Students. Available from: https://www.nmc.org.in/information-desk/for-colleges/pg-curricula-2/. [last accessed on 09 Feb 2022].
7. Singh R, Yadav N, Pandey M, Jones DG. Is inadequate anatomical knowledge on the part of physicians hazardous for successful clinical practice? Surg Radiol Anat 2022;44:83-92.

Article Info

Received: 22 February 2022
Accepted: 22 February 2022
Available online: 17 March 2022

Access this article online	
Quick Response Code:	**Website:** www.jasi.org.in
	DOI: 10.4103/jasi.jasi_34_22

How to cite this article: Singh V, Singh G. Superspecializations in anatomy: A step forward in order to improve medical education and clinical practice. J Anat Soc India 2022;71:1-2.

Original Article

Mutation Analysis of Severe Acute Respiratory Syndrome Coronavirus-2 Genomic Sequences in India and its Geographical Relations

Pradip Rameshbhai Chauhan, Ashish J. Rathva[1], Kinjal Jethva[2]

Department of Anatomy, P.D.U. Government Medical College, Rajkot, [1]Department of Anatomy, GMERS Medical College, Junagadh, [2]Department of Anatomy, SKBS Medical College and Research Institute, Sumandeep Vidhyapeeth, Baroda, Gujarat, India

Abstract

Introduction: Severe acute respiratory syndrome coronavirus-2 (SARS-CoV-2) infection has been spreading all over the world, including India; the virus has been classified in various clades (L, S, V, G, GH, GR, and others) on the base of mutations. India is vulnerable to the health and financial hazards of the SARS-CoV-2 infection. Even after four phases of lockdown, the number of SARS-CoV-2 infections has been increasing in India. Clinical trials for vaccine and ribonucleic acid (RNA)-dependent RNA polymerase inhibitor are going on. The study was conducted to analyze SARS-CoV-2 genomic sequences submitted from India to identify mutations and their geographical distribution. **Material and Methods:** Three hundred and sixty-three sequences submitted from India were archived (GISAID database), compared with reference sequence (Wuhan, China), and phylogenetic tree was prepared. Sequences with more than 1% nucleotide stretching were excluded for mutation analysis, and multiple sequence analysis for 317 sequences was done. Mutations were analyzed as per phases of lockdown and geographical distribution. **Results:** Clade "GH" appears in the second and third phases of lockdown; the clade "V" has not been reported after March 17, 2020, in India. Spike protein mutation D614G was found in 166 sequences, out of which 164 sequences show P323 L mutation of nonstructural protein 12 (nsp12). RNA-dependent RNA polymerase coding nsp12 shows 23 types of 364 amino acid mutations. **Discussion and Conclusion:** SARS-CoV-2 shows increasing mutations with the time and spread of the virus. The mutations in spike protein and nsp12 regions are critical for response to undergoing trials of vaccines and drugs.

Keywords: *Genome, mutation, ribonucleic acid-dependent ribonucleic acid polymerase, severe acute respiratory syndrome coronavirus-2, spike protein*

Introduction

The first case of severe acute respiratory syndrome coronavirus-2 (SARS-CoV-2) disease (COVID-19) was reported on December 31, 2019, in Wuhan, China.[1] The World Health Organization declared the emerging SARS-CoV-2 as a pandemic on March 11, 2020.[2] As of June 2, 2020, reported to the WHO, there have been 6,194,533 confirmed cases of SARS-CoV-2 infection including 376,320 deaths globally and 5,598 deaths in India.[3]

India implemented lockdown in four phases as cautionary measures to combat the spread of the SARS-CoV-2. First phase: March 25, 2020–April 14, 2020; second phase: April 15, 2020–May 3, 2020; and third phase May 4, 2020–May 17, 2020. From May 18, India started the fourth phase of lockdown with many relaxations that ended on May 31. The number of cases has been increasing in India even after four phases of lockdowns. India being a country with the second largest population in the world is vulnerable to the hazards of the SARS-CoV-2 infection.

Genomic structure of severe acute respiratory syndrome coronavirus-2

SARS-CoV-2 is from the SARS-CoV species of subgenus *Sarbecovirus*, genus *Betacoronavirus*, family Coronaviridae; the seventh member of the sphere-shaped enveloped nonsegmented positive-sense ribonucleic acid (RNA) β-coronavirus (SARS-CoV-2) is believed to be originated from the infected bat.[4] Genome sequence of the SARS-CoV-2 is found 96.2% identical to the bat CoV RaTG13 collected in Yunnan province, China, and pangolin is believed as an intermediate host.[5]

Coronavirus genome contains a variable number of open reading frame (ORF);

How to cite this article: Chauhan PR, Rathva AJ, Jethva K. Mutation analysis of severe acute respiratory syndrome coronavirus-2 genomic sequences in India and its geographical relations. J Anat Soc India 2022;71:3-10.

Article Info

Received: 12 June 2020
Accepted: 27 October 2021
Available online: 17 March 2022

Address for correspondence:
Dr. Pradip Rameshbhai Chauhan, Department of Anatomy, P.D.U. Government Medical College, Civil Hospital Campus, Jamanagar Road, Rajkot - 360 001, Gujarat, India.
E-mail: prajjawalitresearch@gmail.com

Access this article online

Website: www.jasi.org.in
DOI: 10.4103/JASI.JASI_109_20
Quick Response Code:

the ORF encodes 16 nonstructural proteins (nsps). The remaining part of the viral genome encodes spike surface glycoprotein (S), a small envelope protein (E), matrix protein (M), and nucleocapsid protein (N), and other accessory proteins.[6]

SARS-CoV-2 genome possesses 14 ORFs encoding 27 proteins. pp1ab and pp1a proteins are encoded by the orf1ab and orf1a genes located at the 5'-terminus of the genome, respectively. The pp1ab and pp1a proteins consist of 15 nsps that include nsp1 to nsp10 and nsp12 to nsp16.[7] Four structural proteins (S, E, M, and N) and Five accessory proteins (ORF3a, ORF6, ORF7a, ORF7b, and ORF8) are encoded by the 3'-terminus of the SARS-CoV-2 genome.[7,8]

The envelope of the SARS-CoV-2 has glycoprotein spikes. The receptor-binding domain (RBD) of the SARS-CoV-2 is closer to GD pangolin-CoV.[9] SARS-CoV-2 binds to angiotensin-converting enzyme-2 (ACE2) receptors through the receptor-binding domain of the spike glycoprotein. The spike glycoprotein contains S1 and S2 subunits with a furin-like cleavage site; S1 domain of the spike glycoprotein interacts with the ACE2 receptor and the S2 subunit allows membrane fusion.[10,11]

Pathogenesis

When the SARS-CoV-2 virus passes through the nasal and larynx mucosa, the patient shows early symptoms such as fever and cough.[12] Around 5–10 days, the patient shows lower respiratory tract infection or pneumonia when the virus reaches the lung through the respiratory tract.[13,14] The virus enters the vascular system through alveoli leading to viremia. SARS-CoV-2 affects the organs such as lungs, kidney, hearts, and gastrointestinal tract which expresses ACE2 receptors.[15] Recent studies show that the virus lowers thrombin and prothrombin time deranging the blood coagulation.[16,17] Clinical data reveal that patients with the SARS-CoV-2 infection show neurological symptoms also as impaired taste, smell, headache, disturbance of consciousness, and epilepsy.[17]

SARS-CoV-2 clades and variants: GISAID database classified the SARS-CoV-2 in four major clades in the context of marker variants relative to WIV04 reference sequence. Clade "L" (Wuhan reference sequence), clade "S" (leucine replaced by serine at the 84th position [L84S mutation] in ns8), clade "V" (leucine replaced by phenylalanine at the 37th position [L37F mutation] in nsp6 and glycine replaced by valine at the 251st position [G251V mutation] in ns3), and clade G (aspartic acid replaced by glycine at the 614th position [D614G mutation] in spike glycoprotein). The clade "G" is further classified as clade "GH" (D614G mutation in spike glycoprotein and glutamine replaced by histidine at the 57th position [Q57H mutation] in ns3) and subclade "GR" (D614G mutation in spike glycoprotein and glycine replaced by arginine at the 204th position [G204R mutation] in nucleocapsid protein).[18]

Because of high replication rate, SARS-CoV-2 is mutating and spreading rapidly. Clinical trials of RNA-dependent RNA polymerase (RdRp) inhibitor drugs are going on to combat the SARS-CoV-2 infection. Mutations of SARS-CoV-2 are critical spread of the virus, morbidity, mortality, vaccine development, and treatment of the infection.

This study was conducted to identify mutations present in SARS-CoV-2 genomic sequences of India and to find out their geographical location. One of the objectives was to find out the progressions of mutation with the phases of lockdown.

Material and Methods

SARS-Cov-2 genomic sequences submitted up to May 26, 2020, were retrieved from GSAID. Three hundred and sixty-three complete genome sequences from India were retrieved from the data source. The data contain information of various parameters such as viral strain name, data of sample collection, country, and state of origin of the sample along with the accession number of the sequence. The sequences were compared with the reference sequence (sequence id in GISAID: hCov-19/Wuhan/WIC04/2019 and access id in NICB database: NC_045512 sequence from the Wuhan, China). The study does not involve any living human or animal so does not require ethical committee approval.

Phylogenetic tree was constructed using maximum likelihood method and the Tamura–Nei model,[19] applying neighbor-join and BIONJ algorithms to a matrix of pairwise distances estimated using the Tamura–Nei model, and then selecting the topology (1000 bootstrap replicates) with superior log-likelihood value. This analysis involved 364 nucleotide sequences. Evolutionary analyses were conducted in MEGA X.[20]

Incomplete genomic sequences and with more than 1% nucleotide stretching were not considered for mutation identification and analysis. Finally, 317 genomic sequences were included for the identification of the mutation. Multiple sequence alignments for nucleotide sequences and the amino acid were done with MAFFT version 7 (Wellcome Genome Campus, Hinxton, Cambridgeshire).[21] Amino acid mutations were distributed according to the geographical area of the sample collection. Demographic data and death rate of Indian SARS-CoV-2 cases according to states were accessed from the Indian COVID-19 dashboard on 9.52 A. M. on the May 31, 2020.[22]

Statistical analysis was performed by the Epi Info 7™ software and R software. After checking the normality of distribution with the Shapiro–Wilk test, continuous variables were analyzed for median, mode, mean, and range. Categorical variables were analyzed for counts and frequency. Fisher's exact test of neutrality for sequence pairs was performed ($P < 0.05$). For the number of mutations per genome related to the states, we used Fisher's exact tests.

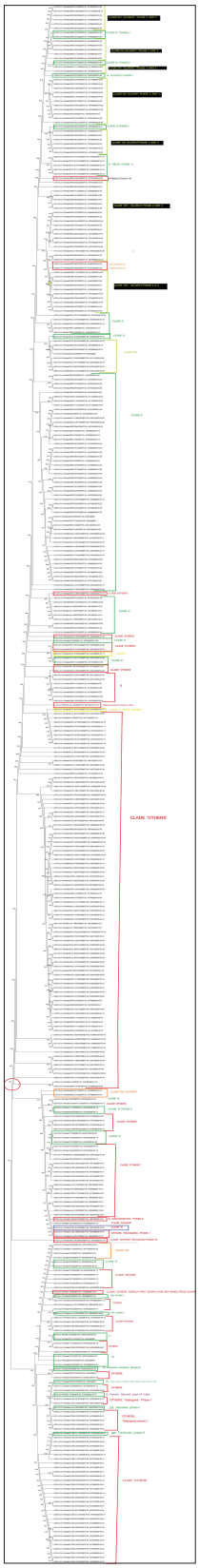

Figure 1: Phylogenetic tree of Indian severe acute respiratory syndrome coronavirus-2 genomic sequences (maximum likelihood and neighbor-joining model) (number in the bracket shows the branch number. Words "G," "GH," "GR," "V," "L," "S," and "others" indicate the clade of the severe acute respiratory syndrome coronavirus-2. Location has been mentioned along with the clade wherever it is necessary)

Results

Phylogenetic tree

Phylogenetic tree [Figure 1] of 364 nucleotide sequences (one of which was the reference sequence hCov-19/Wuhan/WIC04/2019 and NC_045512) was inferred using the maximum likelihood method and Tamura–Nei model. Number in bracket shows the branch number. The phylogenetic tree shows that the first two cases of India (access id EPI_ISL_413522 and EPI_ISL_413523) are closer to the reference sequence from Wuhan, China. A sequence from Telangana (access id EPI_ISL_447866) shows the maximum distance (99.87% similarity) from the reference sequence. A sequence from Madhya Pradesh (access id EPI_ISL_436453) shows the minimum distance (99.99% similarity) from the reference sequence.

Phylogenetic tree shows that SARS-CoV-2 mutates into clade "GH" in the second and third phases of lockdown. As shown at the branch no. 474, sequences marked with clade "others" (which shows more similarity to reference sequence) mutate into clade "G," clade "V," clade "S," and clade "GR." Clade "V" and clade "S" do not show further progression.

Mutation analysis

Three hundred and seventeen SARS-CoV-2 genomic sequences were aligned with the reference sequence (hCov-19/Wuhan/WIC04/2019 and NC_045512). Amino acid and nucleotide mutations were identified and analyzed.

Lockdown phase-wise analysis

Three hundred and seventeen SARS-CoV-2 genomic sequences were classified according to the date of collection in four groups [Figure 2]. The first group was before March 25, 2020 (before lockdown, n = 61); the second group was

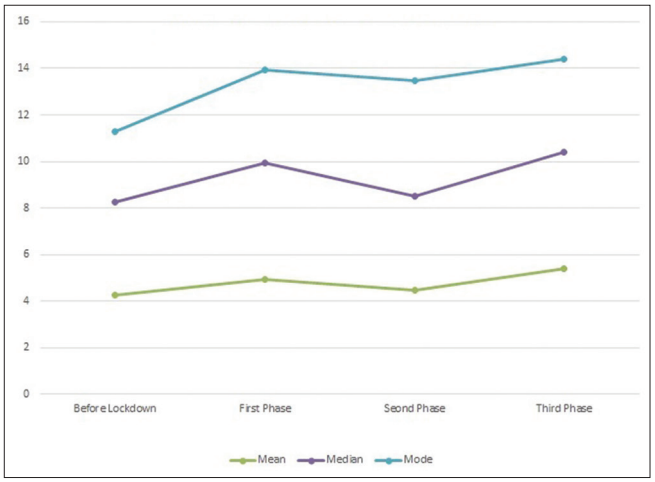

Figure 2: Mutations frequency of severe acute respiratory syndrome coronavirus-2 genomic sequences as per phases of lockdown

from March 25, 2020 to April 14, 2020 (the first phase of lockdown, n = 121); the third group was from April 15, 2020, to May 3, 2020 (the second phase of lockdown, n = 105); and the fourth group was May 4, 2020–May 17, 2020 (the third phase of lockdown, n = 30).

The difference in the means of the mutation among phases of lockdown was statistically significant. (ANOVA, a parametric test for inequality of population means, P = 0.0098 and Bartlett's test for inequality of population variances P = 0.0381); mutations increased significantly during the third phase of the lockdown, which shows that the frequency of mutations increases with the time and spread of the virus.

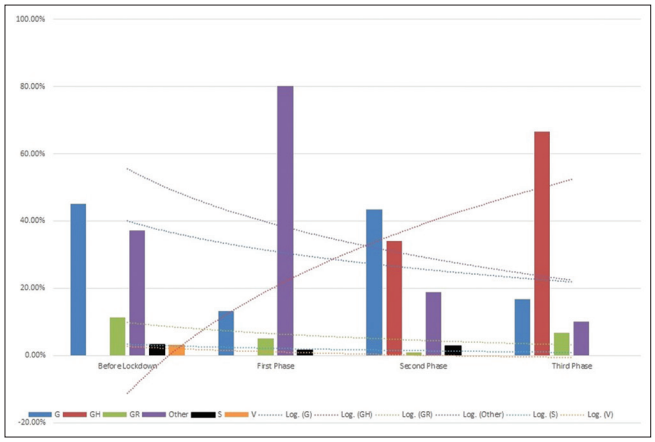

Figure 3: Clades of severe acute respiratory syndrome coronavirus-2 genomic sequences as per phases of lockdown (words "G," "GH," "GR," "V," "L," "S," and "others" indicate the clade of the severe acute respiratory syndrome coronavirus-2. Dotted lines indicate the LogRhythm scale for the clades)

Lockdown phases and severe acute respiratory syndrome coronavirus-2 clades

In this study, SARS-CoV-2 genomic sequences were classified in major clade "L," clade "S," clade "V," clade "G," clade "GH," clade "GR," and "others" to identify their distribution during various phases of lockdown [Figure 3].

Out of 317, only 2 sequences show clade "V"; the clade "V" has not been reported after March 17, 2020, in India. Both sequences were submitted from Delhi – one (access id: EPI_ISL_435109) was from the female of 18 years old and another (access id: EPI_ISL_435108) was of the female of 22 years old.

Clade "GH" appeared after the first phase of lockdown and increased during the second and third phases of lockdown.

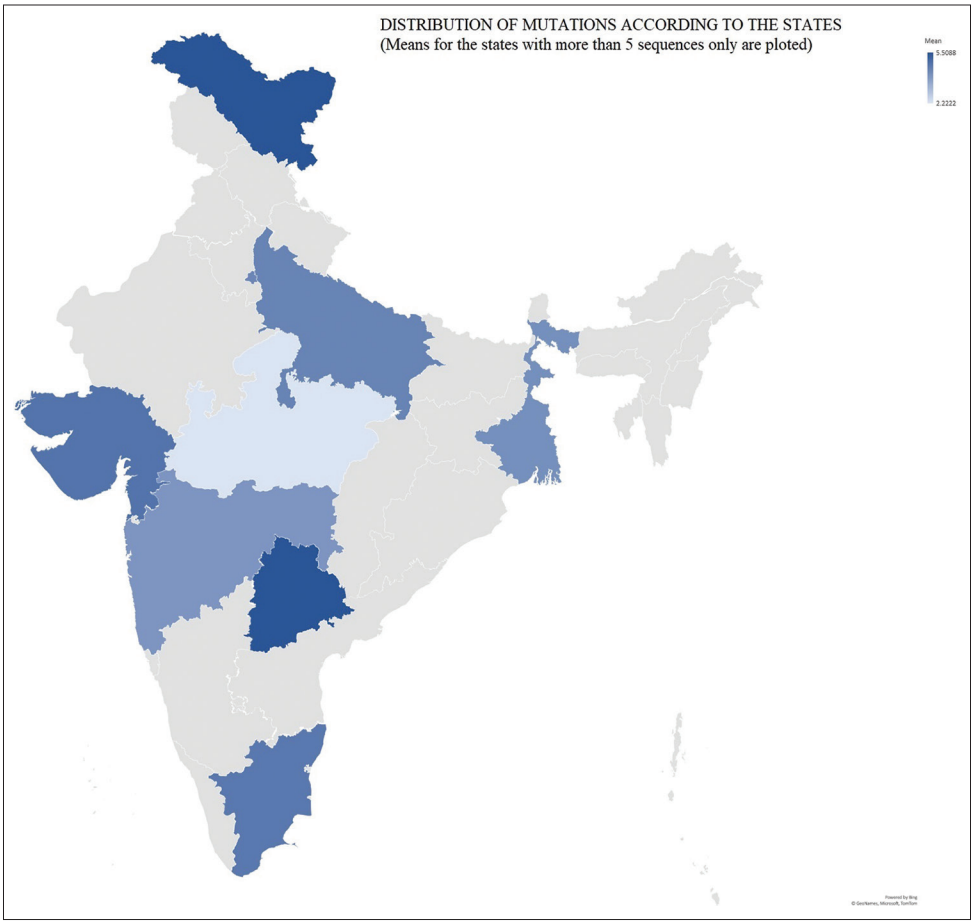

Figure 4: Distribution of severe acute respiratory syndrome coronavirus-2 genomic sequences mutations according to locations (the color density indicates means of mutation, higher the density high means of mutations, states with more than 5 genomic sequences only are plotted on the map)

Table 1: Location-wise clade distribution of severe acute respiratory syndrome coronavirus-2 genomes

States	*n*	Clade					
		G	GH	GR	Other	S	V
Andhra Pradesh	1	0	0	0	1	0	0
Assam	1	0	0	0	1	0	0
Bihar	2	0	0	0	2	0	0
Delhi	35	10	0	3	18	2	2
Gujarat	128	56	55	2	12	3	0
Jammu	1	0	0	0	1	0	0
Karnataka	3	0	0	2	1	0	0
Kerala	2	0	0	0	1	1	0
Ladakh	6	0	0	0	6	0	0
Madhya Pradesh	9	5	1	0	3	0	0
Maharashtra	8	2	0	0	5	1	0
Odisha	1	0	0	0	1	0	0
Punjab	1	1	0	0	0	0	0
Tamil Nadu	15	0	0	1	14	0	0
Telangana	59	2	0	1	56	0	0
Uttar Pradesh	5	1	0	1	3	0	0
West Bengal	8	3	0	2	3	0	0
Unknown*	7	7	0	0	0	0	0
Indian citizen sampled at Iran	14	2	0	3	9	0	0
Italian tourist	5	4	0	0	1	0	0
Indian contacts of Italian tourist	1	1	0	0	0	0	0
Indian contacts of Indian patient having travel history to Italy	4	1	0	0	3	0	0
Total	317	95 (29.97)	56 (17.67)	15 (4.73)	142 (44.79)	7 (2.21)	2 (0.63)

*Location of the sequences was not available. GR: (D614G mutation in spike glycoprotein and G204R mutation in nucleocapsid protein, GH: D614G mutation in the spike glycoprotein and Q57H mutation in ns3

State-wise analysis

Maximum sequences were available from Gujarat (n = 128), followed by Telangana (n = 59) and Delhi (n = 35). Sequences of Indian contact of Indian patients having travel history to Italy (n = 4), Indian citizens tested at Iran (n = 14), Italian tourists (n = 5), and Indian contact of Italian tourists (n = 1) were also analyzed [Figure 4 and Table 1].

Among 317 sequences studied, 1495 amino acid mutations were identified (95% confidence interval; mean = 4.7161, standard deviation = 1.823, median = 5, and mode = 4); Telangana shows a high number of mutations in comparison to the rest of India (mean = 5.508, median = 5, and mode = 5); the difference in frequency of mutation among Telangana and the rest of India was statistically significant (two-tailed Fisher's exact test, P = 0.023).

Out of 317 sequences, 95 sequences were of clade "G" and 56 of "GH" clade. Fifty-five out of 56 clade "GH" were from only Gujarat [Table 1, two-tailed Fisher's exact test, P = 0.000001].

Spike protein mutation

SARS-CoV-2 clade with glycine (G) instead of aspartic acid (D) at the residue 614 in spike glycoprotein is identified as clade "G."[23] S1 subunit of the spike protein that contains the receptor-binding domain shows D614G mutation in 166 sequences. 88.28% (113 out of 128) genomic sequences submitted from Gujarat show the D614G mutation, while genomic sequences from the rest of India show D614G mutation in 28.19% (53 out of 189) of cases. The difference in the spike protein D624G mutation frequency between Gujarat and the rest of India is statistically significant ($P < 0.00001$, two-tailed Fisher's exact test).

Fifty-six sequences show Q57H mutation (glutamine replaced by histidine at the 57th position) in ns3 (orf3 protein) along with D614G mutation of spike protein. Fifteen sequences show G204R mutation (glycine replaced by arginine at the 204th position) in nucleocapsid protein along with D614G mutation of spike protein.

Nonstructural protein 2 mutation

Nineteen sequences show the replacement of valine (V) by isoleucine (I) at the 198th position (V198I mutation) of nsp2. Nine out of 19 sequences were from the Indian citizens sampled at Iran, three were from the Indian contact of Indian patients having travel history to Italy, one was in Italian tourist, and six were from the Ladakh. Seventeen sequences show the replacement of arginine by cysteine at the 27th position of nsp2. Arginine replaced cysteine at the 27th position of nsp2 in 17 sequences; this mutation evolves with the V198I mutation of nsp2.

Nonstructural protein 3 mutation

Lysine (K) instead of threonine (T) at the residue 1198 (T1198K mutation) was found in 121 genomic sequences. 93.22% (55 out of 59) genomic sequences submitted from Telangana show T1198K mutation, while genomic sequences from the rest of India show T1198K mutation in 25.58% (66 out 258) genomic sequences. The difference in the frequency of T1198K mutation between Telangana and the rest of India is statistically significant ($P < 0.05$, two-tailed Fisher's exact test).

Nonstructural protein 6 mutation

L37F mutation (leucine replaced by phenylalanine at the residue 37) was found in 141 genomic sequences. 93.22% (55 out of 59) genomic sequences submitted from Telangana show L37F mutation, while genomic sequences from the rest of India show L37F mutation in 33.33% (86 out 258) genomic sequences. The difference in the frequency of L37F mutation between Telangana and the rest of India is statistically significant ($P = 0.00001$, two-tailed Fisher's exact test).

Nonstructural protein 12 mutation

Total 363 amino acid mutations of 23 types were seen in nsp12 in the studied 317 genome sequences. One or more mutation of nsp12 was found in 296 out of 317 sequences; proline replaced by leucine at the residue 323 (P323 L mutation) being most frequent was present in 167 sequences. Valine replacing alanine at the residue 97 (A97V mutation) was present in 126 sequences. 87.5% (112 out of 128) genomic sequences submitted from Gujarat show the P323 L mutation, while genomic sequences from the rest of India show P323 L mutation in 29.10% (55 out of 189) sequences. The difference in the frequency of P323 L mutation between Gujarat and the rest of India is statistically significant ($P < 0.05$, two-tailed Fisher's exact test).

Both P323 L mutation of nsp12 and D614G mutation of spike glycoprotein were present in 164 sequences, which indicates that P323 L mutation evolves with the D614G mutation.

Nucleocapsid protein mutation

Forty types of 212 mutations in nucleocapsid protein were found in 317 studied sequences. Proline (P) replaced leucine (L) at the residue 13 (P13 L mutation) of nucleocapsid protein in 118 sequences. Figure 5 shows the part of nucleocapsid protein sequence showing P13 L mutation. Fifty-seven out of 59 sequences of Telangana show the P13 L mutation in nucleocapsid protein. One hundred and nine sequences show both T1198K mutation in nsp3 and P13 L mutation in nucleocapsid protein.

Forty sequences show the replacement of leucine (L) by serine (S) at residue 194 in the nucleocapsid protein; 34 out of which were present from Gujarat.

Discussion

In the presented study, 364 sequences were studied for phylogenetic analysis; 317 sequences after deducting sequences with more than 1% nucleotide were considered for mutation analysis.

Replacement of aspartic acid (D) with the glycine (G) at the residue 614 in spike glycoprotein determines the clade "G" of the SARS-CoV-2 [Figure 6].[23,24]

Mutation of nsp12 at residue 323 (P to L) was seen in 164 sequences along with the D614G mutation of spike glycoprotein, which indicates that a P323 L mutation of nsp12 evolves with the D614G mutation of the spike glycoprotein. Previous studies have proved linkage disequilibrium between these two mutations in different populations.[24,25]

In the presented study, 88.28% (113 out of 128) genomic sequences of Gujarat show D614G mutation in the S glycoprotein at the RBD, S1 subunit, that is significantly high than the rest of India. The high number of clade "GH" in Gujarat indicates progressed mutation in Gujarat,

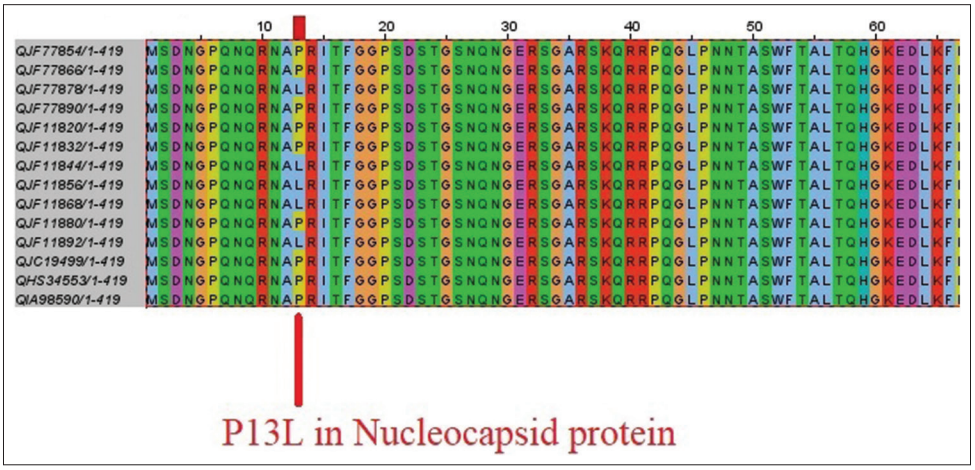

Figure 5: Nucleocapsid protein sequence alignment showing proline replaced by leucine at the 13th position

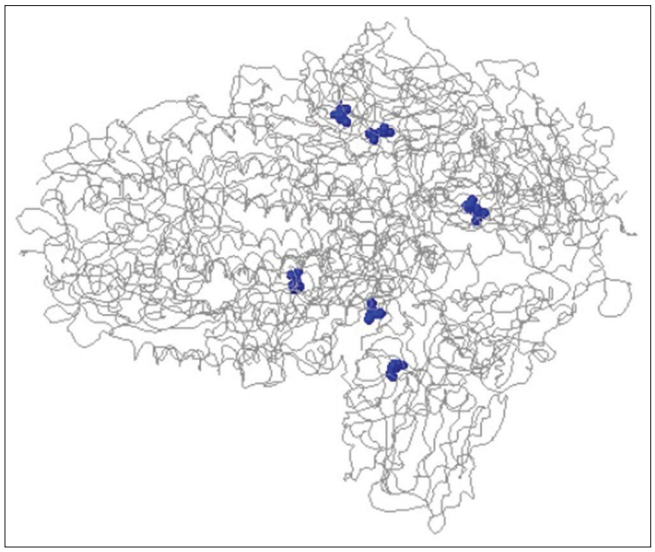

Figure 6: Receptor binding domain of spike glycoprotein of clade GH (D614G mutation in spike glycoprotein and glutamine replaced by histidine at the 57th position [Q57H mutation] in ns3). Blue dot indicates the affected receptor-binding area by the mutation

and it is noticeable that Gujarat has a 6.15% death rate (1007 out of 16356) in the SARS-CoV-2-confirmed cases that are higher than the death rate of the rest of India (2.84%, 5185 out of 182275) as per 9.52 A. M. on May 31, 2020.[22]

S glycoprotein plays an important role in viral entry and pathogenicity of coronavirus. S glycoprotein of the SARS-CoV-2 contains S1 and S2 subunits.[19] S1 subunit is responsible for receptor binding and the S2 subunit allows membrane fusion with the host cell. S1 domain contains RBDs.[24] B-cell epitope is present at the 614 positions of the S1 subunit; D614G mutation affects the conformation of the immunological determinant (amino acids 613-621) that may cause failure to act as a B-cell epitope in SARS-CoV-2.[24] B-cell has an important role in adaptive immunity in virus infection by identifying the antigen. Elimination of B-cell epitope in D614G mutation of the spike glycoprotein reduces immunogenicity and may allow recurrent SARS-CoV-2 infection.[24] It shows that SARS-CoV-2 strain with D614G mutation at the S1 subunit of glycoprotein may have higher mortality than the other clades.

L37F mutation in nsp6 was found in 53.20% (141 out of 317) genomic sequences. nsp6 being a transmembrane protein forms a double-membrane vesicle along with nsp3 and nsp4 protein. Although the 37th residue of nsp6 is a part of the unstructured coil segment, Phe residue at the position in L37F mutants can perform cation–n interaction which may affect the protein–protein interaction.[26]

Twenty-three types of 318 amino acid mutations were seen in nsp12 of the SARS-CoV-2, out of which 126 sequences show the replacement of valine amino acid at residue at 97 with alanine in nsp12. The nsp12 plays an important role in transcription and translation of the viral genome. The nsp12 is the target of choice for RNA-dependent RNA polymerase inhibitors including undertrial drug remdesivir. Nucleoside analog inhibitor (e.g., remdesivir) acts on RNA-dependent RNA polymerase (RdRp); RNA-dependent RNA polymerase (RdRp) of SARS-CoV-2 consists of nsp12 (catalytic subunit) and two accessory subunits (nsp8 and nsp7).[27,28] Mutations in nsp12 and exonuclease site nsp14 are of concern in India as mutations in the nsp12 have been found responsible for resistance to RNA-dependent RNA polymerase inhibitors in other viruses.[29,30]

D614G mutation of spike glycoprotein has shown relation with the P323 L mutation of nsp12; combination of the mutation may affect the response of vaccine and drugs also.

In this study, we found 212 mutations in nucleocapsid protein that is an important site of T-cell epitope.[31] P13 L residue in nucleocapsid protein was the most frequent (118 out of 317 sequences) in this study.

Mutation of the orf3 protein was found more frequently in Gujarat than the rest of India. orf3a along with orf1a, orf1b, and orf10 can dissociate the iron from the porphyrin by attacking the heme on hemoglobin 1-beta chain, leading to reduced hemoglobin to carry oxygen.[32] As mutation of orf3 can affect the virulence and pathogenicity of the SARS-CoV-2 infection, high frequency of mutation of the residue Q57H along with D614G mutation of spike glycoprotein (that determines clade GH) in Gujarat may be one of the factors for high mortality in Gujarat. Although clade "GH" is restricted in Gujarat, after lockdown is relaxed, huge migration has been happened in May; the clade "GH" may spread to other parts of India also. That should be an important concern to combat the mortality and morbidity of SARS-CoV-2 infection.

The study shows that the mutations have been increasing with the spread of infection. Mutations and clades show differences among states. Borders of states are opened after the lockdown is withdrawn that may mix up the different clades in various states. Almost 12 lakh people migrated from Gujarat and 20 lakh people migrated from Maharashtra; such a large migration may spread mutations of Gujarat and Maharashtra other less affected areas.

Limitations

Not enough number of sequences are available from less affected states (e.g. Kerala) that might have helped to identify the correlations of mutation in wider bases; we did not have status data of all patients in the study so could not correlate mutations with actual effect on morbidity and mortality.

Conclusion

SARS-CoV-2 mutations may progress and spread in less affected areas of India after the lockdown is withdrawn. As the mutations are crucial for response of SARS-CoV-2 to the various drugs and vaccines under clinical trials, it is recommended to identify the efficacy of various drugs according to the different mutations and clades of the virus.

Financial support and sponsorship

Nil.

Conflicts of interest

There are no conflicts of interest.

References

1. Hui DS, Azhar E, Madani TA, Ntoumi F, Kock R, Dar O, *et al.* The continuing 2019-nCoV epidemic threat of novel coronaviruses to global health – The latest 2019 novel coronavirus outbreak in Wuhan, China. Int J Infect Dis 2020;91:264-6.
2. Rubino S, Kelvin N, Bermejo-Martin JF, Kelvin D. As COVID-19 cases, deaths and fatality rates surge in Italy, underlying causes require investigation. J Infect Dev Ctries 2020;14:265-7.
3. Coronavirus Disease (Covid-19) Situation Report-134, World Health Organization. https://www.who.int/docs/default-source/coronaviruse/situation-reports/20200602-covid-19-sitrep-134.pdf. [Last accessed on 2020 Jun 4].
4. Yan Y, Shin WI, Pang YX, Meng Y, Lai J, You C, *et al*. The first 75 days of novel coronavirus (SARS-CoV-2) outbreak: Recent advances, prevention, and treatment. Int J Environ Res Public Health 2020;17:2323.
5. Zhou P, Yang XL, Wang XG, Hu B, Zhang L, Zhang W, *et al*. A pneumonia outbreak associated with a new coronavirus of probable bat origin. Nature 2020;579:270-3.
6. Song Z, Xu Y, Bao L, Zhang L, Yu P, Qu Y, *et al.* From SARS to MERS, thrusting coronaviruses into the spotlight. Viruses 2019;11:59.
7. Wu A, Peng Y, Huang B, Ding X, Wang X, Niu P, *et al.* Genome composition and divergence of the novel coronavirus (2019-nCoV) originating in China. Cell Host Microbe 2020;27:325-8.
8. Mousavizadeh L, Ghasemi S. Genotype and phenotype of COVID-19: Their roles in pathogenesis. J Microbiol Immunol Infect 2021;54:159-63.
9. Ye ZW, Yuan S, Yuen KS, Fung SY, Chan CP, Jin DY. Zoonotic origins of human coronaviruses. Int J Biol Sci 2020;16:1686-97.
10. Wu Y, Li C, Xia S, Tian X, Kong Y, Wang Z, *et al.* Identification of human single-domain antibodies against SARS-CoV-2. Cell Host Microbe 2020;27:891-8.e5.
11. Tai W, He L, Zhang X, Pu J, Voronin D, Jiang S, *et al.* Characterization of the receptor-binding domain (RBD) of 2019 novel coronavirus: Implication for development of RBD protein as a viral attachment inhibitor and vaccine. Cell Mol Immunol 2020;17:613-20.
12. Huang JT, Ran RX, Lv ZH, Feng LN, Ran CY, Tong YQ, *et al.* Chronological changes of viral shedding in adult inpatients with COVID-19 in Wuhan, China. Clin Infect Dis 2020;71:2158-66.
13. Khan T, Agnihotri K, Tripathi A, Mukherjee S, Agnihotri N, Gupta G. COVID-19: A worldwide, zoonotic, pandemic outbreak. Altern Ther Health Med 2020;26:56-64.
14. Hu B, Qiu J, Chen H, Tao V, Wang J, Lin H. First, second and potential third generation spreads of the COVID-19 epidemic in mainland China: An early exploratory study incorporating location-based service data of mobile devices. Int J Infect Dis 2020;96:489-95.
15. Lin L, Lu L, Cao W, Li T. Hypothesis for potential pathogenesis of SARS-CoV-2 infection – A review of immune changes in patients with viral pneumonia. Emerg Microbes Infect 2020;9:727-32.
16. Wei XS, Wang X, Niu YR, Ye LL, Peng WB, Wang ZH, *et al.* Diarrhoea is associated with prolonged symptoms and viral carriage in corona virus disease 2019. Clin Gastroenterol Hepatol 2020;18:1753-9.e2.
17. Full Genome Tree Derived from All Outbreak Sequences 2020-06-02, Global Initiative on Sharing All Influenza Data GISAID EpiFlu Database. https://www.epicov.org/epi3/appentities/entities/corona2020/full_genome_tree_derived_from_all_outbreak_sequences.png. [Last accessed on 2020 Jun 8].
18. Li YC, Bai WZ, Hashikawa T. The neuroinvasive potential of SARS-CoV2 may play a role in the respiratory failure of COVID-19 patients. J Med Virol 2020;92:552-5.
19. Tamura K, Nei M. Estimation of the number of nucleotide substitutions in the control region of mitochondrial DNA in humans and chimpanzees. Mol Biol Evol 1993;10:512-26.
20. Kumar S, Stecher G, Li M, Knyaz C, Tamura K. MEGA X: Molecular evolutionary genetics analysis across computing platforms. Mol Biol Evol 2018;35:1547-9.
21. Madeira F, Park YM, Lee J, Buso N, Gur T, Madhusoodanan N, *et al.* He EMBL-EBI search and sequence analysis tools APIs in 2019. Nucleic Acids Res 2019;47:W636-41.
22. Coronavirus Outbreak Update Dashboard in India. Available from: https://www.covid19india.org/. [Last accessed on 2020 May 31, 9:52 A.M.].
23. Bartolini B, Rueca M, Gruber CE, Messina F, Carletti F, Giombini E, *et al.* SARS-CoV-2 phylogenetic analysis, Lazio Region, Italy, February-March 2020. Emerg Infect Dis 2020;26:1842-1845. [Doi: 10.3201/eid2608.201525].
24. Kim SJ, Nguyen VG, Park YH, Park BK, Chung HC. A novel synonymous mutation of SARS-CoV-2: Is this possible to affect their antigenicity and immunogenicity? Vaccines (Basel) 2020;8:220.
25. Veeramachaneni GK, Thunuguntla VB, Bobbillapati J, Bondili JS. Structural and simulation analysis of hotspot residues interactions of SARS-CoV 2 with human ACE2 receptor. J Biomol Struct Dyn 2021;39:4015-25.
26. Cárdenas-Conejo Y, Liñan-Rico A, García-Rodríguez DA, Centeno-Leija S, Serrano-Posada H. An exclusive 42 amino acid signature in pp1ab protein provides insights into the evolutive history of the 2019 novel human-pathogenic coronavirus (SARS-CoV-2). J Med Virol 2020;92(6):688-692. [Doi: 10.1002/jmv. 25758].
27. Hillen HS, Kokic G, Farnung L, Dienemann C, Tegunov D, Cramer P. Structure of replicating SARS-CoV-2 polymerase. Nature 2020;584:154-6.
28. Ahn DG, Choi JK, Taylor DR, Oh JW. Biochemical characterization of a recombinant SARS coronavirus nsp12 RNA-dependent RNA polymerase capable of copying viral RNA templates. Arch Virol 2012;157:2095-104.
29. Shannon A, Le NT, Selisko B, Eydoux C, Alvarez K, Guillemot JC, *et al.* Remdesivir and SARS-CoV-2: Structural requirements at both nsp12 RdRp and nsp14 exonuclease active-sites. Antiviral Res 2020;178:104793.
30. Jorgensen SC, Kebriaei R, Dresser LD. Remdesivir: Review of pharmacology, pre-clinical data, and emerging clinical experience for COVID-19. Pharmacotherapy 2020;40:659-71.
31. Ahmed SF, Quadeer AA, McKay MR. Preliminary identification of potential vaccine targets for the COVID-19 coronavirus (SARS-CoV-2) based on SARS-CoV immunological studies. Viruses 2020;12:254.
32. Ahmadpour D, Ahmadpoor P. How the COVID-19 overcomes the battle? An approach to virus structure. Iran J Kidney Dis 2020;14:167-72.

Original Article

Level of Variations of the Aortic Bifurcation and Distance Measurements between the Aortic Bifurcation and the Common Iliac Bifurcations

Arzu Ekingen, Mehmet Güli Çetinçakmak[1]

Vocational High School of Health Services, Batman University, Batman, [1]Associate Professor, MD, Department of Radiology, Medical School, Dicle University, Diyarbakir, Turkey

Abstract

Introduction: The purpose of the present study was to investigate the vertebral levels of the aortic bifurcation (AB) in patients with and without the abdominal aorta (AA) deviation and to measure the distances between the AB and the right-left common iliac bifurcations (CIBs) which are crucial anatomical information, especially for anterior lumbar interbody fusion surgery. Additionally, we made comparisons levels of the AB according to sex and examined whether the results were statistically significant, which we could not find other studies comparing gender in literature. **Material and Methods:** The images of 721 patients, undergoing angiography with multidetector computed tomography between January 2016 and October 2019, were reviewed retrospectively. The AB levels of the patients with and without the AA deviation were classified and evaluated separately. It was measured the distances between the level of the AB and the right and left CIBs with the 3-dimensional ruler technique in only 207 of 721 patients. **Results:** It was detected seven different vertebral levels of the AB among patients (116 patients) with the AA deviation, in which is the highest L4-upper (27.59%), and 11 different vertebral levels of the AB among patients (605 patients) without the AA deviation, in which is the highest L4-upper (22.48%). When comparing cases with and without AA deviation, a statistically significant difference was found between the sexes ($P < 0.05$). **Discussion and Conclusion:** The presented study demonstrates that there is a significant relationship between the genders at some levels. The preoperative information of the morphological variations of the AB may be very useful for laparoscopic, invasive procedures, and spinal surgery procedures. At the same time, these variation information reveals new information for anatomy.

Keywords: *Abdominal aorta, anatomic variation, aortic bifurcation, common iliac artery, lumbar vertebrae, multidetector computed tomography*

Introduction

The abdominal aorta (AA) is the part of the aorta in the abdomen, the largest artery in the abdomen. The thoracic aorta, which is a part of the aorta in the thorax, takes the name AA after passing in the diaphragm at the level of the 12th thoracic vertebra. As described generally in anatomy books, the AA ends with a bifurcation, which is called aortic bifurcation (AB), at the slightly left side of the midline on the body of L4 and divides into the right and left common iliac arteries (CIAs) which are approximately 5 cm. Each common iliac artery runs toward in the pelvis, then divides into the external iliac and internal iliac arteries on both sides at the anteromedial of the sacroiliac joint. This point where it splits into two is the common iliac bifurcation (CIB).[1-4] Although the AB level and the CIAs are described as described above, various studies have shown that there may be various level variations related to the AB.[5,6]

The AB and CIAs anatomy is very important for anterior lumbar interbody fusion surgery, which is generally preferred for spinal problems such as segmental lordosis, spondylolisthesis, foraminal stenosis, spinal trauma, and scoliosis. In addition, knowledge of the variations of these structures is useful for invasive procedures such as laparoscopic lumbar discectomy, lumbosacral total disc arthroplasty and some cardiovascular diseases such as abdominal aortic aneurysm, aortic stenosis, calcified atherosclerosis of the bifurcation region.[7-14] Furthermore, the anatomy of the AB and the CIB are very crucial for kissing stent reconstruction which is used for aortoiliac disease and external beam radiotherapy which is preferred

How to cite this article: Ekingen A, Çetinçakmak MG. Level of variations of the aortic bifurcation and distance measurements between the aortic bifurcation and the common iliac bifurcations. J Anat Soc India 2022;71:11-7.

Article Info

Received: 10 March 2021
Accepted: 31 October 2021
Available online: 17 March 2022

Address for correspondence:
Dr. Arzu Ekingen, Vocational School of Health Services, Batman University, Batman, Turkey.
E-mail: arzumumcu55@gmail.com

Access this article online

Website: www.jasi.org.in
DOI: 10.4103/jasi.jasi_53_21
Quick Response Code:

in the treatment of carcinoma of the cervix.[14-18] critical complications like vascular injuries can happen in diagnosis and treatment interventions involving the AB and lumbar region. Retroperitoneal major blood vessel injury may cause hypovolemic shock, this can result in shock-related deaths or serious illness. Anatomical information of the AB and the CIB on both sides may reduce the risk of these complications.[19-21]

Advances in radiology such as digital subtraction angiography, magnetic resonance imaging (MRI), and later developed multidetector computed tomography (MDCT) angiography have enabled more reliable images of vascular structures. Especially, the images obtained with the MDCT technique can convert into 3-dimensional (3D) volumetric images and so on it can be make a clearer interpretation of the anatomical structures.[22-27] Variations related to the localization of the AB were mostly investigated by associating lumbar vertebrae and various techniques such as cadaver dissection, pelvic angiography, and computed tomography (CT) were used in these studies.[22] However, the AB and the CIB studies that used MDCT are very few.

Aims and objectives

In this study, we aimed to determine the vertebral levels of the origin of the AB among patients with AA deviation and without AA deviation and to measure the distance between the AB and the bifurcations of the CIAs via MDCT angiography.

Material and Methods

This study was approved by the Dicle University Medical School Noninterventional Clinical Research Ethics Committee (Meeting date, November 14, 2019; Decision no, 52).

In our study, a total of the image records of 721 patients, undergoing angiography with MDCT between 2017 and 2019 at the Department of Radiology of the Dicle University and range 18–85 years, were included in the study. All patients with AA aneurysms, spinal anomalies, and undergoing major abdominal surgery and having poor image quality were excluded. Our study population comprised 339 women and 382 men, the median age of the patients was 49.2 years old.

The MDCT angiography was performed using 64-detector computed tomography (CT) (Brilliance CT System, Philips Medical Systems, Cleveland, OH, USA). Approximately 75-120 mL of nonionic contrast material was injected through a superficial vein located in the forearm region of patients with the supine position at a rate of 3–4 mL/s using an automatic power injector and shooting process started with a delay of 28 s after the start of the injection. Applied CT parameters: Slice collimation, 0.5 mm; gantry rotation, 0.34 s; section thickness, 0.9 mm; tube current, 200–250 mAs; the tube potential, 120 kV. Images obtained in the arterial phase after angiography were sent to a separate workstation (Philips Medical Systems, Philips Extended Brilliance Workspace, Best, The Netherlands). In this workstation, 3D volumetric images were created using the volume rendering (VR) technique. All determinations and measurements of the present study were made on these 3D images obtained.

For determining the level of the AB, 3D images of patients were divided into two groups: patients with AA deviation and patients without AA deviation. Then, the central point of the AB was defined for each case in both groups and the vertebra level matching this central point was determined. To determine the level of the spine where the AB is located, 4 planes including the lumbar vertebrae and intervertebral disc structure were determined: Upper (above the level of the pedicle vertebra), middle (at the level of pedicle vertebra), lower (below level of the pedicle vertebra) and disc level (located at the level of the intervertebral disc) [Figure 1a]. In the images, the plane corresponding to the AB was accepted as the vertebral level of the AB.

For the distance measurements, we were able to evaluate the AB and the bifurcations of the CIAs together in only 207 patients because most of the right-left CIB were out of 3D images and poor image clarity which affects the precise measurement. Firstly, we marked separately the centers of the AB and the bifurcations of the right-left CIAs, second, we measured the distances between the level of the AB and the right and left CIB via the 3D ruler technique [Figure 1b].

Statistical analysis

The obtained data from the radiological images were transferred to the computer environment and all statistical analyzes were performed using the SPSS (IBM SPSS Statistics for Windows, Version 21.0. Armonk, New York, USA). The summary of the data was expressed as mean ± standard deviation, percentage, and frequency. The Independent-Samples *t*-test and Chi-square test were used to compare between the groups according to gender. *P* values with $P < 0.05$ were accepted statistically significant.

Results

The comparison of patients with the AA deviation and without the AA deviation by gender is given in Table 1. The prevalence of women with the AA deviation (58.62%) is higher than men with the AA deviation (41.38%),

Table 1: Comparison of the patients with AA deviation and without abdominal aorta deviation

	Female	Male	Total	χ^2	*P*
With AA deviation	68	48	116	7.471	0.006*
Without AA deviation	271	334	605		
Total, *n* (%)	339 (47)	382 (53)	721 (100)		

*$P<0.05$. AA: Abdominal aorta

whereas the percentage of men without the AA deviation (55.20%) is higher than women without the AA deviation (44.80%). These results are statistically significant ($P < 0.05$) [Table 1].

Considering the results of the AB levels among patients without the AA deviation in Figure 2 and Table 2, the total prevalence of the AB located in above and middle levels of the L3 in women (3.32%) was higher than the total AB prevalence located at the same levels in men (1.80%). The AB prevalence located at the L3 lower (8.86%), the L3-L4 disc levels (24.72%), L4 middle (21.03%) were higher in females. However, the AB prevalence located at the L4 upper (24.25%), L4 lower (17.07%), and L4-L5 disc levels (14.97%) were higher in males. A total percentage of the AB located in the L5 upper and middle levels were higher in women (2.21%) than men (1.80%). When the data were evaluated statistically in this way, a significant difference was found between the genders ($P < 0.05$) [Table 2]. It was found that the L2-L3 intervertebral disc level which was the highest AB level we found, was (0.50%) in 3 of the patients without the AA deviation in total [Figure 3]. However, the highest AB level of patients with the deviation AA was the L3 lower level (2.59%) [Figure 4]. The most common levels of the AB for both patient groups without the AA deviation and with the AA deviation were the L4 upper levels as 22.48% and 27.59%, respectively [Figure 5a and b].

The AB locating at the L5 middle level, lowest vertebral level detected in this study, was (0.50%) in three patients without AA deviation. The AB locating at the L5 upper level, lowest vertebral level detected in patient without AA deviation for this study, was 4 (3.45%) [Figure 6a and b].

In the disc levels, the L3-L4 disc level was observed as 19.67% in the patients without the AA deviation and 9.48% in the cases with the AA deviation [Figure 7a and b]. The L4-L5 disc level was observed as 11.40% in the patients without the AA deviation and 17.24% in the cases with the AA deviation [Figure 8a and b].

When the comparison is made between men and women in the patients with the AA deviation, no significant difference was found between the genders ($P > 0.05$) [Figure 9 and Table 3].

In the distance measurements between the bifurcations of the CIAs and the AA, we founded that the mean value was 57.82 mm in females, 61.09 mm in males on the right side and was 60.41 mm in females, 63.79 mm

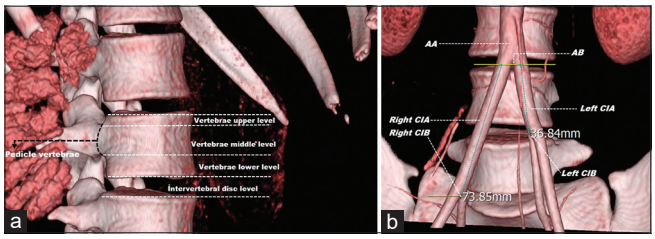

Figure 1: (a) The four planes including the lumbar vertebrae and intervertebral disc to determine levels of the aortic bifurcation; (b) The distance measurements between the aortic bifurcation and the bifurcations of the right-left common iliac artery by the 3-dimensional ruler technique; Abdominal aorta; Aortic bifurcation; common iliac artery; common iliac bifurcation

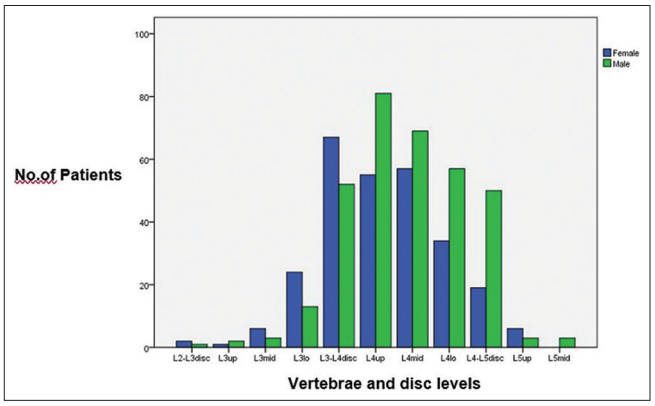

Figure 2: Distribution of the aortic bifurcation levels by gender in patients without the abdominal aorta deviation

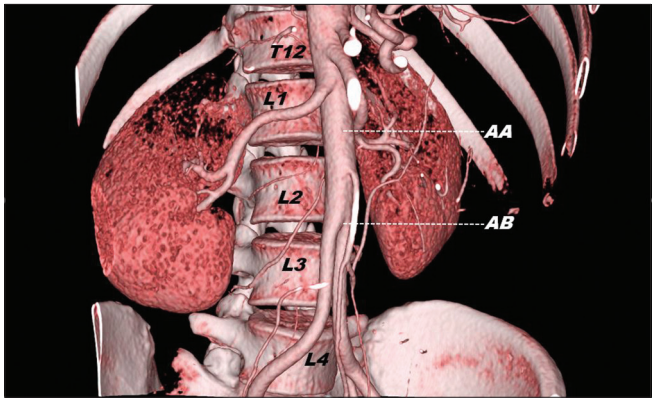

Figure 3: The aortic bifurcation locating at the L2-L3 intervertebral disc level of a patient without abdominal aorta deviation (38 years, male); Abdominal aorta; Aortic bifurcation

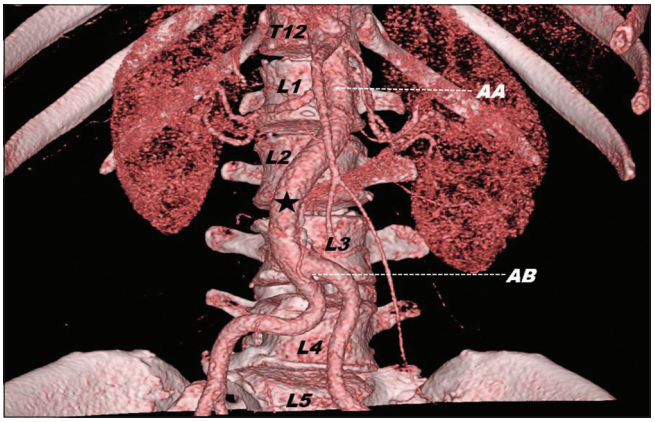

Figure 4: The aortic bifurcation was locating at the L3 lower level of a patient with the abdominal aorta deviation (53 years, female), the abdominal aorta shows deviation to the right at the L2-L3 level (star); Abdominal aorta; Aortic bifurcation

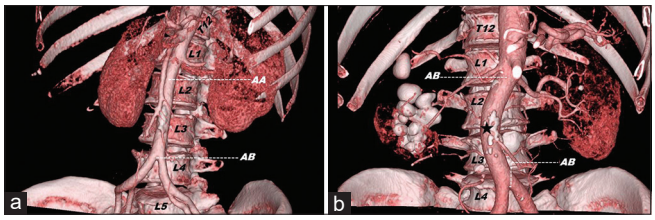

Figure 5: (a) The aortic bifurcation locating at the L4 upper level of a patient without abdominal aorta deviation (49 years, female); (b) The aortic bifurcation locating at the L4 upper level of a patient with abdominal aorta deviation, the abdominal aorta shows deviation to the right at the L2-L3 level (star), (63 years, male); Abdominal aorta; Aortic bifurcation

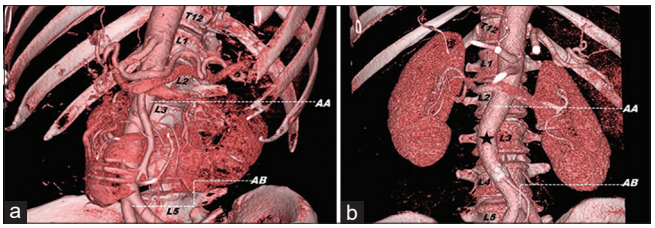

Figure 6: (a) The aortic bifurcation locating at the L5 middle level of a patient without abdominal aorta deviation (75 years, male); (b) The aortic bifurcation locating at the L5 upper level of a patient with abdominal aorta deviation, the abdominal aorta shows deviation to the right at the L3 level (star) (68 years, female); Abdominal aorta; Aortic bifurcation

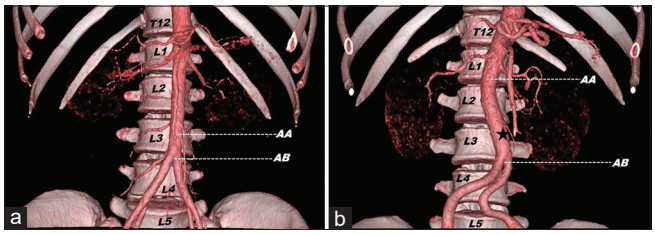

Figure 7: (a) The aortic bifurcation was locating at the L3-L4 intervertebral disc level of a patient without the abdominal aorta deviation (32 years, female); (b) The aortic bifurcation was locating at the L3-L4 intervertebral disc level in a patient with the abdominal aorta deviation which shows deviation to the left at the L3 level (star) (43 years, female); Abdominal aorta; Aortic bifurcation

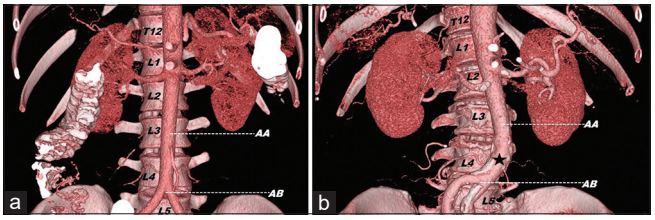

Figure 8: (a) The aortic bifurcation was locating at the L4-L5 intervertebral disc level of a patient without the abdominal aorta deviation (38 years, male); (b) The aortic bifurcation was locating at the L4-L5 intervertebral disc level in a patient with the abdominal aorta deviation which shows deviation to the right at the L4 level (star) (61 years, female); Abdominal aorta; Aortic bifurcation

Table 2: The levels of the aortic bifurcation in patients without abdominal aorta deviation

AB Levels	Sex		Total, *n* (%)	χ^2	*P*
	Female, *n* (%)	Male, *n* (%)			
L2-L3 disc	2 (0.74)	1 (0.30)	3 (0.50)	25.330*	0.001**
L3 upper	1 (0.37)	2 (0.60)	3 (0.50)		
L3 middle	6 (2.21)	3 (0.90)	9 (1.49)		
L3 lower	24 (8.86)	13 (3.89)	37 (6.12)		
L3-L4 disc	67 (24.72)	52 (15.57)	119 (19.67)		
L4 upper	55 (20.30)	81 (24.25)	136 (22.48)		
L4 middle	57 (21.03)	69 (20.66)	126 (20.83)		
L4 lower	34 (12.55)	57 (17.07)	91 (15.04)		
L4-L5 disc	19 (7.01)	50 (14.97)	69 (11.40)		
L5 upper	6 (2.21)	3 (0.90)	9 (1.49)		
L5 middle	0	3 (0.90)	3 (0.50)		
Total	271 (44.79)	334 (55.21)	605 (100)		

*The Chi-square test was calculated by combining prevalences of the "L2-L3 disk + L3 upper + L3 medium" and "L5 upper + L5 middle" levels separately for both sex in in a separate table, ***P*<0.05. AA: Abdominal aorta, AB: Aortic bifurcation

in males on the left side, these results were statistically insignificant [Table 4].

Discussion

Basic anatomy books describe the level of the AB where the AA is divided into right and left CIAs as the level of the 4th lumbar vertebrae. In the following years, the problems preventing blood flow such as atherosclerosis showed that this region should be examined better, because it may have a variety of variations.[28-30] The difficulties encountered in laparoscopic approaches, especially for the L4-L5 intervertebral disc and the increasing morbidity rates have made more important the anatomy of the prevertebral vascular structures in this region and especially, anatomy of the AB and the CIBs.[8,31,32]

In our study, the total AB rate at the L3 levels was found to be 8.11% (49 cases) in patients without the AA deviation. Huang *et al*. explained a high-positioned bifurcation of the AA at the level of the upper L2 body in one case by CT technique.[33] In our study, the L2-L3 intervertebral disc level in 3 (0.50%) patients without the AA deviation and the L3 lower level in 3 (2.59%) patients with the deviation AA were determined as the closest level to the L2 level. Chithriki *et al*. reported that the AB prevalence corresponding to the L3 levels was determined as 9.30% (41 cases) by MRI.[22]

Ponni *et al.* examined the images of 26 patients with cervical cancer and radiotherapy and said that the division of the AA into CIAs occurred at the level of L3-L4 intervertebral space, the body of L4 vertebra and L4-L5 intervertebral space in 53.84%, 30.76% and 15.40% of the patients, respectively.[15] In our study, these prevalences are as follows; 19.67% (L3-L4 disc level), 58.35% (L4 level), 11.40% (L4-L5 disc level). Lakchayapakorn and Siriprakarn[34] and Deswal *et al*.[8] found the L4 levels as the highest level of the AB in 63% and 64%, respectively. Khamanarong *et al*.[35] explained that the AA bifurcated into the CIAs at the level of the L4 vertebra in 131 cases (70.10%), at L4-L5 intervertebral disc in

23 cases (12.30%), and at the level of the L5 vertebra in 33 cases (17.60%) of 187 cadavers. Pirro *et al.*,[21] Chithriki *et al.*,[22] and our current study also showed that the most common levels of the AB were the L4 vertebrae levels [Table 5]. These studies mentioned above showed that the AB is mostly at L4 levels and the results of the level of the studies with CT and MR techniques are lower than the results of the level determined by the cadaver dissection. The reason for that may be due to the fact that the CT technique is more sensitive and reliable as well as enables research in a wider population. The AB prevalence localized at L5 levels was found as 2.50% in the study of Chithriki *et al.*[22] 1.99% in our study, the lowest level detected in our study was the levels of the L5 vertebrae.

When we compared the intervertebral disc levels of the AB in our study, the AB was the most common at the L3-L4 disc level (19.67%) and the least at the L2-L3 disc level (0.50%), and 11.40% at the L4-L5 disc space in patients without the AA deviation and it was 11 cases (9.48%) at the L3-L4 disc level, 20 cases (17.24%) at the L4-L5 disc level in the cases of the AA deviation. But, Deswal *et al*.[8] said that the rate of the AB was 16% at the L4-L5 intervertebral disc and 4% at the L3-L4 disc space. This difference among these studies may be due to the research method.

The difference of our study from other studies, we evaluated the AB data of patients with the deviation AA and with nondeviation AA separately, made comparisons according to sex, and examined whether the results were statistically significant. We did not find studies evaluating patients having the AB with AA deviation separately. Accordingly, a significant difference was found between patients with AA deviation and without the AA deviation, and between patients without AA deviation when comparing among genders in our study ($P < 0.05$) [Tables 1 and 2]. These meaningful results may be related to the genetic and height of women and men.

Deswal *et al.*[8] said that the mean values of length of the CIAs were 56.49 mm on the right side and 53.75 mm on the left side on 25 cadavers and no statistically significant difference was observed. Panagouli *et al.*[36] found that the mean length of the left CIA was 61.2 mm and that of the right one was 60.3 mm in 76 cadavers. In our study, the general mean of the length of the CIAs was 59.43 mm on the right side and 62.07 mm on the left side which these lengths were longer than the lengths written in classical anatomy texts.

Conclusion

The anatomical knowledge of the levels of the AB and the CIB is particularly beneficial during surgical and laparoscopic procedures which are used for both diagnostic and treatment for diseases such as vertebral, spinal cord and

Table 3: The levels of the aortic bifurcation in patients with abdominal aorta deviation

AB levels	Sex		Total, *n* (%)	χ^2	*P*
	Female, *n* (%)	Male, *n* (%)			
L3 lower	2 (2.94)	1 (2.08)	3 (2.59)	1.122*	0.891**
L3-L4 disc	7 (10.29)	4 (8.33)	11 (9.48)		
L4 upper	20 (29.41)	12 (25.00)	32 (27.59)		
L4 middle	13 (19.12)	9 (18.75)	22 (18.97)		
L4 lower	14 (20.59)	10 (20.83)	24 (20.69)		
L4-L5 disc	11 (16.18)	9 (18.75)	20 (17.24)		
L5 upper	1 (1.47)	3 (6.25)	4 (3.45)		
Total	68 (58.62)	48 (41.38	116 (100)		

*The Chi-square test was calculated by combining prevalences of the "L3 lower + L3-L4 disc" and "L4-L5 disc + L5 upper" levels separately for both sex in in a separate table, **P>0.05. AA: Abdominal aorta, AB: Aortic bifurcation

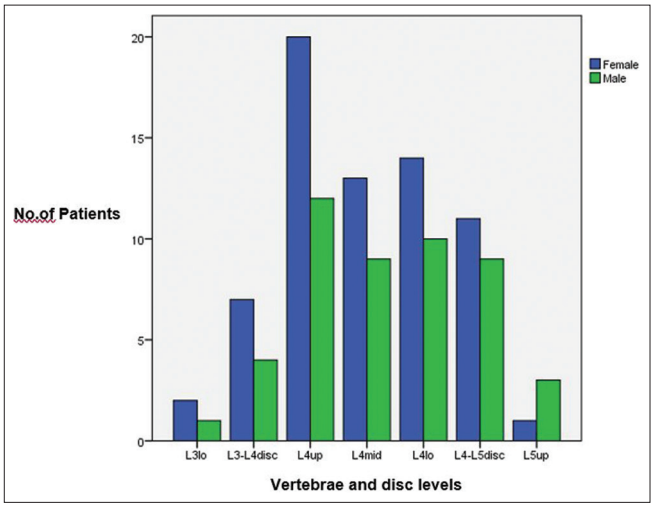

Figure 9: Distribution of the aortic bifurcation levels by gender in patients with the abdominal aorta deviation

Table 4: Measurement distances between the aortic bifurcation and the bifurcations of the right-left common iliac arteries and distribution according to the sex

Distances	Sex	Minimum–maximum (mm)	Mean±SD (mm)	General mean±SD (mm)	*t*	*P*
AB-RCIB	Female (*n*=105)	24.10-93.70	57.82±1.46	59.43±1.69	−1.388	0.167
	Male (*n*=102)	25.20-105.00	61.09±1.89			
AB-LCIB	Female (*n*=105)	24.11-98.30	60.41±1.55	62.07±1.77	−1.379	0.169
	Male (*n*=102)	33.10-120.00	63.79±1.95			

AB: Aortic bifurcation, CIAs: The common iliac arteries, RCIB: Right common iliac bifurcation, LCIB: Left common iliac bifurcation, SD: Standard deviation

Table 5: Comparison of the different studies and the present study related to the aortic bifurcation levels

	Chithriki *et al*.(2002)	Pirró *et al*. (2005)*	Our study
Research year	2002	2005	2020
Research method	MRI	Cadaver dissection	MDCT
AB levels, *n* (%)			
L2-L3 disc	0	0	3 (0.50)
L3 upper	4 (0.90)	1 (2.0)	3 (0.50)
L3 middle	6 (1.40)		9 (1.49)
L3 lower	31 (7.0)		37 (6.12)
L3-L4 disc	59 (13.40)		119 (19.67)
L4 upper	84 (19.10)	21 (50.0)	136 (22.48)
L4 middle	106 (24.0)		126 (20.83)
L4 lower	105 (23.80)		91 (15.04)
L4-L5 disc	34 (7.70)	3 (7.0)	69 (11.40)
L5 upper	7 (1.60)	16 (39.0)	9 (1.49)
L5 middle	4 (0.90)		3 (0.50)
L5 lower	0		0
L5-S1 disc	0	0	0
L5/transitional segment	1 (0.90)	0	0
S1	0	1 (2.0)	0
Total	441	42	605

*Pirró *et al*. noted disc levels and vertebral body levels without separating as upper, middle and lower. AB: Aortic bifurcation, MDCT: Multidedector computed tomography, MRI: Magnetic resonance imaging

disc problems, aortic-iliac atherosclerosis, aortic aneurysm. Knowing the AB levels before these procedures makes a great contribution both to prevent unwanted injuries during surgery and to prevent various complications after surgery.

Financial support and sponsorship

Nil.

Conflicts of interest

There are no conflicts of interest.

References

1. Hansen JT. Netter's Clinical Anatomy. 4th ed. Philadelphia: Elsevier; 2019. p. 157-31.
2. Moses KP, John C, Banks JC, Nava PB, Petersen DK. Atlas of Clinical Gross Anatomy. 2nd ed. Philadelphia: Elsevier, Saunders; 2013. p. 432-45.
3. Netter FH. Atlas of Human Anatomy. 7th ed. Philadelphia, Elsevier; 2019. p. 275-366.
4. Weber EC, Vilensky JA, Carmichael SW, Kenneth S, Lee KS. Netter's Concise Radiologic Anatomy. 2nd ed. Philadelphia: Elsevier; 2019. p. 221-95.
5. Iasiello M, Vafai K, Andreozzi A, Bianco N. Analysis of non-Newtonian effects within an aorta-iliac bifurcation region. J Biomech 2017;64:153-63.
6. Shah PM, Scarton HA, Tsapogas MJ. Geometric anatomy of the aortic – Common iliac bifurcation. J Anat 1978;126:451-8.
7. Baker JF, Chan JC, Moon BG, Robertson PA. Relationship of aortic bifurcation with sacropelvic anatomy: Application to anterior lumbar interbody fusion. Clin Anat. 2021;34:550-55. doi: 10.1002/ca.23598. [doi: 10.1002/ca.23598].
8. Deswal A, Tamang BK, Bala A. Study of aortic- common iliac bifurcation and its clinical significance. J Clin Diagn Res 2014;8:C06-8.
9. Forbang NI, Ix JH, Allison MA, Criqui MH. Associations of cardiovascular disease risk factors and calcified atherosclerosis with aortoiliac bifurcation position: The Multiethnic study of atherosclerosis. Angiology 2015;66:90-5.
10. Golledge J. Abdominal aortic aneurysm: Update on pathogenesis and medical treatments. Nat Rev Cardiol 2019;16:225-42.
11. Khakpour M, Vafai K. Effects of gender-related geometrical characteristics of aorta-iliac bifurcation on hemodynamics and macromolecule concentration distribution. Int J Heat Mass Transf 2008;51:5542-51.
12. Lu K, Lu W, Yang G, Lai J, Wu H, Jiang J. Endovascular treatment of abdominal aortic aneurysm and aortic bifurcation stenosis by unibody bifurcation stent graft. Zhejiang Da Xue Xue Bao Yi Xue Ban 2018;47:612-6.
13. Shakeri A, Shakeri M, Ojaghzadeh Behrooz M, Behzadmehr R, Ostadi Z, Fouladi DF. Infrarenal aortic diameter, aortoiliac bifurcation level and lumbar disc degenerative changes: A cross-sectional MR study. Eur Spine J 2018;27:1096-104.
14. Soares AA, Gonzaga S, Oliveira C, Simões A, Rouboa AI. Computational fluid dynamics in abdominal aorta bifurcation: Non-Newtonian versus Newtonian blood flow in a real case study. Comput Methods Biomech Biomed Engin 2017;20:822-31.
15. Ponni TR, Avinash HU, Janaki MG, Koushik AS, Somashekar MK. Implication of bifurcation of abdominal aorta for radiotherapy planning for cervical cancers. J Clin Diagn Res 2015;9:C01-3.
16. Sharafuddin MJ, Hoballah JJ, Kresowik TF, Sharp WJ. Kissing stent reconstruction of the aortoiliac bifurcation. Perspect Vasc Surg Endovasc Ther 2008;20:50-60.
17. Sharafuddin MJ, Hoballah JJ, Kresowik TF, Sharp WJ, Golzarian J, Sun S, *et al*. Long-term outcome following stent reconstruction of the aortic bifurcation and the role of geometric determinants. Ann Vasc Surg 2008;22:346-57.
18. Taylor A, Rockall AG, Powell ME. An atlas of the pelvic lymph node regions to aid radiotherapy target volume definition. Clin Oncol (R Coll Radiol) 2007;19:542-50.
19. Attwell L, Rosen S, Upadhyay B, Gogalniceanu P. The umbilicus: A reliable surface landmark for the aortic bifurcation? Surg Radiol Anat 2015;37:1239-42.
20. Nezhat C, Childers J, Nezhat F, Nezhat CH, Seidman DS. Major retroperitoneal vascular injury during laparoscopic surgery. Hum Reprod 1997;12:480-3.
21. Pirró N, Ciampi D, Champsaur P, Di Marino V. The anatomical relationship of the iliocava junction to the lumbosacral spine and the aortic bifurcation. Surg Radiol Anat 2005;27:137-41.
22. Chithriki M, Jaibaji M, Steele RD. The anatomical relationship of the aortic bifurcation to the lumbar vertebrae: A MRI study. Surg Radiol Anat 2002;24:308-12.
23. Ekingen A, Tuncer MC, Ertuğrul Ö. Investigation of proper hepatic artery and gastroduodenal artery variations by multidetector computed tomography angiography method. Acta Chir Belg 2020;120:102-15.
24. Ekingen A, Hatipoğlu ES, Hamidi C, Tuncer MC, Ertuğrul Ö. Splenic artery angiography: Clinical classification of origin and branching variations of splenic artery by multi-detector computed tomography angiography method. Folia Morphol (Warsz) 2020;79:236-46.
25. Iacob N, Pusztai AM, Miclăuş GD, Pop E, Matusz P. An

anomalous origin of the gastrosplenic trunk and common hepatic artery arising independently from the abdominal aorta: A case report using MDCT angiography. Rom J Morphol Embryol 2018;59:353-7.
26. Ke J, Cai J, Wen X, Wu X, He Z, Zou Y, *et al.* Anatomic variations of inferior mesenteric artery and left colic artery evaluated by 3-dimensional CT angiography: Insights into rectal cancer surgery – A retrospective observational study. Int J Surg 2017;41:106-11.
27. O'Flynn PM, O'Sullivan G, Pandit AS. Methods for three-dimensional geometric characterization of the arterial vasculature. Ann Biomed Eng 2007;35:1368-81.
28. Standring S. Gray's Anatomy: The Anatomical Basis of Clinical Practice. 42nd ed. London: Elsevier; 2008.
29. Rigatelli G, Zuin M, Dell'Avvocata F, Nanjundappa A, Daggubati R, Nguyen T. Non-invasive evaluation of fluid dynamic of aortoiliac atherosclerotic disease: Impact of bifurcation angle and different stent configurations. J Transl Int Med 2018;6:138-45.
30. Shah PM, Tsapogas MJ, Scarton HA, Jindal PK, Wu KT. Predilection of occlusive disease for the left iliac artery. J Cardiovasc Surg (Torino) 1976;17:420-5.
31. Altunrende EM, Ekin EE. Morphometric analysis of significant vascular structures in posterior disc surgery with computed tomography angiography. Ulus Travma Acil Cerrahi Derg 2019;25:105-10.
32. Nanayakkara BG, Gunarathne C, Sanjeewa A, Gajaweera K, Dahanayake A, Sandaruwan U, *et al.* Geometric anatomy of the aortic – Common iliac bifurcation. Galle Med J 2007;12:8-2.
33. Huang W, Ge G, Meng J, Xu Y. High bifurcation of abdominal aorta upon horseshoe kidney at the level of upper L2 vertebral body: A rare case report. Surg Radiol Anat 2010;32:605-8.
34. Lakchayapakorn K, Siriprakarn Y. Anatomical variations of the position of the aortic bifurcation, iliocava junction and iliac veins in relation to the lumbar vertebra. J Med Assoc Thai 2008;91:1564-70.
35. Khamanarong K, Sae-Jung S, Supa-Adirek C, Teerakul S, Prachaney P. Aortic bifurcation: A cadaveric study of its relationship to the spine. J Med Assoc Thai 2009;92:47-9.
36. Panagouli E, Antonopoulos I, Protogerou V, Troupis T. Anatomical study of the common iliac arteries. Folia Morphol (Warsz) 2020.

Original Article

Ossification of Calcaneal Tendon: Plausible Role of Hypoxia-Induced Factor 1 Alpha

Parul Kaushal, Tara Sankar Roy[1], Tony George Jacob[2], Deep N Srivastava[3], Chetan Sahni[4], Neerja Rani[2]

Department of Anatomy, Pandit Deendayal Upadhyaya National Institute for Persons with Physical Disabilities, [1]Department of Anatomy, NDMC Medical College and Hindu Rao Hospital, Departments of [2]Anatomy and [3]Radiodiagnosis, All India Institute of Medical Sciences, New Delhi, [4]Department of Anatomy, Banaras Hindu University, Banaras, Uttar Pradesh, India

Abstract

Introduction: Tendons may rarely be ossified. The calcaneal tendon (CT) is the largest in the body. The incidence and mechanism of ossification of CT is not known. **Material and Methods:** We carried out a morphological, radiological, histological, and immunohistochemical study on the CT of 50 (30 – male and 20 – female) human cadavers. **Results:** The mean length (cm) of the CT was 27.60 ± 2.30 (right) and 27.51 ± 2.60 (left) in males and 25.43 ± 0.77 on both sides in females. The contribution to the formation of the CT from the two heads of gastrocnemius muscle was greater from medial head in 84%, lateral head in 12%, and equal in 4%. On screening the CT by C-arm radiography, slight opacification at the site of insertion of CT (bilaterally) was noted in an elderly male. Large, bilateral opacification was seen in another elderly male cadaver. Well-defined lamellar bone with osteocytes lying in lacunae and bone marrow amid the tendon collagenous tissue was noted in hematoxylin- and eosin-stained sections. The osteocytes expressed hypoxia-induced factor 1 alpha. **Discussion and Conclusion:** In this study, we confirmed that the radiological opacification in the CT was ossification that may have been triggered by hypoxia.

Keywords: *Achilles tendon, heterotopic ossification, osteocytes, tendocalcaneum*

Introduction

Tendons are dense, regular connective tissue structures, which transmit force from muscle to bone. They consist of collagen (mostly Type I) and elastin embedded in a proteoglycan-rich matrix. The tendon matrix is produced by the tenoblasts and tenocytes that lie parallel between the longitudinally arranged collagen fibers.[1] Any kind of stress or trauma (both micro and macro) predisposes them to changes in their physicochemical composition.[2] The tendons possess a poor healing capacity owing to their low vascularity and cellularity.[3,4] Recent studies have identified tendon stem/progenitor cells (TSPCs) in the tendons, which play a crucial role in healing and repair of the tendons, by promoting either tenogenic (into tenocytes) or nontenogenic (into chondrocytes, osteocytes, etc.) differentiation following trauma.[2] However, the factors and the mechanisms regulating them have not been studied in detail.

Tendocalcaneum or Achilles tendon or calcaneal tendon (CT) is the largest in the body and is formed by the union of the aponeuroses of medial and lateral heads of gastrocnemius with the tendon of soleus. This tendon gets inserted onto the posterior surface of the calcaneum. The three muscles are together referred to as triceps surae.[5] CT is the chief plantar flexor of the foot at the ankle joint and mediates powerful heel rise during each gait cycle. Therefore, the CT is subjected to high tensile load of up to 3.9 and 7.7 times of the body weight during walking and running, respectively.[6] These factors make the CT a potential candidate for tendinopathies and degenerative diseases. Calcification, ossification, and decreased oxygen tension have been suggested as the most plausible consequences of degenerative changes in this tendon, and among them, ossification is a rare condition as only sporadic cases have been reported in literature since 1908.[7] Ossification of CT is characterized by the presence of one or more segments of variable-sized ossified mass within the substance of the CT.[8,9] Its presence is usually asymptomatic but may present as pain or weakness in the tendon, especially during dorsiflexion at the ankle joint.[9] On reviewing the literature,

How to cite this article: Kaushal P, Roy TS, Jacob TG, Srivastava DN, Sahni C, Rani N. Ossification of calcaneal tendon: Plausible role of hypoxia-induced factor 1 alpha. J Anat Soc India 2022;71:18-23.

Article Info

Received: 01 November 2021
Accepted: 03 November 2021
Available online: 17 March 2022

Address for correspondence:
Dr. Neerja Rani, Department of Anatomy, All India Institute of Medical Sciences, New Delhi - 110 029, India.
E-mail: neerja.sirohi@gmail.com

Access this article online

Website: www.jasi.org.in
DOI: 10.4103/jasi.jasi_178_21
Quick Response Code:

we came across few clinical case reports documenting ossification or calcification in the CT, however, most of them were associated with either previous history of tendon surgery or trauma.[10,11] Most of the reported sporadic cases included radiological evaluations without histopathological correlations. Further, none of the studies have considered the immunoexpression of plausible factors influencing the ossification of CT in humans. Although the exact mechanism of ossification of CT remains unclear, various factors such as previous surgery for tenotomy,[12] rupture of tendon,[10] correction of club foot,[11] trauma,[12] repetitive microtrauma,[13,14] degenerative changes,[15] in addition other predisposing conditions such as diabetes mellitus,[16] fluorosis,[17] retinoid therapy,[18] and syphilis[19] have been hypothesized to play a role in ossification of CT. Besides these factors, low vascularity of the CT in the midsection,[4] has been proposed as one of the factors predisposing CT to hypoxia. Hypoxia-induced factor 1 alpha (HIF1α) is one of the key regulators of the cellular and systemic homeostatic response to hypoxia and activates transcription of many genes including those involved in osteogenesis.[7,20] Since hypoxia is postulated as one of the underlying causes of ossification of CT, therefore we planned to study the immunoexpression of HIF1α in those cases in which we found opacities within the CT during routine human cadaveric dissection and radiological survey of the lower limbs.

Material and Methods

Morphology and morphometry

One hundred (100) CTs from 50 cadavers (30 – male and 20 – female) were studied during routine anatomical dissection.[21] All the cadavers used in the study were donated for teaching and research. Hence, the need for clearance from the Ethics Committee was precluded in this study. Lower limbs with any signs of surgery or injury were excluded from the study. The length of the CT was measured by a standardized measuring tape (with minimum reading of 1 mm). The length of CT was measured from the point of fusion of the muscle bellies of the medial and lateral heads of gastrocnemius up to the calcaneal tubercle. We also noted the contribution made by the two heads of the gastrocnemius based on the extent of the muscle fibers, as described previously.[22] Further, all the tendons were physically examined for the presence of any mass.

Radiology

The tendons with the presence of mass were also screened by a C-arm radiography machine (HF49 DIPIQ, Allengers, India) for the presence of any radiopacities, which was further confirmed by a digital radiography machine (GE Definium XR 656, GE Healthcare, USA).

Histology

The hard mass, identified by these techniques, was excised, fixed in 4% paraformaldehyde, decalcified in 10% solution of ethylenediaminetetraacetic acid, and on completion of decalcification (confirmed by radiograph) was processed for embedding and blocking in paraffin. Hematoxylin and eosin (H and E) staining and immunohistochemistry (IHC) were carried out on 7-μm thick sections of the tissue.

Immunohistochemistry

For IHC, antigen retrieval was done in citrate buffer (pH = 6) at 100°C for 20 min, quenching in 3% hydrogen peroxide followed by blocking in normal goat serum. After overnight incubation in HIF1α primary antibody (bs-07370R Bioss rabbit polyclonal, 1:100) and horseradish peroxidase-tagged secondary antibody (Ultravision Plus Detection System, Thermo Scientific), the expression of HIF1α was visualized by using chromogen diaminobenzidine followed by counterstaining with hematoxylin. The slides were dehydrated, cleared, and mounted with DPX. The slides were examined under the light microscope (Nikon E 600 mounted with DS cooled camera) and photographed. Negative controls were incubated with normal goat serum instead of primary antibody. Two independent observers, unaware of the study, examined the sections for qualitative assessment. These observers commented on individual, high-magnification, digital images of five random fields from both the tissues.

Statistical analysis

The measurements of the tendons were represented as mean ± standard deviation. Paired Student's *t*-test was used to compare the difference among the right and left limbs of both the sexes. The categorical data of morphometric parameters of males and females were analyzed by the Chi-square test. An overall $P < 0.05$ was considered statistically significant. All analysis was carried out by Statistical Package for the Social Sciences (SPSS), IBM (International Business Machines), USA.

Results

Morphology and morphometry

The mean length (cm) of the CT in males was 27.60 ± 2.30 (right) and 27.51 ± 2.60 (left), while in the case of females, the corresponding value was 25.43 ± 0.77 for both the limbs. Table 1 shows the contribution from the medial and lateral heads of gastrocnemius to the formation of CT in both the lower limbs of all the cadavers. However, no statistically significant difference was noted in either of the two parameters studied, between male and female cadavers. Large, bilateral ossification was seen in the CT of a male cadaver (62 years) [Figure 1].

Radiology

While screening the CT of the cadavers with the C-arm, we came across extensive bilateral radiopacities in the CT of one of the male cadavers (62 years) while we encountered slight opacification (bilateral) at the point of insertion of the CT in another male cadaver (59 years). The lateral view X-ray of the lower limbs revealed 6.99-cm long and 7.05-cm long radiopaque masses in the right and left sides, respectively [Figure 2].

Histology

Photomicrographs obtained from the H- and E-stained slides revealed the presence of well-defined collagenous fibers with interspersed flattened nuclei. Small empty spaces containing cells with well-defined nuclei were seen lying in between concentric lamellae. Empty space containing some cellular components with clear nucleus and cytoplasm was also noted [Figure 3].

Immunohistochemistry

The sections that were HIF1α immunostained revealed that HIF1α expression was predominantly localized in the cells lying within the lacunae between the lamellae described above [Figure 4].

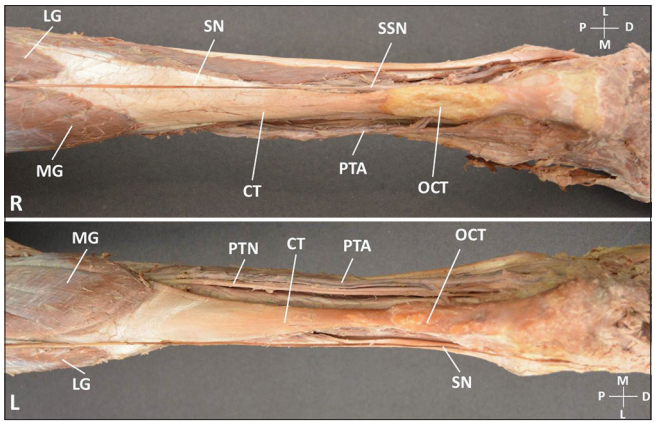

Figure 1: Right and left lower limbs showing the ossification in the calcaneal tendon. OCT: Ossified calcaneal tendon, CT: Calcaneal tendon, MG: Medial head of gastrocnemius, LG: Lateral head of gastrocnemius, SN: Sural nerve, SSN: Neuroma in sural nerve, PTA: Posterior tibial artery, PTN: Posterior tibial nerve

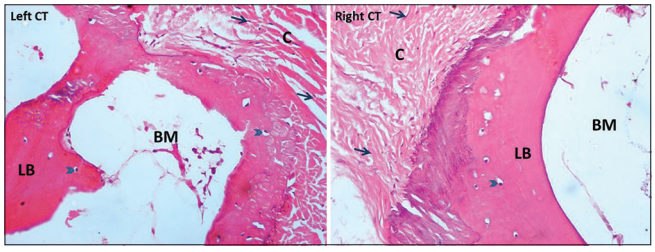

Figure 3: Photomicrographs (×20) showing hematoxylin- and eosin-stained sections obtained from the right and left calcaneal tendons. Note the osteocytes (arrowheads) located in lacunae of the lamellar bone and the bone marrow. Collagen bundles (C) are seen with intervening fibrocyte nuclei (arrows) in the calcaneal tendon

Discussion

The results of the present study demonstrated no significant difference in the morphology of the CT of the right and left sides, with a mean length being 27.56 ± 2.47 cm in males and 25.43 ± 0.77 cm in females. The medial head of gastrocnemius contributed more muscle fibers to the formation of CT in majority of the cases. Out of 100 CTs examined radiologically, well-defined opacification was noted in one, while another male cadaver presented

Table 1: The contribution of medial and lateral heads of gastrocnemius to the formation of calcaneal tendon

Feature on CT	Sex	Side	*n* (%)
Greater contribution by medial head	Male	Right	25 (83.3)
		Left	25 (83.3)
	Female	Right	17 (85)
		Left	17 (85)
Greater contribution by lateral head	Male	Right	4 (13.3)
		Left	4 (13.3)
	Female	Right	2 (10)
		Left	2 (10)
Equal contribution by both heads	Male	Right	1 (3.3)
		Left	1 (3.3)
	Female	Right	1 (5)
		Left	1 (5)

CT: Calcaneal tendon

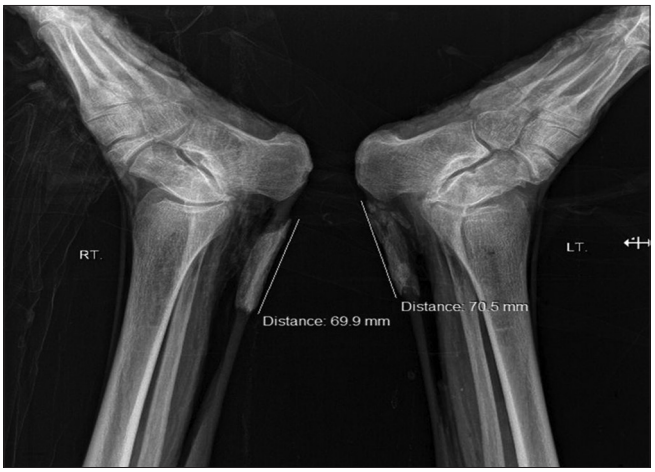

Figure 2: Plain radiograph (lateral view) of both lower limbs showing ossification in the right (69.9 mm) and left (70.5 mm) calcaneal tendons

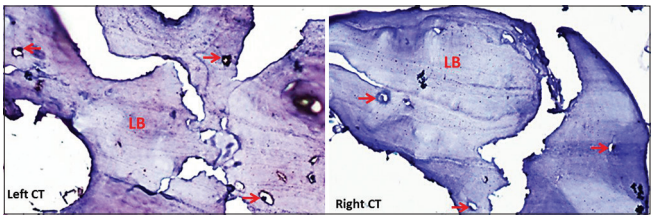

Figure 4: Photomicrographs (×20) showing hypoxia-induced factor 1 alpha-immunostained sections obtained from the left and right calcaneal tendons. Note the localization in the osteocytes (arrowheads) located in the lacunae interspersed in the lamellar bone

a small opacification toward the insertion of the CT. Histological evaluation of the mass revealed features characteristic of ossification, with well-defined concentric lamellae interspersed with lacunae containing osteocytes. Immunoexpression of HIF1α was noted in the cells residing in the lacunae corresponding to osteocytes.

The length of CT was observed ranges between 19 and 27 cm,[22] which corroborates with the findings of the present study. They observed greater contribution by medial head of gastrocnemius (93.3%), while only 6.7% of cases received greater or equal contribution from the lateral head, which was like the pattern observed in the present study [Table 1]. Another study done on 60 cadavers, highlighted the importance of knowledge of variations in the formation of the musculotendinous junction to determine the level of appropriate placement of instruments used in endoscopic recession of gastrocnemius. Further, greater contribution by the medial head of gastrocnemius in majority of the cases points toward the role of these fibers in lateral foot stabilization.[23,24] These workers, however, did not comment on the presence of ossified mass in any of the 60 cadavers studied. No statistically significant difference in the length of CT (between right and left sides) was noted in a study conducted by Kumar *et al*. using 64 dissected lower limbs. These investigators have also not commented on the presence of ossification in any of the 64 limbs studied. Acquaintance with the morphologic and morphometric parameters of the CT serves as an important landmark in its anthropometric evaluation and biomechanical characteristics, besides aiding sports physicians and surgeons for the diagnosis and planning treatment for CT injuries, besides being imperative to achieve successful outcomes and minimizing complications while performing either open, minimally invasive, or percutaneous surgery in this region.[25]

First described by 1908, ossification of CT is a rare clinical condition characterized by the occurrence of one or more fragments of variable-sized ossified mass in any part of the substance of the tendon. Plain radiograph has been reported to reliably demonstrate the ossified mass and define the contour of the tendon in majority of the cases.[8] Depending on their anatomical location, radiopaque densities have been classified into three types: type I – at the insertion or superior pole of calcaneum, Type II – 1–3 cm proximal to CT insertion, and Type III – 3–12 cm from the insertion of the tendon. The lesion was further subcategorized based on the degree of ossification as A: partial ossification and B: total ossification of the tendon, respectively.[26] The lower limb observed with extensive ossification in the present study corresponded to Type II with partial ossification while the minor ossification corresponded to Type I. The ossification of the CT may appear as an outgrowth from the periosteum of the calcaneum[19] or the body of the tendon.[15,19] Although calcification of CT has been reported in various clinical reports,[8-10] cases reporting true ossification in tendon are scarce. The two can be differentiated as calcification involves deposition of amorphous calcium phosphate or carbonate, while ossification involves the formation of hydroxyapatite crystals in an observable histological pattern; however, both are indistinguishable in radiographs. Therefore, histological evaluation of the mass excised was carried out and it revealed lamellar bone formation with the presence of lacunae lodging osteocytes and a distinguishable bone marrow cavity [Figure 3].

Ossification of CT has been reported to be twice as common in males,[13] although enlargement of the tendon ossification has been reported with time.[14] Congenital occurrence of ossification of CT cannot be ruled out as Ghormley and John have reported a case of ossification in CT with deficiency of the neural arch of the first sacral segment,[19] although no other study till date has reported congenital ossification of CT. Genetic predisposition of ossified CT was contemplated by Cortbaoui *et al*. after observing ossified CT in three siblings having no history of trauma, surgery or systemic, metabolic, and infections, however, these investigators did not substantiate their conclusions with any molecular or genetic study.[27] The ossified mass is usually asymptomatic, however, its fracture following trauma may lead to pain.[9,12] Furthermore, cases associated with either of the predisposing factors must be distinguished from the ones occurring idiopathically. This is important as cases with bilateral ossification of CT with no history of trauma, previous surgery, or metabolic diseases have scarcely been reported in literature.[15,28] Tamam *et al*. observed a 1.8 cm × 0.7 cm (left) and 3.2 cm × 2.4 cm (right) sized ossification near the CT insertion of a 41-year-old male patient with no history of direct trauma or previous surgery where the person was involved in extensive physical activity.[15] The radiopaque mass that we observed in the CT measured 6.99 and 7.05 cm, which is one of the largest masses reported in the CT. Small calcific spurs at the insertion site of CT have been reported, especially in healthy individuals, who are physically active, and in patients with rheumatic and articular diseases.[29,30] Since this study was based on cadaveric dissection, we do not have access to the occupational history and lifestyle of the deceased person.

In the literature, there are limited reports revealing the detailed histology of the ossified CT. Histologic observations of ossified CT have been observed by various workers and they have suggested either of the following patterns of ossification: endochondral or intramembranous ossification, lamellar bone formation, calcified cartilage, and osteoid formation.[10,14,31] Hatori *et al*. observed lamellar bone formation and bone marrow in tendon tissue excised from two patients with ossification in CT. These investigators attributed the ossification to the repetitive microtrauma as the patients provided previous history of heavy manual work. Furthermore, these investigators have documented

the presence of both endochondral and intramembranous ossifications in the CT.[14] Majeed *et al*. observed avascular fibroconnective tissue containing a well-circumscribed nodular area composed of mature cancellous bone along with bony trabeculae separated by vascular spaces in an ossified mass obtained from CT.[31] Development of mature bone following an insult with no inflammatory or degenerative changes in the ossification of CT has been reported.[10] In the present study, we observed well-defined ossification areas with osteocytes lying in the lacunae interspersed between the lamellae of bone [Figure 3].

The exact mechanism of ossification of CT has not been elucidated; however, its ossification has been associated with osteogenesis from circulating osteoblasts, bone growth from injured periosteum, bone formation by fibroblasts or osteoblasts that have originated from fibroblasts[16] or TSPCs, or because of degenerative changes in collagen.[2,32] Furthermore, vascular pericytes have been reported to possess the capacity to differentiate into both chondrocytes and osteoblasts, thereby permitting them to act as a reservoir of primitive precursor cells giving rise to cells of multiple lineages.[33] Zhang and Wang identified TSPCs as the functional repairing tendon cells and hypothesized malfunction of these cells due to differential expression of various factors may result in tendinopathies. These investigators proposed differentiation of TSPCs into osteoblasts instead of tendon fibroblasts (tenocytes) as the basis of ossification of tendons.[34]

Decrease in the oxygen tension has been reported to play a crucial role in the transformation of tendon into bone. Persistent lowering of the tissue oxygen tension causes transformation of tendon into regions of fibrocartilage in which chondrocytes mediate deposition of calcium at multiple foci.[35] To elucidate the molecular mechanism of heterotopic ossification in the CT, Lin *et al*. performed Achilles tenotomy in rat. Based on their observations, these investigators proposed endochondral bone formation as the mechanism of ossification in the CT. Furthermore, they also highlighted the role played by hypoxia in chondrogenesis as they noted a significant increase in the mRNA levels of hypoxia-inducible factor HIF1α.[7] This transcriptional regulator has been associated with bone formation by modulating the expression of various downstream genes, especially those mediating adaptive responses.[36] Wang *et al*. have implicated the role of HIFα in angiogenesis and osteogenesis by elevating the levels of VEGF in osteoblasts of developing bone in mouse models.[37]

Conclusion

Our observations of expression of HIF1α in the osteocytes of ossified CT corroborate the findings of these investigators. It has been postulated that, on sensing decreased oxygen tension, osteoblasts (bone-forming cells) activate the HIFα pathway, which leads to many downstream modifications.[37,38] Location and mechanism of formation of ossified mass in the CT in this study is also substantiated by the pattern of gross blood supply of CT wherein a watershed zone with limited blood supply in the region 2–6 cm proximal to the insertion of CT has been described.[4] Taken together, the observations of the present study conclude that the radiological opacification in the CT was ossification and HIF1α may be a crucial factor mediating the ossification of the CT.

Acknowledgments

We thank all the body donors and their families who donated their bodies for teaching and research at All India Institute of Medical Sciences, New Delhi. We also thank Mr. Kulwant Singh Kapoor for helping with the statistical analysis.

Financial support and sponsorship

Nil.

Conflicts of interest

There are no conflicts of interest.

References

1. Ross MH, Pawlina W. Histology: A Text and Atlas. 5th ed. Philadelphia: Lippincott Williams and Wilkins; 2005.
2. Zhang X, Lin YC, Rui YF, Xu HL, Chen H, Wang C, *et al.* Therapeutic roles of tendon stem/progenitor cells in tendinopathy. Stem Cells Int 2016;2016:4076578.
3. Leong NL, Kator JL, Clemens TL, James A, Enamoto-Iwamoto M, Jiang J. Tendon and ligament healing and current approaches to tendon and ligament regeneration. J Orthop Res 2020;38:7-12.
4. Chen TM, Rozen WM, Pan WR, Ashton MW, Richardson MD, Taylor GI. The arterial anatomy of the Achilles tendon: Anatomical study and clinical implications. Clin Anat 2009;22:377-85.
5. Standring S. Gray's Anatomy: The Anatomical Basis of Clinical Practice. 41st ed. Edinburg, London: Elsevier Churchill Livingstone; 2016.
6. Giddings VL, Beaupré GS, Whalen RT, Carter DR. Calcaneal loading during walking and running. Med Sci Sports Exerc 2000;32:627-34.
7. Lin L, Shen Q, Xue T, Yu C. Heterotopic ossification induced by Achilles tenotomy via endochondral bone formation: Expression of bone and cartilage related genes. Bone 2010;46:425-31.
8. Yu JS, Witte D, Resnick D, Pogue W. Ossification of the Achilles tendon: Imaging abnormalities in 12 patients. Skeletal Radiol 1994;23:127-31.
9. Akhaddar A. Painless extensive ossification of the Achilles tendon: A diagnostic trap? Pan Afr Med J 2014;17:120.
10. Richards PJ, Braid JC, Carmont MR, Maffulli N. Achilles tendon ossification: Pathology, imaging and aetiology. Disabil Rehabil 2008;30:1651-65.
11. Manfreda F, Ceccarini P, Corzani M, Petruccelli R, Antinolfi P, Rinonapoli G, *et al*. A silent massive ossification of Achilles tendon as a suspected rare late effect of surgery for club foot. SAGE Open Med Case Rep 2018;6:2050313X18775587.
12. Ishikura H, Fukui N, Takamure H, Ohashi S, Iwasawa M, Takagi K, *et al.* Successful treatment of a fracture of a huge

Achilles tendon ossification with autologous hamstring tendon graft and gastrocnemius fascia flap: A case report. BMC Musculoskelet Disord 2015;16:365.

13. Lotke PA. Ossification of the Achilles tendon. Report of seven cases. J Bone Joint Surg Am 1970;52:157-60.
14. Hatori M, Matsuda M, Kokubun S. Ossification of Achilles tendon - Report of three cases. Arch Orthop Trauma Surg 2002;122:414-7.
15. Tamam C, Yildirim D, Tamam M, Mulazimoglu M, Ozpacaci T. Bilateral Achilles tendon ossification: Diagnosis with ultrasonography and single photon emission computed tomography/computed tomography. Case report. Med Ultrason 2011;13:320-2.
16. Sobel E, Giorgini R, Hilfer J, Rostkowski T. Ossification of a ruptured achilles tendon: A case report in a diabetic patient. J Foot Ankle Surg 2002;41:330-4.
17. Gupta R, Kumar AN, Bandhu S, Gupta S. Skeletal fluorosis mimicking seronegative arthritis. Scand J Rheumatol 2007;36:154-5.
18. Wuenschel M, Trobisch P. Achilles tendon ossification after treatment with acitretin. J Dermatolog Treat 2010;21:111-3.
19. Ghormley JW. Ossification of the Tendo Achillis. J Bone Joint Surg 1938;20:153-60.
20. O'Brien EJ, Frank CB, Shrive NG, Hallgrímsson B, Hart DA. Heterotopic mineralization (ossification or calcification) in tendinopathy or following surgical tendon trauma. Int J Exp Pathol 2012;93:319-31.
21. Romanes GJ. Cunningham's Manual of Practical Anatomy. 15th ed. New York: Oxford University Press; 2008.
22. Nitya J, Mariya. Morphological aspects of triceps surae – A cadaveric study. IJIRD 2013;2:372-6.
23. Vieira TM, Minetto MA, Hodson-Tole EF, Botter A. How much does the human medial gastrocnemius muscle contribute to ankle torques outside the sagittal plane? Hum Mov Sci 2013;32:753-67.
24. Tashjian RZ, Appel AJ, Banerjee R, DiGiovanni CW. Endoscopic gastrocnemius recession: Evaluation in a cadaver model. Foot Ankle Int 2003;24:607-13.
25. Kumar N, Aithal AP, Nayak SB, Patil J, Padavinangadi A, Ray BB. Morphometric evaluation of human tendocalcaneus: A cadaveric study of south Indian male population. Muscles Ligaments Tendons J 2017;7:62-8.
26. Morris KL, Giacopelli JA, Granoff D. Classifications of radiopaque lesions of the tendo Achillis. J Foot Surg 1990;29:533-42.
27. Cortbaoui C, Matta J, Elkattah R. Could ossification of the Achilles tendon have a hereditary component? Case Rep Orthop 2013;2013:539740.
28. Arora AJ, Arora R. Ossification of the bilateral Achilles tendon: A rare entity. Acta Radiol Open 2015;4:1-3.
29. Bassiouni M. Incidence of calcaneal spurs in osteo-arthrosis and rheumatoid arthritis, and in control patients. Ann Rheum Dis 1965;24:490-3.
30. Resnick D, Feingold ML, Curd J, Niwayama G, Georgen TG. Calcaneal abnormalities in articular disorders: Rheumatoid arthritis, ankylosing spondylitis, psoriatic arthritis, and Reiter's syndrome. Radiology 1977;125:355-66.
31. Majeed H, Deall C, Mann A, McBride DJ. Multiple intratendinous ossified deposits of the Achilles tendon: Case report of an unusual pattern of ossification. Foot Ankle Surg 2015;21:e33-5.
32. Yang G, Rothrauff BB, Tuan RS. Tendon and ligament regeneration and repair: Clinical relevance and developmental paradigm. Birth Defects Res C Embryo Today 2013;99:203-22.
33. Doherty MJ, Ashton BA, Walsh S, Beresford JN, Grant ME, Canfield AE. Vascular pericytes express osteogenic potential: *In vitro* and *in vivo*. J Bone Joint Surg 1998;13:828-38.
34. Zhang J, Wang JH. Moderate exercise mitigates the detrimental effects of aging on tendon stem cells. PLoS One 2015;10:e0130454.
35. Uhthoff HK, Loehr JW. Calcific tendinopathy of the rotator cuff: Pathogenesis, diagnosis, and management. J Am Acad Orthop Surg 1997;5:183-91.
36. Semenza GL. Hypoxia-inducible factor 1: Oxygen homeostasis and disease pathophysiology. Trends Mol Med 2001;7:345-50.
37. Wang Y, Wan C, Deng L, Liu X, Cao X, Gilbert SR, *et al.* The hypoxia-inducible factor alpha pathway couples angiogenesis to osteogenesis during skeletal development. J Clin Invest 2007;117:1616-26.
38. Sullivan D, Pabich A, Enslow R, Roe A, Borchert D, Barr K, Cook B. Extensive ossification of the Achilles tendon with and without cute fracture: A scoping review. J Clin Med 2021;10:3480.

Original Article

Morphometric Analysis of Normal and Variant Anatomy of Posterior Cerebral Artery and the Incidence of Fetal Posterior Cerebral Artery in Uttar Pradesh Region: A Computed Tomography Angiographic Study

Abstract

Introduction: The aim is to study morphometric analysis of normal and variant anatomy of posterior cerebral artery (PCA) and incidence of fetal PCA (FPCA) in Uttar Pradesh region. The PCA and its cortical branches supply blood to the occipital lobe, inferomedial temporal lobe, and portions of posterior inferior parietal lobe. Fetal-type PCA is a common anatomic variation of PCA that is closely associated with intracranial aneurysm. The present study provides the description of PCA regarding its normal morphology, morphometry, and variations in Uttar Pradesh region. **Material and Methods:** The study evaluated 100 computed tomography angiograms. **Results:** Among arteries that displayed normal anatomy, mean diameter of PCA was observed to be 4.29 ± 0.74 mm on the right side and 2.47 ± 0.74 mm on the left side. Mean diameter in males and in females was found to be 2.48 ± 0.73 mm and 2.47 ± 0.74 mm, respectively. In 56.5% of cases, the diameters of P1 segment of PCAs ranged from 2.1 to 3 mm whereas >3 mm diameter was observed in 18.5% cases. Nineteen percent cases showed 1.1–2 mm. In 6% cases, hypoplasia (≤1 mm) of PCA was observed. FPCA was observed in 26% cases. Unilateral observed in 17% cases and bilateral in 9% cases and the difference was statistically significant ($P < 0.000$). **Discussion and Conclusion:** Anomalies of PCA may assume considerable significance in surgeries of head and neck, which require ligation of internal carotid and common carotid artery. Awareness of these anatomical variations described shall prove to be useful for any cerebrovascular procedures.

Keywords: *Fetal posterior cerebral artery, variations, vertebrobasilar system*

Arvind Kumar Pankaj, Sarah Sko Sangma[1], Jyoti Chopra, Garima Sehgal

Department of Anatomy, King George's Medical University, Lucknow, Uttar Pradesh, [1]Department of Anatomy, All India Institute of Medical Sciences, New Delhi, India

Introduction

Anterior and posterior circulations provide the primary blood circulation of the brain. Anterior circulation comprises internal carotid artery and its branches. Posterior circulation comprises the vertebral arteries, its main branch posterior inferior cerebellar arteries, the basilar artery (BA) and its branches anterior inferior cerebellar arteries, superior cerebellar arteries, and terminal branch posterior cerebral artery (PCA)[1] [Figure 1]. Most adult humans have the classic vascular anatomy in which both left and right PCAs originate from the BA and are part of the vertebrobasilar system or posterior circulation. PCA is divided into four segments, P1 to P4. The P1 segment is between the termination of the BA and the posterior communicating artery (PCOM)[2] [Figure 1]. An anatomic variant of the PCA, known as fetal-type or fetal PCA (FPCA), has been detected by anatomic,[3] and angiographic,[4-6] studies in 11% to 46% of adult humans, either unilaterally or bilaterally. FPCA is called a full FPCA if the P1 segment is not visualized on computed tomography angiography, magnetic resonance angiography [Figure 2] or after injection of contrast into the vertebral artery; a partial FPCA if the P1 segment is smaller than the PCOMA [Figure 3] or an intermediate FPCA if the P1 segment is as large as the PCOMA[7] [Figure 4].

Various authors have studied the morphometry of the PCA in different populations and the results have been seen to vary in different races. In the present study, we have made an attempt to make a normal morphometry of P1 segment of PCA and observe the variations associated with it such as hypoplasia and fenestration. A solid understanding of the pathophysiology of a

How to cite this article: Pankaj AK, Sangma SS, Chopra J, Sehgal G. Morphometric analysis of normal and variant anatomy of posterior cerebral artery and the incidence of fetal posterior cerebral artery in Uttar Pradesh region: A computed tomography angiographic study. J Anat Soc India 2022;71:24-9.

Article Info

Received: 03 July 2021
Accepted: 14 October 2021
Available online: 17 March 2022

Address for correspondence:
Dr. Sarah Sko Sangma, Department of Anatomy, All India Institute of Medical Sciences, New Delhi, India. E-mail: sarahssangma@gmail.com

Access this article online

Website: www.jasi.org.in
DOI: 10.4103/jasi.jasi_115_21
Quick Response Code:

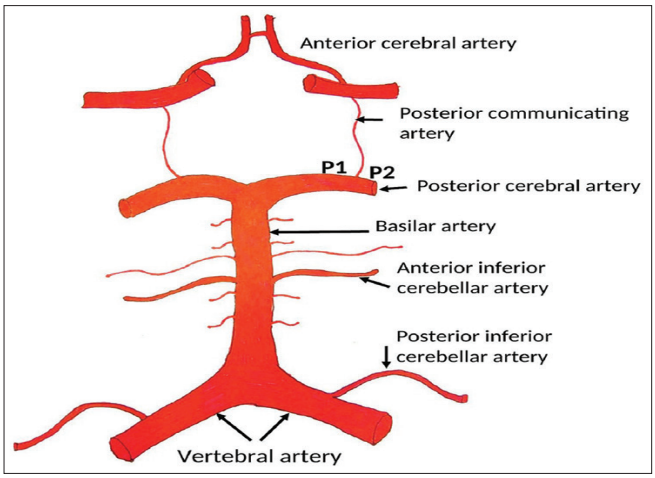

Figure 1: Schematic diagram showing normal vertebrobasilar system and circle of Willis, where P1: P1 segment of posterior cerebral artery, P2: P2 segment of posterior cerebral artery

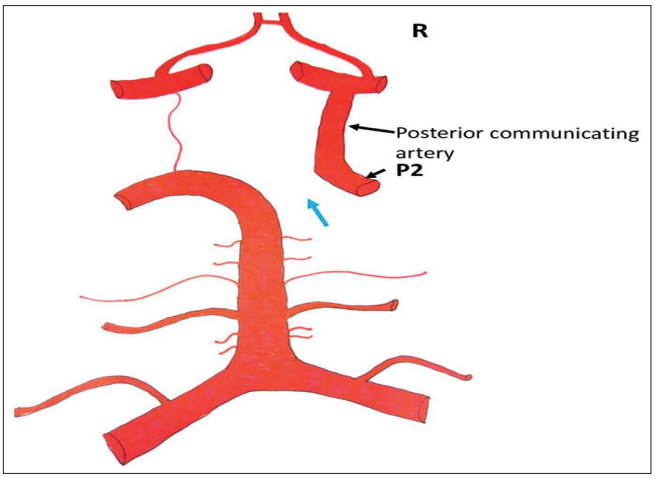

Figure 2: Schematic diagram showing full fetal posterior cerebral artery, blue arrow

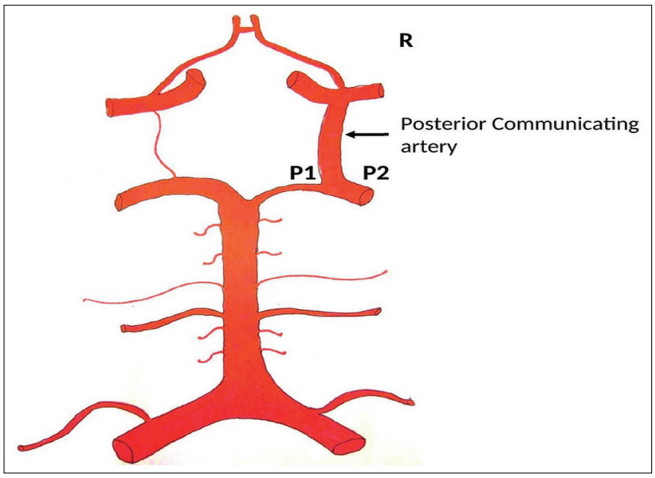

Figure 3: Schematic diagram showing partial fetal posterior cerebral artery

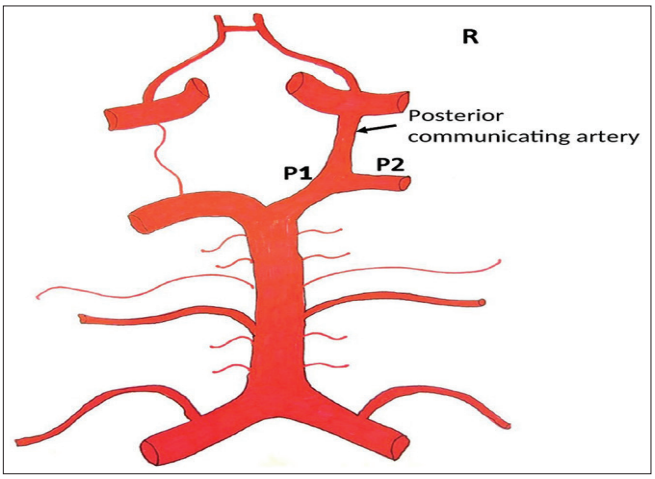

Figure 4: Schematic diagram showing intermediate fetal posterior cerebral artery

PCA stroke as well as the syndrome relating to it requires adequate knowledge of the structures and vascular anatomy of the brain.

Material and Methods

Ethical clearance

Approval for this observational, descriptive, cross-sectional study was obtained from Ethical review board of University with the Helsinki Declaration of 1975, as revised in 2000.

Study design

The present study is an observational, descriptive, cross-sectional, study.

Subjects

The study evaluated 100 computed tomography (CT) angiograms of patients of all age groups of either sex that visited the Department of Radiodiagnosis between September 2016 and August 2017 for undergoing head-and-neck CT angiography.

Duration of study

September 2016 to August 2017.

Inclusion criteria

- All age groups
- Patients undergoing brain angiography, craniovertebral junction angiography
- Willing to participate in the study.

Exclusion criteria

- Refusal to participate in the study
- Pregnancy
- Allergy to iodine
- Renal insufficiency
- Uninterruptable scans
- History of head trauma, cerebral surgery, vasculitis syndrome, vertebrobasilar dissection or near-complete occlusion and space-occupying intracranial lesions likely to distort the vascular anatomy.

Preprocedure precautions

- Patients were enquired to rule out the presence of any drug allergy to avoid the occurrence of any untoward anaphylactic reaction during the procedure
- They were asked to come empty stomach
- They were advised to drink only water just before the procedure
- Blood urea and creatinine levels were evaluated before procedure.

Computed tomography angiography protocol

CT angiography was performed on a 64-slice multidetector computed tomography (MDCT) scanner (BRILLIANCE CT, Philips medical system, Netherland, B. V.5684 PC Best. The Netherlands). CT angiography of all patients was done after overnight fasting. Patients were trained for the breath holding method which was required during the procedure.

Procedure

CT angiography was performed after receiving a written informed consent from the concerned subject. The patient was positioned supine and head immobilized by adhesive strap. The images were acquired on a 64-slice MDCT. The area from C3 vertebra to the vertex was scanned. Plain CT followed by CT angiography was performed. 80–100 ml of nonionic contrast medium was injected at the rate of 5 ml/s followed by saline of flush 40 ml through the antecubital vein with 18 gauge cannula using power injector. The time of delay was chosen by bolus tracking. Common carotid artery was monitored in real-time with low-dose dynamic scanning at C5 vertebra. The diagnostic scan was manually started once contrast reached the common carotid artery. Source images thus obtained were transferred to the workstation dedicated to the scanner where the processing was done. The final postprocessed images along with the axial slices were used for analysis and reporting.

Image analysis

Images were processed on an extended brilliance workspace version 4.0. CT image interpretation was done using various techniques such as multiplanar reconstructions, maximum intensity projection, and volume-rendered technique. Axial source images [Figures 5 and 6] and three-dimensional reconstructed images were helpful in evaluating complex vascular anatomy. Interpretation was done by radiologists and anatomists. Image analysis was done for both right and left P1 segment of PCA for appreciating normal anatomy and variations such as:

- Fenestration: Duplication of a portion of the artery[5] [Figure 7]
- Hypoplasia: PCA: Diameter ≤1 mm[5] [Figure 8]
- FPCA [Figures 8 and 9].

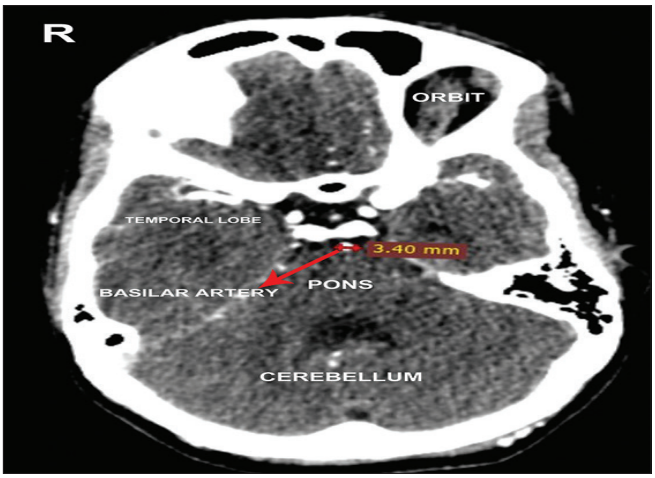

Figure 5: Axial source image of computed tomography angiography of brain showing measurement of basilar artery

Data analysis

The statistical analysis was carried out on SPSS (Statistical Package for the Social Sciences) 16.0 version (Chicago, Illinois, Inc., USA). The results were presented in frequencies and percentages. Chi-square test was used for the assessment of associations. One-way analysis of variance was used to compare the mean diameters of arteries among age groups.

Results

One hundred (100) patients were included in the study (males = 52 and females = 48). Age ranged from 21 to 80 years with mean age = 48.86 ± 16.73 years.

The analysis of images revealed 100 P1 segments of PCAs on both right and left sides. PCA hypoplasia was seen in 6% of cases and fenestrated PCA was seen in 1% of cases. Among the arteries that displayed normal anatomy, the mean diameter of PCA was observed to be 4.29 ± 0.74 mm on the right side and 2.47 ± 0.74 mm on the left side. Mean diameter in males and in females was found to be 2.48 ± 0.73 mm and 2.47 ± 0.74 mm, respectively. The difference in mean diameter with laterality and gender was statistically insignificant.

In 56.5% of cases, the diameters of P1 segment of PCAs ranged from 2.1 to 3 mm whereas >3 mm diameter was observed in 18.5% of cases. In 19% of cases, it was observed to be 1.1–2 mm. In 6% cases, hypoplasia (≤1 mm) of PCA was observed [Table 1 and Figure 10].

The mean diameter of P1 segment of PCA did not show any consistent relation with age groups. It was maximum in <20-year age group then it decreased in 20–40-year age group. In 41–60-year age group, it was wider as compared to 20–40-year age group but lesser than <20-year age group. The diameter then again decreased in 61–80-year age group and was minimum among all values observed in various age groups. The difference in mean diameter

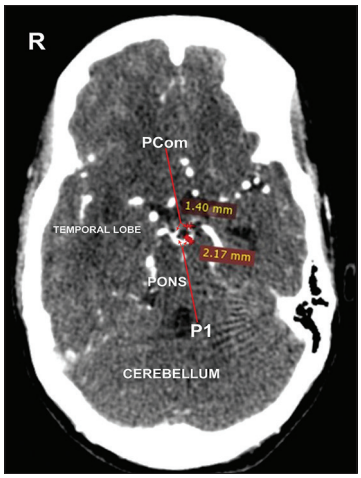

Figure 6: Axial source image of computed tomography angiography of brain showing measurement of normal posterior communicating artery and P1 segment

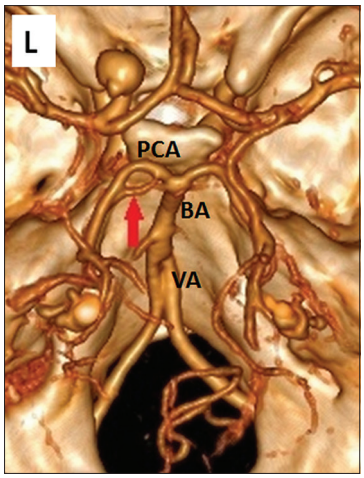

Figure 7: Three-dimensional volume-rendered image of computed tomography angiography of brain showing fenestration of left P1 segment

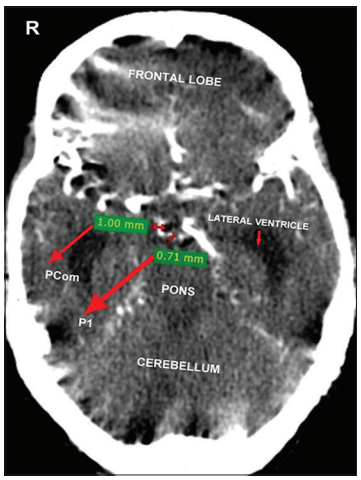

Figure 8: Axial source image of computed tomography angiography of brain showing hypoplasia of P1 segment and partial F posterior cerebral artery on the right side

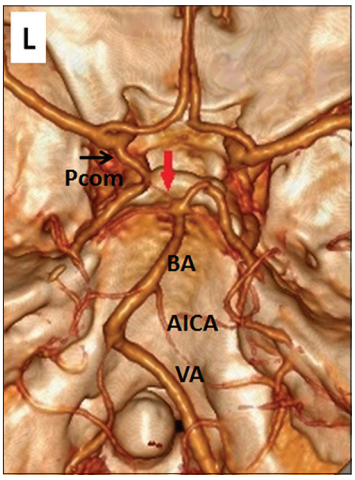

Figure 9: Three-dimensional volume-rendered image of computed tomography angiography of brain showing partial F posterior cerebral artery on left side

Table 1: Prevalence of different range of diameters of P1

Range (mm)	Right, *n* (%)	Left, *n* (%)	Total, *n* (%)
≤1	6 (3)	6 (3)	12 (6)
1.1-2	18 (9)	20 (10)	38 (19)
2.1-3	58 (29)	55 (27.5)	113 (56.5)
3.1-4	17 (8.5)	18 (9)	35 (17.5)
>4	1 (0.5)	1 (0.5)	2 (1)

among different age groups was statistically insignificant [Table 2 and Figure 11].

Variations of partial FPCA: In the present study, FPCA was observed as partial type in 26% cases. Unilateral PCA was observed in 17% cases [Figure 12] and bilateral FPCA in 9% cases [Figure 12] and the difference was statistically significant ($P < 0.000$). The prevalence of unilateral FPCA was found to be more common in males (11%) as compared to females (6%) and on the right side (11%) as compared to the left (6%). Bilateral FPCA was observed to be more common in males than females [Table 3 and Figure 12].

Discussion

PCA was observed in 100 cases. The mean diameter of P1 segment of PCA was observed to be larger on the right side (4.29 ± 0.74 mm) as compared to the left side (2.47 ± 0.74 mm). Our findings were similar with that of Patel *et al*. who also found right PCA (2.53 mm) to be larger than left PCA (2.49 mm).[3] Similarly, Akgun *et al*. also found right P1 to be larger (2.56 ± 0.43 mm) as compared to the left side (2.43 ± 0.34 mm).[5]

The diameters measured by these authors were not in concurrence with the present study. The difference in measurement could be due to different modalities used by the authors. The readings noted by Pai *et al*. were comparatively lesser though they also reported that right P1 (2.76 mm) was marginally wider than left (2.5 mm).[8] In a cadaveric study done in 30 fresh

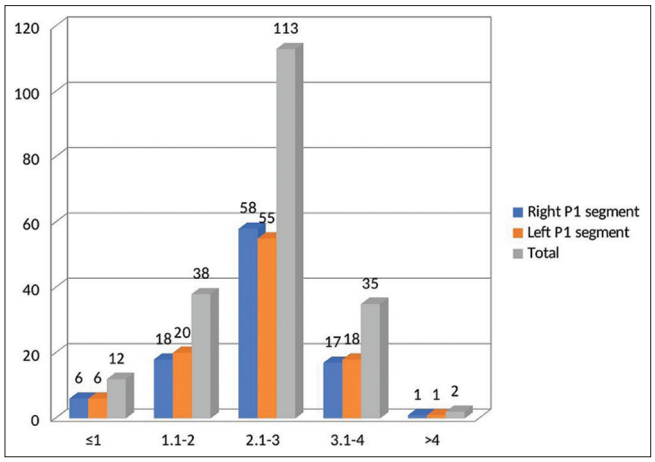

Figure 10: Bar diagram showing prevalence of different range of diameters of P1 segment

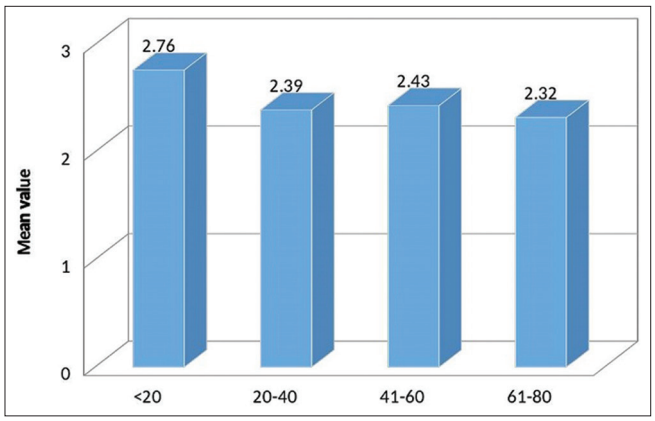

Figure 11: Bar diagram showing mean diameter of P1 segment in different age groups

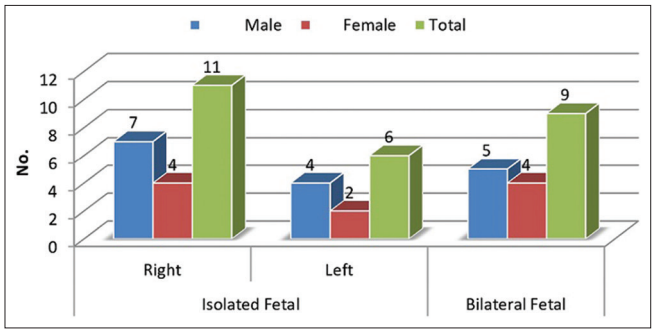

Figure 12: Bar diagram showing prevalence of partial fetal posterior cerebral artery

cadaveric brain specimens, Canaz *et al*. found that in 18 (60%) brains, right PCA was wider than left PCA.[9]

We also noted that mean diameter of P1 was marginally larger in males (2.48 ± 0.73 mm) as compared to females (2.47 ± 0.74 mm), but the difference among gender groups was statistically insignificant. Rai *et al*. observed that the mean diameter was equal in both genders (2.2 ± 0.4 mm).[10] Their findings were not in parallel to the present study.

Table 2: Mean diameter of P1 segment of posterior cerebral artery in different age groups

Age groups (years)	Mean diameter±SD (mm)
<20	2.76±0.59
20-40	2.39±0.58
41-60	2.43±0.67
61-80	2.32±1.16
P	0.68

ANOVA: Analysis of variance, SD: Standard deviation

Table 3: Prevalence of fetal posterior cerebral artery

	Male (%)	Female (%)	Total (%)
Isolated fetal PCA			
Right	7	4	11
Left	4	2	6
Total	11	6	17
Bilateral fetal PCA	5	4	9
Total	16	10	26
P		0.000	

ANOVA: Analysis of variance, PCA: Posterior cerebral artery

PCA occlusion or blockage may result in many clinical conditions such as thalamic syndrome and Weber's syndrome, therefore, thorough knowledge of the morphometry will help clinicians to deal with lesions of posterior circulation.[3] It will also enhance knowledge to radiologists and surgeons for proper diagnosis and treatment of the pathology of PCA.

In the present study, diameter of P1 ranged from 1.1 to 4 mm. In majority of arteries (56.5%), it ranged from 2.1 to 3 mm, so we can infer that normal range of diameter of P1 in the UP region of North India is 2.1–3 mm. Patel *et al*. found the range of diameter of PCA to be 2.07–3.6 mm in Gujurat population.[3] The range of diameter of PCA was found to be 0.3 mm to 3.8 mm in a study of 56 formalin fixed brains done by Saha *et al*.[11]

The knowledge about range of normal diameter of arteries is important to acknowledge hypolasia and/or dilatation to avoid any misinterpretation of the clinical condition. Hypoplastic arteries may alter the hemodynamic balance and cause intracranial stroke. Dilated arteries may be a risk factor for development of aneurysms.

The mean diameter of P1 segment of PCA did not show any consistent relation with age groups in the present study. However, Rai *et al*. found a significant increase in arterial caliber of PCA in patients aged ≥60 years compared with those aged 40–59 years which was not in congruence with the present study.[10]

The posterior circulation measurements showed an increase in arterial caliber with age. This baseline information may be useful in planning neurovascular procedures and endovascular device development.[10]

Along the course of our study, various types of variant

forms were encountered which included hypoplasia and fenestration of P1 segment of PCA.

P1 segment hypoplasia was seen in 6% of cases and fenestration was seen in 1% of cases. Gunnal *et al*. found hypoplastic P1 segment in 5.29% and fenestration in 1.17%.[12] Akgun *et al*. also reported fenestrated PCA in 1 case on the left side.[5]

Fenestration is the duplication of a portion of an artery into two separate and parallel channels which rejoin distally.[5] They are rare anomalies which results from incomplete fusion of primitive embryologic vessels. They may be associated with aneurysms, arteriovenous malformations, and venous angiomas.[13]

FPCA was observed in 26% of cases which was of partial FPCA type. Unilateral PCA was observed in 17% of cases and bilateral FPCA in 9% of cases. The present findings were similar to the findings of He and Wan who found unilateral FPCA in 25% and bilateral in 7.4%.[14] Akgun *et al*. found that isolated FPCA was in 3 cases.[5] Pai *et al*. found in 10% cases.[8] Lambert *et al*. reported 2 cases of concurrent inferior cerebellar arteries (ICA)-PCA territory infarction in the setting of a unilateral FPCA.[7]

Blood supply of the PCA on the fetal type side is exclusively from the ipsilateral ICA, or from both the ipsilateral ICA and the BA, but predominantly from the ICA. Under normal circumstances, intracranial blood supply on both sides simultaneously relies on the cervical and vertebral basilar system, and the cerebral blood flow pressure remains similar between both sides. In the case of fetal type, the blood flow of the ICA and vertebral basilar system is unbalanced, leading to a series of hemodynamic changes in circle of Willis components.[11]

Emboli can move up the ICA, enter and occlude the FPCA or its branches, and result in a paradoxical PCA territory infarction with or without occlusion of other ICA branches.[10]

Conclusion

These variations are probably genetically determined and may alter the occurrence, severity of symptoms, treatment options, and recovery from certain cerebrovascular disorders, namely stroke and aneurysms. The present study was focused to provide a nomogram for morphometry of PCA and presence of its normal and anatomical variants. A detailed knowledge of the normal vascular anatomy and its variants is useful to surgeons in planning shunt operations, keeps away inadvertent vascular traumas during surgeries, and avoids potential diagnostic pitfalls.

Acknowledgments

The authors sincerely thank those who donated their bodies to science so that anatomical research could be performed. Results from such research can potentially increase mankind's overall knowledge that can then improve patient care. Therefore, these donors and their families deserve our highest gratitude.

Financial support and sponsorship

Nil.

Conflicts of interest

There are no conflicts of interest.

References

1. Standring S, Anand N, Jawaheer G, Tubbs RS, Birch R, Smith AL, *et al.* Gray's Anatomy. Elsevier; 41st edition, London, UK: 2016.
2. Kuybu O, Dossani RH. Posterior Cerebral Artery Stroke. In: StatPearls. Treasure Island (FL): StatPearls Publishing; 2018: https://www.ncbi.nlm.nih.gov/books/NBK532296/. [Last accessed on 2021 Sep 29].
3. Patel SK, Zalavadiya DI, Patel SV, Vaniya VH. Morphometry of posterior cerebral artery. International Journal of Anatomy, Radiology and Surgery. 2017 Oct ;6(4): AO35-AO37.
4. Bulsara KR, Zomorodi A, Provenzale JM. Anatomic variant of the posterior cerebral artery. AJR Am J Roentgenol 2007;188:W395.
5. Akgun V, Battal B, Bozkurt Y, Oz O, Hamcan S, Sari S, *et al.* Normal anatomical features and variations of the vertebrobasilar circulation and its branches: An analysis with 64-detector row CT and 3T MR angiographies. ScientificWorldJournal 2013;2013:620162.
6. Kovač JD, Stanković A, Stanković D, Kovač B, Šaranović D. Intracranial arterial variations: A comprehensive evaluation using CT angiography. Med Sci Monit 2014;20:420-7.
7. Lambert SL, Williams FJ, Oganisyan ZZ, Branch LA, Mader EC. Fetal-Type Variants of the Posterior Cerebral Artery and Concurrent Infarction in the Major Arterial Territories of the Cerebral Hemisphere. Journal of Investigative Medicine High Impact Case Reports; 2016:1-7.
8. Pai BS, Varma RG, Kulkarni RN, Nirmala S, Manjunath LC, Rakshith S. Microsurgical anatomy of the posterior circulation. Neurol India 2007;55:31-41.
9. Canaz H, Arslan M, Hacioglu H, Tokmak M, Canaz G, Cavdar S. Morphometric analysis of arteries of Willis polygon. Rom Neurosurg 2018;32:56-64.
10. Rai AT, Rodgers D, Williams EA, Hogg JP. Dimensions of the posterior cerebral circulation: An analysis based on advanced non-invasive imaging. J Neurointerv Surg 2013;5:597-600.
11. Saha A, Sarkar A, Mandal S. A cadaveric study of bilateral configuration of posterior bifurcation of posterior communicating artery in Indian population. J Clin Diagn Res 2015;9:C01-4.
12. Gunnal SA, Farooqui MS, Wabale RN. Study of posterior cerebral artery in human cadaveric brain. Anat Res Int 2015;2015:681903.
13. Osborn RE, Kirk G. Cerebral arterial fenestration. Comput Radiol 1987;11:141-5.
14. He Z. Wan Y. Is fetaltype posterior cerebral artery a risk factor for intracranial aneurysm as analyzed by multislice CT angiography. Exp Ther Med 2018;15:838-46.

Original Article

Estimation of Length of Femur from its Distal Segment

Aswathy Maria Oommen, Suja Robert Joseph Sarasammal, Sheena Kalyani Sukumaran

Department of Anatomy, Government Medical College, Thiruvananthapuram, Kerala, India

Abstract

Introduction: The stature of an individual, one of the key elements of identification, can be calculated from the length of long bones in the body, of which the femur has the highest correlation with stature. Many a times, forensic anthropologists have to identify unknown dead bodies from fragments of bones that are available. Studies have proven that the total length of a bone can be estimated from fragments using population-specific regression equations. In the present study, the objective was to estimate the total length of the femur (TFL), in an Indian population, from measurements of its distal segment, using regression equations. **Material and Methods:** One hundred and twenty-one intact adult femurs were studied. The TFL and four variables from its distal segment were measured. Linear regression analysis was performed, and regression equations were derived to calculate the TFL from each of the variables. **Results:** The mean TFL was 41.9 ± 3.4 cm. All the four parameters of the distal segment showed a significant positive correlation with the total femoral length ($P < 0.001$), and of these, the width measured between the two epicondyles showed the maximum correlation. Multivariate and univariate regression equations were derived to estimate the TFL from these variables. **Discussion and Conclusion:** The TFL can be reliably calculated from the measurements of the distal fragments. These measurements can be used by forensic anthropologists for the estimation of the stature of an unknown individual.

Keywords: *Distal fragments, femur, linear regression analysis, regression equations*

Introduction

Age, sex, ancestry, and stature are the four elements of forensic anthropology used to establish the identity of an individual.[1] Stature can be estimated from different bones such as the limb bones, vertebrae, sternum, and skull.[2-9] It is best calculated from the length of long bones of lower limbs, and the femur is the better option.[10] Reconstruction of the length of the femur from fragments of bone that are recovered from scenes of crime, accidents, and burial grounds is an essential step in the estimation of stature in forensic investigations.[9] Physical characteristics of people of different races and ethnicity are different[3,10,11] and hence regression formulae used for estimating the length of femur from fragments must be population specific. In this study, we aimed to drive regression equations for the reconstruction of the length of femur from its distal fragments in an Indian population.

Material and Methods

This study was approved by the Institutional Review Board and Human Ethics Committee of the institution (IEC. No. 11/05/2017/MCT dated November 03, 2017). It was conducted as a cross-sectional study using 121 intact adult femora (right-54 and left-67). Bones with any gross deformities or damages were not included in the study. Age, ethnicity, and sex were not known. The length of femur was measured using an osteometric board, and all other measurements were taken with digital vernier calipers.

Five variables were measured [Figures 1a-d]:

1. TFL - Total length of femur. It was measured from the highest point on the head of femur to the lowest point on the condyles The other four measurements were taken from the distal end of femur.
2. WE - Width of the lower end of femur, measured between the two epicondyles
3. MAP - Anteroposterior length of the medial condyle, measured between the most convex points, anteriorly and posteriorly

How to cite this article: Oommen AM, Sarasammal SR, Sukumaran SK. Estimation of length of femur from its distal segment. J Anat Soc India 2022;71:30-3.

Article Info

Received: 17 September 2020
Accepted: 27 October 2021
Available online: 17 March 2022

Address for correspondence:
Dr. Suja Robert Joseph Sarasammal,
Ebenezer, JNPRA 76,
Jayaprakash Lane,
Kudappanakunnu,
Thiruvananthapuram, Kerala, India.
E-mail: sujarobert@gmail.com

Access this article online

Website: www.jasi.org.in
DOI: 10.4103/jasi.jasi_190_20
Quick Response Code:

4. LAP - Anteroposterior length of the lateral condyle, measured between the most convex points, anteriorly and posteriorly
5. WIC - Width of the intercondylar notch.

Quantitative variables were expressed as a minimum, maximum, mean, and standard deviation. Comparison of quantitative variables between the right and left was analyzed using independent sample *t*-test. $P < 0.05$ was considered statistically significant. The relationship between TFL and each of the other four quantitative variables was analyzed by Pearson's correlation analysis. $P < 0.05$ was considered statistically significant. Linear regression formulae were derived to estimate TFL from measurements of the different variables. Data analysis was performed using trial versions of the IBM Corp. Released 2013. IBM SPSS Statistics for Windows, Version 22.0. Armonk, NY: IBM Corp.

Results

The total length and the dimensions of the different variables of 121 femora (54-right and 67-left) were measured, subjected to statistical analysis, and compared. Comparison of quantitative variables between right and left showed that the difference was statistically insignificant [Table 1]. None of the variables qualified for discriminant analysis. The mean TFL was 41.9 ± 3.4 cm. Pearson's correlation done to analyze the correlation between TFL and each of the other four quantitative variables was statistically significant ($P < 0.05$). Descriptive statistics of the measurements of the variables of femur are tabulated in Table 2.

Linear regression analysis was done to establish the relationship of TFL with the different variables at the lower end of femur. All the four parameters of the distal segment that were measured showed a significant positive correlation with the TFL ($P < 0.001$). Of these, WE showed the maximum correlation. Linear regression equations were derived for the estimation of the length of femur from the measured variables. Correlation coefficients ranged from 0.338 to 0.693, with WE showing the highest and WIC the least values [Table 3]. Regression model from multivariate analysis reveals that R^2 is 0.584, i.e., 58% variation in TFL could be explained by these measurements.

Multivariate equation: TFL = 12.268+ (1.893 × WE) + (1.356 × MAP) + (1.684 × LAP) − (.226 X WIC)

Univariate equations:
1. TFL = 15.672 + (3.767 × WE)
2. TFL = 21 + (3.905 × MAP)

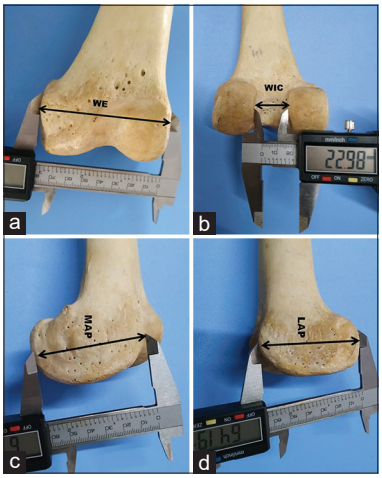

Figure 1: (a) The measurement of the distance between the two epicondyles (WE). (b) The measurement of the width of the intercondylar notch (WIC). (c) The measurement of the anteroposterior length of medial condyle (MAP). (d) The measurement of the anteroposterior length of lateral condyle (LAP)

Table 1: Independent sample *t*-test to compare the quantitative variables of the right and left femora

Parameter	Mean±SD			*t*	*P*
	Right (*n*=54)	Left (*n*=67)	Total (*n*=121)		
TFL	41.7±3.0	41.9±3.7	4.18±0.34	−0.178	0.859
WE	7.11±0.66	7.04±0.63	7.07±0.64	−0.932	0.353
MAP	5.41±0.58	5.26±0.59	5.33±0.59	−1.714	0.089
LAP	5.57±0.50	5.70±0.66	5.64±0.60	0.695	0.488
WIC	2.18±0.33	2.16±0.41	2.17±0.38	−0.085	0.933

All measurements are in cm. TFL: Total length of femur, WE: Width of the lower end of femur, measured between the two epicondyles, MAP: Anteroposterior length of medial condyle, LAP: Anteroposterior length of lateral condyle, measured between the most convex points, WIC: Width of the intercondylar notch, SD: Standard deviation

Table 2: Descriptive statistics of measurements of femur

Parameter	*n*	Mean±SD (cm)
TFL	121	41.9±3.40
WE	121	7.08±0.64
MAP	121	5.33±0.58
LAP	121	5.64±0.59
WIC	121	2.16±0.37

WE: Width of the lower end of femur, measured between the two epicondyles, MAP: Anteroposterior length of medial condyle, LAP: Anteroposterior length of lateral condyle, measured between the most convex points, WIC: Width of the intercondylar notch, SD: Standard deviation

Table 3: Linear regression analysis to estimate the total length of femur from the variables measured from the distal segment of femur

Parameter	Equation	*R*	R^2	SE
WE	TFL=15.672 + (3.767 × WE)	0.693**	0.481	2.466
MAP	TFL=21 + (3.905 × MAP)	0.660**	0.435	2.572
LAP	TFL=19.782 + (3.922 × LAP)	0.675**	0.456	2.524
WIC	TFL=35.15 + (3.125 × WIC)	0.338**	0.114	3.222

**$P<0.001$. WE: Width of the lower end of femur, measured between the two epicondyles, MAP: Anteroposterior length of medial condyle, LAP: Anteroposterior length of lateral condyle, measured between the most convex points, WIC: Width of the intercondylar notch, SE: Standard error, TFL: Total length of femur

3. TFL = 19.782 + (3.922 × LAP)
4. TFL = 35.15+ (3.125 × WIC).

Discussion

Estimation of the antemortem stature of an unknown individual is an important aspect of forensic anthropological investigations and was described way back in 1878 by Thomas Dwight in his essay on "Identification of the human skeleton."[12] Later in 1956, Georges fully developed the "anatomical method" and used all bones from the skull to calcaneum to reconstruct the stature of an individual.[13] Karl Pearson developed the first formal stature regression formula to estimate stature.[14] A method of estimating stature from long bones was also developed by Totter and Glesser.[10,15] They derived regression equations from the length of long bones and calculated stature (mathematical method). There is the most commonly used method for stature estimation.[8,10]

Airplane crashes, bomb blasts in crowded locations, mass fatalities and natural disasters, exhumation of skeletonized human bodies or individual parts that are days or even months old are not a rarity nowadays. Usually, an intact skeleton is not obtained from the scene of an accident or crime, and the actual length of bones must be estimated from the fragments of bone that are obtained. Assuming that the height of an individual is dependent on the length of long bones, stature is estimated from the projection of length of long bones using regression formulae specific for that population for identification of the individual.

In the present study, measurements were taken from the distal segment of femur. The TFL was also measured. There is a difference in the lengths of the right and left side bones. However, studies have shown that the difference in length of femur of the right and left sides is statistically insignificant.[3,16,17] A comparison between the variables of the right and left sides in the present study also showed that it was not statistically significant. The TFL measured in the present study and other studies are shown in Table 4. Steele and McKern studied long bones such as femur, tibia, and humerus in a sample obtained from archaeological sites in the Southeastern United States.[18] Regression formulae were established to obtain the length of the long bones from various fragments. Jubilant Kwame Abledu worked on a Ghanaian population to reconstruct the length of femur.[9] Measurements were taken from both proximal and distal fragments. Of all the segments measured, subtrochanteric transverse diameter measured between the medial and lateral surfaces at the proximal end of the diaphysis just below the lesser trochanter was found to be the best estimator of femoral length. Bidmos MA did a study on complete skeletons obtained from a South African population of European descent to reconstruct stature from fragmentary femora.[23,25]

Studies were also conducted in the Indian population. Sandeep Singh calculated femoral length from measurements of the intertrochanteric crest in a Central Indian population.[20] Solan's work was on femora obtained from a South Indian population.[21] Total femoral length and various dimensions from the proximal and distal end of femur were measured. Parmar *et al*. study was also on the reconstruction of femoral length from both proximal and distal fragments. The sample was obtained from Rajasthan, India.[22] Regression equations were derived for different variables, including the distance between medial and lateral epicondyles, as in the present study. In all these studies, the length of femur measured was higher than values obtained in the present study, reinforcing the fact that the length of bones is population specific.

Shroff *et al*. measured the length of the femur from various fragments, and results obtained for the length of femur were comparable to the present study.[19] Mukhopadhyay correlated the maximum length of femur from epicondylar breadth in a population of West Bengal, India. The results were consistent with the present study.[24]

Linear regression equations were derived from the variables to predict the length of femur. There is a significant positive

Table 4: Comparison of the total length of femur in the different studies

Name of authors	Total length of femur (cm), mean±SD
Steele and McKern[18]	Male-44.90 (1.71) Female-41.51 (1.28)
Shroff *et al*.[19]	42.01 (2.75)
Singh *et al*.[20]	43.26 (2.67)
Solan and Kulkarni[21]	43.48 (2.60)
Parmar *et al*.[22]	Right-43.24 (3.38) Left-44.45 (2.36)
Abledu *et al*.[9]	449.7 (23.4) (measured in mm)
Bidmos[23]	Male-465.22 (27.56) (measured in mm) Female-433.80 (22.18) (measured in mm)
Mukhopadhyay *et al*.[24]	41.82 (3.05)
Present study	41.90 (3.4)

SD: Standard deviation

Table 5: Comparison of linear regression equations derived for calculating total length of femur from the epicondylar breadth (measured between the medial and lateral epicondyles of femur)

Name of authors	Regression equation for estimating femoral length
Parmar *et al*.[22]	Right-13.19 + (3.96 × D_1) Left-27.70 + (2.15 × D_1)
Abledu *et al*.[9]	187.80 + (3.39 × EB) (measured in mm)
Mukhopadhyay *et al*.[24]	7.02 + (4.83 × x)
Khanal *et al*.[16]	22.45 + (2.60 × ECB)
Present study	15.672 + (3.767 × WE)

D_1, EB, x, ECB, WE – all these variables denote epicondylar breadth. (In the present study also, WE refers to 'width of the lower end of femur, measured between the two epicondyles' i.e., epicondylar breadth).EB: epicondylar breadth, ECB: epicondylar breadth

correlation between each of these measurements and TFL. The error estimates of the linear regression equations were low (2.466–3.222) indicating that the difference between the calculated and actual TFL was comparatively low. Compared to all the other parameters, WE were the best parameter to assess TFL. The regression equations of this study and other similar studies that have measured variables from the fragments of femur are shown in Table 5.

Conclusion

From this study, regression equations were derived to calculate the length of femur from fragments of its distal segment that may be recovered from a scene of crime or accidents. From the calculated length of femur, it is possible to obtain the height of the individual using formulae that are available. It will be quite appropriate to conclude that these formulae will prove to be extremely helpful to forensic anthropologists and archaeologists as well as anatomists everywhere.

Financial support and sponsorship

Nil.

Conflicts of interest

There are no conflicts of interest.

References

1. Swanson CR, Chamelin NC, Territo L. Criminal Investigation. Noida, India: McGraw-Hill; 2003.
2. Jantz RL, Kimmerle EH, Baraybar JP. Sexing and stature estimation criteria for Balkan populations. J Forensic Sci 2008;53:601-5.
3. Hauser R, Smoliński J, Gos T. The estimation of stature on the basis of measurements of the femur. Forensic Sci Int 2005;147:185-90.
4. De Mendonça MC. Estimation of height from the length of long bones in a Portuguese adult population. Am J Phys Anthropol 2000;112:39-48.
5. Dayal MR, Steyn M, Kuykendall KL. Stature estimation from bones of south African whites. S Afr J Sci 2008;104:124-8.
6. Mall G, Hubig M, Büttner A, Kuznik J, Penning R, Graw M. Sex determination and estimation of stature from the long bones of the arm. Forensic Sci Int 2001;117:23-30.
7. Menezes RG, Kanchan T, Kumar GP, Rao PP, Lobo SW, Uysal S, *et al*. Stature estimation from the length of the sternum in South Indian males: A preliminary study. J Forensic Leg Med 2009;16:441-3.
8. Pelin IC, Duyar I. Estimating stature from tibia length: A comparison of methods. J Forensic Sci 2003;48:708-12.
9. Abledu JK, Offei EB, Osabutey CK. Reconstruction of femoral length from fragmentary femora. Anat Cell Biol 2016;49:206-9.
10. Trotter M, Gleser GC. A re-evaluation of estimation of stature based on measurements of stature taken during life and of long bones after death. Am J Phys Anthropol 1958;16:79-123.
11. Chikhalkar B, Mangaonkar A, Nanandkar S, Peddawad R. Estimation of stature from measurements of long bones, hand and foot dimensions. J Indian Acad Forensic Med 2010;32:329-33.
12. Thomas D. Methods of estimating the height from parts of the skeleton. Med Rec (1866-1922) 1894;46:293.
13. Fully G. New method of determination of the height. Ann Med Leg Criminol Police Sci Toxicol 1956;36:266-73.
14. Pearson, Karl. "Mathematical Contributions to the Theory of Evolution. V. On the Reconstruction of the Stature of Prehistoric Races." *Philosophical transactions - Royal Society. Mathematical, physical and engineering sciences* 192: 169-244.
15. Trotter M, Gleser GC. Estimation of stature from long bones of American Whites and Negroes. Am J Phys Anthropol 1952;10:463-514.
16. Khanal L, Shah S, Koirala S. Estimation of total length of femur from its proximal and distal segmental measurements of disarticulated femur bones of Nepalese population using regression equation method. J Clin Diagn Res 2017;11:C01-5.
17. Lee JH, Kim YS, Jeong YG, Lee NS, Han SY, Tubbs RS, *et al*. Sex determination from partial segments and maximum femur lengths in Koreans using computed tomography. Folia Morphol (Warsz) 2014;73:353-8.
18. Steele DG, McKern TW. A method for assessment of maximum long bone length and living stature from fragmentary long bones. Am J Phys Anthropol 1969;31:215-27.
19. Shroff A, Panse A, Diwan C. Estimation of length of femur from its fragments. J Anat Soc India 1999;48:1-5.
20. Singh S, Nair SK, Anjankar V, Bankwar V, Satpathy D, Malik Y. Regression equation for estimation of femur length in central Indians from inter-trochanteric crest. J Indian Acad Forensic Med 2013;35:223-6.
21. Solan S, Kulkarni R. Estimation of total length of femur from its fragments in south Indian population. J Clin Diagn Res 2013;7:2111-5.
22. Parmar AM, Shah KP, Goda J, Aghera B, Agarwal G. Reconstruction of total length of femur from its proximal and distal fragments. Int J Anat Res 2015;3:1665-8.
23. Bidmos MA. Stature reconstruction using fragmentary femora in south Africans of European descent. J Forensic Sci 2008;53:1044-8.
24. Mukhopadhyay PP, Ghosh TK, Dan U, Biswas S. Correlation between maximum femoral length and epicondylar breadth and its application in stature estimation: A population specific study in Indian Bengali males. J Indian Acad Forensic Med 2010;32:204-7.
25. Bidmos MA. Fragmentary femora: Evaluation of the accuracy of the direct and indirect methods in stature reconstruction. Forensic Sci Int 2009;192: 5.e1-5.

Original Article

Effects of Maternal Iron Deficiency Anemia on Placenta and Cord Blood Iron Status with Specific Reference to the Iron Transport Protein Ferroportin 1

Abstract

Introduction: Iron deficiency anemia is the most prevalent nutritional deficiency disorder in pregnant women. During pregnancy, nutrients, including iron, are transferred from the mother to the fetus through the placenta, in which the placental transport protein Ferroportin1 (FPN1) plays a crucial role. It has been frequently observed that developing fetus is immune to anemia despite the presence of anemia in the mother, the mechanisms underlying which have not been identified. We, therefore, planned the present study to explore the effect of maternal iron deficiency anemia on the expression of FPN1 in the placenta. **Material and Methods:** Two hundred pregnant women recruited were divided into anemic and nonanemic groups based on their predelivery hemoglobin levels (<11 g/dl and ≥11 g/dl, respectively). After delivery, placental expression of FPN1 was studied by immunohistochemistry and mRNA analysis, and neonatal anthropometry was performed. **Results:** Of the 200 women, 59% were anemic. FPN1 protein immunohistochemical staining in placenta showed a statistically significant increase with increasing severity of anemia. Similarly, placental mRNA expression levels of the FPN1 gene were observed to be higher in anemic mothers when compared with nonanemic mothers. **Discussion and Conclusion:** Thus, our study for the first time shows that maternal iron deficiency increases placental FPN1 protein and mRNA expression, thereby probably facilitating increased transport of iron from the mother to the fetus.

Keywords: *Anaemia, cord blood, ferroportin1, iron deficiency, pregnancy*

Shravanthi Gadhiraju, Thathapudi Sujatha[1], Uday Kumar Putcha[1], Mullapudi Venkata Surekha[2]

Department of Obstetrics and Gynecology, Gandhi Hospital, Secunderabad, [1]Division of Pathology and Microbiology, National Institute of Nutrition, [2]Division of Pathology and Microbiology, National Institute of Nutrition (Indian Council of Medical Research), Hyderabad, Telangana, India

Introduction

Iron deficiency anemia is the most prevalent nutritional deficiency disorder in the world.[1] According to WHO, globally, 38.2% of pregnant women are affected by anemia,[2] leading to low birth weight and increased risk of maternal and perinatal mortality.[3]

During pregnancy, the placenta forms an interface between the mother and the fetus, and the nutrients are transported from the mother to the fetus through specialized nutrient transporters located on the placental villi.[4] Ferroportin (FPN) is a transmembrane protein that transports iron from inside the cell to outside and is the only known iron exporter.[5] In the placental syncytiotrophoblast cells, iron is transferred across the cell and is released into fetal circulation with the help of FPN.

Maternal iron deficiency leads to the development of anemia in the developing fetus; however, it is observed that the degree of deficiency seen in the fetus is of lesser severity than that of the mother, but the mechanisms behind this adaptation have not been identified. Our earlier study showed interesting results in which we observed newborns of anemic mothers had normal blood cell parameters despite the presence of anemia in mothers. Literature search performed by us revealed few to nil studies on FPN1 expression in the placenta in the condition of maternal iron deficiency. Thus, we planned this study to investigate the effect of maternal iron deficiency anemia on the expression levels of FPN1 in the placenta.

Material and Methods

This was a cross-sectional study in which 200 pregnant women in their third trimester of pregnancy, attending the Obstetrics and Gynecology Department of Gandhi hospital, Hyderabad, for

How to cite this article: Gadhiraju S, Sujatha T, Putcha UK, Surekha MV. Effects of maternal iron deficiency anemia on placenta and cord blood iron status with specific reference to the iron transport protein ferroportin 1. J Anat Soc India 2022;71:34-41.

Article Info

Received: 17 August 2020
Accepted: 30 September 2021
Available online: 17 March 2022

Address for correspondence:
Dr. Mullapudi Venkata Surekha, Division of Pathology and Microbiology, National Institute of Nutrition (Indian Council of Medical Research), Jamai-Osmania, Tarnaka, Hyderabad - 500 007, Telangana, India.
E-mail: surekha_mv@yahoo.com

Access this article online

Website: www.jasi.org.in
DOI: 10.4103/jasi.jasi_158_20
Quick Response Code:

their delivery, were enrolled. The institutional ethical committee report of both the National Institute of Nutrition (NIN) and Gandhi hospital was obtained before the start of the study.

The subjects, found to be anemic on admission, were asked to participate in the study after signing an informed consent form. Information on sociodemographic factors, dietary intake and clinical status was collected. The weight, height, and body mass index (BMI) were also noted.

Study groups

Anemic group

Pregnant women with Hb <11 g/dL as defined by the World Health Organization.

Nonanemic group

Healthy pregnant women with Hb ≥11 g/dL.

Inclusion criteria

18–45 years age, 36–42 weeks of gestation, and single pregnancy (primiparous or multiparous).

Exclusion criteria

Hemolytic anemia, hypertension, diabetes mellitus, thyroid disease and HIV, hepatitis C virus, and hepatitis B surface antigen positive women.

Sociodemographic and anthropometric information

Using a well-designed questionnaire, information on age, family history, socioeconomic status, and clinical history of the subjects were obtained. Weight and height of the mothers were recorded for calculating BMI. After birth, anthropometric measurements of newborns were noted.

Sample collection and processing

1. About 10 ml of blood was drawn before delivery from the mothers and collected in ethylenediaminetetraacetic acid and plain vacutainers (Beckton Dickinson). After delivery, 10 ml of cord blood was collected in similar types of vacutainers, and both maternal and cord blood samples, after collection, were immediately transported in ice to Pathology lab of NIN
2. Collection of placentas
   The placentas were collected within 30 min of delivery. For m-RNA analysis, fresh samples were collected from the maternal side, within 5 cm of the radius of the umbilical cord insertion, omitting the membranous layer, about 1 cm deep below the surface and kept in vials containing 5 ml of RNA later solution and stored at −80°C until further analysis.
3. Histopathology of placentas
   After collection of samples for m-RNA analysis, the remaining whole placentas were stored at room temperature, in containers filled with 10% neutral buffered formalin.
4. Parameters studied in maternal and cord blood Hb, red cell indices, and ferritin.
5. Parameters studied in the placenta
   i. Weight, size, gross anomalies, histomorphology (ii) FTN-1 expression by immunohistochemistry and m-RNA analysis (iv) cord length, morphology.
6. Parameters studied in the Newborns
   Weight, crown-rump length, head, mid-arm circumference, and skinfold thickness.
7. Hemoglobin estimation and complete blood count (CBP) was performed within 06 h of sample collection, in an automated Coulter counter (ADVIA 120, Seimens). Hb, differential count, total leukocyte count (TLC), red blood cell count (RBC), mean corpuscular volume (MCV), mean corpuscular hemoglobin (MCH), MCH concentration (MCHC), red cell distribution width (RDW), and hemoglobin distribution width (HDW) were analyzed. The serum was separated and stored at −80°C until further analysis for ferritin.
8. Estimation of serum ferritin by ELISA method
   Serum ferritin was estimated using ferritin SA ELISA kit of Calbiotech, Inc., which uses solid phase sandwich assay method, based on the streptavidin-biotin principle.
9. Histopathology

The placentas were weighed after removal of cords and membranes, their size, shape, and gross findings were noted. After overnight fixation in 10% neutral buffered formalin, four sections were taken, about 5 cm from within the radius of insertion of the cord, away from the margins, and close to the maternal surface. The tissues were processed in an automatic tissue processor (Shandon), embedded in paraffin, and their 5 μ thick sections taken.

The immunohistochemical expression for FPN-1proteinwas studied in formalin-fixed and paraffin-embedded placental tissues. The primary antibody used was polyclonal rabbit SLC40A1from Biorbyt, and the secondary antibody was Dako Real Flex Mini Envision Detection with Peroxidase/ Wash buffer/Antigen retrieval buffer/DAB+, Rb/Mo One-Step Method. The stained sections were studied under a light microscope (Nikon Eclipse E800) by two histopathologists, and relevant images were captured in a digital camera attached to the microscope.

Immunohistochemical analysis

Immunoreactivity was classified by estimating the percentage (P) of placental trophoblast cells showing the characteristic staining (from an undetectable level or 0%, to homogeneous staining or 100%) and by estimating the intensity (I) of staining (1 – weak staining, 2 – moderate staining, and 3 – intense staining). Results were scored by multiplying the percentage of positive cells by the intensity, i.e., by the so-called quick score (Q) ($Q = P \times I$; maximum = 300).[6]

9. Real-time polymerase chain reaction (RT-PCR) analysis of FPN1 gene.

The mRNA expression of FPN1 gene was analyzed using the manual Trizol method. About 20 mg of placental tissue was treated with 1 ml of the TRI reagent in a 1.5 ml microcentrifuge tube. The isolated RNA's quantity and purity were measured spectrophotometrically by measuring the OD at absorbance ratios of 260/280 and 260/230, respectively, using Nanodrop 2000c spectrophotometer (Thermoscientific). The RNA isolated (1 ug) per target was treated with DNase1, according to the manufacturer's instructions. The total RNA (200 ng) was reverse-transcribed into cDNA by using the transcriptor cDNA synthesis kit (Bio-Rad). Reverse transcription reaction was carried out using a thermocycler (Applied Biosystems), under the following conditions; 25°C for 5 min, 46°C for 20 min, 95°C for 1 min with a hold at 4°C. RT-PCR reactions were carried out using light cycler CFX 96 (Bio-Rad), and each reaction contained 0.5 µl of the primer (Bioartis), 10 µl 2x SYBR Green PCR Mastermix (Thermoscientific), 8 µl of nuclease-free water, and 1 µl of 15 ng/µl of cDNA in a 15 µl reaction. The PCR reactions were set at 95°C for 3 min, 95°C for 15 s, and finally 57°C for 30 s (40 repeats). The results were obtained as cycle threshold, and single melt curves were obtained for all samples, indicating that a single PCR product was generated. β-actin was used as an endogenous control gene with relative expression of a gene expressed as $2^{-\Delta CT}$. Each sample was pipetted into 96-well plates were run in duplicate. Negative control of PCR-grade H_2O and positive control (human placental tissues) were used. The primer was designed using National Center for Biotechnology Information sequence ID and purchased from Bio-Artis: Ferroportin: Forward: 5'-TTACCAGAAAACCCCAGCTC-3', reverse 5'-CAGGGGTTTTGGCTCAGT AT-3' and β-actin: Forward: 5′-CCAACCGCGAGAAGA TGA-3′, reverse: 5′-CCA GAG GCG TAC AGG GAT AG-3′.Plate-to-plate variation was controlled by normalizing gene expression to β-actin and control by using the ΔΔCT method.[7]

Statistical analysis

Assuming a 95% confidence interval, a prevalence of 15% anemia in newborns and the margin of error being 5%, the required sample size calculated was 196.

Data processing and statistical analyses were performed using SPSS version 19.0 (SPSS Inc., Chicago, IL, USA). Continuous data were summarized as means ± standard deviation (SD) and categorical data as numbers (%). Descriptive statistics such as mean, SD, and prevalence were calculated for all variables. Mean values for all variables were compared by unpaired *t*-test across both healthy and anemia groups. Correlation coefficients calculated relationships between Hb, MCV, MCH, MCHC, RBC, RDW, HDW, serum ferritin. and Chi-square test was performed for associations. A nonparametric test was done wherever required. Pearson's correlation analysis was carried out to evaluate the correlation between different variables. The level of significance was considered as 0.05.

Results

Nearly 59% of the pregnant mothers recruited were anaemic among with 60% having moderate anaemia, 28% mild anaemia and 12% severe anaemia.

Table 1 shows that 72% of the women were in the age group of 18–23 years, among whom 38% are anemic. A BMI >23 was observed in 75% of the women. Nineteen women (9.6%) were college educated, whereas 89 (45.2%) each were illiterate and school educated. 53 (59.6%) of these illiterate women were anemic. Among the 171 (86.8%) unemployed women, 60.2% were anemic. The monthly family income of 68.7% was between Rs. 5000 and 10,000. Maternal red cell parameters are displayed in Table 2, in which Hb, RBC count, PCV, MCV, MCH, and MCHC including serum ferritin are significantly lower in anemic mothers, while RDW and HDW values are significantly higher. Table 3 shows that Hb, PCV, RBC,

Table 1: Sociodemographic and economic characteristics of pregnant women

Variables	Values	Anaemic mothers (Hb <11 g/dl), *n* (%)	Nonanaemic mothers (Hb ≥11 g/dl), *n* (%)	All mothers, *n* (%)	*P*
Age (years)	18-23	37 (38.5)	59 (61.5)	96 (100)	0.52
	>23	9 (31)	29 (69)	29 (100)	
BMI (kg/m^2)	<18.5	0 (0)	1 (100)	1 (100)	0.55
	18.5-23	16 (33.3)	32 (66.7)	48 (100)	
	>23	66 (44.3)	83 (55.7)	149 (100)	
Education status	Illiterate	53 (59.6)	36 (40.4)	89 (100)	0.13
	Schooling	48 (53.9)	41 (46.1)	89 (100)	
	College	15 (78.9)	4 (21.1)	19 (100)	
Occupation	Working	13 (50)	13 (50)	26 (100)	0.39
	Not-working	103 (60.2)	68 (39.8)	171 (100)	
Monthly income of family (Rs.)	<5000	9 (69.2)	4 (30.8)	13 (100)	0.65
	5000-10,000	80 (58.8)	56 (41.2)	136 (100)	
	10,000-50,000	27 (55.1)	22 (44.9)	49 (100)	

P value was considered significant if $P<0.05$. BMI: Body mass index, Hb: Haemoglobin

Table 2: Blood cell parameters in anaemic and nonanaemic pregnant women

Variables	Anaemic mothers (Hb <11 g/dl)	Nonanaemic mothers (Hb ≥11 g/dl)	All mothers	*P*
Hb (g/dl)	8.86±1.54 (3.7-10.9)	12.44±1.09 (11-15.4)	10.33±2.23 (3.7-15.4)	0.00***
RBCs (/L)	11.38±4.97 (1.08-5.16)	13.33±4.79 (2.84-0.09)	12.18±4.97 (1.08-5.16)	0.00***
PCV (%)	25.48±5.02 (9.30-2.60)	35.55±31.91 (24.80-323.00)	29.6±21.30 (9.30-323.00)	0.00**
MCV (fl)	71.61±10.63 (44.79-118.00)	75.49±7.90 (60.50-103.00)	73.20±9.77 (44.79-118.00)	0.00**
MCH (pg)	25.11±4.47 (15.00-42.60)	29.35±3.17 (22.30-38.90)	26.85±4.49 (15.00-42.60)	0.00***
MCHC (g/dl)	35.02±4.00 (24.17-49.70)	39.00±3.46 (31.70-45.30)	36.65±4.26 (24.17-49.70)	0.00***
RDW (%)	16.85±2.85 (11.70-24.80)	14.64±2.53 (10.70-24.00)	15.94±2.93 (10.70-24.80)	0.00***
HDW (%)	3.76±1.49 (0.96-14.60)	3.72±1.52 (1.06-13.40)	3.74±1.50 (0.96-14.60)	0.88
Ferritin (ng/ml)	16.70±23.50 (1.04-147.30)	32.15±28.87	23.07±26.88 (1.04-147.3)	0.00***

*P<0.05, **P<0.01, ***P<0.001. All values are in mean±SD and those within brackets are in the range. Hb: Haemoglobin, RBC: Red blood cells, PCV: Packed cell volume/hematocrit, MCV: Mean corpuscular volume, MCH: Mean corpuscular haemoglobin, MCHC: Mean corpuscular haemoglobin concentration, RDW: Red cell distribution width, HDW: Hemoglobin distribution width, SD: Standard deviation

Table 3: Comparison of blood cell parameters between cord blood of newborns of anaemic and nonanaemic mothers

Variables	Cord blood anaemic mothers (Hb <11 g/dl)	Cord blood nonanaemic mothers (Hb ≥11 g/dl)	Total (n=191)†	*P*
Hb (g/dl)	15.83±2.08 (11.10-23.30)	15.63±2.25 (7.40-21.70)	15.75±2.15 (7.40-23.30)	0.51
RBCs (/L)	4.37±0.52 (3.27-5.80)	4.31±0.56 (2.12-5.49)	4.35±0.54 (2.12-5.80)	0.46
PCV (%)	42.42±7.85 (21-65.8)	39.47±6.75 (18.8-58)	41.22±7.54 (18.8-65.8)	0.00**
MCV (fl)	97.17±11.54 (73.6-146.4)	91.6±9.97 (65.1-116.4)	94.9±11.24 (65.1-146.4)	0.00**
MCH (pg)	36.23±2.29 (28.1-45.1)	36.23±2.92 (25.1-45.4)	36.23±2.56 (25.1-45.4)	0.99
RDW (%)	15.45±2.77 (9.9-25.8)	16.1±3.34 (10.3-32)	15.73±3.03 (9.9-32)	0.12
Cord ferritin (ng/ml)	96.94±79.05 (5.57-352.7)	134.72±87.87 (11.36-478.90)	112.46±84.65 (5.57-478.9)	0.00**

*P<0.05, **P<0.01, ***P<0.001. †The cord blood of the remaining nine newborns was clotted and hence could not be analyzed. All values are in mean±SD, and those within brackets are in the range. Hb: Hemoglobin, RBC: Red blood cells, PCV: Packed cell volume/hematocrit, MCV: Mean corpuscular volume, MCH: Mean corpuscular hemoglobin, MCHC: Mean corpuscular hemoglobin concentration, RDW: Red cell distribution width, HDW: Hemoglobin distribution width, SD: Standard deviation

MCV, and MCH are higher while serum ferritin levels are significantly lower in cord blood of anemic mothers. Table 4 shows that all neonatal anthropometric parameters are lower in newborns of anemic mothers. Pearson's correlations in Table 5 highlight the negative correlation of maternal Hb with cord blood Hb, but significant positive correlation with cord blood ferritin. Cord blood Hb shows a negative correlation with maternal ferritin.

Graph 1 shows that serum ferritin values were significantly lower in anemic mothers. Graph 2 shows that, among the different grades of anaemia, serum ferritin is lowest in severe anaemia. Graph 3 shows higher levels of serum ferritin in cord blood when compared to the mother's blood. Graph 4 shows a statistically significant increase in immunohistochemical staining for FPN1 in placental cells with increasing severity of anemia. Graph 5 demonstrates that mRNA expression of FPN1 gene is higher in anemic women in comparison to nonanemic women.

Figures 1–4 show the immunohistochemical staining in trophoblasts, which was observed to be weak in mild anemia and strongly positive in severe anemia.

Table 4: Anthropometric data of newborns of anemic and nonanemic mothers

Variables	Anemic group	Nonanemic group	*P*
Placental weight (g)	416.03±90.65	422.82±91.66	0.609
Birth weight (kg)	2.80±0.38	2.87±0.49	0.258
Crown-rump length (cm)	30.48±1.47	30.52±1.68	0.882
Skinfold thickness (cm)	1.24±0.19	1.27±0.26	0.300
Head circumference (cm)	30.70±1.48	30.78±1.65	0.702
Mid-arm circumference (cm)	12.90±1.09	12.91±1.17	0.937

All values are in mean±SD. SD: Standard deviation

Discussion

The placenta is an essential organ for the development of a fetus and forms an interface for nutrient transfer between the mother and the fetus. Iron transfer from mother to fetus takes place across the placenta with the help of iron transport proteins.[8] Surprisingly, the fetus seldom seems to develop anemia, despite the presence of maternal anaemia.

The WHO considers anemia in pregnant women as a serious public health problem when the prevalence is higher than 40%. We enrolled 200 pregnant women in the present study, 59% of whom were anemic. The prevalence of anemia observed in our study was higher than the National prevalence of 50.3% and 49.8% state prevalence.[9] However, other studies have reported a lower prevalence of anemia.[10,11] The high prevalence of anemia is an important finding in our study indicating that maternal anemia is still

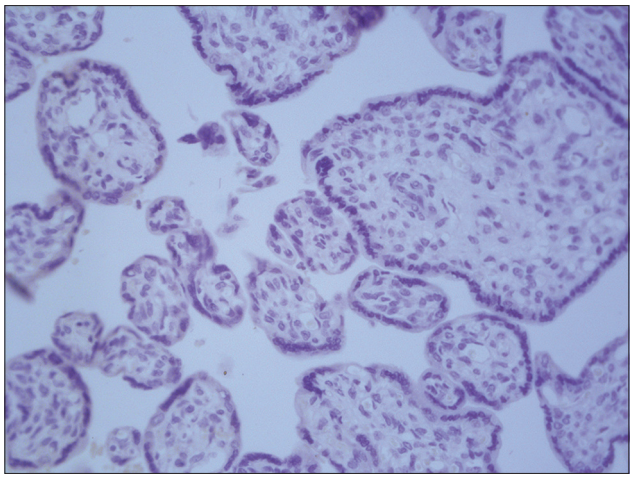

Figure 1: Microphotograph is of negative control, in which the trophoblastic cells show no immunostain as the only secondary antibody is added (×40)

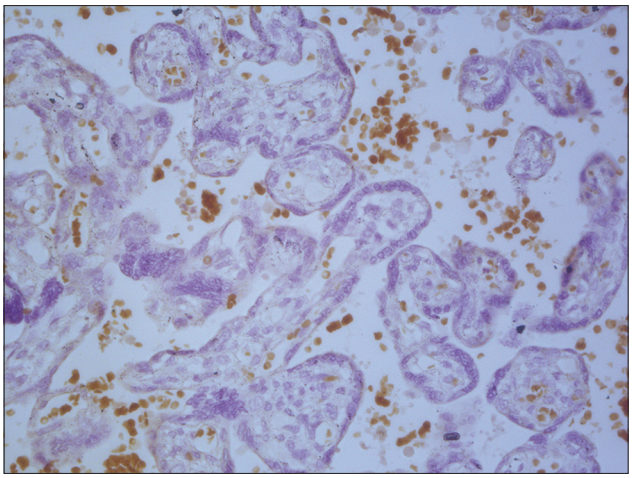

Figure 2: Microphotograph shows immunostaining for ferroportin in placentas from mothers with mild anemia. A mild degree of immunostaining is observed in the cytoplasm of the trophoblastic cells. Ferroportin immunostain; (×40)

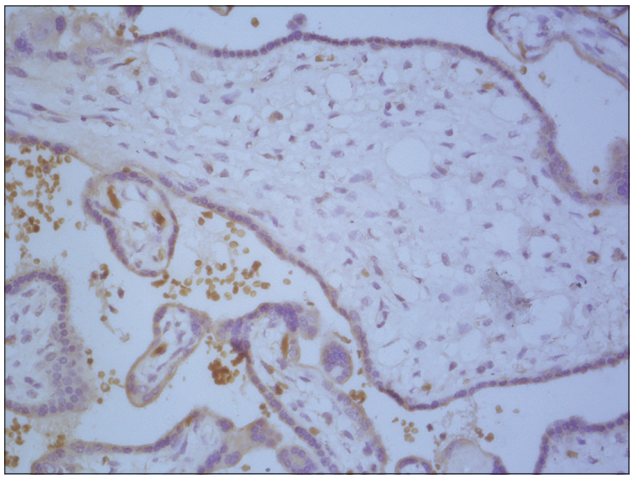

Figure 3: Microphotograph shows immunostaining for ferroportin in placentas from mothers with moderate anemia. A moderate degree of immunostaining is observed in the cytoplasm of the trophoblastic cells. Ferroportin immunostain; (×40)

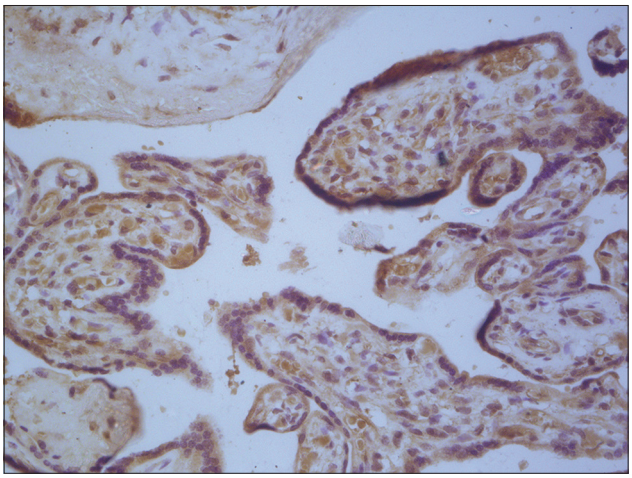

Figure 4: Microphotograph shows immunostaining for ferroportin in placentas from mothers with severe anemia. Intense staining is observed in the cytoplasm of the trophoblastic cells. Ferroportin immunostain; (×40)

a rampant problem in our part of the country, which needs to be tackled at the community level at the earliest. The majority (60%) of women presented with moderate anemia, followed by 28% with mild anemia and the least (12%) with severe anemia. Contrary to the present study, other studies, however, reported mild anemia being the most common.[9,12-14] The reason for the higher incidence of moderate anemia (60%), in our study, could be either poor compliance of the women in taking iron and folic acid tablets supplied by the government or associated Vitamin B12 and folate deficiency. Moreover, it is also a disturbing finding which calls for more in-depth analysis of the cause and also measures to tackle it, as maternal anemia has numerous long-term adverse effects on the fetus.

The majority of the women (75%) had an association between anemia and a high BMI >23, which is similar to other studies.[15,16] Although obesity and iron deficiency usually represent opposite ends of the spectrum of malnutrition, the association between high BMI and anemia in our study proves to be a significant finding and thus needs to be addressed as a measure of nutritional and health status.

We observed that most of the anemic women were illiterate and unemployed in our study. Kefiyalew *et al*.[16] had similarly reported a significant number of women with anemia being illiterate and unemployed. These findings highlight the fact that illiteracy, low family income and lower levels of education are risk factors for the development of anemia either due to inaccessibility of the women to food or due to a lack of their knowledge on the intake of iron-rich food which thus leads to the development of anemia.

Maternal red cell parameters such as Hb, RBC count, PCV, MCV, MCH, and MCHC, including serum ferritin, were significantly low in anemic mothers, which is consistent

Table 5: Pearson's correlations between maternal and cord blood parameters

Parameters	Hb (mothers)	RBC (mothers)	PCV (mothers)	MCV (mothers)	MCH (mothers)	MCHC (mothers)	RDW (mothers)	HDW (mothers)	S.Ferritin (mothers)
Hb (cord blood)	−0.023	0.854***	0.809***	0.314***	0.412***	−0.080	−0.139*	0.113	−0.133*
RBC (cord blood)	−0.008	0.113	0.726***	0.051	−0.116	−0.154**	−0.068	0.102	−0.125
PCV (cord blood)	−0.164**	0.726***	−0.019	0.684***	0.259***	−0.595***	−0.325***	0.067	−0.150**
MCV (cord blood)	−0.241**	0.051	0.684***	0.266**	0.514***	−0.779***	−0.415***	−0.013	−0.110
MCH (cord blood)	−0.025	−0.116	0.259***	0.514***	−0.07	0.118	−0.137*	0.048	−0.035
MCHC (cord blood)	0.270***	−0.154**	−0.595***	−0.779***	0.118	0.473**	0.402***	0.074	0.117
RDW (cord blood)	0.105	−0.068	−0.325***	−0.415***	−0.137*	0.402***	−0.09	0.840***	−0.037
HDW (cord blood)	0.073	0.102	0.067	−0.013	0.048	0.074	0.840***	0.135	−0.065
S.Ferritin (cord blood)	0.201**	−0.125	−0.150*	−0.110	−0.035	0.117	−0.037	−0.065	00.053

*Correlation is significant at the 0.05 level (two-tailed), **Correlation is significant at the 0.01 level (two-tailed), ***Correlation is significant at the 0.001 level (two-tailed). Hb: Hemoglobin, RBC: Red blood cell, PCV: Packed cell volume, MCV: Mean corpuscular volume, MCH: Mean corpuscular haemoglobin, MCHC: Mean corpuscular haemoglobin concentration, RDW: Red cell distribution width, HDW: Hemoglobin distribution width, S.Ferritin: Serum ferritin

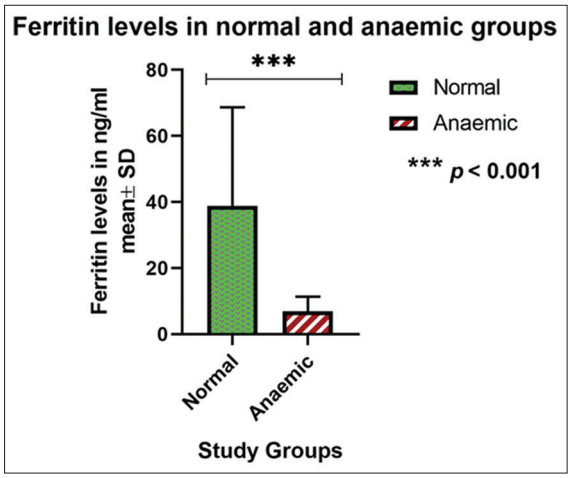

Graph 1: A comparison of serum ferritin values between anemic and nonanemic pregnant mothers

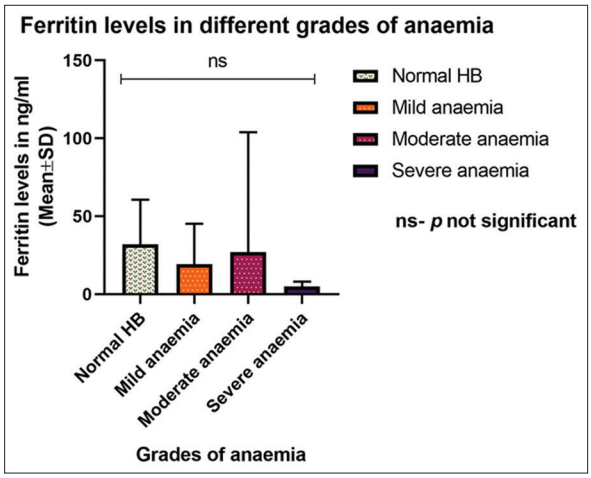

Graph 2: Serum ferritin values in pregnant mothers with different grades of anemia

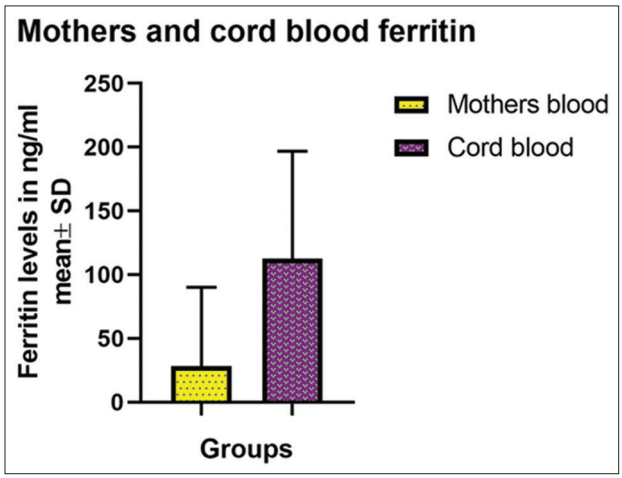

Graph 3: A comparison of serum ferritin values between the mothers and cord blood

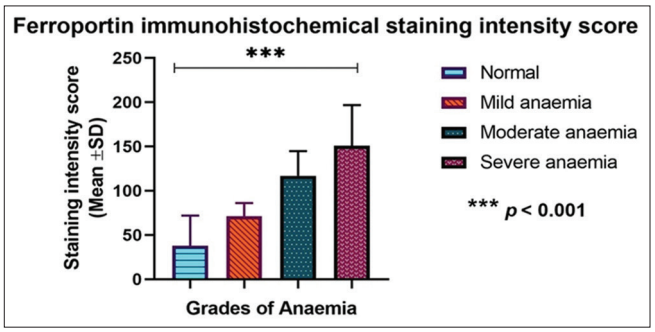

Graph 4: The immunohistochemistry staining intensity score for ferroportin in the placenta, in different grades of anemia in the mothers

with other studies.[14] Another parameter useful for the diagnosis of iron deficiency is RDW, which is a quantitative measure of anisocytosis. Increased RDW levels indicate a heterogeneous population of erythrocytes, formed by cells of various sizes. In iron deficiency, RDW levels are always found to be increased. In our study, too, RDW of anemic pregnant women was observed to be higher when compared to nonanaemic ones, thus corroborating the literature.[17]

Many studies have been carried out in maternal and cord blood. While some have reported a negative impact of maternal iron deficiency anemia on the iron stores of the newborns,[18] others could not find any relationship.[19]

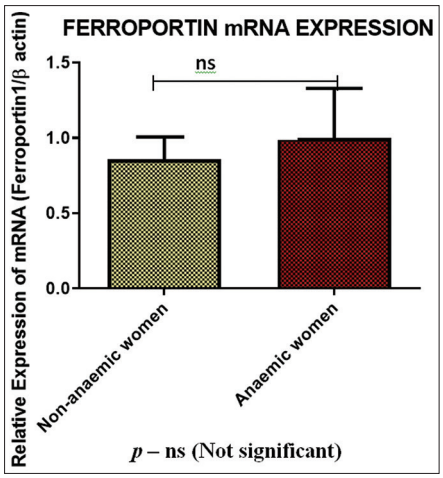

Graph 5: m-RNA expression levels of ferroportin in the placentas of anemic and nonanemic mothers

However, Jaime-Pérez *et al*. and other investigators[11,14,20] had reported normal to above normal Hb levels in the cord blood, thus corroborating with our mean Hb value of 15.75 ± 2.15 g/dl, which is above the average cord blood Hb value of 13 g/dl. This finding shows that the fetus can maintain normal Hb levels irrespective of maternal Hb levels.

A negative correlation was found between cord blood Hb and mother's Hb, RBC, PCV, MCV, and MCH. This finding thus indicates that cord blood Hb values are independent of the mother's values, unlike Timilsina *et al*., who found a positive correlation.[21]

Placental weight, the weight of newborns, crown-rump length, mid-arm, and head circumference, all were observed to be lower in the newborns of anemic mothers when compared to the nonanemic women, consistent with other studies.[22,23] This highlights the crucial role played by iron as an essential nutrient for the development and growth of the fetus.

FPN is one of the iron transporter proteins located on the basolateral side of syncytiotrophoblasts and is a crucial protein required for the efflux of the iron out of the trophoblasts of the placenta into the fetal circulation. Few animal studies show that, in the presence of a low supply of micronutrients in the maternal diet, signals from the fetus can upregulate the expression of micronutrient transporters in the placenta for its nutrition.[24,25]

These findings are in line with cell culture studies by Li *et al*.,[26] in which the BeWo placental cell line was treated with the iron chelator desferrioxamine when FPN mRNA levels were found to be increased. However, there are very few to none studies on the behavior of FPN1 in human subjects, especially in the context of anemia in pregnancy. The only one of such studies in pregnant mothers,[27] however, showed no significant effect of maternal anemia on the placental FPN1 expression. A previous study conducted by us revealed an interesting finding of increased Hb and hematological values in the cord blood, despite the presence of anemia in the mothers. This finding prompted us to undertake the present study in which we hypothesized that maternal iron deficiency increases placental FPN1expression by upregulating the FPN1 gene in order to facilitate increased transport of iron across the placenta. We found immunohistochemical staining for the FPN1 protein was localized to the cytoplasm of the trophoblastic cells. We also studied FPN1 immunoexpression in different grades of anemia and observed a statistically significant increase in the immunoexpression with increasing severity of anemia. In mild anemia, the trophoblastic cells showed a weak staining intensity, while in severe anemia, the cells showed intense positive staining.

In order to further strengthen our findings and test our hypothesis, we also studied the expression of FPN1at the genetic level by performing the mRNA analysis of the FPN1 gene in the placental tissue. Consistent with the protein expression, we observed that m-RNA expression too was higher in anemic women when compared to the nonanemic women. However, our results are not in agreement with Li *et al*.,[27] who found no significant change in either protein or mRNA expression of FPN1 in the maternal anemia groups. The reason for this discrepancy could be due to their small sample size (40 cases). Thus, our study, with greater sample size, for the first time showed that, in maternal iron deficiency anemia, there is upregulation of FPN1 gene, leading to increased expression of FPN1 protein and mRNA in the placenta, thus confirming our hypothesis.

Conclusion

Our study thus shows that, apart from a high prevalence of moderate anemia in pregnant women of our city, there is increased expression of the placental iron transport protein FPN1 in the placenta at both protein and mRNA level which probably explains the immunity of fetus to the development of anemia despite the presence of maternal anemia by facilitating increased transport of iron to the fetus.

Acknowledgement

All the authors acknowledge Indian Council of Medical Research and National Institute of Nutrition for funding this study and also want to thank all the participants of this study. The manuscript has been read and approved by all the authors, and the requirements for authorship as stated earlier in this document have been met, and each author believes that the manuscript represents honest work.

Financial support and sponsorship

This study was financially supported by Indian Council of Medical Research and National Institute of Nutrition for funding this study (Fund number: 16 PT-03).

Conflicts of interest

There are no conflicts of interest.

References

1. WHO. Microdeficiencies: Iron Deficiency, Anaemia. Available from: http://www.who.int/nutrition/topics/ida/en/. [Last accessed on 2020 Aug 15].
2. Horton S, Levin C. Commentary on "evidence that iron deficiency anemia causes reduced work capacity". J Nutr 2001;131:691S-6S.
3. Horton S, Ross J. The economics of iron deficiency. Food Policy 2003;28:51-75.
4. Sibley CP. Understanding placental nutrient transfer – Why bother? New biomarkers of fetal growth. J Physiol 2009;587:3431-40.
5. Ward DM, Kaplan J. Ferroportin-mediated iron transport: Expression and regulation. Biochim Biophys Acta 2012;1823:1426-33.
6. Charafe-Jauffret E, Tarpin C, Bardou VJ, Bertucci F, Ginestier C, Braud AC, *et al*. Immunophenotypic analysis of inflammatory breast cancers: Identification of an 'inflammatory signature'. J Pathol 2004;202:265-73.
7. Best CM, Pressman EK, Cao C, Cooper E, Guillet R, Yost OL, *et al*. Maternal iron status during pregnancy compared with neonatal iron status better predicts placental iron transporter expression in humans. FASEB J 2016;30:3541-50.
8. Srai SK, Bomford A, McArdle HJ. Iron transport across cell membranes: Molecular understanding of duodenal and placental iron uptake. Best Pract Res Clin Haematol 2002;15:243-59.
9. International Institute for Population Sciences (IIPS) and ICF. National Family Health Survey (NFHS-4), 2015-16: India. Mumbai: IIPS; 2017.
10. Koura GK, Ouedraogo S, Le Port A, Watier L, Cottrell G, Guerra J, *et al*. Anaemia during pregnancy: Impact on birth outcome and infant haemoglobin level during the first 18 months of life. Trop Med Int Health 2012;17:283-91.
11. Jaime-Pérez JC, García-Arellano G, Méndez-Ramírez N, González-Llano Ó, Gómez-Almaguer D. Evaluation of hemoglobin performance in the assessment of iron stores in feto-maternal pairs in a high-risk population: Receiver operating characteristic curve analysis. Rev Bras Hematol Hemoter 2015;37:178-83.
12. Vanderjagt DJ, Brock HS, Melah GS, El-Nafaty AU, Crossey MJ, Glew RH. Nutritional factors associated with anaemia in pregnant women in northern Nigeria. J Health Popul Nutr 2007;25:75-81.
13. Cogill B. Anthropometric Indicators Measurement Guide. Washington, DC: Food and Nutrition Technical Assistance (FANTA) Project, FHI 360; 2003.
14. de Sá SA, Willner E, Duraes Pereira TA, de Souza VR, Teles Boaventura G, Blondet de Azeredo V. Anemia in pregnancy: Impact on weight and in the development of anemia in newborn. Nutr Hosp 2015;32:2071-9.
15. Nair KM, Fernandez-Rao S, Nagalla B, Kankipati RV, Punjal R, Augustine LF, *et al*. Characterisation of anaemia and associated factors among infants and pre-schoolers from rural India. Public Health Nutr 2016;19:861-71.
16. Kefiyalew F, Zemene E, Asres Y, Gedefaw L. Anemia among pregnant women in Southeast Ethiopia: Prevalence, severity and associated risk factors. BMC Res Notes 2014;7:771.
17. Karaoglu L, Pehlivan E, Egri M, Deprem C, Gunes G, Genc MF, *et al*. The prevalence of nutritional anemia in pregnancy in an east Anatolian province, Turkey. BMC Public Health 2010;10:329.
18. El-Farrash RA, Ismail EA, Nada AS. Cord blood iron profile and breast milk micronutrients in maternal iron deficiency anemia. Pediatr Blood Cancer 2012;58:233-8.
19. Paiva Ade A, Rondó PH, Pagliusi RA, Latorre Mdo R, Cardoso MA, Gondim SS. Relationship between the iron status of pregnant women and their newborns. Rev Saude Publica 2007;41:321-7.
20. Shao J, Lou J, Rao R, Georgieff MK, Kaciroti N, Felt BT, *et al*. Maternal serum ferritin concentration is positively associated with newborn iron stores in women with low ferritin status in late pregnancy. J Nutr 2012;142:2004-9.
21. Timilsina S, Karki S, Gautam A, Bhusal P, Paudel G, Sharma D. Correlation between maternal and umbilical cord blood in pregnant women of Pokhara Valley: A cross sectional study. BMC Pregnancy Childbirth 2018;18:70.
22. Agboola A. Effect of type and duration of anemia on placental weight and villous histology. J Natl Med Assoc 1979;71:1067-9.
23. Mongia SM, Jain SK, Yadav M. Placenta: The wonder organ. J Indian Acad Forensic Med 2011;33:140-2.
24. McArdle HJ, Gambling L, Kennedy C. Iron deficiency during pregnancy: The consequences for placental function and fetal outcome. Proc Nutr Soc 2014;73:9-15.
25. McArdle HJ, Lang C, Hayes H, Gambling L. Role of the placenta in regulation of fetal iron status. Nutr Rev 2011;69 Suppl 1:S17-22.
26. Li YQ, Bai B, Cao XX, Yan H, Zhuang GH. Ferroportin 1 and hephaestin expression in BeWo cell line with different iron treatment. Cell Biochem Funct 2012;30:249-55.
27. Li YQ, Yan H, Bai B. Change in iron transporter expression in human term placenta with different maternal iron status. Eur J Obstet Gynecol Reprod Biol 2008;140:48-54.

Original Article

Carrying Angle of the Elbow Joint in Young Caucasian and Indian American Population: A Descriptive Cross-Sectional Study

Abstract

Introduction: To establish normative anthropometric data about the carrying angle, length of the forearm, hip circumference, and body height for young Indian American and Caucasian population and to test statistically the ethnic and gender differences. The objective was also to compare the right and left carrying angle in the ethnic groups. **Material and Methods:** The present study included 200 students from the American population. Among them, 100 were Caucasians (50 females and 50 males), and 100 were Indian Americans (50 females and 50 males). These participants were aged between 18 and 30 years. Goniometer was used to measure the carrying angle, the hip circumference, body height, and length of forearm were also determined. **Results:** The present study observed that there was no statistical significance for the carrying angle compared between sides and genders of both the ethnic groups ($P > 0.05$). The carrying angle was higher ($P < 0.05$) in Caucasians than in the Indian Americans, both over the right and left upper extremities. This was observed in both the genders. The comparison between genders showed that, carrying angle was higher for females ($P < 0.05$) than the males in both Caucasians and Indian Americans. **Discussion and Conclusion:** This investigation contributes the morphological database in Indian Americans and Caucasians for the carrying angle. The morphological findings of this study could be used as reference values for the clinical application and ergonomics. The knowledge about the carrying angle is imperative during the surgical procedures at the elbow joint.

Keywords: *Asian Indian Americans, Caucasian race, elbow joint*

Chakravarthy Marx Sadacharan, Sukaina B. Alikhan[1], Vasanthakumar Packirisamy[2], B. V. Murlimanju[3]

School of Biological Sciences (SBS), Morgane 120, 11 Hills Beach Road, University of New England (UNE), Biddeford, Maine, USA, [1]Medical Student, College of Medicine, American University of Antigua, Antigua, Antigua and Barbuda, [2]Basic Sciences, College of Applied Medical Sciences, King Saud Bin Abdulaziz University for Health Sciences, Al Ahsa, Saudi Arabia, King Abdullah International Medical Research Centre, Al Ahsa, Saudi Arabia, [3]Department of Anatomy, Kasturba Medical College, Mangalore, Manipal Academy of Higher Education, Manipal, India

Article Info

Received: 02 August 2020
Accepted: 30 September 2021
Available online: 17 March 2022

Address for correspondence:
Dr. Chakravarthy Marx Sadacharan, Associate Professor of Anatomy, School of Biological Sciences (SBS), Morgane 120, 11 Hills Beach Road, University of New England (UNE), Biddeford, Maine, USA - 04005.
E-mail: csadacharan@une.edu

Access this article online

Website: www.jasi.org.in
DOI: 10.4103/JASI.JASI_145_20
Quick Response Code:

Introduction

In the normal anatomical position, the long axes of brachium and ante brachium form an acute angle medially; this angle at the elbow joint is known as the carrying angle.[1] The trochlear groove of humerus is vertically oriented anteriorly, and there is oblique orientation posteriorly. This provides the carrying angle.[2] The carrying angle provides the range of mobility at the elbow joint and allows the forearm to move away from the hip during the swing phase of walking. The movement of forearms away from the hip joint is also important while carrying the objects. However, a higher carrying angle will contribute to the formation of conditions such as elbow pain, instability, and valgus deformity. This may also cause difficulty in throwing the objects like in the sports. Increased carrying angle will reduce the elbow flexion, can cause dislocation and fracture when one falls on an outstretched hand. The best example is the fracture of distal humeral epiphysis.[3-5] The normal data of the carrying angle is essential during the anthropological evaluation during the sex determination of skeletal remains in medicolegal circumstances. It will also help in lessening the complications following the supracondylar fractures of the humerus, including the cosmetic deformities. Information about the carrying angle may also help in designing the total elbow prosthesis following the elbow injury.[6,7]

In the literature, there are few studies available which compared the carrying angle with respect to the sides and genders. The comparison was also done between the dominant and nondominant extremities. However, there are only few reports which focus on the ancestor-based variations in the carrying angle. The data are not available about the carrying angle in younger population of Caucasians and Indian Americans.

How to cite this article: Sadacharan CM, Alikhan SB, Packirisamy V, Murlimanju BV. Carrying angle of the elbow joint in young Caucasian and Indian American population: A descriptive cross-sectional study. J Anat Soc India 2022;71:42-6.

Aims and objectives

The aim of this present study was to obtain the normal anthropometric data about the carrying angle, length of the forearm, hip circumference, and height of the person from Indian American and Caucasians young population and compare them statistically. The objective was also to compare the right and left carrying angle in the ethnic groups.

Material and Methods

The present study included 200 students from the American population [Figure 1]. Among them, 100 were Caucasians [50 from each gender, Figure 1a and b], and 100 were Indian Americans [50 from each gender, Figure 1c and d]. These are from younger population, who were aged between 18 and 30 years. The individuals with the previous history of upper extremity fractures, congenital bony deformities, and nutritional skeletal disorders were not included in this study. The goniometer was used to measure the carrying angle. The measurement was performed as per the Ruparelia *et al*.,[7] however, there was slight modification. The other parameters such as hip circumference, length of forearm, height, and age were also determined. The present study was approved by the Ethics Committee of American University of Antigua, College of Medicine.

Measurement of carrying angle

The participants of this study were requested to stand in the anatomical position. The arm of the goniometer was placed in a straight line, and its measurement plate was placed at the fulcrum of the elbow joint. The arm of the goniometer was aligned with the central part of the participant's upper arm. The other arm of the goniometer was swung until it was aligned with the center of the participant's forearm. The measurement plate of the goniometer gave the reading of carrying angle, and the same procedure was repeated for the other elbow joint.[8]

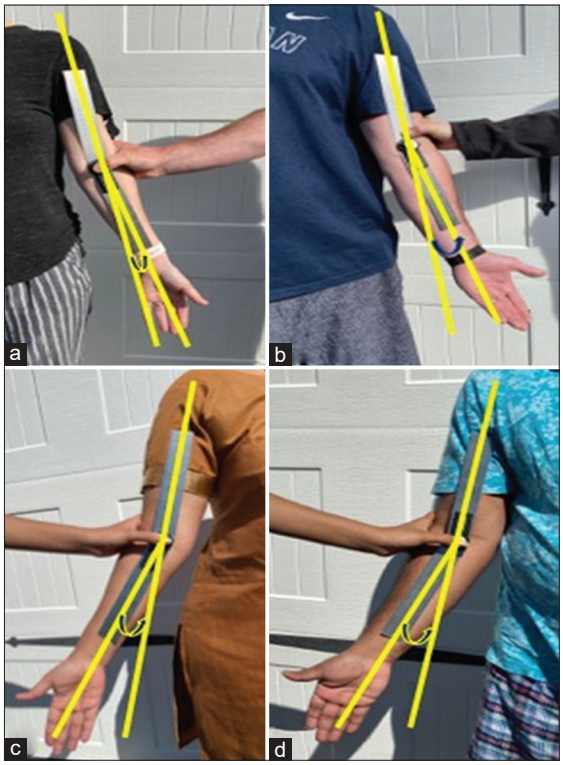

Figure 1: Schematic representation of the carrying angle in Caucasian male (a), Caucasian female (b), Indian American female (c) and Indian American male (d)

Measurement of height, forearm length, and hip circumference

Height

The height was measured using stature meter from vertex to heel with barefoot.[8]

Forearm length

The length of forearm was measured by using the digital Vernier caliper of 16". The distance between the medial epicondyle of humerus and styloid process of ulna was considered as the length of forearm.

Hip circumference

The width of the hip (waist) was determined with a simple measuring meter.

Measurements

All the measurements were performed by two same persons. The values were given as centimeters, and the carrying angle was read in degrees. Special care and comfort were offered to the participants while performing these measurements. Three readings were taken for each measurement by the same observer. The third reading was taken when the first two readings exhibited a larger discrepancy. The two closer readings were considered to minimize the errors, and the mean reading was calculated.

Analysis of the data

Graph Pad Prism software (version 3.00, San Diego, California, USA) was used to perform the statistical analysis. The mean and standard deviation were calculated for each of the measurements in both the genders of both ethnic groups. The values were compared statistically using the two-way factorial analysis of variance. The statistical significance was considered at 5% ($P < 0.05$), with two-tailed values. The independent *t*-test was applied by categorizing the participants into groups. Pearson correlation analysis was performed among the age and other anthropometric parameters.

Results

Comparison of carrying angle over the right and left sides

The present study observed that there was no statistical significance [Table 1] for the carrying angle compared over the left and right sides ($P > 0.05$). There was no statistically

Table 1: Comparison of the carrying angle over right and left sides

Population	Right (dominant) side	Left (nondominant) side	*P*
Male Caucasian (*n*=50)	10.02±3.06	9.66±3.36	0.59
Male Indian American (*n*=50)	7.88±3.76	7.11±3.9	0.28
Female Caucasian (*n*=50)	13.68±3.63	13.04±4.63	0.15
Female Indian American (*n*=50)	11.17±4.86	10.26±3.8	0.09

Measurements are in degree (°), mean±SD, paired *t*-test, statistical significance *P*>0.05. SD: Standard deviation

significant difference observed ($P > 0.05$) in both genders of both ethnic groups.

Comparison of the data among male Caucasian and Indian Americans

The present study observed that the Caucasians were taller ($P < 0.05$) than the Indian Americans with respect to male population [Table 2]. The difference was not significant statistically with respect to the hip circumference ($P > 0.05$). The forearm length was higher in Caucasians than the Indian Americans ($P < 0.05$) in both the sides. The carrying angle was higher ($P < 0.05$) in Caucasian males than the Indian American males both over the right and left sides.

Comparison of the data among female Caucasian and Indian Americans

The present study observed that the Caucasians were taller ($P < 0.05$) than the Indian Americans [Table 3] with respect to female groups. The difference was not significant statistically with respect to the hip circumference ($P > 0.05$). The forearm length was not different statistically ($P > 0.05$) when compared between these ethnic groups over both the sides. However, the carrying angle was higher ($P < 0.05$) in Caucasian females than the Indian American females on both the sides.

Comparison of the data among female and male Caucasians

The present study observed that the males were taller than the females ($P < 0.05$) in Caucasians [Table 4]. The significant difference was not observed statistically between the females and males ($P > 0.05$) in relation to the hip circumference. The forearm length was higher for males ($P < 0.05$) than in females in Caucasians. The carrying angle was more ($P < 0.05$) in female Caucasians than the male Caucasians over both the sides.

Comparison of the data among female and male Indian Americans

The present study observed that the males were taller than the females ($P < 0.05$) in the Indian American Population [Table 5]. The comparison between male and female did not reveal statistical significance ($P > 0.05$) in relation to the hip circumference. The forearm length was also not significant statistically when compared between the genders ($P > 0.05$) in the Indian American population. The reading of carrying angle was more ($P < 0.05$) in female Indian Americans than the male Indian Americans over the left and right sides.

Table 2: Comparison of the data among male Caucasian (*n*=50) and Indian (*n*=50) Americans

	Male Caucasian	Male Indian American	*P*
Age	24.9±2.2	25.1±2.1	
Height	179.5±3.46	175.94±6.81	0.038*
Hip circumference	103.44±12.8	99.05±8.8	0.92
Forearm length right side	31.5±1.19	28.5±2.38	0.048*
Forearm length left side	31.4±1.31	28.7±2.54	0.039*
Carrying angle right side	10.02±3.06	7.88±3.76	0.029*
Carrying angle left side	9.66±3.36	7.11±3.91	0.031*

Measurements are in centimetres and degree (°), mean±SD, paired *t*-test, *statistical significance *P*>0.05. SD: Standard deviation

Table 3: Comparison of the data among female Caucasians (*n*=50) and Indian Americans (*n*=50)

	Female Caucasian	Female Indian American	*P*
Age	27.2±3.5	24.2±2	
Height	166.84±7.85	159.63±8.16	0.013*
Hip circumference	100.1±13.4	97.1±12.9	0.62
Forearm length right side	25.08±2.23	25.16±1.84	0.91
Forearm length left side	25.29±2.24	25.24±1.95	0.94
Carrying angle right side	13.68±3.63	11.17±4.86	0.041*
Carrying angle left side	13.04±4.63	10.26±3.8	0.035*

Measurements are in centimetres and degree (°), mean±SD, paired *t*-test, *Statistical significance *P*>0.05. SD: Standard deviation

Table 4: Comparison of the data among female (*n*=50) and male (*n*=50) Caucasian Americans

	Female Caucasian	Male Caucasian	*P*
Age	27.2±3.5	24.9±2.2	
Height	166.84±7.85	179.5±3.46	0.001*
Hip circumference	100.1±13.4	103.44±12.8	0.56
Forearm length right side	25.08±2.23	31.5±1.19	0.01
Forearm length left side	25.29±2.24	31.4±1.31	0.01
Carrying angle right side	13.68±3.63	10.02±3.06	0.017*
Carrying angle left side	13.04±4.63	9.66±3.36	0.012*

Measurements are in centimetres and degree (°), mean±SD, unpaired *t*-test, *Statistical significance *P*>0.05. SD: Standard deviation

The present study carrying angle data were compared with the previous reports of other populations and are represented in Table 6.

Discussion

The wider pelvis and small shoulders, offer higher carrying angle in females than the males.[14,15] However, some studies report that there is no difference in the carrying angles of males and females.[9,15] Few studies reported that, carrying angle will be higher in the dominant upper limb than the nondominant.[14,16,17] In this study, the statistically significant difference was not observed ($P > 0.05$) between the side-based and gender-based comparison in both ethnic groups. The muscle bulk may be more for the dominant upper limb, and there may be slighter greater carrying angle over the right side, but this was not statistically significant ($P > 0.05$). This research observed the highest carrying angle in females ($P < 0.05$) than in the males, in both the population. Khare *et al*.[18] opined that carrying angle is not correlated with the width of pelvis, and it is not a secondary sexual character. However, there is overlapping of the carrying angle in males and females.[15,19] Carrying angle differs from individual to individual; hence, it is important to compare both the elbow joints during the evaluation. The present study compared the carrying angle with different ethnic groups globally [Table 6], and there were lots of variations. This may be due to ancestral and geographic variations. Carrying angle may help in the sex determination and is of interest to the anthropologists. The anthropometry varies between genders, ancestry, food intake, geography, and the environment.[20] It was reported that the data of certain population cannot be applied to other population[21] and this requires data for a particular region. The United States is a country, which has many ethnic groups who migrated there for the occupation. The morphometric data of these ethnic groups are not recorded separately. Indians in America are the second-largest migratory group in the United States. The data available for the American population have been taken from the Caucasians and therefore these data cannot be used for the Indian Americans.

The anthropometric data of various ethnic and ancestral groups need to be determined for establishing the normal database.[22] The elbow surgeries performed on the Indian American patient require the data from Indian American population only. The instruments and prosthesis cannot be taken from the Caucasian size. Hence, it is suggested to obtain data from different ethnic groups to determine the reference values for that particular population. There are few studies available from Indian populations within India for the carrying angle.[7,14] However, there are no reports available about the carrying angle of the elbow with other parameters in Indian American population. Indian Americans are the Indians who migrated to the United States. Most of the Indian Americans in this present study were born in the United States, but their parents or grandparents have migrated to the United States from India. The American data are not accurate to be used for this Indian American population. Even the Indian data cannot be considered because these individuals have lived in the United States for the longer time. There will be environmental, geographical, genetic, ancestral, and nutritional variations. The height, hip circumference, forearm length, and carrying angle were higher for the Caucasians ($P > 0.05$) than the Indian Americans. This is because the Caucasians are tall and robust in comparison to the Indians. The age of the Caucasian students was slightly higher than the Indian American students, because Caucasians join the school, slightly later in their age. Indian students join the schools according to their age. The data of Indian American are essential to treat the patients of this ethnic group during the conditions like elbow surgeries. The data regarding the carrying angle with other parameters may help the operating surgeon during the orthopedic procedures like correction of cubitus varus deformity.

The present study has few limitations like few of the participants of this study have lived in different continents.

Table 5: Comparison of the data among female (*n*=50) and male (*n*=50) Indian Americans

	Female Indian American	Male Indian American	*P*
Age	24.2±2	25.1±2.1	
Height	159.63±8.16	175.94±6.81	0.001*
Hip circumference	97.1±12.9	99.05±8.8	0.65
Forearm length right side	25.16±1.84	28.5±2.38	0.41
Forearm length left side	25.24±1.95	28.7±2.54	0.57
Carrying angle right side	11.17±4.86	7.88±3.76	0.045*
Carrying angle left side	10.26±3.8	7.11±3.91	0.047*

Measurements are in centimetres and degree (°), mean±SD, unpaired *t*-test, *Statistical significance $P>0.05$. SD: Standard deviation

Table 6: Global comparison of the carrying angle in other ethnic younger population

Authors	Population	Male right side (°)	Male left side (°)	Female right side (°)	Female left side (°)
Sharma *et al*.[9]	Nepalese	4.55	7.03	4.95	7.8
Chinweife *et al*.[10]	Nigerian	12.30±1.88	10.99±1.87	13.82±1.65	12.55±1.76
Açıkgöz *et al*.[11]	Turkish	9.77±2.82	9.85±2.95	13.94±3.97	14.03±4.08
Allouh *et al*.[12]	Arabian	13.0±0.2	10.4±0.2	17.50±0.3	16.0±0.6
Allouh *et al*.[12]	Malayan	14.1±0.2	12.5±0.2	15.7±0.4	14.3±0.3
Kothapalli *et al*.[13]	Indian	12.09±4.66	10.20±4.53	13.54±6.44	11.90±5.61
Present study	Indian American	7.88±3.76	7.11±3.91	11.17±4.86	10.26±3.8
Present study	Caucasian	10.02±3.06	9.66±3.36	13.68±3.63	13.04±4.63

For example, they have lived both in India and the United States. The data will be more accurate if the participants belong to the same geographical location from their ancestors of three, four generations. The sample size of one hundred in each population group studied may be lesser for this study. The data will be more accurate with a larger sample size. The present study did not correlate the carrying angle radiologically. The carrying angle can be calculated radiologically using the software like "Radiant," after obtaining the X-ray films.

Conclusion

The present study has provided the data about the carrying angle and other parameters such as forearm length, hip circumference in Indian Americans and Caucasians. These data can be used as reference data for these population subgroups. The data of the present study have implications in the shoulder and elbow surgery. The data are also enlightening to the anthropologists and morphologists.

Financial support and sponsorship

Nil.

Conflicts of interest

There are no conflicts of interest.

References

1. Williams PL, Bannister LH, Berry MM, Collins P, Dyson M, Dussek JE, *et al.* Gray's Anatomy. 38th ed. London: Churchill Livingstone; 1995. p. 642-3.
2. Kapandji IA. The physiology of the joints, Vol 1, upper limb. New York: Churchill. Livingstone; 1982. p. 72-97.
3. Cain EL Jr., Dugas JR, Wolf RS, Andrews JR. Elbow injuries in throwing athletes: A current concepts review. Am J Sports Med 2003;31:621-35.
4. Hutchinson MR, Wynn S. Biomechanics and development of the elbow in the young throwing athlete. Clin Sports Med 2004;23:531-44.
5. Van Roy P, Baeyens JP, Fauvart D, Lanssiers R, Clarijs JP. Arthro-kinematics of the elbow: Study of the carrying angle. Ergonomics 2005;48:1645-56.
6. Punia RS, Sharma R, Usmani JA. The carrying angle in an Indian population. J Anat Soc India 1994;43:107-10.
7. Ruparelia S, Patel S, Zalawadia A, Shah S, Patel SV. Study of carrying angle and its correlation with various parameters. Nat J Int Res Med 2010;1:28-32.
8. Rajesh B, Reshma VR, Jaene RC, Somasekhar IT, Vaithilingam A. An evaluation of the carrying angle of the elbow joint in adolescents. Int J Med Biomed Res 2013;2:221-5.
9. Sharma K, Mansur DI, Khanal K, Haque MK. Variation of carrying angle with age, sex, height and special reference to side. Kathmandu Univ Med J (KUMJ) 2013;11:315-8.
10. Chinweife KC, Ejimofor OC, Ezejindu DN. Correlation of carrying angle of the elbow in full extension and hip-circumference in adolescents of Nnewi people in Anambra state. Int J Sci Res Pub 2014;4:1-8.
11. Açıkgöz AK, Balci RS, Göker P, Bozkir MG. Evaluation of the elbow carrying angle in healthy individuals. Int J Morphol 2018;36:135-9.
12. Allouh MZ, Abu Ghaida JH, Jarrar AA, Khasawneh RR, Mustafa AG, Bashaireh KM. The carrying angle: Racial differences and relevance to inter-epicondylar distance of the humerus. Folia Morphol (Warsz) 2016;75:388-92.
13. Kothapalli J, Murudkar PH, Seerla LD. The carrying angle of elbow – A correlative and comparative study. Int J Curr Res Rev 2013;5:71.
14. Tükenmez M, Demirel H, Perçin S, Tezeren G. Measurement of the carrying angle of the elbow in 2,000 children at ages six and fourteen years. Acta Orthop Traumatol Turc 2004;38:274-6.
15. Steel FL, Tomlinson JD. The carrying angle in man. J Anat 1958;92:315-7.
16. Paraskevas G, Papadopoulos A, Papaziogas B, Spanidou S, Argiriadou H, Gigis J. Study of the carrying angle of the human elbow joint in full extension: A morphometric analysis. Surg Radiol Anat 2004;26:19-23.
17. Yilmaz E, Karakurt L, Belhan O, Bulut M, Serin E, Avci M. Variation of carrying angle with age, sex, and special reference to side. Orthopedics 2005;28:1360-3.
18. Khare GN, Goel SC, Saraf SK, Singh G, Mohanty C. New observations on carrying angle. Indian J Med Sci 1999;53:61-7.
19. Zampagni ML, Casino D, Zaffagnini S, Visani AA, Marcacci M. Estimating the elbow carrying angle with an electrogoniometer: Acquisition of data and reliability of measurements. Orthopedics 2008;31:370.
20. Wankhede KP, Kamdi NY, Parchand MP, Anjankar VP, Bardale RV. Estimation of stature from maxillo-facial anthropometry in a central Indian population. J Forensic Dent Sci 2012;4:34-7.
21. Siddiqui MA, Shah MA. Estimation of stature from long bones of Punjabis. Indian J Med Res 1944;32:105-8.
22. Kunjur J, Sabesan T, Ilankovan V. Anthropometric analysis of eyebrows and eyelids: An inter-racial study. Br J Oral Maxillofac Surg 2006;44:89-93.

Original Article

Retromolar Canals and Mandibular Third Molar Position: Is there a Possible Connection?

Oğuzhan Demirel, Aslıhan Akbulut[1]

Bolu Abant İzzet Baysal University, Faculty of Dentistry, Department of Dentomaxillofacial Radiology, BOLU, [1]Department of Dentomaxillofacial Radiology, Faculty of Dentistry, İstanbul Medipol University, Fatih, İstanbul, Turkey

Abstract

Introduction: The retromolar canal (RMC) is an anatomical variation of the posterior part of the mandibular canal. It is thought that this variation is related to histological vestiges of the gubernacular canal and RMC presence may be associated with mandibular third molar (MTM) malposition. This study aims to investigate the relationship between MTM position and RMC existence. **Material and Methods:** Patients who had undergone cone-beam computed tomography examination for various purposes were included in the study. All of the patients had unilateral or bilateral MTM teeth. MTM impaction patterns were classified according to Winter and Pell-Gregory classifications. RMC existence, type, retromolar foramen (RMF) position, RMF dimensions, and distance from RMF to second and third molars were recorded. **Results:** Three hundred and forty-six retromolar areas with MTM of 244 patients were evaluated. RMCs were present in 11.5% of the patients. No statistically significant relationship between RMC and MTM impaction patterns was observed. A1-type RMC was found to be the most prevalent. The mean distance from RMF to the third molar was 6.09 ± 4.20 mm and was found to be higher in male patients. The mean distance from RMF to the second molar was 15.28 ± 4.73 mm. The average dimensions of the RMF were 1.4 ± 0.47 mm. **Discussion and Conclusion:** RMC is a relatively common anatomical variation of the mandibular canal. Although no correlation was observed between MTM impaction pattern and RMC existence, further research including more samples may be helpful to explain a possible correlation.

Keywords: *Impaction, mandibular third molar, retromolar canal, retromolar foramen*

Introduction

The retromolar canal (RMC) can be defined as an anatomic variant that branches from the mandibular canal and exits at retromolar foramen (RMF) in the retromolar area.[1]

The canal contains a thinly myelinated nerve with tiny arteries and venules, and the nerve is associated with innervation of the retromolar pad and buccal gingiva of two molar teeth anterior to the foramen.[2] Therefore, clinically it is of importance to define this canal before any surgical procedures involving the posterior part of the mandible. They may be related to extensive hemorrhage during surgical procedures, postsurgical sensory deficiencies, development of traumatic neuroma, and anesthetic failure. Furthermore, in elderly people using prosthetic appliances, following resorption of the alveolar crest, discomfort may be seen due to pressure on the nerve.[3]

The prevalence of the RMC ranges between 8% and 75.4%.[3,4] The wide range of observed frequency is associated with racial differences, investigation methods, and the criteria used to define the RMC existence.[5] A study using cone-beam computed tomography (CBCT) and panoramic radiography concluded with a prevalence of 24.6% when evaluated with CBCT and with a prevalence of 6.6% when the evaluation was made using panoramic radiography. Of the detected 18 RMCs on CBCT, only 4 were detected on panoramic radiographs.[6] The results of the study indicate the importance of assessment using three-dimensional methods to avoid limitations of two-dimensional techniques such as superimpositions and low diagnostic success.

Moreno Rabie *et al*. stated that the RMC may be a histological vestige of the gubernacular canal – the canal that contains the gubernacular cord which connects tooth in formation with gums and takes a role in tooth eruption.

How to cite this article: Demirel O, Akbulut A. Retromolar canals and mandibular third molar position: Is there a possible connection? J Anat Soc India 2022;71:47-53.

Article Info

Received: 23 September 2020
Revised: 23 November 2021
Accepted: 25 November 2021
Available online: 17 March 2022

Address for correspondence:
Dr. Oğuzhan Demirel, Department of Dentomaxillofacial Radiology, School of Dental Medicine, Bahçeşehir University, Sahrayı Cedit Mahallesi, Batman Sk. No: 66, Kadıköy 34734, İstanbul, Turkey.
E-mail: dtoguzhandemirel@gmail.com

Access this article online

Website: www.jasi.org.in
DOI: 10.4103/jasi.jasi_194_20
Quick Response Code:

In their study to investigate the possible connection between two structures, they hypothesized that if there was a connection between the gubernacular canal and RMC, RMCs should have been more common in dental malpositions.[1]

Winter classification and Pell-Gregory classifications are widely used to categorize mandibular third molar (MTM) impaction patterns.[7] Winter classification uses the third molar angulation according to the long axis of the second molar. Third molars are classified as vertical (−10°–10°), mesioangular (11°–79°), distoangular (−11° to −79°), horizontal (80°–100°), and others (101 to −80°).[8,9]

In Pell-Gregory classification, the definition of depth of third molars is made according to the relationship between occlusal levels of third molars and second molars: the third molar occlusal level is at the same level with second molar (A), the third molar occlusal level is between occlusal level and cervical level of the second molar (B), and the third molar occlusal level is below cervical level of second molar (C). Third molar-ramus relation is classified as: MTM is fully anterior to ramus (1), the third molar is partially inside ramus (2), and the third molar is fully inside ramus (3).[10]

In this study, the initial purpose is to define the relationship between RMCs and the impaction pattern of the MTMs using CBCT; also, it is aimed to evaluate the types of RMCs, RMF positions, dimensions, and their distance to second and third molars.

Material and Methods

Ethical approval was obtained from İstanbul Medipol University Non-Interventional Clinical Research Ethics Committee (no. 10840098-604.01.01-E.65173).

Patient selection

CBCT scans of patients who had undergone CBCT examination for various purposes were included in the study. All the patients had unilateral or bilateral MTM teeth. Exclusion criteria were as follows: any radiographic sign of surgical procedures, trauma or pathologic defects in the retromolar area, and CBCT artifacts that may influence the diagnostic quality of the radiographic image. In the case of unilateral MTM existence, only the side with the third molar was evaluated.

Image acquisition

CBCT scans were taken using iCAT (Imaging Sciences International, Hatfield, PA, USA) with exposure parameters 80 kVp, 5–7 mA, and 14.7–17.8 s with a 0.25-mm voxel size. Vision (Imaging Sciences International, Hatfield, PA, USA) software is used for assessment. Multiplanar reconstructions were made for the evaluation of third molars and RMCs.

Assessment of retromolar canal existence

RMC existence was determined with the consensus of two dentomaxillofacial radiologists. RMC was defined as a radiolucent canal with radiopaque borders, leaving the bone at the retromolar area. RMCs were categorized according to the classification that Patil *et al*.[3] described:

- Type A1: Canal branches from the mandibular canal, moves posterosuperiorly, and opens into the retromolar fossa
- Type A2: Canal branches from the mandibular canal; continues anteriorly, turns posterosuperiorly, and opens into the retromolar fossa
- Type B: Canal originates from the apical portion of the third molar with no radiographic evidence of a connection with the mandibular canal, runs posterosuperiorly, and opens into the retromolar fossa.
- Type C: Canal branches from mandibular foramen, moves anteriorly, and opens into retromolar fossa [Figures 1 and 2]

Evaluation of mandibular third molar position

MTMs were classified as mesioangular, distoangular, horizontal, vertical, and others according to their angular relationship with mandibular second molar [Figure 3].

Pell-Gregory (P-G) depth classification was used for the classification of the inferosuperior position of the third molar according to the cervical level of the mandibular second molar. Third molars were categorized as levels A, B, and C.

Pell-Gregory ramus classification which determines the mesiodistal orientation of MTM according to mandibular ramus was used. MTMs were classified as classes I, II, and III [Figure 4].

Assessment of retromolar foramen

Buccolingual positions of RMFs were classified depending on their position in the retromolar area as buccal, buccolingual, and lingual.

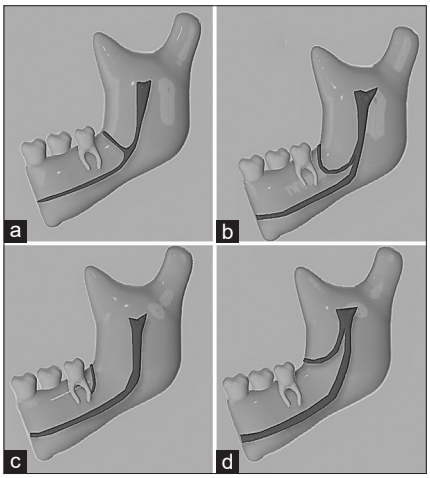

Figure 1: Retromolar canal types: (a) Type A1, (b) Type A2, (c) Type B, (d) Type C

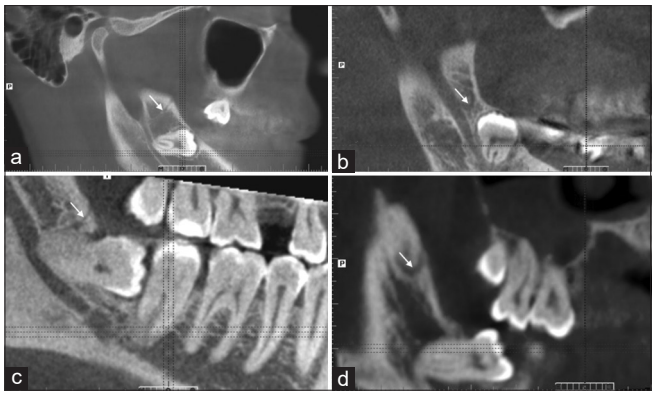

Figure 2: Retromolar canals on cone-beam computed tomography images: (a) Type A1, (b) Type A2, (c) Type B, (d) Type C

On panoramic reconstructions, the distance from the RMF to the distal end of the second molar crown and the distal end of the third molar crown was measured. Mesiodistal dimensions of RMFs were measured on panoramic reconstructions.

Statistical analysis

For quantitative measures, analysis results were presented as average ± standard deviation, and for categorical data, frequency and percentages were presented. Statistical analysis of nonparametric data was performed with Chi-square test. Normal distribution of parametric data was evaluated with Kolmogorov–Smirnov test, and homogeneity of variance was evaluated with Levene's test. For the analysis of parametric data, two-group comparisons were performed with Student's *t*-test and *z*-test. One-way ANOVA test was used for comparisons between RMC types. Statistical significance was set at $P < 0.05$.

Results

Demographics

CBCT scans of 244 patients and a total of 346 sides with MTMs were evaluated. While unilateral MTMs were evident in 142 patients, 102 patients had bilateral third molars.

One hundred and forty (57.4%) of the patients were female and 104 (42.6%) were male. The mean age of the evaluated patients was 30.94 ± 10.02 (28.93 ± 8.97 females and 33.65 ± 10.79 males). The average age of male patients was significantly higher than females ($z = 3.85$; $P < 0.01$).

Retromolar canal existence

RMCs were evident in 28 (11.5%) of the 244 patients and 29 (8.4%) of the evaluated 346 sides with MTMs. RMCs were seen in 17 (12.1%) female patients and 11 (10.6%) male patients. No statistical significance was observed between genders in terms of RMC existence ($P = 0.94$, $P > 0.05$). The average age of the 28 patients with RMCs was 34.61 ± 10.71, and the average age of the patients without RMCs was 30.47 ± 9.88. The average age of the patients with RMCs was significantly higher than patients without ($z = 2.10$; $P = 0.035$, $P < 0.05$).

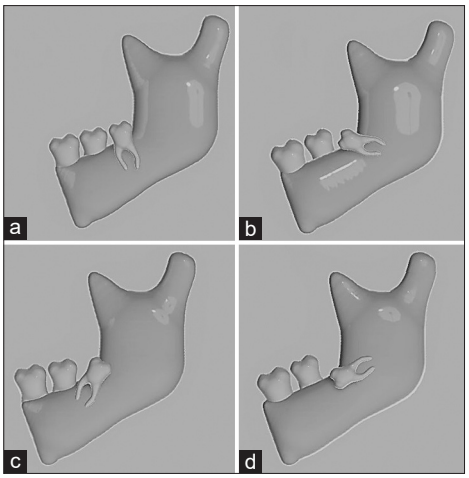

Figure 3: Winter classification of mandibular third molars: (a) Vertical, (b) Mesioangular, (c) Distoangular, (d) Horizontal

Third molar position

According to Winter classification, 169 (48.8%) of the evaluated 346 MTMs were in mesioangular position, followed by 76 (22%) – horizontal position, 56 (16.2%) – vertical position, 35 (10.1%) – distoangular position, and 10 (2.9%) – other positions. The frequency of RMC existence in hemi-mandibles with third molars positioned horizontal, vertical, mesioangular, distoangular, and others was 13.2%, 8.9%, 7.1%, 5.7%, and 0%, respectively. No statistically significant relationship between the positions and RMC existence was observed ($\chi^2 = 2.860$; $P = 0.413$, $P > 0.05$).

Pell-Gregory depth frequencies were 11.9%, 39%, and 49.1% for A, B, and C levels, respectively. RMCs were observed in 6 (14.6%) of the hemi-mandibles with A level, 12 (8.9%) of the hemi-mandibles with B level, and 11 (6.5%) of the hemi-mandibles with C level MTMs. No statistically significant relationship was observed between levels of depth and RMC existence ($\chi^2 = 2.94$; $P = 0.229$, $P > 0.05$).

In the context of Pell-Gregory ramus classification of MTMs, Class III was most frequent (52%), followed by Class I (29.8%) and Class II (18.2%). While 6.1% of the hemi-mandibles with Class III third molar showed RMCs, 7.8% and 18.9% of the hemi-mandibles with Class I and Class II third molars showed RMCs, respectively. No statistically significant relationship was observed between the third molar-ramus relation and RMCs ($\chi^2 = 5.86$; $P = 0.053$, $P > 0.05$).

Retromolar canal types

Table 1 demonstrates the frequency and distribution of RMC types and their relationship with the third molar position.

Table 1: Third molar positions and retromolar canal types

	RMC types				Total
	A1, *n* (%)	A2, *n* (%)	B, *n* (%)	C, *n* (%)	
Winter					
Mesioangular	5 (50)	3 (50)	2 (33.3)	2 (28.6)	12
Distoangular	0	0	1 (16.7)	1 (14.3)	2
Vertical	1 (10)	2 (33.3)	2 (33.3)	0	5
Horizontal	4 (40)	1 (16.7)	1 (16.7)	4 (57.1)	10
Total	10 (100)	6 (100)	6 (100)	7 (100)	29
P-G depth					
A	0	2 (33.3)	0	4 (57.1)	6
B	4 (40)	2 (33.3)	5 (83.3)	1 (14.3)	12
C	6 (60)	2 (33.3)	1 (16.7)	2 (28.6)	11
Total	10 (100)	6 (100)	6 (100)	7 (100)	29
P-G ramus					
1	1 (10)	2 (33.3)	3 (50)	2 (28.6)	8
2	3 (30)	2 (33.3)	1 (16.7)	4 (57.1)	10
3	6 (60)	2 (33.3)	2 (33.3)	1 (14.3)	11
Total	10 (100)	6 (100)	6 (100)	7 (100)	29

RMC: Retromolar canal

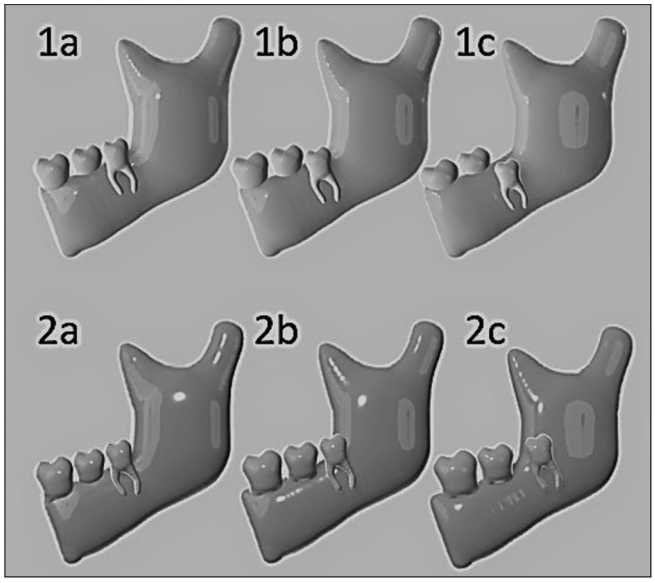

Figure 4: Pell-Gregory classification of mandibular third molars: (1a) Level A, (1b) Level B, (1c) Level C, (2a) Class I, (2b) Class II, (2c) Class III

A1-type RMC was found to be the most frequent. Ten (34.5%) of the observed 29 RMCs was type A1, followed by 7 (24.1%) – type C and 6 (20.7%) – type A2 and 6 (20.7%) – type B.

Buccolingual position of retromolar foramen

Eighteen (62%) of the evaluated 29 RMFs were located on the lingual aspect of the retromolar area. Nine (31.1%) were positioned buccolingually and only 2 (6.9%) were on the buccal aspect.

Table 2 demonstrates the location of RMFs and their relationship with RMC types.

Mesiodistal position of retromolar foramen

The mean distance from RMF to the third molar was 6.09 ± 4.20 mm. This value was observed as 4.35 ± 2.08 mm for females and 8.54 ± 5.24 mm for males. The average distance was significantly higher in male patients compared to all patients' averages ($z = 2.017$; $P = 0.021$, $P < 0.05$).

The mean distance from RMF to the second molar was 15.28 ± 4.73 mm. Females showed an average distance of 13.49 ± 4.12 mm, and males showed an average distance of 17.82 ± 4.51 mm. The average distance was significantly higher in male patients compared to all patients' averages ($z = 1.857$; $P = 0.031$, $P < 0.05$).

Table 3 demonstrates the relationship between RMC type and the distance between RMF and third molar and the distance between RMF and second molar.

Retromolar foramen dimensions

The average mesiodistal dimension of RMF was 1.4 ± 0.47 mm. The average dimensions were 1.41 ± 0.44 mm for female patients and 1.37 ± 0.52 mm for male patients. No statistically significant difference between genders was observed ($P = 0.824$, $P > 0.05$).

The average mesiodistal dimension of RMF located on the buccal aspect was 1.35 ± 0.32 mm, located buccolingually was 1.66 ± 0.62 mm, and located on the lingual aspect was 1.27 ± 0.34 mm. Dimensions of RMF located buccolingually were significantly higher than the RMF located on the lingual aspect ($t = 2.116$; $P = 0.044$, $P < 0.05$).

Average RMF mesiodistal dimensions were 1.51 ± 0.53 mm, 1.62 ± 0.67 mm, 1.20 ± 0.24 mm, and 1.21 ± 0.23 mm for A1-, A2-, B-, and C-type RMCs, respectively. In terms of foramen dimensions, there was no statistically significant difference between canal types ($P = 0.267$, $P > 0.05$).

Discussion

Variations of the mandibular canal may be seen at various levels along the course of the canal.[11] The RMC is an anatomic variation that arises from the mandibular canal and opens to the retromolar area with a foramen called "retromolar foramen."[12,13]

Histological studies showed that the canal contains myelinated nerves, small arteries, and venules; therefore, contents of the canal are of clinical importance which may be associated with complications such as extensive bleeding during surgical procedures to the posterior mandible, insufficient anesthesia, and postsurgical discomfort.[14-16]

It has been stated that there may be a link between the RMC and gubernaculum chord, and if such a connection exists, RMCs should have been seen more commonly with dental malpositions.[1]

The primary goal of the present study was to define the relationship between MTM positions and RMC existence. Prevalence and characteristics of the RMC and the RMF were also investigated.

Previous reports about the prevalence of RMC and foramen range between 8% and 75.4%.[3,4] Two major methods were used in previous studies: retrospective CBCT analysis and macro-anatomical assessment using dry mandibles. In CBCT studies, although the vast majority of reported prevalence of the RMCs were around 25%, percentages vary between 8.5% and 75.4%.[1,3,6,11-14,16,17] Lizio *et al*.'s CBCT assessment excluded RMCs with a RMF below 1 mm, and the observed prevalence was 14.6%.[16] Similarly, in Han and Hwang's research, 0.5 mm was the lower limit for the RMF diameter for the RMC inclusion criteria, and a prevalence of 8.5% was observed.[17] RMF was investigated in macro-anatomical studies, and the frequency is reported between 8% and 71.4%.[1,2,4,5,14,18] Inclusion criteria were performed in one study, which reported the lowest prevalence. The insertion of a nonbeveled needle with 1.0 mm in diameter to the foramen was defined for inclusion criteria.[4] In a study conducted by Capote *et al*., 500 panoramic radiographs were evaluated and a frequency of 8.8% is reported.[15] Kim *et al*.[5] and Motamedi *et al*.[2] in their studies reported 27.3% and 40.4% prevalence, respectively. Both studies used histologic investigations to define the characteristics of RMF and canal.

In this study, a prevalence of 11.5% is observed. Differences between observed values among CBCT studies may be the consequence of varying patient selection criteria, exposure parameters, and associated radiographic artifacts caused by patient movement or metallic objects.

This study group consisted of patients who had at least one MTM, and the presence of a dense object in the imaging field may obstruct the visibility of anatomic structures below 1 mm as a result of stripe-like artifacts.[19] Similarly, Patil *et al*.'s study included patients who had undergone CBCT examination for MTM impaction, and in the study, a prevalence of 75.4% is reported. The difference between results can be explained with imaging parameters they used, such as a smaller field of view and smaller voxel size which allows visualization of smaller subjects.[3] Another factor that may influence the visibility of these anatomic structures may be the metal and the motion artifacts. A recent study, performed by Rabie *et al*., investigated 89 dry mandibles with third molars. They defined retromolar foramina in 73 of the mandibles in macroscopic evaluation; also, in CBCT assessment, RMCs were evident in 64 of the mandibles.[1] At this point, motion artifacts may be responsible for differing results compared to our study. Motion artifacts are reported as high as 48.2% of the CBCT scans.[20] Therefore, scanning a dry mandible, rather than scanning a living person, may result in fewer motion artifacts. We excluded CBCT scans that have artifacts decreasing the overall image quality; however, as such an anatomic structure with submillimeter dimensions is investigated, our exclusion criteria may be inadequate. RMF dimensions are also investigated in our study, and the smallest foramen was around 0.9 mm. RMCs and RMFs below this value may be unseen due to the abovementioned reasons. As we consider the studies, which used dimensional exclusion criteria, consistency with our results can be seen.[16,17]

Patient age was not investigated in the vast majority of previous reports, except Patil *et al*.'s, which reported no significant relationship between age groups.[3] In this study, the average age of the patients with RMCs was found to be significantly higher than the patients without RMCs.

Various classifications are made for RMCs according to their course inside the posterior mandible.[3,5,12-14,17] We used the classification that Patil *et al*. described, which adds one more type of RMC. Type B RMC courses between the RMF and apical portion of the third molar, and has no connection with the mandibular canal on CBCT images. They found this type of canal in the majority of their study group, followed by type A1 and type A2. Type C canal was observed in only one subject.[3] In another study, type B RMC, corresponding to type A2 in our study, was found to be the most frequent canal type.[14] In our study, of the

Table 2: Retromolar foramen location and retromolar canal types

	RMC type				Total
	A1	A2	B	C	
Buccolingual, *n* (%)	3 (33.3)	2 (22.2)	1 (11.1)	3 (33.3)	9 (31.1)
Buccal, *n* (%)	0	0	0	2 (100)	2 (6.9)
Lingual, *n* (%)	7 (38.9)	4 (22.2)	5 (27.8)	2 (11.1)	18 (62)
Total	10	6	6	7	29

RMC: Retromolar canal

Table 3: Retromolar canal type and distance from retromolar foramen to third molar and second molar

	RMF third molar distance (mm)	*z*	*P*	RMF second molar distance (mm)	*z*	*P*
A1	5.10±3.18	−0.744	0.459	13.99±3.56	−0.861	0.389
A2	4.86±3.06	−0.716	0.471	14.58±1.76	−0.361	0.718
B	3.28±0.35	−1.636	0.101	15.36±2.67	0.041	0.968
C	10.94±4.57	3.050	0.002*	17.67±8.19	1.334	0.183
Overall	6.09±4.20			15.28±4.73		

*P<0.05. RMF: Retromolar foramen

observed 29 canals, 10 were type A1, 7 were type C, 6 were type A2, and 6 were type B.

Despite the significant number of studies focused on the prevalence and properties of RMCs and foramina, only one study investigated their relationship with third molars. Moreno Rabie *et al*. hypothesized that, if RMCs are the histological vestiges of the gubernacular canal, which is a structure involved in tooth eruption, they should be more common with dental malpositions. They investigated 112 hemi-mandibles with third molars, and 58 of the hemi-mandibles showed RMCs. They found no correlation between the third molar position and the presence of RMCs.[1]

In this study, a more comprehensive categorization of third molars is made according to Winter and Pell-Gregory classifications. We investigated the angular position, depth, and ramus relation of MTMs and evaluated the connection between these positions and RMC presence. No statistically significant relationship between the pattern of impaction and RMC presence was observed. However, although no statistical assessment was made because of the small sample group, all type B RMCs, which course between the RMF and apical portion of the third molar, were evident in hemi-mandibles with level B and C third molars. No type B RMCs were seen in hemi-mandibles with level A third molars. A similar situation can be mentioned for type A1 RMCs. Although our results cannot indicate a relationship between RMC presence and third molar impaction pattern, the link between type B RMCs and impaction depth of the third molar should be considered. As described before, these types of canals do not have a radiographic connection with the mandibular canal and they course between the apical portion of the third molar and the RMF. Therefore, rather than being an anatomical variant of the mandibular canal, this type of canal may be a histological vestige of the gubernacular canal. Further research, including more samples, should be performed to clarify the possible relationship.

The buccolingual position of the RMF is of importance to avoid complications. In one study, it was found that more than half of the retromolar foramina were located in the middle of the retromolar triangle, followed by the lingual aspect and buccal aspect.[5] Park *et al*. stated that retromolar foramina were more common on the buccal side than the lingual.[14] In our study, the majority of the foramina were located on the lingual side, followed by buccolingual foramina which were located in the middle of the retromolar fossa. Only two foramina were observed on the buccal aspect, and both were the foramina of type C canals.

The distance to RMF from the distal end of the third molar and second molar was investigated in previous reports. Patil *et al*. reported average distances for type A, type B, and type C canal foramina from the distal end of the third molar as 7.0 mm, 7.1 mm, and 14.3 mm, respectively.[3] Park *et al*. defined the average distance from RMF to the second molar as 12.1 mm, and to the third molar as 5.8 mm.[14] These values were 16.8 mm and 10.5 mm for second and third molars, respectively, in Gamieldien *et al*.'s study.[4] Another study reported the average distance from the second molar to foramen as 14.08 mm with no significant difference between genders.[17] Von Arx *et al*. stated that the distance from the distal end of the second molar to RMF is higher in younger age patients.[13] In only one research, a statistically significant difference between genders was defined for the distance between the third molar and RMF.[12] For the second molar-RMF distance and third molar-RMF distance, we observed a statistically significant difference between genders. These measurements were higher in male patients. Another important finding of these measurements was that, when the canal types are considered, the distance from foramina of C type canals to the third molar was significantly higher, compared to other types. Although no statistical significance was observed, foramina of B-type canals had the lowest average distance from third molars (3.28 ± 0.35 mm). This finding should be considered for our hypothesis that type B canals might be associated with the gubernacular canal and should be evaluated in further research.

RMF dimensions were assessed in previous reports. Han and Hwang measured the width of the RMC on sagittal sections, 3 mm below RMF. They found the mean width of RMC 1.13 mm.[17] Kikuta *et al*., in their research performed on 50 CBCT scans, found the average diameter of RMF as 1.1 mm.[12] The average mesiodistal width of RMCs was found to be 1.05 mm in another research.[6] Von Arx *et al*. measured RMC 3 mm below RMF, and the mean width of the RMC was 0.99 mm.[13] Motamedi *et al*. in their cadaveric study defined the average width of RMF as 1.7 mm.[2] In this study, the mean mesiodistal dimension of foramen was 1.4 mm and it was found that the mean dimensions of foramina located on buccolingual position are significantly higher than the foramina located on the lingual position. No statistically significant relationship was observed between canal types in terms of average canal dimensions. However, despite the lack of statistical significance, B-type canals showed the lowest average dimensions (1.20 ± 0.24 mm). Solely based on this finding, it is impossible to proclaim a connection between B-type canals and gubernacular canals.

The limitation of this study is the inadequacy of collected RMC samples, and this may be related to the exclusion criteria we used. This research was a retrospective CBCT analysis, and only the images which were considered to be "diagnostically insufficient" were excluded. CBCT scans were not performed to determine the RMC existence. RMCs, as discussed before, may have submillimeter dimensions, and the artifacts on CBCT images, seen as a result of various reasons, may obstruct their visibility.

Conclusion

In this study, the prevalence of the RMC was 11.5%. No statistically significant relationship between RMC existence and the MTM position was observed. A1-type RMCs, which have a vertical course from the mandibular canal, were the most frequent, followed by C-type RMC, which branches from mandibular foramen. Although no statistically significant finding suggests a relationship between MTM position and RMC existence, type B RMCs were only observed with MTMs below the occlusal level of second molars. There may be a possible relationship between type B RMCs and the position of MTMs. Furthermore, the radiographic properties of type B RMCs support a possible connection between the gubernacular canal and type B RMCs. Further radiographic and anatomic studies will be helpful to determine the relationship.

Ethics statement

Ethical approval was taken from İstanbul Medipol Non-Interventional Clinical Research Ethics Committee (no. 10840098-604.01.01-E.65173).

Financial support and sponsorship

Nil.

Conflicts of interest

There are no conflicts of interest.

References

1. Rabie CM, Vranckx M, Rusque MI, Deambrosi C, Ockerman A, Politis C, *et al*. Anatomical relation of third molars and the retromolar canal. Br J Oral Maxillofac Surg 2019;57:765-70.
2. Motamedi MH, Gharedaghi J, Mehralizadeh S, Navi F, Badkoobeh A, Valaei N, *et al*. Anthropomorphic assessment of the retromolar foramen and retromolar nerve: Anomaly or variation of normal anatomy? Int J Oral Maxillofac Surg 2016;45:241-4.
3. Patil S, Matsuda Y, Nakajima K, Araki K, Okano T. Retromolar canals as observed on cone-beam computed tomography: Their incidence, course, and characteristics. Oral Surg Oral Med Oral Pathol Oral Radiol 2013;115:692-9.
4. Gamieldien MY, Van Schoor A. Retromolar foramen: An anatomical study with clinical considerations. Br J Oral Maxillofac Surg 2016;54:784-7.
5. Kim HJ, Kang H, Seo YS, Kim DK, Yu SK. Anatomic evaluation of the retromolar canal by histologic and radiologic analyses. Arch Oral Biol 2017;81:192-7.
6. Palma LF, Buck AF, Kfouri FÁ, Blachman IT, Lombardi LA, Cavalli MA. Evaluation of retromolar canals on cone beam computerized tomography scans and digital panoramic radiographs. Oral Maxillofac Surg 2017;21:307-12.
7. Akarslan ZZ, Kocabay C. Assessment of the associated symptoms, pathologies, positions and angulations of bilateral occurring mandibular third molars: İs there any similarity? Oral Surg Oral Med Oral Pathol Oral Radiol 2009;108:26-32.
8. Yilmaz S, Adisen MZ, Misirlioglu M, Yorubulut S. Assessment of third molar ımpaction pattern and associated clinical symptoms in a central anatolian Turkish population. Med Princ Pract 2016;25:169-75.
9. Ishii S, Abe S, Moro A, Yokomizo N, Kobayashi Y. The horizontal inclination angle is associated with the risk of inferior alveolar nerve injury during the extraction of mandibular third molars. Int J Oral Maxillofac Surg 2017;46:1626-34.
10. Eshghpour M, Nezadi A, Moradi A, Shamsabadi RM, Rezaei NM, Nejat A. Pattern of mandibular third molar impaction: A crosssectional study in northeast of Iran. Niger J Clin Pract 2014;17:673-7.
11. Orhan K, Aksoy S, Bilecenoglu B, Sakul BU, Paksoy CS. Evaluation of bifid mandibular canals with cone-beam computed tomography in a Turkish adult population: A retrospective study. Surg Radiol Anat 2011;3:501-7.
12. Kikuta S, Iwanaga J, Nakamura K, Hino K, Nakamura M, Kusukawa J. The retromolar canals and foramina: Radiographic observation and application to oral surgery. Surg Radiol Anat 2018;40:647-52.
13. von Arx T, Hänni A, Sendi P, Buser D, Bornstein MM. Radiographic study of the mandibular retromolar canal: An anatomic structure with clinical importance. J Endod 2011;37:1630-5.
14. Park MK, Jung W, Bae JH, Kwak HH. Anatomical and radiographic study of the mandibular retromolar canal. J Dent Sci 2016;11:370-6.
15. Capote TS, Gonçalves MA, Bonini Campos JA. Retromolar canal associated with age, side, sex, bifid mandibular canal, and accessory mental foramen in panoramic radiographs of Brazilians. Anat Res Int 2015;2015:434083.
16. Lizio G, Pelliccioni GA, Ghigi G, Fanelli A, Marchetti C. Radiographic assessment of the mandibular retromolar canal using cone-beam computed tomography. Acta Odontol Scand 2013;71:650-5.
17. Han SS, Hwang YS. Cone beam CT findings of retromolar canals in a Korean population. Surg Radiol Anat 2014;36:871-6.
18. Alves N, Deana NF. Anatomical and radiographical study of the retromolar canal and retromolar foramen in macerated mandibles. Int J Clin Exp Med 2015;8:4292-6.
19. Spin-Neto R, Matzen LH, Schropp L, Gotfredsen E, Wenzel A. Movement characteristics in young patients and the impact on CBCT image quality. Dentomaxillofac Radiol 2016;45:20150426.
20. Nardi C, Taliani GG, Castellani A, De Falco L, Selvi V, Calistri L. Repetition of examination due to motion artifacts in horizontal cone beam CT: Comparison among three different kinds of head support. J Int Soc Prev Community Dent 2017;7:208-13.

Original Article

Evaluation of Pharyngeal Airway by Cone-Beam Computed Tomography after Mono- and Bimaxillary Orthognathic Surgery

Merve Sarı, Esengül Şen, Nihat Akbulut, Seval Bayrak[1], Osman Demir[2]

Departments of Oral and Maxillofacial Surgery and [2]Biostatistics, Tokat Gaziosmanpasa University Faculty of Dentistry, Tokat, [1]Department of Oral and Maxillofacial Radiology, Faculty of Dentistry, Bolu Abant Izzet Baysal University, Bolu, Turkey

Abstract

Introduction: The aim of this study was to evaluate the changes of the pharyngeal airway obtained using mono-and bimaxillary orthognathic surgery in patients with skeletal malocclusion. **Material and Methods:** The analysis was conducted on cone-beam computed tomography images taken preoperatively and postoperatively of patients undergoing mono-or bimaxillary orthognathic surgery. The pharyngeal airway was divided into four airway volume segments and measured by planimetry. **Results:** The bimaxillary surgery group showed an increase in nasopharynx and velopharynx volumes and a decrease in glossopharynx and hypopharynx volumes ($P < 0.05$). The mandibular setback surgery group showed decreases in glossopharynx, hypopharynx, oropharynx, and pharynx volumes ($P < 0.05$). The mandibular advancement surgery group showed increases in glossopharynx, hypopharynx, oropharynx, and pharynx volumes ($P < 0.05$). The maxillary advancement surgery group showed increases in nasopharynx, velopharynx, and pharynx volumes ($P < 0.05$). **Discussion and Conclusion:** Mandibular setback surgery had a narrowing effect on the pharyngeal airway volume. Maxillary advancement surgery compensated for the constrictive effect of mandibular setback surgery on both the oropharynx and pharynx volumes. Although maxillary and mandibular advancement surgery affected different sites, these were the operations that contributed most to the increase in pharyngeal volume.

Keywords: *Cone-beam computed tomography, orthognathic surgery, pharyngeal airway*

Introduction

Orthognathic surgery and orthodontics are applied together with the overall aim of correcting dentofacial deformities through both functional and aesthetic changes.[1] Orthognathic surgery provides the ideal dental occlusion and facial esthetics to bring the patients to their desired position both socially and psychologically. Skeletal movements in orthognathic surgery can also cause changes in the pharyngeal airway space by pushing or stretching the soft tissues while changing the positions of the jaw and soft tissues to the required maxillomandibular relationship and esthetics.[2,3]

In the last 20 years, the pharyngeal airway has been a prominent issue in orthognathic surgery operations.[4-9] The maxilla and mandible are directly or indirectly connected to the tongue, soft palate, hyoid bone, and many muscles. Therefore, movement in these bones leads to spatial changes in bone-associated structures, while causing tension in the associated soft tissues and muscles. As a result, skeletal movement will result in changes in the nasal and oral cavity and airway volumes.[4-9] The main cause of concern is the fact that the pharyngeal airway space may narrow after orthognathic surgery, impeding airway during breathing. Orthognathic surgery involves skeletal movements in different directions, so the effects of these operations on the pharyngeal airway will also differ.[10] The aim of this study was to evaluate the effects of mono-or bimaxillary orthognathic surgery operations on the pharyngeal airway using cone-beam computed tomography (CBCT) images in patients with skeletal class II (maxillary hyperplasia and/or mandibular hypoplasia) or class III (maxillary hypoplasia and/or mandibular hyperplasia) and associated malocclusions. This information was also used to inform patients before surgery and to ensure necessary precautions before the operation when risk factors

How to cite this article: Sarı M, Şen E, Akbulut N, Bayrak S, Demir O. Evaluation of pharyngeal airway by cone-beam computed tomography after mono- and bimaxillary orthognathic surgery. J Anat Soc India 2022;71:54-60.

Article Info

Received: 16 September 2020
Accepted: 31 October 2021
Available online: 17 March 2022

Address for correspondence:
Dr. Merve Sarı, Department of Oral and Maxillofacial Surgery, Tokat Gaziosmanpasa University Faculty of Dentistry, Tokat/ Turkey.
E-mail: mervexsari3@gmail.com

Access this article online

Website: www.jasi.org.in
DOI: 10.4103/jasi.jasi_189_20
Quick Response Code:

(e.g., septum deviation and obesity) were present that could cause airway narrowing in the patient.

Material and Methods

This study was approved by Tokat Gaziosmanpaşa University Faculty of Medicine Clinical Research Ethics Committee and conformed to the Declaration of Helsinki (approval no: 18-KAEK-100). This retrospective study included images of 42 patients (This retrospective study included images of 42 patients (15 males; 27 females) who had skeletal class II (maxillary hyperplasia and/or mandibular hypoplasia) or class III (maxillary hypoplasia and/or mandibular hyperplasia) with associated malocclusions treated with mono-or bimaxillary orthognathic surgery at Tokat Gaziosmanpaşa University, Faculty of Dentistry, Department of Oral and Maxillofacial Surgery, during the period of 2015-2019. Patients without syndromes, who had skeletal class II (maxillary hyperplasia and/or mandibular hypoplasia) or class III (maxillary hypoplasia and/or mandibular hyperplasia) with associated malocclusions treated with mono-or bimaxillary orthognathic surgery, who had preoperative and postoperative CBCT records were included to the study. Patients with syndromes or craniofacial abnormalities (e.g., cleft lip and palate), who had previously undergone orthognathic or orthodontic treatment, or who had undergone genioplasty or rhinoplasty operations were excluded from the study. All patients provided written informed consent. The sex and age of the patients were recorded.

The patients were divided into the following four different groups according to the orthognathic surgical treatment method:

- Group 1: Patients with maxillary advancement + mandibular setback
- Group 2: Patients with mandibular setback alone
- Group 3: Patients with mandibular advancement alone
- Group 4: Patients with maxillary advancement alone.

All operations were performed by the same surgical team. Bilateral sagittal split ramus osteotomy and/or Le fort I osteotomy were performed in all patients who underwent mono-or bimaxillary orthognathic surgery. Both jaws were subjected to rigid internal fixation.

Cephalometric films were obtained for all patients 2 weeks before the surgery (T0) and 6 months after the surgery (T1). Cephalometric films were evaluated using a modified analysis method.[11] In this method, the plane with an angle of + 7° to the Sella-Nasion line is the horizontal reference plane, and the strut lowered to this plane from the Nasion point was used as a vertical reference plane. The distances of the hard and soft tissue landmarks to these 2 planes were measured on cephalometric films taken before and 6 months after the operation and the difference between them was recorded as the amount of hard tissue movement.

CBCT images were obtained for all patients to evaluate the three-dimensional changes in the pharyngeal airway 2 weeks before the surgery (T0) and 6 months after the surgery (T1). The CBCT images were obtained with a Galileos device under conditions of 98 kVp, 15–30 mA, 15 mm × 15 mm imaging area, 0.25 mm^3 voxel size, 2–5 s irradiation, and 14 s scanning time. While the images were being obtained, the patient was adjusted in a standing position so that the Frankfurt horizontal plane was parallel to the floor and the sagittal plane was perpendicular to the floor. Preoperative (T0) and postoperative 6^{th} month (T1) images were obtained with the same devices for each patient.

The Cavalieri Principle was applied to calculate the airway volume on the CBCT images. DICOM files of these images were transferred to the 3D-DOCTOR (3D-DOCTOR Able Software Corp., Lexington, USA) image analysis program. Measurements were performed on sagittal sections. The image was divided into 0.3 mm sequential sections. No gap was left between the sections. Airway volume measurements were performed in four sections: Nasopharynx, velopharynx, glossopharynx, and hypopharynx.

Planes drawn from the following anatomical points were used when separating these sections[12] [Figure 1]:

a. Nasopharynx: The region between the top of the upper airway and the hard palate plane (the plane between anterior nasal spine and posterior nasal spine). The line passing between posterior nasal spine and ala of vomer is its anterior border
b. Velopharynx: The region between the hard palate plane and the tip of the uvula
c. Glossopharynx: The region between the tip of the uvula and the upper part of the epiglottis
d. Hypopharynx: The region between the upper end and lower end of the epiglottis.

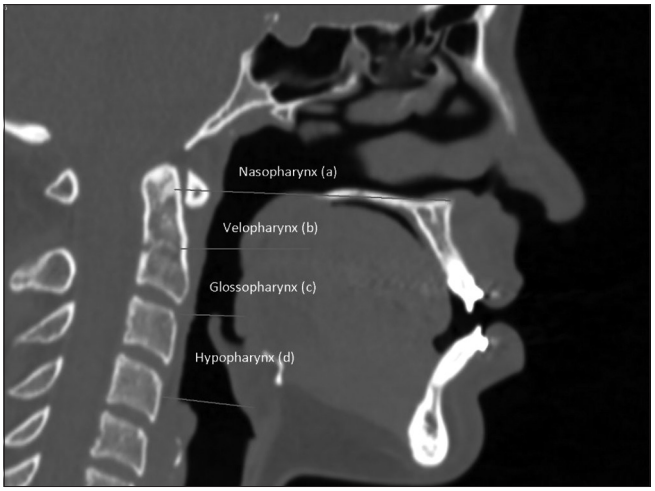

Figure 1: The pharyngeal airway volume was divided into four sections: (a) Nasopharynx; (b) Velopharynx; (c) Glossopharynx; (d) Hypopharynx

The oropharynx volume was obtained as the total of the velopharynx and glossopharynx volumes. The pharynx volume was obtained as the total of the nasopharynx, velopharynx, glossopharynx, and hypopharynx volumes. Thus, six-volume parameters were created from four airway volume segments.

The volume was calculated with the current program by determining the surface area of the related region on each section using a planimetry method. The boundaries of the related area on each section were manually drawn using a computer mouse [Figure 2]. Upon completion of the drawing, the program automatically multiplied the total surface area by the section thickness and calculated the total volume in mm^3. This procedure was performed for the nasopharynx, velopharynx, glossopharynx, and hypopharynx on pre- and postoperative images for all patients. The preoperative and postoperative images of each patient were measured twice by the same maxillofacial radiologist and their mean values were calculated.

Statistical analysis

Student's *t*-test and one-way ANOVA were used when comparing the means of quantitative variables between groups. A paired samples test was used for dependent groups. $P < 0.05$ was considered statistically significant. Ready Statistics software was used for the calculations (IBM SPSS Statistics 19, SPSS inc., an IBM Co., Somers, NY).

Results

In total, images of 42 treated patients were included in the study. The included patients were aged 15–34 years and had a mean age of 21.29 ± 4.45 years. The sex and age distributions of the subjects according to orthognathic surgical treatment method are shown in Table 1. No statistically significant difference was noted between the groups in terms of age ($P > 0.05$). Amounts of surgical movement in orthognathic surgical treatment groups are summarized in Table 2. No statistically significant difference was evident between the groups in terms of the extent of surgical movement ($P > 0.05$).

The volumetric changes in the pharyngeal airway volume segments are summarized in Table 3. In the bimaxillary group, the nasopharynx and velopharynx volumes increased and the glossopharynx and hypopharynx volumes decreased ($P < 0.05$). In the mandibular setback group, the glossopharynx, hypopharynx, oropharynx, and pharynx volumes all decreased ($P < 0.05$). In the mandibular advancement group, the glossopharynx, hypopharynx, oropharynx, and pharynx volumes all increased ($P < 0.05$). In the maxillary advancement group, the nasopharynx, velopharynx, and pharynx volumes increased ($P < 0.05$).

Discussion

Orthognathic surgery is widely applied for the correction of dentofacial deformities as well as for aesthetic improvement.[13] The effects of these operations on airway dimensions have been the subject of research for the past 30 years. In particular, studies focusing on mandibular setback operations have reported narrowing of the airway area.[7,14,15] Orthognathic surgery may cause changes in the surrounding structures and pharyngeal airway space by pulling forward or pushing backward the soft tissues as the positions of the jaws are altered to achieve the required maxillomandibular aesthetic and functional relationships.[2,3,16] A positional change in the maxilla affects the nasopharyngeal space, the posterior part of the nose, and the superior part of the soft palate. A change in the mandible position may affect hard and soft tissues in the oral and maxillofacial regions, including the upper respiratory tract.[13]

In the present study, the airway volume was evaluated at four levels - the nasopharynx, velopharynx, glossopharynx, and hypopharynx - and six-volume parameters were established. The volume measurements of the pharyngeal airway were the measurements used in airway determination referenced in the study by Chen *et al*.[12] As in the study of Tepecik

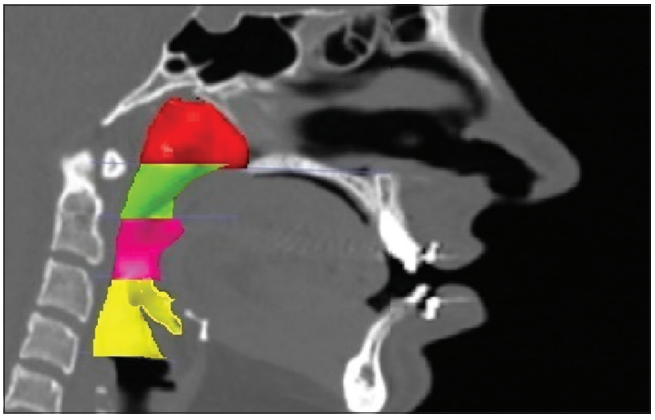

Figure 2: The 3D image of pharyngeal airway volume

Table 1: The sex and age distributions of the subjects according to orthognathic surgical treatment method

Orthognathic surgical treatment method	Male	Female	Mean age±SD
Maxillary advancement + mandibular setback (Group 1)	8	17	21.72±5.04
Mandibular setback (Group 2)	2	6	20.38±4.57
Mandibular advancement (Group 3)	3	1	21±2.16
Maxillary advancement (Group 4)	2	3	20.8±2.77

SD=Standard deviation

Table 2: Amounts of surgical movement in orthognathic surgical treatment groups

Amount of surgical movement (mm)	Orthognathic surgical treatment method, mean±SD				*P*
	Maxillary advancement + mandibular setback (Group 1)	Mandibular setback (Group 2)	Mandibular advancement (Group 3)	Maxillary advancement (Group 4)	
Amount of mandibular setback	4.73±1.71	5.13±1.83	-	-	0.578
Amount of mandibular advancement	-	-	7.13±1.03	-	-
Amount of maxillary advancement	5.33±1.3	-	-	6.7±2.33	0.070

P* value is significant at the 0.05 level. (P*<0.05). SD=Standard deviation

Table 3: The volumetric changes in the pharyngeal airway volume segments

Orthognathic surgical treatment method	Pharyngeal airway volume segments	Volumetric change (mm^3) mean±SD			
		T0	T1	ΔT	*P*
Maxillary advancement + mandibular setback (Group 1)	Nasopharynx volume	5704.6±1803.57	7036.2±2249.95	1331.6±1215.35	<0.001*
	Velopharynx volume	6178.56±2771.07	7903.16±3473.02	1724.6±1722.28	<0.001*
	Glossopharynx volume	5599.68±3104.56	4247.44±2070.55	−1352.24±1545.05	<0.001*
	Hypopharynx volume	5975.28±2161.9	4475.52±1949.89	−1499.76±1054.31	<0.001*
	Oropharynx volume	11,778.36±5152.22	12,150.6±4936.6	743.73±2068.45	0.400
	Pharynx volume	23,458.32±7507.23	23,662.32±7900.18	203.96±3103.23	0.745
Mandibular setback (Group 2)	Nasopharynx volume	5267.75±2438.09	5277.38±2455.38	9.63±24.9	0.978
	Velopharynx volume	5025.75±2296.49	5005.88±2297.61	−19.87±119.24	0.969
	Glossopharynx volume	6008.88±3921.26	4659.88±3192.84	−1349±1161.93	0.007*
	Hypopharynx volume	6218.25±1886.39	4647.25±1383.38	−1571±962.23	<0.001*
	Oropharynx volume	11,034.75±5947.3	9665.88±5317.24	−1368.97±1198.68	0.014*
	Pharynx volume	22,520.75±7315.3	19590.5±6657.17	−2930.43±1744.6	0.002*
Mandibular advancement (Group 3)	Nasopharynx volume	5788.5±2403.37	5746.25±2424.07	−42.25±35.69	0.932
	Velopharynx volume	6408.5±1602.45	6338±1671.28	−70.5±96.42	0.923
	Glossopharynx volume	3777.5±628.22	5698.5±1102.97	1921±558.79	0.007*
	Hypopharynx volume	3759±1821.03	5298±2541.09	1539±800.23	0.003*
	Oropharynx volume	10,185.75±2055.01	12,036.75±2273.28	1850.94±543.41	0.006*
	Pharynx volume	19,732.75±4493.32	23,081±5234.2	3348.04±922.93	0.005*
Maxillary advancement (Group 4)	Nasopharynx volume	4786.4±620.33	6200.8±926.13	1414.4±579.87	0.003*
	Velopharynx volume	5073.2±846.5	6563±1499.51	1489.8±1493.45	0.028*
	Glossopharynx volume	4398.6±2895.63	4356.8±2869.19	−41.8±45.01	0.945
	Hypopharynx volume	4075±1919.55	4059±1867.42	−16±99.31	0.971
	Oropharynx volume	9472±2380.03	10,919.8±3678.43	1447.91±1487.75	0.095
	Pharynx volume	18,333.2±2618.89	21,179.4±3733.1	2846.39±1275.87	0.008*

P* value is significant at the 0.05 level. (P*<0.05). T0=2 week preoperatively, T1=6 months postoperatively, ΔT=Difference between T1 and T0 (T1–T0). SD=Standard deviation

et al.,[16] the authors used reference points on soft tissue instead of vertebral reference points when separating airway segments. This was because the use of vertebral points for reference points does not provide an exact match of the boundaries of the velopharyngeal and glossopharyngeal regions that are most responsible for obstructive sleep apnea (OSA).[16] In addition, the vertebral lengths, upper or lower limits, and the locations do not correspond to the same site in each patient, so different regions are compared as a result. Therefore, the velopharyngeal and glossopharyngeal regions are more appropriately measured using points determined from the anatomical structures that form the boundaries or are adjacent to these structures.[16]

The literature shows two main trends regarding the changes in the pharyngeal airway as a result of bimaxillary surgery, but one trend is that the pharyngeal airway decreases[10,17,18] and then in the second trend, the oropharyngeal airway remains unchanged.[15,19-22] In the present study, the authors noted a significant decrease in pharyngeal volume in the mandibular setback group but no significant change in the bimaxillary group. Uesugi *et al*.[22] reported a reduction in the pharyngeal airway volume in the monomaxillary group of 40 class III patients undergoing mono-and bimaxillary surgery, whereas the change in the bimaxillary group was not significant. Park *et al*.[21] reported no significant decrease in pharyngeal airway space after mandibular setback surgery and found no physiological adaptation to maintain airway capacity in the pharyngeal airway. Some studies have suggested that bimaxillary surgery compensates for the pharyngeal airway narrowing caused by mandibular

setback surgery.[9,21] This probably reflects a balancing of the airway contraction after mandibular setback with the forward movement of the velopharyngeal muscular system due to maxillary advancement.[23]

In the present study, a significant increase was observed in the pharynx volume in the mandibular advancement and maxillary advancement groups. Hernández-Alfaro *et al*.[24] evaluated the effect of mono-and bimaxillary advancement on the pharyngeal airway with CBCT. They reported an average increase in pharyngeal airway volume of 69.8% in the bimaxillary advancement group, 78.3% in the mandibular advancement group, and 37.7% in the maxillary advancement group. In that study, a greater effect on the pharyngeal airway volume was suggested for mandibular advancement than for maxillary advancement.[24] Achilleos *et al*.[5] and Alves *et al*.[25] also reported an increased pharyngeal airway volume after mandibular advancement.

The nasopharyngeal airway was not included in previous assessments of the effect of only mandibular operations on airway sizes, as it was considered to be unaffected by movement of the mandible.[7,8,15,26] Present study revealed no significant change in the nasopharynx volume in the mandibular setback and advancement groups, which included only surgery on the mandible. A few studies have evaluated the changes in the nasopharynx after mandibular setback surgery but reported no significant change.[14,21]

In the present study, the authors observed a significant increase in the nasopharynx volume in the bimaxillary and maxillary advancement groups. Progression of the maxilla and subsequent forward movement of the soft palate has been previously reported to increase the volume of the nasopharynx.[27] In most studies, although the nasopharynx volume tends to increase, no significant changes have been reported after bimaxillary surgery.[16,18,21,22] Li *et al*.[18] reported an increase in the nasopharyngeal volume from 6.07 cm^3 to 6.10 cm^3 at 6 months after bimaxillary surgery. However, despite the forward movement of the maxilla, the volume of the nasopharynx remained almost the same, in contradiction to present findings.[18] Li *et al*.[18] reported a mean forward motion of the maxilla of 3.5 ± 0.8 mm, whereas the authors found a mean movement of 5.33 ± 1.3 mm. This difference in findings may reflect the amount of forward movement of the maxilla and increase in the airway. Becker *et al*.[23] reported an increase in nasopharynx volume after bimaxillary surgery.

Many studies have reported that mandibular setback surgery decreases the pharyngeal airway space.[9,20,22,23] A posteroinferior displacement of the hyoid bone, which moves the tongue in a similar direction, is observed after mandibular setback surgery.[4,13,26] An increase in the angle of contact between the posteriorly displaced tongue and the soft palate may narrow the glossopharyngeal area, thereby decreasing the volume of the oropharynx.[4,26] Enacar *et al*.[4] emphasized a need for careful monitoring of the decrease in the oropharyngeal airway space after mandibular setback. Several studies have shown a decrease in the size of glossopharyngeal and hypopharyngeal airways after mandibular setback surgery.[2,6,9,13] In the present study, the decrease in the glossopharynx, oropharynx, and hypopharynx volumes in the mandibular setback group was statistically significant, but no significant change was evident in the velopharynx volume. The glossopharynx and hypopharynx probably undergo narrowing due to the contraction of the hyoglossus and consequent retroposition of the tongue corpus. Yang *et al*.[28] reported a decrease in the velopharynx, glossopharynx, oropharynx, and hypopharynx volumes after mandibular setback. In that study, a velopharyngeal constriction was reported as a result of soft palate lengthening and elevation caused by posterior movement of the tongue when the mandible was moved backward. Similar to the present study, other studies also have reported a decrease in oropharynx and hypopharynx volumes after mandibular setback surgery during short and long follow-up periods.[21,26]

In the present study, in the maxillary advancement group, the velopharynx and oropharynx volumes increased, but only the increase in the velopharynx volume was statistically significant. An increase in these regions is expected due to the anterior movement of the supporting structures. The increase in velopharynx volume and decrease in glossopharynx and hypopharynx volumes were significant in the bimaxillary group, whereas the change in oropharynx volume was not significant. Hatab *et al*.[3] and Tepecik *et al*.[16] reported no change in velopharyngeal airway volume after bimaxillary surgery. However, other studies have reported significant constriction of the velopharyngeal airway volume after surgery.[10,21] Some studies report no change in the glossopharyngeal volume after bimaxillary surgery[3,16,21] while others report a significant decrease.[10] In the present study, the absence of any significant change in the oropharynx volume in the bimaxillary group was consistent with the findings of some studies,[22] although Tepecik *et al*.,[16] Li *et al*.,[18] and Lee *et al*.[20] reported a decrease in the volume of oropharynx after bimaxillary surgery. By contrast, Jakobsone *et al*.[19] reported a significant increase in oropharynx and hypopharynx volumes after bimaxillary surgery. In the present study, the authors observed that maxillary advancement in the bimaxillary group increased the velopharynx volume, while mandibular setback decreased the glossopharynx volume, to produce a balancing effect on oropharynx volume obtained by summing velopharynx and glossopharynx volumes. This indicates that maxillary advancement decreases the constructive effect of a mandibular setback on the oropharynx volume.

In the present study, the bimaxillary group showed a significant increase in velopharynx volume compared to the mandibular setback group. In their meta-analysis,

Christovam *et al*.[29] reported a decrease in velopharyngeal and glossopharyngeal airway volumes after mandibular setback surgery, whereas the velopharyngeal airway volume decreased and glossopharyngeal airway volume increased after bimaxillary surgery. This appears contradictory and is exactly the opposite of the expected result. Brunetto *et al*.[17] suggested that surgeries in which both jaws move in the same direction tend to have more predictable results. In addition, when the base of the tongue moves backward, the soft palate may be pushed in the same direction, resulting in a decrease in the velopharyngeal volume.[17] In addition, the decrease in the hypopharynx volume in the mandibular setback and bimaxillary groups is expected, due to the posteroinferior movement of the hyoid bone in response to the posterior movement of the mandible. Becker *et al*.[23] reported a decrease in the volume of the hypopharynx after bimaxillary surgery.

A significant increase was detected in the glossopharynx, oropharynx, and hypopharynx volumes in the mandibular advancement group. Mandibular advancement has been previously reported to increase the glossopharyngeal airway volume.[29] Jiang *et al*.[30] and Sahoo *et al*.[31] reported a significant increase in the oropharyngeal and hypopharyngeal airway space as a result of mandibular advancement.

Conclusion

Mandibular setback had a constrictive effect on the pharyngeal airway volume. Therefore, extensive surgical movements should be avoided in the presence of a mandibular setback indications, unless airway dimension is greater than normal prior to surgery. Although maxillary advancement and mandibular advancement affect different sites, they are operations that contribute to increased pharyngeal volume. Therefore, these surgeries should be the first choice, especially in patients at risk for OSA. Maxillary advancement compensated for the constrictive effect of mandibular setback on both the oropharynx and pharynx volumes, even if bimaxillary operations included mandibular setback surgery. If the patient has predisposing factors for the development of OSA, such as obesity, macroglossia, short neck, and large uvula, then bimaxillary surgery should be preferred over mandibular setback, or, if possible, only maxillary advancement should be performed.

However, this study had some limitations. The number of samples was not homogeneous, and the postoperative period could not be evaluated for longer than 6 months. Sample sizes for mandibular setback, mandibular advancement, and maxillary advancement groups are too small to make conclusive evidence of airway changes. Therefore, future studies should be conducted on larger and more homogenous patient groups for longer periods and should include a minimum of three axial area parameters. However, to the best of our knowledge, this study is the first to use Cavalieri Principle to calculate the volume of pharyngeal airway.

Financial support and sponsorship

Nil.

Conflicts of interest

There are no conflicts of interest

References

1. Selber JC, Rosen HM. Aesthetics of facial skeletal surgery. Clin Plast Surg 2007;34:437-45.
2. Lye KW. Effect of orthognathic surgery on the posterior airway space (PAS). Ann Acad Med Singap 2008;37:677-82.
3. Hatab NA, Konstantinović VS, Mudrak JK. Pharyngeal airway changes after mono- and bimaxillary surgery in skeletal class III patients: Cone-beam computed tomography evaluation. J Craniomaxillofac Surg 2015;43:491-6.
4. Enacar A, Aksoy AU, Sençift Y, Haydar B, Aras K. Changes in hypopharyngeal airway space and in tongue and hyoid bone positions following the surgical correction of mandibular prognathism. Int J Adult Orthodon Orthognath Surg 1994;9:285-90.
5. Achilleos S, Krogstad O, Lyberg T. Surgical mandibular advancement and changes in uvuloglossopharyngeal morphology and head posture: A short- and long-term cephalometric study in males. Eur J Orthod 2000;22:367-81.
6. Samman N, Tang SS, Xia J. Cephalometric study of the upper airway in surgically corrected class III skeletal deformity. Int J Adult Orthodon Orthognath Surg 2002;17:180-90.
7. Kawakami M, Yamamoto K, Fujimoto M, Ohgi K, Inoue M, Kirita T. Changes in tongue and hyoid positions, and posterior airway space following mandibular setback surgery. J Craniomaxillofac Surg 2005;33:107-10.
8. Muto T, Yamazaki A, Takeda S, Kawakami J, Tsuji Y, Shibata T, *et al.* Relationship between the pharyngeal airway space and craniofacial morphology, taking into account head posture. Int J Oral Maxillofac Surg 2006;35:132-6.
9. Chen F, Terada K, Hua Y, Saito I. Effects of bimaxillary surgery and mandibular setback surgery on pharyngeal airway measurements in patients with Class III skeletal deformities. Am J Orthod Dentofacial Orthop 2007;131:372-7.
10. Shin JH, Kim MA, Park IY, Park YH. A 2-year follow-up of changes after bimaxillary surgery in patients with mandibular prognathism: 3-dimensional analysis of pharyngeal airway volume and hyoid bone position. J Oral Maxillofac Surg 2015;73:9.e1-9.
11. Lew KK, Loh FC, Yeo JF, Loh HS. Evaluation of soft tissue profile following intraoral ramus osteotomy in Chinese adults with mandibular prognathism. Int J Adult Orthodon Orthognath Surg 1990;5:189-97.
12. Chen X, Liu D, Liu J, Wu Z, Xie Y, Li L, *et al.* Three-dimensional evaluation of the upper airway morphological changes in growing patients with skeletal class III malocclusion treated by protraction headgear and rapid palatal expansion: A comparative research. PLoS One 2015;10:e0135273.
13. Athanasiou AE, Toutountzakis N, Mavreas D, Ritzau M, Wenzel A. Alterations of hyoid bone position and pharyngeal depth and their relationship after surgical correction of mandibular prognathism. Am J Orthod Dentofacial Orthop 1991;100:259-65.
14. Chen CM, Lai S, Chen KK, Lee HE. Correlation between the

pharyngeal airway space and head posture after surgery for mandibular prognathism. Biomed Res Int 2015;2015:251021.

15. Muto T, Yamazaki A, Takeda S, Sato Y. Effect of bilateral sagittal split ramus osteotomy setback on the soft palate and pharyngeal airway space. Int J Oral Maxillofac Surg 2008;37:419-23.
16. Tepecik T, Ertaş Ü, Akgün M. Effects of bimaxillary orthognathic surgery on pharyngeal airway and respiratory function at sleep in patients with class III skeletal relationship. J Craniomaxillofac Surg 2018;46:645-53.
17. Brunetto DP, Velasco L, Koerich L, Araújo MT. Prediction of 3-dimensional pharyngeal airway changes after orthognathic surgery: A preliminary study. Am J Orthod Dentofacial Orthop 2014;146:299-309.
18. Li YM, Liu JL, Zhao JL, Dai J, Wang L, Chen JW. Morphological changes in the pharyngeal airway of female skeletal class III patients following bimaxillary surgery: A cone beam computed tomography evaluation. Int J Oral Maxillofac Surg 2014;43:862-7.
19. Jakobsone G, Neimane L, Krumina G. Two- and three-dimensional evaluation of the upper airway after bimaxillary correction of Class III malocclusion. Oral Surg Oral Med Oral Pathol Oral Radiol Endod 2010;110:234-42.
20. Lee Y, Chun YS, Kang N, Kim M. Volumetric changes in the upper airway after bimaxillary surgery for skeletal class III malocclusions: A case series study using 3-dimensional cone-beam computed tomography. J Oral Maxillofac Surg 2012;70:2867-75.
21. Park SB, Kim YI, Son WS, Hwang DS, Cho BH. Cone-beam computed tomography evaluation of short- and long-term airway change and stability after orthognathic surgery in patients with Class III skeletal deformities: Bimaxillary surgery and mandibular setback surgery. Int J Oral Maxillofac Surg 2012;41:87-93.
22. Uesugi T, Kobayashi T, Hasebe D, Tanaka R, Ike M, Saito C. Effects of orthognathic surgery on pharyngeal airway and respiratory function during sleep in patients with mandibular prognathism. Int J Oral Maxillofac Surg 2014;43:1082-90.
23. Becker OE, Avelar RL, Göelzer JG, Dolzan AN, Haas OL Jr., De Oliveira RB. Pharyngeal airway changes in class III patients treated with double jaw orthognathic surgery - Maxillary advancement and mandibular setback. J Oral Maxillofac Surg 2012;70:e639-47.
24. Hernández-Alfaro F, Guijarro-Martínez R, Mareque-Bueno J. Effect of mono- and bimaxillary advancement on pharyngeal airway volume: Cone-beam computed tomography evaluation. J Oral Maxillofac Surg 2011;69:e395-400.
25. Alves M Jr., Franzotti ES, Baratieri C, Nunes LK, Nojima LI, Ruellas AC. Evaluation of pharyngeal airway space amongst different skeletal patterns. Int J Oral Maxillofac Surg 2012;41:814-9.
26. Irani SK, Oliver DR, Movahed R, Kim YI, Thiesen G, Kim KB. Pharyngeal airway evaluation after isolated mandibular setback surgery using cone-beam computed tomography. Am J Orthod Dentofacial Orthop 2018;153:46-53.
27. Rosário HD, Oliveira GM, Freires IA, de Souza Matos F, Paranhos LR. Efficiency of bimaxillary advancement surgery in increasing the volume of the upper airways: A systematic review of observational studies and meta-analysis. Eur Arch Otorhinolaryngol 2017;274:35-44.
28. Yang Y, Yang K, Zhao Y. Three-dimensional changes in the upper airway of skeletal class III patients after different orthognathic surgical procedures. J Oral Maxillofac Surg 2018;76:155-64.
29. Christovam IO, Lisboa CO, Ferreira DM, Cury-Saramago AA, Mattos CT. Upper airway dimensions in patients undergoing orthognathic surgery: A systematic review and meta-analysis. Int J Oral Maxillofac Surg 2016;45:460-71.
30. Jiang C, Yi Y, Jiang C, Fang S, Wang J. Pharyngeal airway space and hyoid bone positioning after different orthognathic surgeries in skeletal class II patients. J Oral Maxillofac Surg 2017;75:1482-90.
31. Sahoo NK, Jayan B, Ramakrishna N, Chopra SS, Kochar G. Evaluation of upper airway dimensional changes and hyoid position following mandibular advancement in patients with skeletal class II malocclusion. J Craniofac Surg 2012;23:e623-7.

Original Article

Typing and Morphometric Analysis of the Pterion on Human Skull of Central Anatolia

Duygu Akin Saygın[1], Anıl Didem Aydin Kabakci[1], Şerife Alpa[2], Mustafa Buyukmumcu[3], Mehmet Tuğrul Yilmaz[1]

[1]Department of Anatomy, Meram Faculty of Medicine, University of Necmettin Erbakan, Konya/Turkey, [2]Department of Anatomy, Faculty of Medicine, University of Karatay, Konya/Turkey, [3]Department of Anatomy, Faculty of Medicine, University of Bezmialem, Istanbul/Turkey

Abstract

Introduction: Pterion is seen in the norma lateralis of the skull and is shaped like the letter H. Pterional approach such as retro-orbital, sellar, sub-frontal, replate areas, anterior circulation, and olfactory meningiomas, tumors involving downstream of the frontal lobe such as the orbital, basilar artery aneurysm is a commonly preferred surgical approach. The present study focused on the typing of the pterion and morphometric measurements between the pterion and surrounding important anatomic spots. **Material and Methods:** The present study was performed with pterion typing of 107 skull (a total of 214 sides including the right and left sides) within Anatomy Laboratories of Necmettin Erbakan University, Meram Faculty of Medicine, and KTO Karatay University, Medicine Faculty. Distance between the pterion and some important (mid-point of the superior edge of the zygomatic arch, the anterior and posterior edge of the frontozygomatic suture, the tip of the mastoid process, and anterosuperior edge of suprameatal spine and asterion) spots were measured through a digital caliper in millimeter. In addition to the classification made by Murphy, three different classifications were made. The pterion was classified into seven types. **Results:** The rates of the types were sphenoparietal type by 55.60%, epipteric type by 3.73%, stellate type by 2.33%, frontotemporal type by 0.4%, wormian type by 5.14%, frontoparietal type by 8.87%, and frontoparietal sphenoidtype by 23.83%. **Discussion and Conclusion:** Morphometric characteristics of the pterion were detected in detail by the present study. Moreover, the knowledge of typing would serve as an important guide for surgical planning and procedures and may contribute to further anthropological studies. This study is aimed at the Central Anatolia population and can be conducted among other populations.

Keywords: *Anatomic, skull, morphometry, pterion*

Introduction

Pterion is a "H" shape. Small but also important marking point on the intersection point of four bones including the frontal, parietal, frontal, squamous part of the temporal bone, and major wing of the sphenoid bone.[1,2] Such point indicates the anterior branch of the medial meningeal artery and located between the skull base and calvarium adjacent to important formations such as lesions on the motor speaking region of the left Broca, insula, and lateral sulcus (Sylvian fissure).[3,4] Pterion is used in the treatment of patients with transcranial aneurysm, removal of some tumors in neurosurgery, intervention to middle meningeal artery and internal carotid artery, in surgical approaches various diseases such as traumatic "optic" neuropathy. These approaches bring advantages such as minor tissue damage, less brain retraction, a good cosmetic result and shorter surgical time.[5] However there are ethnic and gender differences for location of pterion, symmetrical and asymmetrical pterion types are important for surgical procedure.[1] The difference between the right and left sides is closed; however, it should be noted that the procedure is performed on the left side of the skull due to differences in superficial anatomic indicators and underlying soft tissue. Variations of the pterion may cause surgical complications.[2,5] The first classification was identified by Broca[4] as sphenoparietal, frontotemporal, and stellate. Another classification was defined by Murphy[6] in four types including sphenoparietal, frontotemporal, stellate, and epipteric types. Six types were identified in studies conducted by Wang *et al.*,[7]

The present study aimed to determine pterion types on the skulls obtained from the Central Anatolian region and to reveal

How to cite this article: Saygın DA, Aydin Kabakci AD, Alpa Ş, Buyukmumcu M, Yilmaz MT. Typing and morphometric analysis of the pterion on human skull of central anatolia. J Anat Soc India 2022;71:61-70.

Article Info

Received: 17 January 2021
Accepted: 20 April 2021
Available online: 17 March 2022

Address for correspondence:
Dr. Duygu Akin Saygin, Department of Anatomy, Meram Faculty of Medicine, University of Necmettin Erbakan, 42090 Meram, Konya, Turkey.
E-mail: d.akin.42@hotmail.com

Access this article online

Website: www.jasi.org.in
DOI: 10.4103/JASI.JASI_7_20
Quick Response Code:

some important anatomic points as well as the distance between such points on the pterion which is important for surgical procedures.

Material and Methods

The present study was conducted on typing of 107 skull (totally 214 sides as right and left) in the collection of Anatomy Laboratory of Meram Faculty of Medicine within Necmettin Erbakan University and Faculty of Medicine of KTO Karatay University. The morphometric measurements of 57 skull (fully intact anatomic points for measurement) were measured. All measurements were performed on the skulls with unknown gender which were obtained as a result of excavations in Central Anatolia. Measurements of the skull were performed through a digital caliper and provided in millimeters (mm). The consent for the study was obtained through Decision 2016/011 of Ethical Committee for Non-Pharmaceutical and Medical Device Researches of Faculty of Medicine within KTO Karatay University.

Pterion morphometric measurements

Pterion-anterior edge of frontozygomatic suture (PFZSa)

The shortest distance between the anterior edge of the frontozygomatic suture and the center of the pterion.

Pterion-posterior edge of frontozygomatic suture (PFZSp)

The shortest distance between the posterolateral edge of frontozygomatic suture and the center of the pterion.

Pterion- zygomatic angle (PZangle)

The distance between the lowest point of the zygomatic angle and the center of the pterion.

Pterion-posterior edge of temporozygomatic suture (PTZSp)

The distance between the posterior edge of temporozygomatic suture and the center of the pterion.

Pterion -zygomatic arch (PZarch)

The distance between the middle point of the zygomatic arch and the center of the pterion.

Pterion- mandibular fossa (PMF)

The shortest distance between the base of the mandibular fossa and the center of the pterion.

Pterion-mastoid process (PMP)

The shortest distance between the lowest edge of the mastoid process and the center of the pterion.

Pterion -suprameatal spine (PSS)

The shortest distance between suprameatal spine and the center of the pterion.

Pterion –asterion (PA)

The shortest distance between asterion and the center of the pterion.

The schematic drawing of all measurement points is shown in Figure 1.

Pterion types

Typing of the pterion was identified on both sides of the skull by Murphy.[6] Furthermore, three different types were revealed in our study.

Sphenoparietal type (Type 1)

The first type is the sphenoparietal type where sphenoid and parietal bones union directly.

Frontotemporal type (Type 2)

The second type is the frontotemporal type that frontal and temporal bones reversely contact with each other.

Epipteric type (Type 3)

The third type includes a small suture bone between the parietal bone and the major wing of the sphenoid bone.

Stellate type (Type 4)

The fourth type is the stellate type which appears by the intersection of four bones including frontal, temporal, parietal, and sphenoid bones.

Frontoparietal type (Type 5)

The fifth type appears by the union of frontal and parietal bones.

Frontoparietosphenoid type (Type 6)

The sixth type occurs by the union of frontal, parietal, and sphenoid bones.

Wormian type (Type 7)

The seventh type is revealed by some researchers and identified as the existence of wormian bone on the sphenoparietal type.

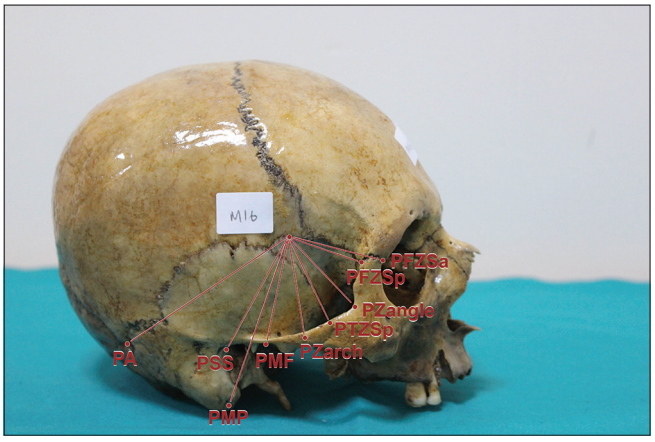

Figure 1: Linear measurements related to the pterion and neighboring structures. (PFZSa: Pterion-anterior edge of frontozygomatic suture, PFZSp: Pterion-posterior edge of frontozygomatic suture, PZangle: Pterion-zygomatic angle, PTZSp: Pterion temporozygomatic suture posterior, PZarch: Pterion-zygomatic arch, PMF: Pterion-mandibular fossa, PSS: Pterion-suprameatal spine, PMP: Pterion-mastoid process, PA: Pterion-asterion

Both the schematic shapes (in the upper corner of the pictures) and the original photographs of all pterion types are given in Figure 2. The data obtained were evaluated by SPSS 21.0 (IBM, New York, USA).Data were analyzed by descriptive (mean value, standart deviation (SD), maximum (max.) and minimum (min.) values, percentages) and quantitative methods. Results were evaluated statistically at a confidence level of 95%; differences at a $P < 0.01$ were accepted as statistically significant.

Results

The present study was performed under two groups including morphometric measurements and pterion typing. Morphometric measurements of the pterion were done on 114 pterion points including 57 right and 57 left points as well as adjacent formations. PSS, PMP were found larger on the left side when compared with the right. There was not any significant difference in linear measurements of the pterion between the right and left sides of the skull [Table 1].

In our study, we classified the pterion-forming bone combination into 7 types. The incidence on the right side is as follows; type 1 (55.1%) >type 6 (25.2%>type 5 (8.4%) >type 3 (4.7%) > type 7 (3.7%) > type 4 (2.8%). Type 2 was not detected in any skull on the right side. On left side, their frequency were found as type 1 (56.1%) > type 6 (22.4%) > type 5 (9.3%) > type 3 (5.6%) > type 7 (3.7%) > type 2 (0.9%) [Figure 2]. Seven combinations were detected among various types on both sides of the skull [Table 2]. The sphenoparietal pterion was the predominant type in both right and left sides by 55.1% and 56.1%, respectively. The frontotemporal was detected as the least type on both sides [Figure 2]. Symmetrical combinations were higher (%75.7) in type 1 (Sp) (46.7%) and type 6 (18.7%) [Table 2].

The common observed asymmetrical combinations were sphenoparieatal-epipteric (type 1–3, 24.3%) and frontoparietal-frontoparietosphenoidal (type 5–6, 4.7%), respectively. Type 2 has not presented a combination with any other type, except type 1 (0.9%). The distance between the pterion and the anterior and posterior edge of frontozygomatic suture, the distance between pterion and the midpoint of the zygomatic arch were measured.

A comparison was also done between the left and right sides of all skulls. The study revealed a significantly higher pterion on the right side according to the left. However, there was not any difference on the sides [Table 1]. Vertical distance between the upper edge of the zygomatic arch and center of the pterion was 39.52 ± 7.09 on the left and 41.06 ± 6.01 mm on the right on 57 skulls. The correlation associations between right and left pterion measurements were revealed in Table 3 and 4. A positive and strong association was found between all linear measurements on the right and left except Pterion- anterior edge of frontozygomatic suture.

Discussion

Pterion type and distance of the pterion to adjacent formations are very important for neurosurgery. Pterion

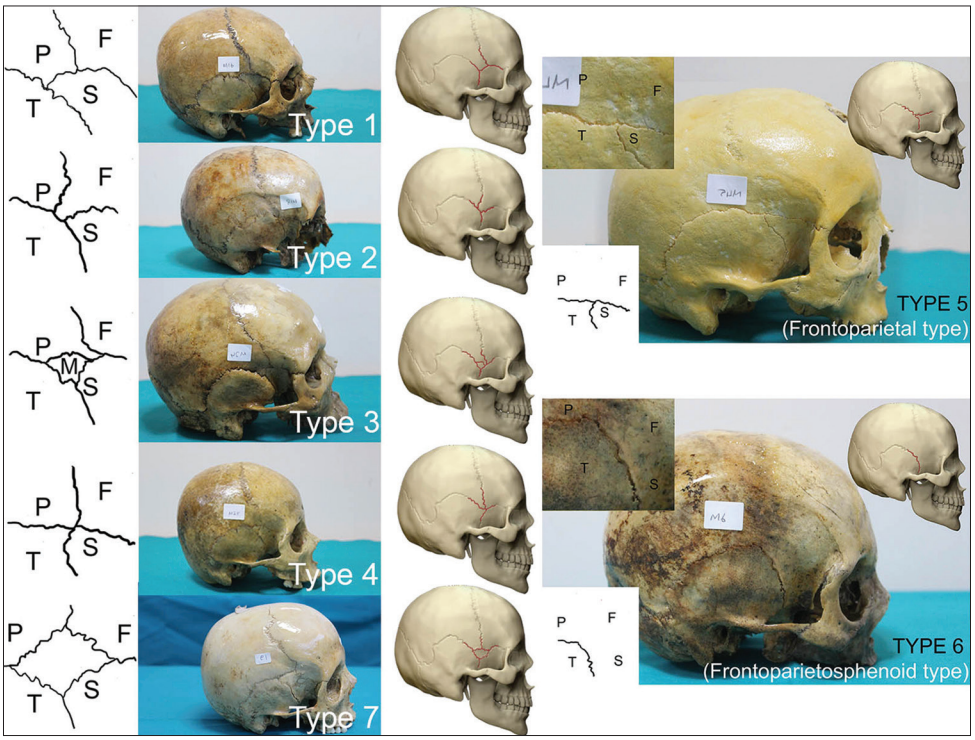

Figure 2: Classification of the shape of the pterion. (Type 1: Sphenoparietal, Type 2: Frontotemporal, Type 3: Epipteric, Type 4: Stellate, Type 5: Frontoparietal, Type 6: Frontoparietosphenoidal, Type 7: Wormian)

Table 1: Mean and standard deviations of the linear distances between pterion and specific bony landmarks according to sides (mm)

Parameters	Right				Left				*P*
	n	Min.	Max.	Mean±SD	*n*	Min.	Max.	Mean±SD	
PFZSa	57	19.59	56.13	37.89±6.86	57	15.56	65.45	37.56±7.31	0.768
PFZSp	57	17.76	50.2	32.70±6.43	57	22.31	54.34	32.23±6.34	0.549
PZangle	57	28.8	59.62	41.73±6.73	57	28.95	78.43	41.07±7.84	0.458
PTZSp	57	27.6	59.98	41.9±6.69	57	5.62	81.05	40.09±8.68	0.193
PZarch	57	26.14	58.62	41.06±6.01	57	27.51	79.03	39.52±7.09	0.066
PMF	57	30.54	64.51	46.64±6.3	57	31.47	82.75	45.71±7.42	0.346
PSS	57	39.64	71.37	56.12±6.79	57	31.58	95.95	56.90±9.1	0.440
PMP	57	40.48	102.23	80.29±11.44	57	42.73	123.23	80.52±10.48	0.875
PA	57	55.17	282.77	89.21±27.49	57	51.55	126.57	87.19±10.57	0.573

P<0.05 differences between group. *Mean*: Average, *SD*: Standard deviation, *PFZSa*: Pterion-anterior edge of frontozygomatic suture, *PFZSp*: Pterion-posterior edge of frontozygomatic suture, *PZangle*: Pterion-zygomatic angle, *PTZSp*: Pterion temporozygomatic suture posterior, *PZarch*: Pterion-zygomatic arch, *PMF*: Pterion-mandibular fossa, *PSS*: Pterion-suprameatal spine, *PMP*: Pterion-mastoid process, *PA*: Pterion-asterion

Table 2: The comparison of the incidences of the pterion types according to sides (*n*=107)

Pterion types	Side		Total, *n* (%)
	Right, *n* (%)	Left, *n* (%)	
Type 1	59 (55.1)	60 (56.1)	119 (55.6)
Type 2	0	1 (0.9)	1 (0.5)
Type 3	4 (3.7)	4 (3.7)	8 (3.7)
Type 4	3 (2.8)	2 (1.9)	5 (2.3)
Type 5	9 (8.4)	10 (9.3)	19 (8.9)
Type 6	27 (25.2)	24 (22.4)	51 (23.8)
Type 7	5 (4.7)	6 (5.6)	11 (5.1)
Total	107 (100)	107 (100)	214 (100)

Type 1: Sphenoparietal, Type 2: Frontotemporal,
Type 3: Epipteric, Type 4: Stellate, Type 5: Frontoparietal,
Type 6: Frontoparietosphenoidal, Type 7: Wormian

which is called Sylvian point is a great importance due to the separation of the anterior branch of middle meningeal artery and the separation of the lateral sulcus to the ascendens and posterior ramus behind this point. Also, Broca's motor speech central was located approximately the width of a finger above the pterion.[1-4] Bleeding in the anterior branch of the medial meningeal artery is the most frequent cause for acute epidural hematoma and pterion is used as a guide for the location of such anterior branch. Nevertheless, the pertional approach is used for neurosurgical procedures such as aneurysms, cellar and supracellar lesions, frontotemporal lesions and sphenoid bridge meningiomas.[1] Furthermore, the pterion known as the anterolateral fontanella has a membranous structure during birth and fetal life. As the skull passes through the birth canal during birth, the membranous structures overlap and allow it to pass more easily.[6] Our current study was carried out in the skull of a Central Anatolian human. Murphy[6] reported that the variations that may be seen in pterion may vary with environmental and genetic factors. Wang *et al.,*[7] in their study on mouse models, they found that the variations in the suture pattern were responsible for the joints of the MSX 2 gene (ten 5q35,2) belonging to the homeobox family.

In the literature, pterion is generally classified into 4 types.[6,7,9-41] In our study, unlike other studies, pterion was classified into 7 types. In the studies carried out up to this time, many researchers have classified Murphy[6] as 4 types (Sphenoparietal, Frontotemporal, Epipteric, and Stellate) considering the classification he made in 1956. In our study, three different types were revealed as the type in which 2 (type 5 and 6) formed wormian bones, which are formed by the fusion of bones and 1 (type 7) resembles the epipteric type but between 4 bones. In the previous studies, frontotemporal, stellate, and epipteric types have wide variations; however, the most common type was detected as sphenoparietal type in our study [Table 2,5]. Ethnic differences are obvious in the bone configuration of the pterion. However, the differences between the studies may depend on the differences in management and classification. The sphenoparietal type was also detected more by 55.6% than other types in the present study.

There are a limited number of studies on pterion typing in the bones of the Turkish population.[1,2,5,31] Oguz *et al*.,[5] found sphenoparietal type by 88% (96% right, 79% left) in their study where the location of the medial meningeal artery and pterion was investigated; Aksu *et al*.,[1] detected sphenoparietal type by 85.2% (42.2% right, 43% left) in their study conducted on adult skulls in Western Anatolia; Sindel *et al*.,[31] found the ratio of sphenoid type as 63% in their morphometric study. Ersoy *et al*.,[2] detected the ratio as 87.35% in their study "epiteric bones in pterion may be a surgical pitfall;" however, distribution on the right and left sides was not reported [Table 5]. The ratio was found 55.6% (55.1% right, 56.1% left) in the present study. Lower rates found in the present study may be caused by the fact that craniums in the studies belong to different regions. Since Oguz *et al*.,[5] studies on male skulls, Aksu *et al*.,[1] study on human craniums

Table 3: Pearson correlation coefficient between parameters belonging to right pterion.

Parameters (Right)	PFZSa	PFZSp	PZangle	PTZSp	PZarch	PMF	PMP	PSS	PA
PA									
r	0.274*	0.219	0.350**	0.330*	0.250	0.332*	0.341**	0.464**	1
P	0.039	0.102	0.008	0.012	0.061	0.012	0.010	0.000	
PSS									
r	0.508**	0.397**	0.461**	0.470**	0.439**	0.594**	0.692**	1	
P	0.000	0.002	0.000	0.000	0.001	0.000	0.000		
PMP									
r	0.430**	0.341**	0.506**	0.616**	0.647**	0.853**	1		
P	0.001	0.009	0.000	0.000	0.000	0.000			
PMF									
r	0.488**	0.439**	0.588**	0.668**	0.782**	1			
P	0.000	0.001	0.000	0.000	0.000				
PZarch									
r	0.603**	0.717**	0.821**	0.888**	1				
P	0.000	0.000	0.000	0.000					
PTZSp									
r	0.734**	0.764**	0.955**	1					
P	0.000	0.000	0.000						
PZangle									
r	0.818**	0.851**	1						
P	0.000	0.000							
PFZSp									
r	0.850**	1							
P	0.000								
PFZSa									
r	1								
P									

*Correlation is significant at the 0.05 level (two-tailed), **Correlation is significant at the 0.01 level (two-tailed), $P<0.05$ differences between group.[8] PFZSa: Pterion-anterior edge of frontozygomatic suture, PFZSp: Pterion-posterior edge of frontozygomatic suture, PZangle: Pterion-zygomatic angle, PTZSp: Pterion temporozygomatic suture posterior, PZarch: Pterion-zygomatic arch, PMF: Pterion-mandibular fossa, PSS: Pterion-suprameatal spine, PMP: Pterion-mastoid process , PA: Pterion-asterion

of Western Anatolia and we analyzed the craniums of the Central Anatolian population. A significant difference was observed. Furthermore, we identified three different types as follows; frontoparietal (type 5), frontosphenoid (type 6), and wormian type (type 7) [Table 2,5].

Data on comparison of the previous studies for classification of pterion were limited due to differences such as epipteric variations and association of these with wormian bones.[3,9,10] We observed the wormian pterion type of which we classified as type 7 in 3.7% of the cases. In the present study, a small bone exists between the sphenoid bone and parietal bone in the epipteric (type 3) type; a single and large bone exists in the wormian type that we identified as type 7. There was not any typing in the studies conducted until the present day. The reason for such identification is the presence of a single and large bone; we believe that surgical procedures may be performed without disrupting bone integrity by removing the wormian bone. Similarly, recognition of the epipteric type which was identified as type 3 is important for surgical procedures in this area. In the literature, the percentages of epipteric types have been shown by many researchers on different races [Table 5].

The percentages of epipteric pterions were found to be 5.1% Center Anatolian populations in our study, and these findings are similar to those reported for other Anatolian skulls Ersoy *et al*.,[2] Oguz *et al*.,[5] Ilknur *et al*.,[14] Aksu *et al*.,[1] Sindel *et al*.[31] However, Lee *et al*.,[12] 40.3% Korean, Murphy[6] 18.3% Australian, Manjunath and Thomas,[10] 17.3% South Indian populations reported higher percentages of epipteric pterions among, respectively.

Satpute and Wahane[24] conducted a study on 85 skulls and identified the "atypical type" of which we identified as type 6 in 1.76% of all skulls and 2.35% and 1.17% on the right and left side, respectively. In the present study, we found type 6 in 23.8% of all skulls, 25.2% on the right, and 22.4% on the left. The most common type that we identified as type 2. The sphenoparietal type was not revealed by any other researcher. Furthermore, Satpute and Wahane[24] detected the frontotemporal type with the lowest rate which is similar to the present study.

Esenkaya *et al.,*[42] reported that numeric differences in morphometric measurements obtained on dry bone samples may be caused by wearing on superficial. Angular or edge

Table 4: Pearson correlation coefficient between parameters belonging to left pterion.

Parameters (Left)	PFZSa	PFZSp	PZangle	PTZSp	PZarch	PMF	PPM	PMP	PA
PA									
r	−0.027	0.212	0.495**	0.373**	0.459**	0.614**	0.744**	0.754**	1
P	0.842	0.114	0.000	0.005	0.000	0.000	0.000	0.000	
PSS									
r	0.004	0.522**	0.720**	0.488**	0.666**	0.762**	0.870**	1	
P	0.977	0.000	0.000	0.000	0.000	0.000	0.000		
PMP									
r	−0.032	0.410**	0.592**	0.455**	0.574**	0.822**	1		
P	0.813	0.002	0.000	0.000	0.000	0.000			
PMF									
r	−0.073	0.382**	0.588**	0.562**	0.749**	1			
P	0.588	0.003	0.000	0.000	0.000				
Pzarch									
r	0.260	0.648**	0.845**	0.673**	1				
P	0.051	0.000	0.000	0.000					
PTZSp									
r	0.164	0.565**	0.646**	1					
P	0.228	0.000	0.000						
Pzangle									
r	0.455**	0.818**	1						
P	0.000	0.000							
PFZSp									
r	0.449**	1							
P	0.000								
PFZSa									
r	1								
P									

*Correlation is significant at the 0.05 level (two-tailed), **Correlation is significant at the 0.01 level (two-tailed), $P<0.05$ differences between group.[8] *PFZSa*: Pterion-anterior edge of frontozygomatic suture, *PFZSp*: Pterion-posterior edge of frontozygomatic suture, *PZangle*: Pterion-zygomatic angle, *PTZSp*: Pterion temporozygomatic suture posterior, *PZarch*: Pterion-zygomatic arch, *PMF*: Pterion-mandibular fossa, *PSS*: Pterion-suprameatal spine, *PMP*: Pterion-mastoid process, *PA*: Pterion-asterion

zones appeared on dry bone samples in time. However, although we performed typing on 107 (214 pterion) bones in the present study. We performed morphometric measurements for pterion on 57 dry skulls considering that worn or broken skulls would not provide accurate results.

In the literature, there are studies measuring the distances of the pterion from the anterior, middle, and posterior edges of the frontozygomatic suture (FZS).[1,13,14,16,19,21-23,27-30,32,33,36,39-41,43-45,47,54] In our study, the distance of the pterion from both the anterior and posterior edges of the FZS was measured.

In our study, the distance to both the anterior and posterior edges of the FZS has been given. Because posterior edge is a more prominent point. In our study, the distance of the pterion from FZS to its central point was not taken.

Natekar and De Souza Fatima[15] reported that pterion laid 3.5 cm posterior tip FZS where as Sindel *et al*.,[31] reported that pterion lied 3.4 cm behind the FZS. Aksu *et al*.,[1] reported the mean distance between the center of the pterion and the FZS as 40.02 ± 4.06 mm and 39.88 ± 4 mm on the right and left sides, respectively. According to our measurements, pterion lied 37.89 ± 6.86 mm on the right and 37.56 ± 7.31mm behind the anterior edge of FZS. Furthermore, the distance between pterion and the posterior edge of FZS was measured in the present study. According to our measurements, pterion laid 32.70 ± 6.43 mm on the right and 32.23 ± 6.34mm behind the posterior edge of FZS. Some researchers have measured the distance between this suture and the pterion. However, they did not specify exactly where the measurement was taken from the FZS.[1,13,16,19,21-23,27,29,30,33,39,40,43,44-46]

Aksu *et al*.,[1] have shown that the mean distance between pterion and posterior edge of the FZS were 31.80 ± 4.51 mm and 31.44 ± 4.73mm on the right and left sides, respectively. Oğuz *et al.,*[5] determined these values as 33.0 ± 4.0 mm and 34.4 ± 3.9 mm, respectively, in the Turkish population. The difference in our results may be due to the fact that all of the skulls in the study of Oğuz *et al.,*[5] consisted of male skulls. It is known that male skulls have a larger size than female skulls. Mwachaka *et al*.,[43] reported that the pterion laid 30.35 ± 3.61 mm posterior to the FZS in Kenyans. Our results are similar to this study. It was previously reported that the pterion

Table 5: Comparison of the percentage of pterion types in different populations (%)

Authors	Population	Samples	Sphenoparietal	Frontotemporal	Stellat	Epipterik	Atypical
Murphy[6]	Australian	388	73	7.5	1	18.3	0
Matsumura *et al*.[9]	Japanese	614	79.10	2.6	0.6	17.7	0
Manjunath and Thomas[10]	South Indian	172	93.55	3.52	2.93	17.30	0
Asala and Mbajiorgu[11]	Nigerian	212	82.1	23.60	0	5.70	0
Lee *et al*.[12]	Korean	149	76.5	0	0	40.30	0
Saxena *et al*.[3]	North Indian	203	87.72	10.01	5.17	0.00	0
Ersoy *et al*.[2]	Turkish	300	87.35	3.47	8.98	0.20	0
Oguz *et al*.[5]	Turkish	26	88.00	10.00	0	2.00	0
Zalawadia *et al*.[13]	Western Indian	42	91.7	2.40	1.20	4.80	0
Ilknur *et al*.[14]	Byzantine male	16	87.5	6.25	0	6.25	0
Ilknur *et al*.[14]	Comtemporary	28	89.2	3.6	3.6	3.6	0
Natekar and De Souza Fatima[15]	Indian	79	66.00	15.00	12.00	7.00	0
Nayak *et al*.[16]	Odisha	50	85	0	5	10	0
Saheb *et al*.[17]	Indian	125	69.25	17.35	9.70	3.70	0
Morales *et al*.[18]	Spanish	85	90.00	2.35	4.12	3.53	0
Praba and Venkatramaniah[19]	South Indian	50	74.00	3.00	9.00	14.00	0
Khatri *et al*.[20]	Gujarat	311	96.9	2.9	0.2	0	0
Ukoha *et al*.[21]	Nigerian	56	75.5	19.60	1.80	3.60	0
Kumar *et al*.[22]	Uttarakhand	40	86.25	11.25	2.5	0	0
Adejuwon *et al*.[23]	Adult Nigerian	37	86.1	8.30	5.60	0	0
Satpute and Wahane[24]	Vidarbha Regio	85	82.94	2.94	5.29	7.05	1.76
Sudha *et al*.[25]	South Indian	150	80.00	0.30	5.30	0	0
Kumar *et al*.[26]	-	40	86.25	11.25	2.50	0	0
Eboh and Obaroefe[27]	Nigerian	50	83	5	6	6	0
Mahajan[28]	North Indian	50	89.00	7.00	4.00	12.00	0
Aksu *et al*.[1]	West Anatolian	128	85.20	1.10	5.50	8.20	0
Gindha *et al*.[29]	North Indian	65	72.31	4.61	0	23.08	0
Anjana *et al*.[30]	South Canada	32	82.8	3.1	4.7	9.4	0
Sindel *et al*.[31]	Turkish	150	63.00	2	19	16	0
Warille and Mandloi[32]	India	71	80.3	5.6	7	7	0
Walulkar *et al*.[33]	Maharashtra	350	82.2	9	3.7	5	0
Ruiz *et al*.[34]	Brazil	55	90	4.54	1.82	3.64	0
Kalthur *et al*.[35]	India	100	78	4	1	17	0
Dutt *et al*.[36]	India		82.7	3.2	11.54	2.56	0
Modasiya and Kanani[37]	North Gujarat	110	80.9	0	10.9	8.18	0
Vasudha *et al*.[38]	İndia	150	69.33	5.67	11	14	0
Rathnakar *et al*.[39]	India	50 dry	72	18	8	2	0
Sarvaiya *et al*.[40]	India	326	80.21	5.22	3.68	10.89	0
Nikola *et al*.[41]	Serbian	50	86 R 88 L	0		14 R 12L	0
Current study	Central Anatolia	107	55.6	0.5	2.3	5.1	23.8

is 26.8 ± 4.5 mm from the center of the FZS in Koreans. Ma, *et al*.,[45] also reported that the pterion was located at a mean of 26.6 ± 4 mm behind the posterolateral edge of the FZS. These differences might have resulted from ethnic or genetic factors. Adejuwon *et al*.,[23] found the distance between pterion and the center of the FZS as 31.52 ± 0.677 on the left and 30.82 ± 0.809 on the right; the difference was not statistically significant ($p = 0.505$).

In comparison to the skull sides, the distance between pterion and anterior edge of the FZS were found to be 37.89 ± 6.86 mm and 37.56 ± 7.31 mm for the right and left sides, respectively. For the posterior edge of the FSZ, these values were found to be 32.70 ± 6.43 mm and 32.23 ± 6.34 mm for the right and left sides, respectively. The data obtained from the study of Warille and Mandloi[32] were also found to be compatible with our study [Table 6].

In the Turkish population, the pterion was found to be localized above the zygomatic arch at a distance ranging from 34 to 41.06 mm on average.[1,5,31] Natekar

and De Souza Fatima[15] reported that pterion lied 4 cm above the Zarch; Sindel *et al*.,[31] found this distance as 3.4 cm. In our study, these distances were found to be 41.06 ± 6.01 mm and 39.52 ± 7.09 mm for the right and left sides, respectively. It was not statistically significant between the sides (p = 0.066). It was determined that this value varied between 25.4 and 45 mm in different populations [Table 6].

To the best of our knowledge, the distance betwen pterion and temporozygomatic suture (TZ) was performed for the first time by Gupta *et al.,*[46]. In their study, they determined this distance as 43.1 mm. In our study, this distance was determined as 41.8 mm. The difference may be of racial origin. Similarly, while Gupta *et al.,*[46] determined the distance between pterion and suprameatal spine (SS) as 57.2 mm in their study, this value was determined as 56.51 mm in our study.

Ilknur *et al*.,[14] Aksu *et al*.,[1] Warille and Mandloi[32] Rathnakar *et al*.,[39] and Nikola *et al*.,[41] measured the distance between pterion and mastoid process (MP). Studies conducted on different societies have stated that this distance will be around 79.18 mm on average, although not very different from each other.

Aksu *et al*.,[1] found the distance between the center of the pterion and the upper border of the external acoustic meatus was 53.29 ± 4.55 mm and 56.22 ± 4.60 mm on the right and left sides, respectively. In the present study, the distances were found as 56.12 ± 6.79 mm on the right and 56.90 ± 9.1 mm on the left, respectively. The data obtained from other races were found to be consistent with those obtained in our study with Aksu *et al.,*[1]

There are very few studies that have measured the distance between pterion and asterion.[14] In our study, the PA was found to be 89.21 ± 27.49 mm on the right side and 87.19 ± 10.57 mm on the left side. Ilknur *et al*.,[14] the PA measurements are closer to the measurements in the contemporary group than the Byzantium male group [Table 7].

Despite clinical importance, pterion is an important anatomical landmark; therefore, current major

Table 6: According to the researchers, the distance measurements between pterion, frontozygomatic suture and zygomatic arch (mm).

Authors	Population	*n*	RPFZ	LPFZ	RPZarch	LPZarch
Oguz *et al*.[5]	Turkish	37	33.0±4.0^{m}	34.4±3.9^{m}	40.5±3.9	38.5±2.5
Mwachaka *et al*.[43]	Kenyan	50	30.35±3.4	30.34±4.30	38.88±3.49	38.24±3.47
Ilknur *et al*.[14]	Byzantine male	16	39±4^{a}	39±4.2^{a}	45±4	39±4.6
Ilknur *et al*.[14]	Comtemporary	28	38±5^{a}	41±7^{a}	42±3	43±2
Zalawadia *et al*.[13]	Western Indian	42	37.3±5.1	35.5±4.2	31.2±4.4	29.7±3.3
Bhargavi *et al*.[44]	İndia	70	M:39.3±3.7	M:38.02±4	M:45.2±3.2	M:44.58±3.5
			F:35.38±4.2	F:34.72±3.7	F:41±4.4	F:41.05±3
Ma *et al*.[45]	India	76	26±4		25±4	
Kumar *et al*.[22]	Uttarakhand	40	35.0±4.4	34.1±4.8	34±4	34±4
Adejuwon *et.al*.[23]	Nigerian	37	31.52±0.67	30.82±0.80	37.7±3.5	36.9±3.0
Ukoha *et al*.[21]	Nigeria	56	27.4±0.7	27.4±0.6	39.1±0.58	38.77±0.63
Aksu *et al*.[1]	West Anatolian	128	31.80±4.51	31.44±4.73	40.2±0.5	40.1±0.3
Mahajan[28]	India	50	31±4.4^{p}	34±4^{p}	40.02±4.06	39.88±4.01
Gupta *et al*.[46]	India	60	34.8±4.8	40.2±4.3	41±45	44±3.2
Eboh and Obaroefe[27]	Nigerian	50	32.06±2.62		31.08±2.24	
Anjana *et al*.[30]	Southern India	32	30.0±4.0	29.0±2.0	37.1±3.9	36.8±3.5
Walulkar *et al*.[33]	Maharashtra	350	27.2±0.6	27.0±0.5	40.0±5.0	40.0±2.0
Gindha *et al*.[29]	North India	65	38.71±3.10	36.29±3.73	40.1±0.5	39.2±0.3
Warille and Mandloi[32]	Jhansi UP	71	31.9±3.8^{p}	32.0±4.0^{p}	39.00±2.56	37.00±3.35
			37.4±3.6^{a}	36.3±4.1^{a}		
Nayak *et al*.[35]	Odisha	50	34.8±2.1	34.1±1.6	36.2±3.5	36.7±3.5
Dutt *et al*.[36]			29.35±3.60^{p}	27.37±5.80^{p}	40.1±1.9	39.4±2.0
Rathnakar *et al*.[39]	India	50	40	40	37.74±3.66	37.07±4.19
Sarvaiya *et al*.[40]	India	523	30.17±3.91	29.23±3.85	32	32
Nikola *et al*.[41]	Serbian	50	M:39.98±3.85^{a}	M:9.67±4.61^{a}	37.36±3.62	36.34±3.54
			F:37.38±6.38^{a}	F:35.94±6.46^{a}		
Current study	Central Anatolia		37.89±6.86^{a}	37.56±7.31^{a}	41.06±6.01	39.52±7.09
			32.70±6.43^{p}	32.23±6.34^{p}		

(*PFZS*: Pterion-frontozygomatic suture, *PZarch*: Pterion-zygomatic arch *R*: Right, *L*: Left, *M*: Male, *F*: Female, *a*: Distance from anterior edge, *p*: Distance from posterior edge, *m*: Midline distance)

Table 7: The comparative measurements on right and left side for the various measurements (mm)

Authors	Population	*n*	RPZangle	LPZangle	RMP	LPMP	RPSS	LPSS	RPA	LPA
Ilknur *et al.*[14]	Byzantime male	16			83±3.4	85±2.6	57±4	59±3.5	89±4	93±6.5
Ilknur *et al.*[14]	Comtemporary	28			82±5	81±7	58±4	59±3	87±7	86±8
Gupta *et al.*[46]	India	60					57.2±4.06			89.2±4.7
Aksu *et al.*[1]	West Anatolian	128	41.54±4.95	41.35±5.14	82.48±5.45	81.81±5.50	53.29±4.55		56.22±4.6	
Warille and Mandloi[32]	Jhansi UP	71	-	-	79.4±5.4	79.3±5.6	51.3±3.7	51.1±3.1		
Rathnakar *et al.*[39]	India	50	-	-	83	83	56	56		
Nikola *et al.*[41]			M:43.93±4.16	M:41.41±2.43	M:78.47±4.12	M:74.83±5.60	M:53.13±2.22	M:50.96±2.15		
			F:42.03±6.82	F:39.76±6.35	F:70.23±6.84	F:67.43±7.02	F:47.74±5.12	F:46.79±5.09		
Current study	Central Anatolia		41.06±6.01	39.52±7.09	80.29±11.44	80.52±10.48	56.12±6.79	56.90±9.1	89.21±27.49	87.19±10.57

(*R*: Right, *L*: Left, *M*: Male, *F*: Female, *PZangle*: Pterion-zygomatic angle, *PMF*: Pterion-mandibular fossa, *PSS*: Pterion-suprameatal spine, *PA*: Pterion-asterion)

inconsistencies in terms of the anterior branch of the medial meningeal artery indicated in previous articles should not be ignored. Pterion was detected to overlap with the anterior branch of the medial meningeal artery in many of the cases; furthermore, it laid several millimeters posterior to the artery in the remaining cases. Besides, we provided the distance between the pterion and the middle point of the Zarch, posterolateral aspect of FZS, and MP which may be palpated externally on the right and left sides through individual regression formula. Injury of any point may be guessed based on other points.[1,5,31,41,45]

In the current study, the examined skulls belonged to the Central Anatolian population. This fact might lead to the differences between the result of previous studies and our study. This information is of great importance for neurosurgical operations in regions where neuronavigation equipment does not work and for anthropological identification of skulls of the Central Anatolian population.

Conclusion

The most common variety of pterion in the present study was found to be of the sphenoparietal type (56.1%). Furthermore, we believe that recognition of typing would significantly guide surgical planning and procedures and also contribute to the studies in anthropologic sciences.

We did not search the genders of the skulls in the present study; this may be a limitation for the present study; however, the information provided for shape and location of the pterion would worth the tips to care for during surgical procedures. We believe that we enlightened anthropologists, forensic medicine pathologists, neurosurgeons, and maxillofacial surgeons by trying to explain variations of typing through different bone markers in different populations.

Financial support and sponsorship

Nil.

Conflicts of interest

There are no conflicts of interest.

References

1. Aksu F, Akyer SP, Kale A, Geylan S, Gayretli O. The localization and morphology of pterion in adult West Anatolian skulls. J Craniofac Surg. 2014;25 (4):1488-91.
2. Ersoy M, Evliyaoglu C, Bozkurt M, Konuskan B, Tekdemir I, Keskil İS. Epipteric bones in the pterion may be a surgical pitfall. Minim Invasive Neurosurg**.** 2003;46 (06):363-5.
3. Saxena R, Bilodi A, Mane S, Kumar A. Study of pterion in skulls of Awadh area--in and around Lucknow. Kathmandu Univ Med J (KUMJ)**.** 2003;1 (1):32-3.
4. Broca P. Instructions craniologiques et craniométriques: Masson; Place De L'ecole-Medecine, 1875.
5. Oguz Ö, Şanli SG, Bozkir M, Soames R. The pterion in Turkish male skulls. SRA. 2004;26 (3):220-4.
6. Murphy T. The pterion in the Australian aborigine. Am J Phys

Anthropol**.** 1956;14 (2):225-44.
7. Wang Q, Opperman LA, Havill LM, Carlson DS, Dechow PC. Inheritance of sutural pattern at the pterion in Rhesus monkey skulls. Anat Rec A Discov Mol Cell Evol Biol. 2006;288 (10):1042-9.
8. Obilor EL, Amadi EC.Test for significance of Pearson's correlation coefficient. IJSR. 2018;6:11-23
9. Matsumura G, Kida K, Ichikawa R, Kodama G. Pterion and epipteric bones in Japanese adults and fetuses, with special reference to their formation and variations. Kaibogaku Zasshi. 1991;66 (5):462-71.
10. Manjunath K, Thomas I. Pterion variants and epipteric ossicles in South Indian skulls. JASI. 1993;42:85-94.
11. Asala S, Mbajiorgu F. Epigenetic variation in the Nigerian skull: sutural pattern at the pterion. East Afr Med J**.** 1996;73 (7):484-6.
12. Lee UY, Park DK, Kwon SO, Paik DJ, Han SH. Morphological analysis of the pterion in Korean. Korean J Phys Anthropol. 2001;14 (4):281-9.
13. Zalawadia A, Vadgama J, Ruparelia S, Patel S, Rathod S, Patel S. Morphometric study of pterion in dry skull of Gujarat region. NJİRM. 2010;1 (4):25-9.
14. Ilknur A, Mustafa KI, Sinan B. A comparative study of variation of the pterion of human skulls from 13th and 20th century Anatolia. Int J Morphol. 2009:1291-8.
15. Natekar P, De Souza Fatima M. Epipteric bones at pterion. An anatomical study and its surgical significance. Indian J Otol. 2010;16:44-6.
16. Nayak G, Mohanty BB, Das SR. Morphometric study of pterion and its clinical significance. Asian J Pharm Clin Res. 2017;10:142-4.
17. Saheb SH, Mavishetter G, Thomas S, Prasanna L, Magi MP. A study of sutural morphology of the pterion and asterion among human adult Indian skulls. Biomed Res. 2011;22 (1):73-5.
18. Morales A, Elizondo O, Guzman L. Estudio morfológico del pterion y asterion en cráneos adultos mexicanos. Rev Argent Anat Clin. 2011;3 (3):77-83.
19. Praba AMA, Venkatramaniah C. Morphometric Study of different types of Pterion and It's relation with middle meningeal artery in dry skulls of Tamil Nadu. J Pharm Biomed Sci. 2012;21 (21).
20. Khatri CR, Gupta S, Soni JS. Study of pterion and incidence of epipteric bones in dry human skulls of Gujarat. Natl J Integr Res Med. 2012;3 (2):57-60.
21. Ukoha U, Oranusi C, Okafor J, Udemezue O, Anyabolu A, Nwamarachi T. Anatomic study of the pterion in Nigerian dry human skulls. Niger J Clin Pract**.** 2013;16 (3):325-8.
22. Kumar S, Anurag A, Munjal S, Chauhan P. Pterion its location and clinical implications-a study compared. Pterion its location and clinical implications-A study compared J Evol Med Dent Sci. 2013;2 (25):4599-608.
23. Adejuwon SA, Olopade FE, Bolaji M. Study of the location and morphology of the pterion in adult Nigerian skulls. ISRN Anat. 2013;2013.
24. Satpute C, Wahane A. To study the morphology of pterion in dry human skull in Vidarbha region. Int J Sci Res. 2013;4 (1):2171-3.
25. Sudha R, Sridevi C, Ezhilarasi M. Anatomical variations in the formation of pterion and asterion in south Indian population. Int J Cur Res Rev. 2013;5 (09):92-101.
26. Kumar S, Anurag SM, Chauhan P, Chaudhary A, Jain SK. Pterion its location and clinical implications-a study compared. J Evolu Med Dent Sci. l2. 2013:4599-608.
27. Eboh D, Obaroefe M. Morphometric study of pterion in dry human skull bones of Nigerians. Int J Morphol. 2014;32 (1):208-13.
28. Mahajan A. Pterion Formation in North Indian Population: An Anatomico-Clinical Study. Int J Morphol. 2014;32 (4).
29. Gindha G, Kaur H, Kaushal S, Singh M. Variations in the articular facets on superior surface of calcaneus in North Indian population: A Dry Bone Study. Hum Bio Rev. 2015;4 (1):27-37.
30. Anjana S, Satheesha K, Bhaskar R, Pai SR. Morphometric Study of Pterion in Adult Dry Skulls in Dakshina Kannada District, Karnataka State, India. Int J Anat Res. 2015;3 (4):1603-06.
31. Sindel A, Ögüt E, Aytaç G, Oguz N, Sindel M. Morphometric study of pterion. Int J Anat Res. 2016;4 (1):1954-57.
32. Warille AA, Mandloi RS. Measurement of the Various Identifiable Bony Landmarks from the Center of Pterion in Human Skulls from Indian Population. Int J Health sci and Res. 2016;6 (2):133-37.
33. Walulkar S, Dehankar R, Walulkar M, Ksheersagar D. Pterion formation and its variations in Human Skull in Vidarbha Region. J Cont Med A Dent. 2016;4 (2):4-10.
34. Ruiz C, Souza G, Scherb T, Nascimento S. Anatomical variations of pterion: analysis of the possible anatomical variations of pterion in human skulls. J Morphol Sci. 2017;33 (4):0
35. Kalthur SG, Vangara SV, Kiruba L, Dsouza AS, Gupta C. Metrical and non-metrical study of the pterion in South Indian adult dry skulls with notes on its clinical importance. Marmara Med J. 2017;30 (1):30-39.
36. Dutt V, Shankar VV, Shetty S. Morphometric study of pterion and asterion in adult human skulls of Indian origin. Int J Anat Res. 2017;5 (2.2):3837-42.
37. Modasiya UP, Kanani SD. Study of pterion and asterion in adult human skulls of north Gujarat region. Ind J Clin Anat Physiol. 2018;5:353-6.
38. Vasudha T, D'Sa DS, Gowd S. Study of morphology of pterion and ıts clinical ımplications. Int J Anat Res. 2017;5: 46748.
39. Rathnakar P, Vinod R, Sinha A. Anthropometric evaluation of pterion in dry human skulls found in Southern India. J Evolution Med Dent Sci. 2019;8:24759.
40. Sarvaiya BJ, Chaudhari JS, Fichadiya NC. Morphometric analysis of pterion ın adult human dry skull of Gujarat region. Int J Anat Res. 2019;7:6204-10.
41. Nikola K, Ljubica SD, Ivan A, Dusica M, Nikolina P, Knezi N, *et al.* Morphology of the pterion in serbian population. Int J Morphol. 2020;38:820-4.
42. Esenkaya I, Aluçlu MA, Kavaklı A, Bulut HT. Radiologic and morphologic evaluation of the lateral sacral mass. Acta Orthop Traumatol Turc. 2003;37:330-9.
43. Mwachaka P, Hassanali J, Odula PO. Anatomic position of the pterion among kenyans for lateral skull approaches. Int J Morphol**.** 2008;26 (4):931-3.
44. Bhargavi C, Saralaya V, Kishan K. Pterion: A site for neurosurgical approach. Int J Biomed Res. 2011;2:588-94.
45. Ma S, Baillie LJ, Stringer MD. Reappraising the surface anatomy of the pterion and its relationship to the middle meningealartery. Clin Anat. 2012;25:330-9.
46. Gupta R, Sinha MB, Aggarwal A, Gupta T, Kaur H, Sahni D, *et al*. Landmarks for keyhole neurosurgical procedures though pterion.Int J Healthc Biomed Res. 2014;2:168-175.

Case Report

A Rare Anomalous Origin of the Right Vertebral Artery from the Right Aortic Arch with the Left Aberrant Subclavian Artery Arising from Kommerell's Diverticulum

Abstract

Right-sided aortic arch (RAA) with left aberrant subclavian artery (LASA) is a rare vascular variant due to the failure in regression process during embryologic development of the aortic arch. The prevalence of it ranges from 0.04% to 0.1% in radiology series. We report the case of a 44-year-old female shown to have the presence of a RAA with LASA arising from the Kommerell's diverticulum, and also in association with an aberrant aortic origin of the right vertebral artery using computed tomography angiography. Considering the diameter of the diverticulum <5 cm and the absence of severe external esophageal or tracheal compression, thoracic surgery was not indicated and it was decided to keep the patient under clinical follow-up at regular intervals. Based upon this present case and literature review, the knowledge of this anomalous anatomy and its embryologic basis appear to be important for diagnostic endovascular interventions and planning thoracic surgery.

Keywords: *Aberrant left subclavian artery, computed tomography angiography, Kommerell's diverticulum, right-sided aortic arch, right vertebral artery*

Gulay Açar, Mustafa Koplay[1]

Department of Anatomy, Meram Faculty of Medicine, Necmettin Erbakan University, Konya, Turkey, [1]Department of Radiology, Faculty of Medicine, Selcuk University, Konya, Turkey

Introduction

Right-sided aortic arch (RAA) is a rare and mostly asymptomatic variant of the aortic arch (AA) with a frequency of <0.1% in adult population. Type II RAA associated with the left aberrant subclavian artery (LASA) arising from the Kommerell's diverticulum (KD) is observed in <50% of the RAA.[1-3] We reported this case with an anomalous aortic origin of the right vertebral artery (RVA) using computed tomography angiography (CTA). An aberrant origin of vertebral artery (VA) observed mostly on the left side may cause vertebrobasilar insufficiency.[4] To the best of our knowledge, this is the second documented report of Type II RAA with an aberrant aortic RVA in the literature.

Case Report

A 44-year-old woman with a history of systemic hypertension presented at the emergency department with severe headache, dizziness, and dyspnea. Furthermore, she had complaints of anxiety episodes, dyspnea on exertion, and no other cardiovascular symptoms. The amplitude of arterial pulse and systolic blood pressure value were found lower in the left upper limb than right on physical examination. Thoracic CTA (128-slice CT scanner; Siemens Somatom Definition Flash, Munich, Germany) was performed to rule out pulmonary embolism after written informed consent was obtained from the patient. Evaluation of CTA images revealed an incidental finding of the RAA with the LASA arising from the KD with a diameter of 3.9 cm, as well as an anomalous aortic origin of the RVA [Figure 1].

The KD has a mild mass effect on the trachea, and the LASA forms a retroesophageal vascular ring. The RVA was found to arise directly from the AA between the right common carotid artery (RCCA) and the right subclavian artery (RSA), and extend upward to the transverse process of cervical vertebrae to pass through the foramen of C4 and all of the upper transverse processes [Figure 2]. Considering her imaging findings and medical history with the absence of dysphagia, the patient was interpreted as unsuitable for surgical intervention.

How to cite this article: Açar G, Koplay M. A rare anomalous origin of the right vertebral artery from the right aortic arch with the left aberrant subclavian artery arising from Kommerell's diverticulum. J Anat Soc India 2022;71:71-3.

Article Info

Received: 23 January 2021
Revised: 31 March 2021
Accepted: 27 October 2021
Available online: 17 March 2022

Address for correspondence:
Dr. Gülay Açar, Department of Anatomy, Meram Faculty of Medicine, Necmettin Erbakan University, Yunus Emre Mh. Unzile Sk., 42090 Meram, Konya, Turkey. E-mail: gulayzeynep73@gmail.com

Access this article online

Website: www.jasi.org.in
DOI: 10.4103/jasi.jasi_17_21
Quick Response Code:

Regular follow-up without medication was recommended to the patient. Furthermore, the patient confirmed written informed consent for publication of this case report with images.

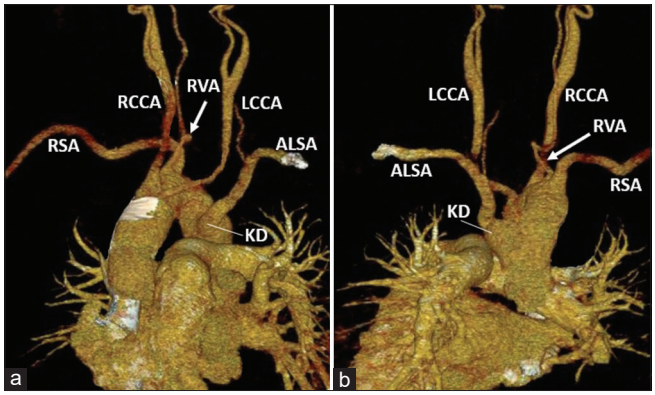

Figure 1: Computed tomography angiography volume-rendered reconstruction showing Type II RAA with aberrant RVA. (a) Anterolateral and (b) posterolateral aspect. RCCA: Right common carotid artery, LCCA: Left common carotid artery, RSA: Right subclavian artery, ALSA: Left aberrant subclavian artery, RVA: Right vertebral artery, KD: Kommerell's diverticulum

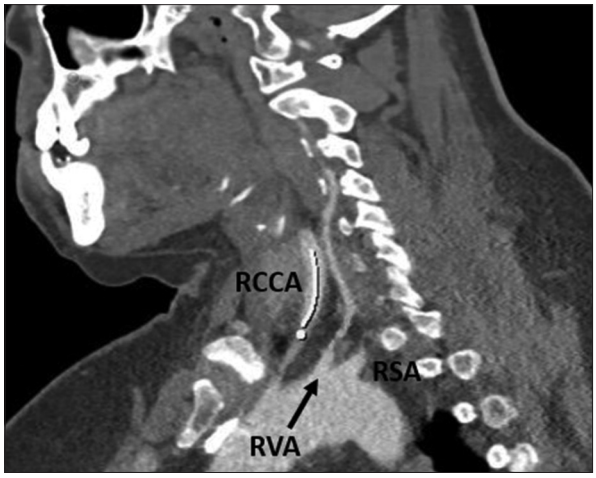

Figure 2: Thoracic computed tomography angiography sagittal maximum intensity projection image showing an aberrant origin of the right vertebral artery from the aortic arch. RCCA: Right common carotid artery, RSA: Right subclavian artery, RVA: Right vertebral artery

Discussion

The classic left-sided AA (LAA) gives rise to three branches from right to left: the brachiocephalic trunk, the left common carotid artery (LCCA), and finally, the left subclavian artery (LSA). Normally, the VA is originated as the first branch of the ipsilateral subclavian artery. In the literature, the AA branching variations are a common finding with a diversity of frequencies ranging from 5% to 35%.[1,3] RAA anomaly has three subtypes based on Edwards classification: mirror image RAA (Type I, 59%), RAA with LASA (Type II, 39.5%), and RAA with direct communication between isolated LSA and pulmonary artery (Type III, 1.5%) [Figure 3].[5,6] The KD is a bulbous dilatation of an anomalous origin of the LASA which leads to a relatively loose vascular ring mostly behind the esophagus. The LASA coexists with congenital heart diseases in 5%–10% of cases. Ichikawa *et al*. reported the prevalence of KD as 100% in Type II RAA, while it was found in 62% in the study by Tyczyński *et al*.[1,7,8] Owing to compression of the esophagus or trachea, the KD can cause miscellaneous symptoms such as dyspnea and dysphagia and rarely results in an aortic dissection or ruptured aneurysm. Considering the diameter (≥5 cm) of the KD and severe symptoms such as an aortic aneurysm and a cerebrovascular insufficiency, surgical intervention can be required.[1,2,9]

Embryology

During the 4th and 8th weeks of intrauterine life, a series of aortic regression and reformation result in the formation of the LAA, which was reported in about 74%–89.4% of cases. Initially, the primitive AA consists of ventral and dorsal aortic trunks. Between these trunks, six paired branchial arch arteries develop and seven cervical intersegmental arteries (CIAs) arise from the dorsal aorta at different stages of the organogenesis. Normally, the LAA is formed by the regression of the dorsal aortic trunk and ductus arteriosus on the right side. In contrast, the failure of this involution results in RAA, which is subdivided into three types.[5,6,9] First, the RAA was identified by Fioratti and Aglietti in 1763. Due to the persistence of the right fourth branchial arch

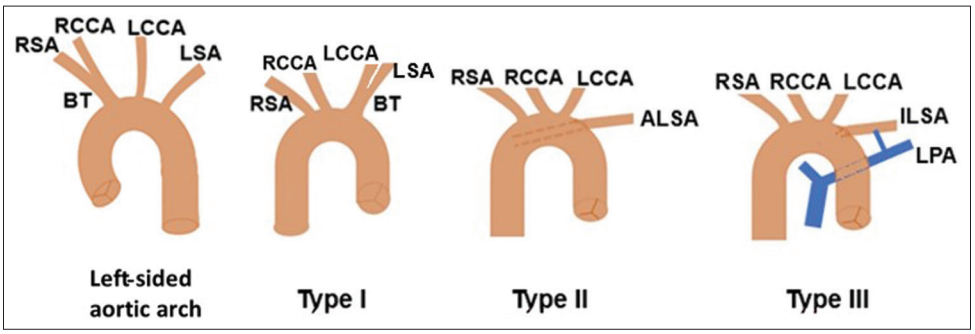

Figure 3: Schematic diagram showing the left-sided aortic arch and subtypes of the right-sided aortic arch. Type I; Mirror image right-sided aortic arch, Type II; Right-sided aortic arch with left aberrant subclavian artery, Type III; Right-sided aortic arch with direct communication between the isolated left subclavian artery and left pulmonary artery

and involution or regression of the left fourth dorsal aortic segment between the LCCA and LSA, the RAA with LASA is formed, and also, the KD develops as a remnant of the fourth primitive dorsal arch during embryonic period. Type II RAA is a rare (0.05%–0.1%) and mostly an asymptomatic incidental finding unless the KD becomes a compressive mass or ruptured.[1-3] After the obliteration of six CIAs, the seventh CIA converts into the proximal subclavian artery giving origin to the VA, which is the further development of the intercostal longitudinal anastomosis. The failure of involution in these developmental stages results in different anomalous origins of the VA. If the first or the second CIA does not regress, the VA arises from the external or internal carotid artery, whereas the persistence of other CIAs (3–6) causes an anomalous origin of the VA from the AA or common carotid artery.[5,9,10,11] Hence, in this case, we suggested that the right anastomosis between the sixth and seventh CIAs may not occur and the sixth CIA fails to regress.

We presented a rare case of Type II RAA having branches, in a proximal to distal progression, with the following order: LCCA, RCCA, RVA, RSA, and LASA arising from the KD. A review of the literature from 2011 to date showed that 32 case reports of Type II were reported. Concerning the higher incidence of ruptured aneurysm or dissection associated with the KD, the prevalence of it was reported by Cinà *et al*. as 53%, by Kouchoukos and Masetti as 20%, and by Austin and Wolfe as 19%.[5,8,12-14] Detailed identification of this aberrant vascular anatomy is crucial for accurate surgical and endovascular intervention planning and to prevent intraoperative vascular complications during surgery and diagnostic cerebral angiography.[1,2,5]

In the recent literature, an aberrant origin of the RVA is less common than the LVA, whereas the prevalence of the aortic origin of the RVA associated with Type II RAA is even more the rarest of all. Generally, an anomalous aortic origin of the RVA most commonly occurs as the last branch of the AA distal to the origin of the LSA.[1,9,10] To our knowledge, an anomalous origin of the RVA from the RAA, with the LCCA as the first branch of the AA followed by RCCA, RSA, and LASA, has been presented only in the study by Tyczyński *et al*.[1] An aberrant origin of the RVA directly from the arch may lead to an increased risk of spinal and right upper limb ischemia.[1,4]

Although this anomaly is found incidentally and mostly asymptomatic, preoperative evaluation using CTA is essential for planning endovascular intervention and surgical approach and avoidance of unexpected outcomes. Identification of this case report with the review of the literature has significant clinical implications in thoracic surgery and endovascular procedures.

Declaration of patient consent

The authors certify that they have obtained all appropriate patient consent forms. In the form, the patient has given her consent for images and other clinical information to be reported in the journal. The patient understands that name and initials will not be published and due efforts will be made to conceal her identity, but anonymity cannot be guaranteed.

Financial support and sponsorship

Nil.

Conflicts of interest

There are no conflicts of interest.

References

1. Tyczyński P, Michałowska I, Wolny R, Dobrowolski P, Łazarczyk H, Rybicka J, *et al.* Left aberrant subclavian artery. Systematic study in adult patients. Int J Cardiol 2017;240:183-6.
2. Zhyvotovska A, Yusupov D, Abdul R, Chandrakumar H, Hartt A, Akter K, *et al.* Right-sided aortic arch with aberrant left subclavian artery in a pregnant female: A case report and literature review. Am J Med Case Rep 2020;8:143-7.
3. Oztas DM, Umutlu M, Ertan M, Beyaz MO, Badem S, Erdinc I, *et al.* Brief review of right aortic arch with aberrant left subclavian artery. Aorta (Stamford) 2019;7:179-80.
4. Lazaridis N, Piagkou M, Loukas M, Piperaki ET, Totlis T, Noussios G, *et al.* A systematic classification of the vertebral artery variable origin: Clinical and surgical implications. Surg Radiol Anat 2018;40:779-97.
5. Edwards JE. Anomalies of the derivates of the aortic arch system. Med Clin North Am 1948;32:925-49.
6. Tong E, Rizvi T, Hagspiel KD. Complex aortic arch anomaly: Right aortic arch with aberrant left subclavian artery, fenestrated proximal right and duplicated proximal left vertebral arteries-CT angiography findings and review of the literature. Neuroradiol J 2015;28:396-403.
7. Ichikawa T, Koizumi J, Tanno K, Okochi T, Nomura T, Shimura S, *et al.* Kommerell diverticulum in adults: Evaluation of routine CT examinations. Tokai J Exp Clin Med 2016;41:65-9.
8. Silveira JV, Junqueira FP, Silveira CG, Consolim-Colombo FM. Kommerell diverticulum: Right aortic arch with anomalous origin of left subclavian artery and duplicity of right vertebral artery in a 16-year-old girl. Am J Case Rep 2019;20:228-32.
9. Morishita A, Tomioka H, Katahira S, Hoshino T, Hanzawa K. Surgical treatment for kommerell's diverticulum associated with a right-sided aortic arch and an aberrant left subclavian artery: Endovascular or hybrid. Ann Vasc Dis 2019;12:228-32.
10. Vitošević F, Vitošević Z, Rasulić L. The right vertebral artery arising from the right common carotid artery: Report of a rare case. Surg Radiol Anat 2020;42:1263-6.
11. Maiti TK, Konar SK, Bir S, Nanda A, Cuellar H. Anomalous origin of the right vertebral artery: Incidence and significance. World Neurosurg 2016;89:601-10.
12. Cinà CS, Althani H, Pasenau J, Abouzahr L. Kommerell's diverticulum and right-sided aortic arch: A cohort study and review of the literature. J Vasc Surg 2004;39:131-9.
13. Kouchoukos NT, Masetti P. Aberrant subclavian artery and Kommerell aneurysm: Surgical treatment with a standard approach. J Thorac Cardiovasc Surg 2007;133:888-92.
14. Austin EH, Wolfe WG. Aneurysm of aberrant subclavian artery with a review of the literature. J Vasc Surg 1985;2:571-7.

Case Report

Unusual Additional Distal Aponeurotic Slips of Biceps Brachii: A Rare Variation

Abstract

Biceps brachii muscle is basically a powerful supinator. Although there is ample literature on variant origin of biceps brachii, variant insertion pattern was minimally reported. Here, we report a case, in which apart from usual insertion of biceps brachii, three distal accessory aponeurotic slips were found on the right arm of 55-year-old embalmed male cadaver. Two slips were arising from the lateral most part of bicipital aponeurosis traversing across the cubital fossa superficial to the brachial artery and median nerve and get attached to deep fascia covering the brachioradialis and pronator teres. Third accessory aponeurotic slip arises from the lateral side of biceps brachii muscle belly, traversing superficial to the musculocutaneous nerve and get attached to deep fascia covering the lateral border of brachioradialis and extensor carpi radialis longus. These extra slips may affect the kinematics of biceps brachii muscle and adds to the differential diagnosis of variety of clinical symptoms of neurovascular syndrome.

Keywords: *Accessory aponeurotic slips, biceps brachii muscle, musculocutaneous nerve, superficial branch of radial nerve*

Ritu Singh[1,2], Pooja Singh[3], Ranjana Verma[4], Rakesh Kumar Diwan[2]

[1]Department of Anatomy, School of Medical Sciences and Research, Sharda University, [2]Department of Anatomy, King George's Medical University, Lucknow, Uttar Pradesh, [3]Department of Anatomy, Shri Shankaracharya Institute of Medical Sciences, Bhilai, Chhattisgarh, [4]Department of Anatomy, Government Institute of Medical Sciences, Greater Noida, India

Introduction

Biceps brachii muscle is one of the flexor groups of muscle in the anterior compartment of arm showing wide anatomical variation both pertaining to its origin and insertion. Although there is ample literature on variant origin of biceps brachii, documentation of anatomical variation of biceps brachii muscle related to the manner of its insertion is minimally reported.[1] Biceps brachii muscle derives its name from its two proximally attached heads, the short and long head both originating from the scapula. The two heads join to form a single muscle belly distally that ends in a flattened tendon which get attached to radial tuberosity. The tendon has a broad medial expansion, the bicipital aponeurosis, that descends medially across the brachial artery to fuse with deep fascia over the origins of the flexor muscles of the arm.[2] The biceps is basically a powerful supinator, especially in rapid and resisted movements of the forearm. It is also flexor of the elbow joint. These functions of muscle are executed by its attachment at the radial tuberosity as well as by bicipital aponeurosis that performs the function of drawing the posterior border of the ulna medially during supination of the forearm, thus stabilizing the distal tendon of biceps brachii.[1] Bicipital aponeurosis also imparts protection to the brachial artery and median nerve running underneath.[3] There was a study mentioning tendinous slip from bicipital aponeurosis giving extension to both pronator teres and flexor carpi ulnaris.[4] In another study, accessory tendon was noted which was an extension from the lateral side of fleshy belly of the muscle on its lower third and get inserted distal to insertion of common tendon.[5] The present case study drew our attention as we observed accessory aponeurotic slip arising from the muscle belly of biceps brachii and bicipital aponeurosis as well, lying over the neurovascular structures present in cubital fossa of the right arm. This type of variation may alter the kinematics of biceps brachii or may lead to neurovascular compression syndrome.

Case Report

During routine dissection for the undergraduate medical students in Anatomy Department at King George's Medical University, Uttar Pradesh, Lucknow, India,

How to cite this article: Singh R, Singh P, Verma R, Diwan RK. Unusual additional distal aponeurotic slips of biceps brachii: A rare variation. J Anat Soc India 2022;71:74-6.

Article Info

Received: 23 May 2020
Accepted: 15 November 2021
Available online: 17 March 2022

Address for correspondence:
Dr. Ritu Singh, Department of Anatomy, School of Medical Sciences and Research, Sharda University, Greater Noida, India. E-mail: dr.ritusingh.in@gmail.com

Access this article online

Website: www.jasi.org.in
DOI: 10.4103/JASI.JASI_97_20
Quick Response Code:

we came across variation in the insertion pattern of biceps brachii muscle on the right arm of 55-year-old embalmed male cadaver. The origin of biceps brachii was normal and was inserted normally on radial tuberosity, and to the antebrachial fascia of the forearm through bicipital aponeurosis. Apart from this usual insertion, three accessory aponeurotic slips were found. Two slips were arising from the lateral most part of bicipital aponeurosis traversing across the cubital fossa superficial to the brachial artery and median nerve [Figure 1]. The medial slip courses superficial to the proximal part of radial artery and superficial branch of radial nerve and get attached to the deep fascia covering the pronator teres while the lateral slip get attached to fascial covering of brachioradialis muscles [Figure 2]. Third accessory aponeurotic slip arises from the lateral side of biceps brachii muscle belly was 10 cm in length arising 7 cm proximal to the lateral epicondyle, coursing downward superficial to the musculocutaneous nerve and was attached to deep fascia covering the lateral border of brachioradialis and extensor carpi radialis longus muscle 3 cm below the lateral epicondyle [Figure 3].

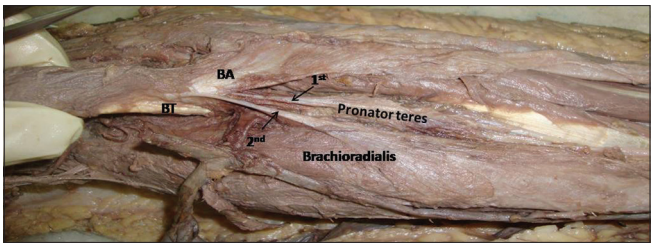

Figure 1: Right cubital fossa showing tendon of Biceps Brachii (BT) muscle and 1st and 2nd additional aponeurotic slips arising from the lateral most part of bicipital aponeurosis (BA) traversing across the cubital fossa and get merged with pronator teres and brachioradialis muscles respectively.

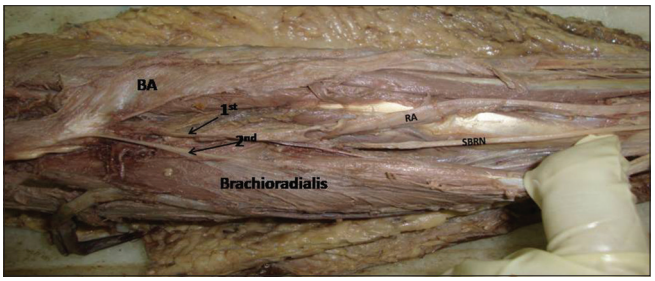

Figure 2: Right cubital fossa and upper part of front of forearm showing the medial slip (1st) courses superficial to the proximal part of radial artery (RA) and superficial branch of radial nerve (SBRN)

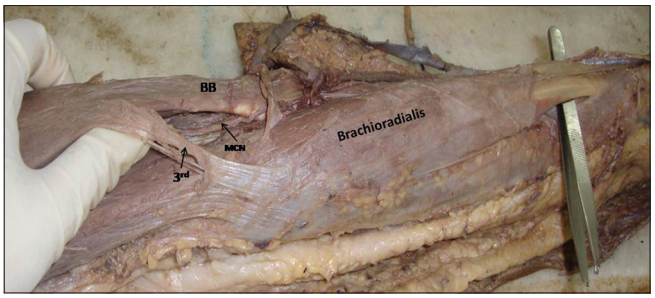

Figure 3: Lower part of front of right arm showing third (3rd) accessory aponeurotic slip arises from the lateral side of biceps brachii muscle (BB) belly, coursing downward superficial to the musculocutaneous nerve (MCN) and was attached to deep fascia covering the lateral border of brachioradialis

Discussion

Variation in the proximal end of biceps brachii is very well recorded in literature, but unusual insertion pattern of biceps brachii muscle is rarely documented and that too accessory aponeurotic slip is further rare.[6] Limbs begins to develop by the end of the 4th week, with the activation of mesenchymal cells in somatic lateral mesoderm. Mesenchymal cells at the posterior margin of the limb bud form an important signaling center in the limb development.[7] Variation of muscle patterns may be result of altered signaling or stimulus between mesenchymal cells. The variant accessory tendinous slip from biceps brachii muscle is said to be the remnant of various muscular or tendinous slips from the distal end of the muscle during the development of fetus in utero.[8]

Variant biceps brachii muscle was reported which gives an abnormal muscle fasciculus from its medial side and continued down as narrow tendinous slip which further subdivided into lateral and medial slips. The lateral slip cross the cubital fossa superficial to the brachial artery and median nerve and get merged with facial covering of flexor carpi ulnaris while the medial slip run deep to the brachial artery and median nerve and get attached to medial supracondylar ridge of humerus.[9] In another cadaveric study, biceps brachii of the left arm was founded to be inserted on the posterior part of radial tuberosity, both by a common tendon and an accessory tendon. This accessory tendon was an extension from the lateral side of fleshy belly of muscle on its lower third and get inserted distal to insertion of common tendon.[5] Bicipital aponeurosis was reported to had two slips, i.e., medial and lateral. Medial slip gave origin to some fibers of pronator teres and flexor carpi radialis and the lateral slip gave origin to some fibers of brachioradialis.[10] Three cases of variant bicipital aponeurosis were reported. In the first case, fibers originated from bicipital aponeurosis and get merged with flexor carpi radialis muscle. In the second case, two tendinous slips arising from medial and lateral most fibers of biceps brachii, medial one passes deep to the brachial artery before merging with bicipital aponeurosis while lateral one merge directly. The third variant was third head of biceps brachii that originated from the superomedial aspect of brachialis and get merged with bicipital aponeurosis.[3] In another study, accessory tendo-aponeurotic slip of bicep brachii was reported which traverses across the forearm, superficial to the proximal part of radial artery as well as the superficial branch of radial nerve, possibly compressing them.[5] In the present study, we observed three accessory aponeurotic slips, two from the lateral aspect of bicipital

aponeurosis and third from the lateral aspect of muscle belly of biceps brachii. The aponeurotic slips arising from the bicipital aponeurosis traverses across the cubital fossa, superficial to neurovascular bundle and get attached to fascia covering the pronator teres and brachioradialis. The third aponeurotic slip arising from the muscle belly of biceps brachii traverses downward superficial to musculocutaneous nerve and get attached to fascia covering the brachioradialis.

These extra slips may affect the kinematics of biceps brachii muscle, thus altering the movements at elbow joint and superior radio ulnar joint. In addition, these slips may produce paresthesia and ischemic symptoms due to the compression of neurovascular bundle.[11] Hence, information on such variation adds to differential diagnosis of variety of clinical symptoms of neurovascular syndrome. The presence of accessory aponeurotic slips may end up in iatrogenic injuries during surgeries around elbow and may create problem for orthopedician because of unpredictable displacement of bone fragments after fracture.[5] Plastic surgeons may find difficulty in elevation and transfer of lateral arm flaps due to the presence of additional aponeurotic slip on the lateral side of biceps brachii muscle.[12]

The mode of insertion of biceps brachii muscle is accountable for its efficient function that is supination and flexion of the forearm. Clinician should also have idea of such slips as it may be one of the reasons of neurovascular compression syndrome. The facts regarding unusual variation in the insertion pattern may help orthopedician to give better outcome while repairing or reconstructing tendon surgeries during avulsion and plastic surgeons while doing the lateral arm flap elevation and transfer.

Financial support and sponsorship

Nil.

Conflicts of interest

There are no conflicts of interest.

References

1. Eames MH, Bain GI, Fogg QA, van Riet RP. Distal biceps tendon anatomy: A cadaveric study. J Bone Joint Surg Am 2007;89:1044-9.
2. Standring S. Gray's Anatomy. The Anatomical Basis of Clinical Practice. 41st ed. UK: Elsevier; 2016.
3. Deopujari R, Quadir N, Athavale S, Gajbhiye V, Kotgirwar S. Variant bicipital aponeurosis: A cadaveric study. Peoples J Sci Res 2014;7:43-6.
4. Bhat Kumar MR, Kulakarni V, Gupta C. Additional muscle slips from the bicipital aponeurosis and a long communicating branch between the musculocutaneous nerve and median nerve. Int J Anat Var 2012;5:41-3.
5. Daimi SR, Siddiqui AU, Wabale RN, Gandhi KB. Additional tendinous insertion of biceps brachii: A case report. Paravara Med Rev 2010;2:16-8.
6. Sanchita R, Mira D, Pandey M, Gupta HD. An aberrant tendo-aponeurotic extension of biceps brachii muscle a possible factor for neurovascular compression in the antibrachium. Int J Anat Var 2014;7:91-2.
7. Moore KL, Persaud TV, Torchia MG. The Developing Human Clinically Oriented Embryology. 9th ed. India: Saunders an Imprint of Elsevier; 2013.
8. Bryce TH. Myology. The muscle and fascia of upper arm-M biceps brachii. In: Sharpey SE, Symington J, Bryce TH, editors. Quain's Elements of Anatomy. 11th ed. London: Longmans, Green & Co; 1923. p. 121.
9. Paval J, Mathew JG. A rare variation of the biceps brachii muscle. Indian J Plast Surg 2006;3937:65-7.
10. Nayak SB, Swamy RS, Shetty P, Maloor PA, Dsouza MR. Bifurcated bicipital aponeurosis giving origin to flexor and extensor muscles of the forearm – A case report. J Clin Diagn Res 2016;10:D01-2.
11. Warner JJ, Paletta GA, Warren RF. Accessory head of the biceps brachii. Case report demonstrating clinical relevance. Clin Orthop Relat Res 1992;280:179-81.
12. Sawant SP, Shaikh ST, More RM. A case report on the median nerve passing through the supernumerary head of the biceps brachii muscle. Int J Anal Pharm Biomed Sci 2012;1:(2).

Case Report

Calcified Brain Metastasis from Ovarian Cancer: A Case Report and Literature Review

Abstract

The overall incidence of ovarian cancer with calcified brain metastasis is low. However, in the absence of edema, it is difficult to distinguish metastasis from isolated brain calcifications. Metastasis should be considered in any cancer patient who presents with brain calcification(s) and symptomatology of the nervous system. The authors report a case of advanced ovarian cancer with multiple calcifications in the brain and edema after multiline treatment, in which metastatic cystadenocarcinoma was confirmed by biopsy.

Keywords: *Brain metastasis, ovarian cancer, pathology*

Jian-Hui Huang, Jian-Zeng Ma[1], Chun-Wei Xu[2], Xue-Ni Liu, Jian Lou, Yan-Ru Xie

Department of Medical Oncology, Lishui Municipal Central Hospital, Lishui, [1]Department of Oncology, Sunshine Union Hospital, Weifang, [2]Department of Pathology, Fujian Cancer Hospital, Fuzhou, China

Introduction

Although ovarian cancer is the second most common cancer of the female reproductive system, brain metastasis from ovarian cancer is relatively rare. According to a literature review, the incidence of brain metastasis of ovarian cancer is approximately 0.29% to 12%.[1] The incidence of calcified brain metastasis is low, which has been confirmed in 1% of surgeries and 6% of autopsies.[2] This report describes a rare case involving a patient exhibiting calcified brain metastasis from ovarian cancer. All protocols used in the present study were approved by the Human Clinical and Research Ethics Committees of the Lishui Municipal Central Hospital (Zhejiang, China) and the Sunshine Union Hospital (Shandong, China). The patient provided written informed consent for treatment and publication of anonymized case details.

Case Report

A 56-year-old woman was diagnosed with ovarian cancer. She had been operated on >9 years previously, and metastasis occurred 3 years ago. Physical examination revealed a performance status score of 1 and a numerical rating scale score of 0. Her consciousness was clear, with no enlargement of the superficial (i.e. bilateral supraclavicular and axillary) lymph nodes. Breath sounds in both lungs were clear; dry and wet rales were not heard. Her heart rate was 100 beats/min with normal rhythm, her abdomen was flat and soft, and the operation scar healed well. The entire abdomen was free of tenderness and rebound pain, the liver and spleen were palpable in the subcostal region, and mobility voiced sounds were negative, with no edema in both lower extremities. Pathological signs were not elicited. The patient was diagnosed with an ovarian tumor in the authors' hospital in July 2010. Subsequently, an ovarian tumor staging operation was performed under general anesthesia. Postoperative pathology revealed bilateral borderline serous cystadenocarcinoma of the ovary [Figure 1]. She was treated with a 3-cycle regimen of paclitaxel + cisplatin (i.e., "TP"). After regular reexamination, stable disease was confirmed. Positron emission tomography-computed tomography (CT) performed in June 2016 revealed postoperative changes in the ovarian tumor and anterior mediastinal metastatic tumors, metastasis of the right side of the anterior mediastinum, subcutaneous metastasis of the right side of the right quarter, metastasis of the left iliopsoas muscle, peritoneal metastasis around the liver, metastasis of the two lungs, and metastasis of the mediastinal lymph nodes. She underwent paclitaxel + carboplatin (i. e., "TC")

How to cite this article: Huang JH, Ma JZ, Xu CW, Liu XN, Lou J, Xie YR. Calcified brain metastasis from ovarian cancer: A case report and literature review. J Anat Soc India 2022;71:77-9.

Article Info

Received: 18 December 2019
Accepted: 25 July 2021
Available online: 17 March 2022

Address for correspondence:
Dr. Yan-Ru Xie, Department of Medical Oncology, Lishui Municipal Central Hospital, 289 Kucang Road, Lishui 323 000, Zhejiang, China.
E-mail: yeruosui@163.com

Access this article online

Website: www.jasi.org.in
DOI: 10.4103/JASI.JASI_241_19
Quick Response Code:

therapy plus a 6-cycle regimen of recombinant human endostatin from September 2016 to January 2017. CT revealed a reduction in the lung lesions, and the patient achieved partial response. Subsequently, she was treated with 12 cycles of paclitaxel combined with endostatin maintenance therapy from February 2017 to January 2018. Reexamination with abdominal CT revealed enlargement of abdominal wall nodules and chest CT revealed enlarged lesions in the lungs. The patient then underwent implantation of radioactive particles in the right abdominal wall metastasis in January 2018 and was treated with local radiotherapy for sternal metastasis in February 2018. From March 2018 to February 2019, the patient was treated with 13 cycles of gemcitabine combined with endostatin. Abdominal CT revealed small nodules on the left side of the pelvic cavity that were enlarged. The patient underwent 7 cycles of irinotecan chemotherapy from March to July 2019. One week previously, the patient experienced weakness in the right upper limb accompanied by unstable gait. Cranial CT revealed multiple calcifications with edema in both cerebral hemispheres, the left cerebellar hemisphere, and vermis [Figure 2]. Brain magnetic resonance imaging (MRI) revealed multiple calcifications with edema [Figure 3]. To clarify the nature of the brain calcification, CT-guided biopsy of the metastatic brain tumor was performed in August 2019, which revealed metastatic cystadenocarcinoma [Figure 4]. The patient underwent whole-brain palliative radiotherapy (DT: 3000cGy/10f/300cGy) combined with simultaneous targeted bevacizumab (400 mg) therapy. The patient exhibited movement of the right upper limb, which recovered after radiotherapy and targeted therapy; however, head MRI examination was not performed. The patient was still undergoing bevacizumab therapy as of this writing.

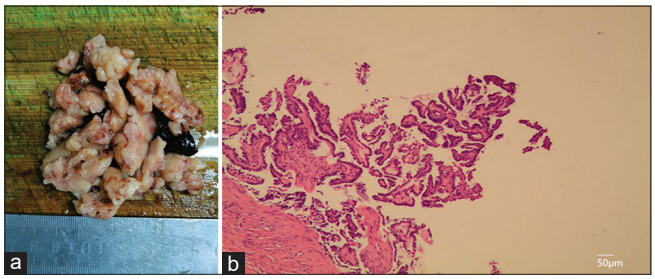

Figure 1: (a) Postoperative specimens of ovarian tumor. (b) Postoperative pathology of ovarian serous cystadenocarcinoma. (×400)

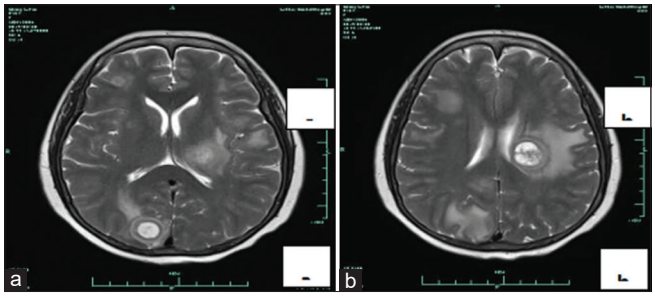

Figure 3: Cranial magnetic resonance imaging revealing multiple calcification metastases with edema (a and b)

Discussion

Primary tumors with a high incidence of brain metastasis of malignant tumors mainly include lung and breast cancers, melanoma, and gastrointestinal tumors,[1] of which brain metastasis of lung cancer accounts for 60% of all brain metastases. Brain metastasis of female reproductive system tumor(s) is rare; the incidence of brain metastasis of ovarian cancer reported in the literature is 1.19%.[3] With recent advances in imaging modalities and targeted drug therapies, the incidence of brain metastasis of ovarian cancer has demonstrated an upward trend.[4] Although the incidence of brain metastasis of ovarian cancer is higher, the incidence of calcified brain metastasis remains very low. Calcified brain metastasis can easily be misdiagnosed as a benign tumor or brain calcification, and calcification may be a sign of long survival of a metastatic tumor.[5] In the present case, multiple metastases were diagnosed and limb symptoms appeared 9 years after surgery and 3 years of treatment. Multiple craniocerebral calcifications were found using transcranial CT and MRI, and craniocerebral calcification metastasis was confirmed using puncture biopsy.

Although the pathogenesis of intracranial calcified metastasis currently remains unclear, it may be related to the destruction of the blood–brain barrier, abundant

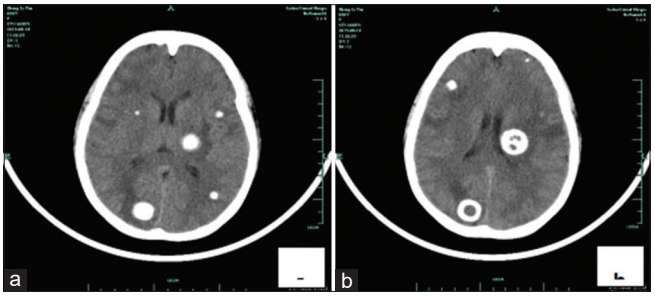

Figure 2: Computed tomography scan revealing multiple calcification metastases with edema (a and b)

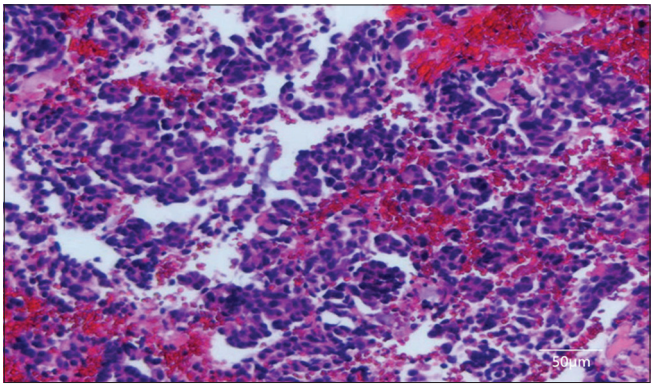

Figure 4: Postoperative pathology of calcified brain metastasis: Metastatic cystadenocarcinoma. (×1000)

tumor cells, and calcium deposition in the tumor area. Tumor blood vessels are necessary to maintain the biological characteristics of the tumor including rapid growth, invasion, and metastasis. It is characterized by neovascularization and incomplete basement membrane of capillaries. This provides favorable conditions for the outward progression, migration, and metastasis of tumor cells and facilitates the deposition of calcium in the blood in tumor cells through blood vessels, which is the basis for the formation of calcification and metastasis. Craniocerebral calcified metastasis is easily misdiagnosed without peritumoral edema and contrast enhancement and can negatively impact patient treatment.[6] Most intracranial calcified metastases are located in the cerebral cortex or the junction of the cerebral cortex and medulla. They are characterized by mild peripheral edema, weak enhancement, and benign lesions.[7]

The treatment of calcified brain metastasis is basically the same as that of ordinary brain metastasis. For patients with multiple brain metastases, whole-brain radiotherapy combined with whole-body therapy can be selected. For patients with single brain metastasis, surgical resection of the metastatic lesions and other targeted radiotherapy may also be helpful in prolonging patient survival. In recent years, targeted drugs and immunological inhibitors have become more widely used. It has been reported that antiangiogenic therapy can be used as a part of a comprehensive treatment strategy for calcified brain metastasis without an increased risk for cerebral hemorrhage.[8]

In conclusion, the occurrence of brain metastasis of ovarian cancer is relatively rare, and the probability of calcification metastasis is even lower. Patients experiencing limb symptoms should be examined using craniocerebral CT/MRI to determine the occurrence/presence of brain metastasis. When obvious calcification is found on CT/MRI, it cannot be considered a benign lesion, and further investigation should be conducted to rule out the possibility of tumor metastasis. The probability of long (er) survival in patients with brain metastasis of ovarian cancer has significantly increased; as such, craniocerebral imaging should be considered in the routine follow-up of those in high-risk groups. The treatment of brain calcification metastasis can be combined with whole-body therapy on the basis of whole-brain radiotherapy, including antiangiogenic drugs, targeted drugs, and immunological inhibitors aimed at prolonging patient survival.

Declaration of patient consent

The authors certify that they have obtained all appropriate patient consent forms. In the form, the patient has given her consent for her images and other clinical information to be reported in the journal. The patient understands that their name and initials will not be published and due efforts will be made to conceal their identity, but anonymity cannot be guaranteed.

Financial support and sponsorship

Nil.

Conflicts of interest

There are no conflicts of interest.

References

1. Barnholtz-Sloan JS, Sloan AE, Davis FG, Vigneau FD, Lai P, Sawaya RE. Incidence proportions of brain metastases in patients diagnosed (1973 to 2001) in the Metropolitan Detroit Cancer Surveillance System. J Clin Oncol 2004;22:2865-72.
2. Tashiro Y, Kondo A, Aoyama I, Nin K, Shimotake K, Tashiro H, *et al*. Calcified metastatic brain tumor. Neurosurgery 1990;26:1065-70.
3. Cohen ZR, Suki D, Weinberg JS, Marmor E, Lang FF, Gershenson DM, *et al*. Brain metastases in patients with ovarian carcinoma: Prognostic factors and outcome. J Neurooncol 2004;66:313-25.
4. Fakour F, Hajizadeh Fallah H, Khajeh Jahromi S, Porteghali P. Central nervous system metastasis in epithelial ovarian carcinoma: A case report and literature review. J Family Reprod Health 2015;9:41-4.
5. Kawamura D, Tanaka T, Fuga M, Yanagisawa T, Tochigi S, Irie K, *et al*. Slow progression of calcified cerebellar metastasis from ovarian cancer: A case report and review of the literature. Neurol Med Chir (Tokyo) 2013;53:722-6.
6. Ricke J, Baum K, Hosten N. Calcified brain metastases from ovarian carcinoma. Neuroradiology 1996;38:460-1.
7. Zhu XH. CT diagnosis of intracranial calcifying metastases. Southwest Mil Med J 2009;11:454.
8. Lin X, DeAngelis LM. Treatment of Brain Metastases. J Clin Oncol 2015;33:3475-84.

The Editorial Process

A manuscript will be reviewed for possible publication with the understanding that it is being submitted to Journal of the Anatomical Society of India alone at that point in time and has not been published anywhere, simultaneously submitted, or already accepted for publication elsewhere. The journal expects that authors would authorize one of them to correspond with the Journal for all matters related to the manuscript. All manuscripts received are duly acknowledged. On submission, editors review all submitted manuscripts initially for suitability for formal review. Manuscripts with insufficient originality, serious scientific or technical flaws, or lack of a significant message are rejected before proceeding for formal peer-review. Manuscripts that are unlikely to be of interest to the Journal of the Anatomical Society of India readers are also liable to be rejected at this stage itself.

Manuscripts that are found suitable for publication in Journal of the Anatomical Society of India are sent to two or more expert reviewers. During submission, the contributor is requested to provide names of two or three qualified reviewers who have had experience in the subject of the submitted manuscript, but this is not mandatory. The reviewers should not be affiliated with the same institutes as the contributor/s. However, the selection of these reviewers is at the sole discretion of the editor. The journal follows a double-blind review process, wherein the reviewers and authors are unaware of each other's identity. Every manuscript is also assigned to a member of the editorial team, who based on the comments from the reviewers takes a final decision on the manuscript. The comments and suggestions (acceptance/ rejection/ amendments in manuscript) received from reviewers are conveyed to the corresponding author. If required, the author is requested to provide a point by point response to reviewers' comments and submit a revised version of the manuscript. This process is repeated till reviewers and editors are satisfied with the manuscript.

Manuscripts accepted for publication are copy edited for grammar, punctuation, print style, and format. Page proofs are sent to the corresponding author. The corresponding author is expected to return the corrected proofs within three days. It may not be possible to incorporate corrections received after that period. The whole process of submission of the manuscript to final decision and sending and receiving proofs is completed online. To achieve faster and greater dissemination of knowledge and information, the journal publishes articles online as 'Ahead of Print' immediately on acceptance.

Clinical trial registry

Journal of the Anatomical Society of India favors registration of clinical trials and is a signatory to the Statement on publishing clinical trials in Indian biomedical journals. Journal of the Anatomical Society of India would publish clinical trials that have been registered with a clinical trial registry that allows free online access to public. Registration in the following trial registers is acceptable: http://www.ctri.in/; http://www.actr.org.au/; http://www.clinicaltrials.gov/; http://isrctn.org/; http://www.trialregister.nl/trialreg/index.asp; and http://www.umin.ac.jp/ctr. This is applicable to clinical trials that have begun enrollment of subjects in or after June 2008. Clinical trials that have commenced enrollment of subjects prior to June 2008 would be considered for publication in Journal of the Anatomical Society of India only if they have been registered retrospectively with clinical trial registry that allows unhindered online access to public without charging any fees.

Authorship Criteria

Authorship credit should be based only on substantial contributions to each of the three components mentioned below:

1. Concept and design of study or acquisition of data or analysis and interpretation of data;
2. Drafting the article or revising it critically for important intellectual content; and
3. Final approval of the version to be published.

Participation solely in the acquisition of funding or the collection of data does not justify authorship. General supervision of the research group is not sufficient for authorship. Each contributor should have participated sufficiently in the work to take public responsibility for appropriate portions of the content of the manuscript. The order of naming the contributors should be based on the relative contribution of the contributor towards the study and writing the manuscript. Once submitted the order cannot be changed without written consent of all the contributors. The journal prescribes a maximum number of authors for manuscripts depending upon the type of manuscript, its scope and number of institutions involved (vide infra). The authors should provide a justification, if the number of authors exceeds these limits.

Contribution Details

Contributors should provide a description of contributions made by each of them towards the manuscript. Description should be divided in following categories, as applicable: concept, design, definition of intellectual content, literature search, clinical studies, experimental studies, data acquisition, data analysis, statistical analysis, manuscript preparation, manuscript editing and manuscript review. Authors' contributions will be printed along with the article. One or more author should take responsibility for the integrity of the work as a whole from inception to published article and should be designated as 'guarantor'.

Conflicts of Interest/ Competing Interests

All authors of must disclose any and all conflicts of interest they may have with publication of the manuscript or an institution or product that is mentioned in the manuscript and/or is important to the outcome of the study presented. Authors should also disclose conflict of interest with products that compete with those mentioned in their manuscript.

Submission of Manuscripts

All manuscripts must be submitted on-line through the website https://review.jow.medknow.com/jasi. First time users will have to register at this site. Registration is free but mandatory. Registered authors can keep track of their articles after logging into the site using their user name and password.

- If you experience any problems, please contact the editorial office by e-mail at editor@jasi.org.in

The submitted manuscripts that are not as per the "Instructions to Authors" would be returned to the authors for technical correction, before they undergo editorial/ peer-review. Generally, the manuscript should be submitted in the form of two separate files:

[1] Title Page/First Page File/covering letter:

This file should provide

1. The type of manuscript (original article, case report, review article, Letter to editor, Images, etc.) title of the manuscript, running title, names of all authors/ contributors (with their highest academic degrees, designation and affiliations) and name(s) of department(s) and/ or institution(s) to which the work should be credited, . All information which can reveal your identity should be here. Use text/rtf/doc files. Do not zip the files.
2. The total number of pages, total number of photographs and word counts separately for abstract and for the text (excluding the references, tables and abstract), word counts for introduction + discussion in case of an original article;
3. Source(s) of support in the form of grants, equipment, drugs, or all of these;
4. Acknowledgement, if any. One or more statements should specify 1) contributions that need acknowledging but do not justify authorship, such as general support by a departmental chair; 2) acknowledgments of technical help; and 3) acknowledgments of financial and material support, which should specify the nature of the support. This should be included in the title page of the manuscript and not in the main article file.
5. If the manuscript was presented as part at a meeting, the organization, place, and exact date on which it was read. A full statement to the editor about all submissions and previous reports that might be regarded as redundant publication of the same or very similar work. Any such work should be referred to specifically, and referenced in the new paper. Copies of such material should be included with the submitted paper, to help the editor decide how to handle the matter.
6. Registration number in case of a clinical trial and where it is registered (name of the registry and its URL)
7. Conflicts of Interest of each author/ contributor. A statement of financial or other relationships that might lead to a conflict of interest, if that information is not included in the manuscript itself or in an authors' form
8. Criteria for inclusion in the authors'/ contributors' list
9. A statement that the manuscript has been read and approved by all the authors, that the requirements for authorship as stated earlier in this document have been met, and that each author believes that the manuscript represents honest work, if that information is not provided in another form (see below); and
10. The name, address, e-mail, and telephone number of the corresponding author, who is responsible for communicating with the other authors about revisions and final approval of the proofs, if that information is not included on the manuscript itself.

[2] Blinded Article file: The main text of the article, beginning from Abstract till References (including tables) should be in this file. The file must not contain any mention of the authors' names or initials or the institution at which the study was done or acknowledgements. Page headers/ running title can include the title but not the authors' names. Manuscripts not in compliance with the Journal's blinding policy will be returned to the corresponding author. Use rtf/doc files. Do not zip the files. **Limit the file size to 1 MB.** Do not incorporate images in the file. If file size is large, graphs can be submitted as images separately without incorporating them in the article file to reduce the size of the file. The pages should be numbered consecutively, beginning with the first page of the blinded article file.

[3] Images: Submit good quality color images. **Each image should be less than 2 MB in size.** Size of the image can be reduced by decreasing the actual height and width of the images (keep up to 1600 x 1200 pixels or 5-6 inches). Images can be submitted as jpeg files. Do not zip the files. Legends for the figures/images should be included at the end of the article file.

[4] The contributors' / copyright transfer form (template provided below) has to be submitted in original with the signatures of all the contributors within two weeks of submission via courier, fax or email as a scanned image. Print ready hard copies of the images (one set) or digital images should be sent to the journal office at the time of submitting revised manuscript. High resolution images (up to 5 MB each) can be sent by email.

Contributors' form / copyright transfer form can be submitted online from the authors' area on https://review.jow.medknow.com/jasi.

Preparation of Manuscripts

Manuscripts must be prepared in accordance with "Uniform requirements for Manuscripts submitted to Biomedical Journals" developed by the International Committee of Medical Journal Editors (October 2008). The uniform requirements and specific requirement of Journal of the Anatomical Society of India are summarized below. Before submitting a manuscript, contributors are requested to check for the latest instructions available. Instructions are also available from the website of the journal (www.jasi.org.in) and from the manuscript submission site https://review.jow.medknow.com/jasi.

Journal of the Anatomical Society of India accepts manuscripts written in American English.

Copies of any permission(s)

It is the responsibility of authors/ contributors to obtain permissions for reproducing any copyrighted material. A copy of the permission obtained must accompany the manuscript. Copies of any and all published articles or other manuscripts in preparation or submitted elsewhere that are related to the manuscript must also accompany the manuscript.

Types of Manuscripts

Original articles:

These include randomized controlled trials, intervention studies, studies of screening and diagnostic test, outcome studies, cost effectiveness analyses, case-control series, and surveys with high response rate. The text of original articles amounting to up to 3000 words (excluding Abstract, references and Tables) should be divided into sections with the headings Abstract, Key-words, Introduction, Material and Methods, Results, Discussion and Conclusion, References, Tables and Figure legends.

An abstract should be in a structured format under following heads: **Introduction, Material and Methods, Results,** and **Discussion and Conclusion.**

Introduction: State the purpose and summarize the rationale for the study or observation.

Material and Methods: It should include and describe the following aspects:

Ethics: When reporting studies on human beings, indicate whether the procedures followed were in accordance with the ethical standards of the responsible committee on human experimentation (institutional or regional) and with the Helsinki Declaration of 1975, as revised in 2000 (available at http://www.wma.net/e/policy/17-c_e.html). For prospective studies involving human participants, authors are expected to mention about approval of (regional/ national/ institutional or independent Ethics Committee or Review Board, obtaining informed consent from adult research participants and obtaining assent for children aged over 7 years participating in the trial. The age beyond which assent would be required could vary as per regional and/ or national guidelines. Ensure confidentiality of subjects by desisting from mentioning participants' names, initials or hospital numbers, especially in illustrative material. When reporting experiments on animals, indicate whether the institution's or a national research council's guide for, or any national law on the care and use of laboratory animals was followed. Evidence for approval by a local Ethics Committee (for both human as well as animal studies) must be supplied by the authors on demand. Animal experimental procedures should be as humane as possible and the details of anesthetics and analgesics used should be clearly stated. The ethical standards of experiments must be in accordance with the guidelines provided by the CPCSEA and World Medical Association Declaration of Helsinki on Ethical Principles for Medical Research Involving Humans for studies involving experimental animals and human beings, respectively). The journal will not consider any paper which is ethically unacceptable. A statement on ethics committee permission and ethical practices must be included in all research articles under the 'Materials and Methods' section.

Study design:

Selection and Description of Participants: Describe your selection of the observational or experimental participants (patients or laboratory animals, including controls) clearly, including eligibility and exclusion criteria and a description of the source population. *Technical information*: Identify the methods, apparatus (give the manufacturer›s name and address in parentheses), and procedures in sufficient detail to allow other workers to reproduce the results. Give references to established methods, including statistical methods (see below); provide references and brief descriptions for methods that have been published but are not well known; describe new or substantially modified methods, give reasons for using them, and evaluate their limitations. Identify precisely all drugs and chemicals used, including generic name(s), dose(s), and route(s) of administration.

Reports of randomized clinical trials should present information on all major study elements, including the protocol, assignment of interventions (methods of randomization, concealment of allocation to treatment groups), and the method of masking (blinding), based on the CONSORT Statement (http://www.consort-statement.org).

Reporting Guidelines for Specific Study Designs

Initiative	Type of Study	Source
CONSORT	Randomized controlled trials	http://www.consort-statement.org
STARD	Studies of diagnostic accuracy	http://www.consort-statement.org/stardstatement.htm
QUOROM	Systematic reviews and meta-analyses	http://www.consort- statement.org/Initiatives/MOOSE/moose.pdf statement.org/Initiatives/MOOSE/moose.pdf
STROBE	Observational studies in epidemiology	http://www.strobe-statement.org
MOOSE	Meta-analyses of observational studies in epidemiology	http://www.consort- statement.org/Initiatives/MOOSE/moose.pdf

Statistics: Whenever possible quantify findings and present them with appropriate indicators of measurement error or uncertainty (such as confidence intervals). Authors should report losses to observation (such as, dropouts from a clinical trial). When data are summarized in the Results section, specify the statistical methods used to analyze them. Avoid non-technical uses of technical terms in statistics, such as 'random' (which implies a randomizing device), 'normal', 'significant', 'correlations', and 'sample'. Define statistical terms, abbreviations, and most symbols. Specify the computer software used. Use upper italics (*P* 0.048). For all *P* values include the exact value and not less than 0.05 or 0.001. Mean differences in continuous variables, proportions in categorical variables and relative risks including odds ratios and hazard ratios should be accompanied by their confidence intervals.

Results: Present your results in a logical sequence in the text, tables, and illustrations, giving the main or most important findings first. Do not repeat in the text all the data in the tables or illustrations; emphasize or summarize only important observations. Extra- or supplementary materials and technical detail can be placed in an appendix where it will be accessible but will not interrupt the flow of the text; alternatively, it can be published only in the electronic version of the journal.

When data are summarized in the Results section, give numeric results not only as derivatives (for example, percentages) but also as the absolute numbers from which the derivatives were calculated, and specify the statistical methods used to analyze them. Restrict tables and figures to those needed to explain the argument of the paper and to assess its support. Use graphs as an alternative to tables with many entries; do not duplicate data in graphs and tables. Where scientifically appropriate, analyses of the data by variables such as age and sex should be included.

Discussion: Include summary of *key findings* (primary outcome measures, secondary outcome measures, results as they relate to a prior hypothesis); *Strengths and limitations* of the study (study question, study design, data collection, analysis and interpretation); *Interpretation and implications* in the context of the totality of evidence (is there a systematic review to refer to, if not, could one be reasonably done here and now?, what this study adds to the available evidence, effects on patient care and health policy, possible mechanisms); *Controversies* raised by this study; and *Future research directions* (for this particular research collaboration, underlying mechanisms, clinical research).

Do not repeat in detail data or other material given in the Introduction or the Results section. In particular, contributors should avoid making statements on economic benefits and costs unless their manuscript includes economic data and analyses. Avoid claiming priority and alluding to work that has not been completed. New hypotheses may be stated if needed, however they should be clearly labeled as such. About 30 references can be included. These articles generally should not have more than six authors.

Review Articles:

These are comprehensive review articles on topics related to various fields of Anatomy. The entire manuscript should not exceed 7000 words with no more than 50 references and two authors. Following types of articles can be submitted under this category:

- Newer techniques of dissection and histology
- New methodology in Medical Education
- Review of a current concept

Please note that generally review articles are by invitation only. But unsolicited review articles will be considered for publication on merit basis.

Case reports:

New, interesting and rare cases can be reported. They should be unique, describing a great diagnostic or therapeutic challenge and providing a learning point for the readers. Cases with clinical significance or implications will be given priority. These communications could be of up to 1000 words (excluding Abstract and references) and should have the following headings: Abstract (unstructured), Key-words, Introduction, Case report, Discussion and Conclusion, Reference, Tables and Legends in that order.

The manuscript could be of up to 1000 words (excluding references and abstract) and could be supported with up to 10 references. Case Reports could be authored by up to four authors.

Letter to the Editor:

These should be short and decisive observations. They should preferably be related to articles previously published in the Journal or views expressed in the journal. They should not be preliminary observations that need a later

paper for validation. The letter could have up to 500 words and 5 references. It could be generally authored by not more than four authors.

Book Review: This consists of a critical appraisal of selected books on Anatomy. Potential authors or publishers may submit books, as well as a list of suggested reviewers, to the editorial office. The author/publisher has to pay INR 10,000 per book review.

Other:

Editorial, Guest Editorial, Commentary and Opinion are solicited by the editorial board.

References

References should be *numbered* consecutively in the order in which they are first mentioned in the text (not in alphabetic order). Identify references *in text*, tables, and legends by Arabic numerals in superscript with square bracket after the punctuation *marks. References cited only* in tables or figure legends should be numbered in accordance with the sequence established by the first identification in the text of the particular table or figure. Use the style of the examples below, which are based on the formats used by the NLM *in Index Medicus*. The titles of journals *should be abbreviated* according to the style used in Index Medicus. Use complete name of the journal for non-indexed journals. Avoid using abstracts as references. Information from manuscripts submitted but not accepted should be cited in the text as "unpublished observations" with written permission from the source. Avoid citing a "personal communication" unless it provides essential information not available from a public source, in which case the name of the person and date of communication should be cited in parentheses in the text. The commonly cited types of references are shown here, for other types of references such as newspaper items please refer to ICMJE Guidelines (http://www.icmje.org or http://www.nlm.nih.gov/bsd/uniform_requirements.html).

Articles in Journals

1. Standard journal article (for up to six authors): Parija S C, Ravinder PT, Shariff M. Detection of hydatid antigen in the fluid samples from hydatid cysts by co-agglutination. Trans. R.Soc. Trop. Med. Hyg.1996; 90:255–256.
2. Standard journal article (for more than six authors): List the first six contributors followed by *et al*.

Roddy P, Goiri J, Flevaud L, Palma PP, Morote S, Lima N. *et al*., Field Evaluation of a Rapid Immunochromatographic Assay for Detection of Trypanosoma cruzi Infection by Use of Whole Blood. J. Clin. Microbiol. 2008; 46: 2022-2027.

3. Volume with supplement: Otranto D, Capelli G, Genchi C: Changing distribution patterns of canine vector borne diseases in Italy: leishmaniosis vs. dirofilariosis. Parasites & Vectors 2009; Suppl 1:S2.

Books and Other Monographs

1. Personal author(s): Parija SC. Textbook of Medical Parasitology. 3rd ed. All India Publishers and Distributors. 2008.
2. Editor(s), compiler(s) as author: Garcia LS, Filarial Nematodes In: Garcia LS (editor) Diagnostic Medical Parasitology ASM press Washington DC 2007: pp 319-356.
3. Chapter in a book: Nesheim M C. Ascariasis and human nutrition. In Ascariasis and its prevention and control, D. W. T. Crompton, M. C. Nesbemi, and Z. S. Pawlowski (eds.). Taylor and Francis,London, U.K.1989, pp. 87–100.

Electronic Sources as reference

Journal article on the Internet: Parija SC, Khairnar K. Detection of excretory *Entamoeba histolytica* DNA in the urine, and detection of *E. histolytica* DNA and lectin antigen in the liver abscess pus for the diagnosis of amoebic liver abscess. *BMC Microbiology* 2007, **7**:41. doi:10.1186/1471-2180-7-41. http://www.biomedcentral.com/1471-2180/7/41

Tables

- Tables should be self-explanatory and should not duplicate textual material.
- Tables with more than 10 columns and 25 rows are not acceptable.
- Number tables, in Arabic numerals, consecutively in the order of their first citation in the text and supply a brief title for each.
- Place explanatory matter in footnotes, not in the heading.
- Explain in footnotes all non-standard abbreviations that are used in each table.
- Obtain permission for all fully borrowed, adapted, and modified tables and provide a credit line in the footnote.
- For footnotes use the following symbols, in this sequence: *, †, ‡, §, ‖,¶ , **, ††, ‡‡
- Tables with their legends should be provided at the end of the text after the references. The tables along with their number should be cited at the relevant place in the text

Illustrations (Figures)

- Upload the images in JPEG format. The file size should be within 1024 kb in size while uploading.
- Figures should be numbered consecutively according to the order in which they have been first cited in the text.
- Labels, numbers, and symbols should be clear and of uniform size. The lettering for figures should be large enough to be legible after reduction to fit the width of a printed column.
- Symbols, arrows, or letters used in photomicrographs

should contrast with the background and should be marked neatly with transfer type or by tissue overlay and not by pen.
- Titles and detailed explanations belong in the legends for illustrations not on the illustrations themselves.
- When graphs, scatter-grams or histograms are submitted the numerical data on which they are based should also be supplied.
- The photographs and figures should be trimmed to remove all the unwanted areas.
- If photographs of individuals are used, their pictures must be accompanied by written permission to use the photograph.
- If a figure has been published elsewhere, acknowledge the original source and submit written permission from the copyright holder to reproduce the material. A credit line should appear in the legend for such figures.
- Legends for illustrations: Type or print out legends (maximum 40 words, excluding the credit line) for illustrations using double spacing, with Arabic numerals corresponding to the illustrations. When symbols, arrows, numbers, or letters are used to identify parts of the illustrations, identify and explain each one in the legend. Explain the internal scale (magnification) and identify the method of staining in photomicrographs.
- Final figures for print production: Send sharp, glossy, un-mounted, color photographic prints, with height of 4 inches and width of 6 inches at the time of submitting the revised manuscript. Print outs of digital photographs are not acceptable. If digital images are the only source of images, ensure that the image has minimum resolution of 300 dpi or 1800 x 1600 pixels in TIFF format. Send the images on a CD. Each figure should have a label pasted (avoid use of liquid gum for pasting) on its back indicating the number of the figure, the running title, top of the figure and the legends of the figure. Do not write the contributor/s' name/s. Do not write on the back of figures, scratch, or mark them by using paper clips.
- The Journal reserves the right to crop, rotate, reduce, or enlarge the photographs to an acceptable size.

Protection of Patients' Rights to Privacy

Identifying information should not be published in written descriptions, photographs, sonograms, CT scans, etc., and pedigrees unless the information is essential for scientific purposes and the patient (or parent or guardian, wherever applicable) gives informed consent for publication. Authors should remove patients' names from figures unless they have obtained informed consent from the patients. The journal abides by ICMJE guidelines:

1. Authors, not the journals nor the publisher, need to obtain the patient consent form before the publication and have the form properly archived. The consent forms are not to be uploaded with the cover letter or sent through email to editorial or publisher offices.
2. If the manuscript contains patient images that preclude anonymity, or a description that has obvious indication to the identity of the patient, a statement about obtaining informed patient consent should be indicated in the manuscript.

Sending a revised manuscript

The revised version of the manuscript should be submitted online in a manner similar to that used for submission of the manuscript for the first time. However, there is no need to submit the "First Page" or "Covering Letter" file while submitting a revised version. When submitting a revised manuscript, contributors are requested to include, the 'referees' remarks along with point to point clarification at the beginning in the revised file itself. In addition, they are expected to mark the changes as underlined or colored text in the article.

Reprints and proofs

Journal provides no free printed reprints. Authors can purchase reprints, payment for which should be done at the time of submitting the proofs.

Publication schedule

The journal publishes articles on its website immediately on acceptance and follows a 'continuous publication' schedule. Articles are compiled in issues for 'print on demand' quarterly.

Copyrights

Checklist

Covering letter

- Signed by all contributors
- Previous publication / presentations mentioned
- Source of funding mentioned
- Conflicts of interest disclosed

Authors

- Last name and given name provided along with Middle name initials (where applicable)
- Author for correspondence, with e-mail address provided
- Number of contributors restricted as per the instructions
- Identity not revealed in paper except title page (e.g. name of the institute in Methods, citing previous study as 'our study', names on figure labels, name of institute in photographs, etc.)

Presentation and format

- Double spacing
- Margins 2.5 cm from all four sides
- Page numbers included at bottom
- Title page contains all the desired information
- Running title provided (not more than 50 characters)
- Abstract page contains the full title of the manuscript
- Abstract provided (structured abstract of 250 words for original articles, unstructured abstracts of about 150 words for all other manuscripts excluding letters to the Editor)
- Key words provided (three or more)
- Introduction of 75-100 words
- Headings in title case (not ALL CAPITALS)
- The references cited in the text should be after punctuation marks, in superscript with square bracket.
- References according to the journal's instructions, punctuation marks checked
- Send the article file without 'Track Changes'

Language and grammar

- Uniformly American English
- Write the full term for each abbreviation at its first use in the title, abstract, keywords and text separately unless it is a standard unit of measure. Numerals from 1 to 10 spelt out
- Numerals at the beginning of the sentence spelt out
- Check the manuscript for spelling, grammar and punctuation errors
- If a brand name is cited, supply the manufacturer's name and address (city and state/country).
- Species names should be in italics

Tables and figures

- No repetition of data in tables and graphs and in text
- Actual numbers from which graphs drawn, provided
- Figures necessary and of good quality (colour)
- Table and figure numbers in Arabic letters (not Roman)
- Labels pasted on back of the photographs (no names written)
- Figure legends provided (not more than 40 words)
- Patients' privacy maintained (if not permission taken)
- Credit note for borrowed figures/tables provided
- Write the full term for each abbreviation used in the table as a footnote

Journal of
The Anatomical Society of India

Salient Features:

- Publishes research articles related to all aspects of Anatomy and Allied medical/surgical sciences.
- Pre-Publication Peer Review and Post-Publication Peer Review
- Online Manuscript Submission System
- Selection of articles on the basis of MRS system
- Eminent academicians across the globe as the Editorial board members
- Electronic Table of Contents alerts
- Available in both online and print form.

The journal is registered with the following abstracting partners:
Baidu Scholar, CNKI (China National Knowledge Infrastructure), EBSCO Publishing's Electronic Databases, Ex Libris – Primo Central, Google Scholar, Hinari, Infotrieve, Netherlands ISSN center, ProQuest, TdNet, Wanfang Data

The journal is indexed with, or included in, the following:
SCOPUS, Science Citation Index Expanded, IndMed, MedInd, Scimago Journal Ranking, Emerging Sources Citation Index.

Impact Factor® as reported in the 2018 Journal Citation Reports® (Clarivate Analytics, 2019): 0.168

Editorial Office:
Dr. Vishram Singh, Editor-in-Chief, JASI
OC-5/103, 1st floor, Orange County Society,
Ahinsa Khand-I, Indirapuram, Ghaziabad,
Delhi, NCR- 201014.
Email: editorjasi@gmail.com
(O) | Website: www.asiindia.in

The journal is owned and run by The Anatomical Society of India